Development of Preparative Microfluidic Techniques for Lysis of Microbial Cells and Affinity Purification of Proteins

A thesis submitted to University College London for the degree of Doctor of Philosophy

By Hani El-Sabbahy

Department of Biochemical Engineering
University College London
Torrington Place
London
WC1E 7JE
UK

Declaration

I, Hani El-Sabbahy, confirm that the work presented in this thesis is my own. Where information has been derived from other sources, I confirm that this has been indicated in the thesis.

Signed……………………..

Date………………………

I Abstract

In order to fully realise the benefits of microscale mammalian cell culture and microbial fermentation systems, a device capable of online sample preparation to enable further investigation of product quality is a key requirement. The aim of this work is to move toward such a device by designing and characterising a microfluidic lysis device and microaffinity chromatography device that are compatible with each other. The resulting microfluidic lysis device is useful for preparatory lysis of microbial cells. It works by mixing a lysis reagent (BugBuster Mastermix™), with microbial culture, using a T-Piece connection. Lysis takes place in a 700µm internal diameter fused silica capillary. The device was able to successfully lyse microbial cells with similar active Glutathione S Transferase release to sonication. The operating flowrate range of the device was 3.207µL min^{-1} to 6.414 µL min^{-1} and the device volume was 30µL - 60µL. The microaffinity chromatography column performed well in studies with pure Glutathione S Transferase. It showed good loading and elution behaviour. The breakthrough and elution curves, and quantity of protein eluted per unit bed volume, were similar to lab scale. The difference being as a result of experimental error. The column also performed well with a 100% clarified *Escherichia coli* lysate containing recombinant Glutathione S Transferase from *Schistosoma japonicum*. The eluate had a purity of 55% and concentration of 2.24 mg/ml. The column was fabricated from inexpensive fused silica capillary. It had an internal diameter of 700µm, a length of 5cm (the same length as a typical lab scale Glutathione Affinity column), and a bed volume of approximately 19µL. The operating flowrate range for the column was the same as the microlysis device.

II Table of Contents

III List of Tables

Hani El-Sabbahy

IV List of Figures

syringe adaptor (IDEX Health and Science, Washington, USA); (4) double winged peak nut with 1/32" ferrule (Agilent Technologies, Cheshire, UK); (5) PeekSil tubing 100µm internal diameter, 1/32" external diameter (IDEX Health and Science, Washington, USA); (6) Agilent 1100 HPLC diode array detector using a semi-micro flowcell (Agilent Technologies, Cheshire, UK), (7) Microcolumn in holder...168

Figure 5.3 – A typical blue dextran transition curve, obtained at a flowrate of 50 cm hr^{-1}, without the micro column in place. The system was first flushed with PBS pH7.4 and then loaded with 1 mg/mL Blue dextran 2000 in PBS pH7.4. 176

Figure 5.4 – A typical blue dextran transition derivative curve, with the micro-column removed, fitted to a Weibull distribution. The derivative curve shown (solid line) is for the blue dextran transition at 50cm hr^{-1}. The dashed line represents the predicted derivative curve when the data is fitted to a Weibull distribution...177

Figure 5.5 – Blue dextran transition curve obtained at a flowrate of 50 cm hr^{-1}. The column was first washed with PBS pH7.4 and then loaded with 1 mg/ mL Blue dextran 2000 in PBS pH7.4 179

Figure 5.6 - First order derivatives of the averaged blue dextran transitions. 1 mg/ mL blue dextran 2000 was loaded on to the column at different flowrates and the resulting transitions for each flowrate were averaged and differentiated to give the above curves. The solid line is the first order derivative of the averaged blue dextran transitions obtained at a linear velocity of 50 cm hr^{-1} the dashed line is the first order derivative of the averaged blue dextran transitions obtained at is 75 cm hr^{-1} and the dotted line is the first order derivative of the averaged blue dextran transitions obtained at 100 cm hr^{-1} 180

Figure 5.7 – Typical blue dextran transition derivative curve showing the estimation of the void volume by fitting the curve with a Weibull distribution. The derivative curve shown is for the blue dextran transition at 50 cm hr^{-1}. The dashed line represents the predicted derivative curve when the data is fitted to a Weibull distribution...181

Figure 5.8 - Typical acetone pulse. A 360µL 0.1% acetone (v/v) in PBS pH7.4 was loaded on to the 10 mL XK16 column at 50cm hr^{-1}..................................185

Figure 5.9 - 0.2% acetone transition with its first order derivative. The transition was performed 100 cm hr^{-1} by switching flow between PBS pH7.4 and 0.2% (v/v) acetone in PBS pH7.4...186

Figure 5.10 - Plot of HETP versus flowrate. The (●) show Gaussian HETP versus flowrate for the 10 mL XK16 lab scale column. The (○) show Gaussian HETP versus flowrate for the 19µl micro column which was calculated using Equation 5.2 and Equation 5.3. The (△) shows corrected Gaussian HETP versus flowrate for the 19µL micro column, these HETP values were corrected to remove extra column dispersion using Equation 5.10 to calculate the variance resulting from the column by subtracting the extra column variance from the total variance. The (□) shows non-Gaussian HETP versus flowrate for the 19µl micro column calculated using Equation 5.4, Equation 5.8 and Equation 5.9...191

V Acknowledgements

First and foremost I would like to thank Almighty God for all the gifts and opportunities that he has given me. I am, and will be, eternally grateful and will strive to be worthy of them and of his love.

Secondly I would like to thank my family. I would like to express my admiration for, and gratitude to, my father for his encouragement and all that he has taught me, my mother for her support, my wife and children for their support and encouragement, the sacrifices they have made, and the understanding they have shown while I was completing this work. I would also like to thank my brother for his support.

My supervisor Dr Paul Dalby and advisor Dr Daniel Bracewell have both taught me so much. I am very grateful for the knowledge they have entrusted to me and for their guidance, support, patience and encouragement during this research.

I am grateful to Professor Nigel Titchener-Hooker for encouraging me to undertake this project and for his inspirational teaching during my undergraduate degree. I would also like to make clear my upmost respect for all the lecturers in the Department of Biochemical Engineering. I am grateful for the opportunity to learn from some of the best minds in the field.

I would also like to express my gratitude to my fellow researchers in the Department for their help and support. In particular, I would like to thank Omar Al Ramadhani, Wasim Domah, Niqash Raja, Spyros Gerontas, and Shaukat Ali for their encouragement and friendship.

I have enjoyed working with colleagues in the Engineering workshop who built some of the equipment and fittings that I used in this work. I am particularly grateful to Martin and Graham for their hard work and kind words.

Finally I would like to thank HSE for giving me the time off to undertake this PhD, and my colleagues at HSE for their kind words and support.

VI Nomenclature

$\triangle P$	pressure drop	bar
A	contribution of eddy diffusion to plate height,	cm
a	width the peak to the right of the maximum at 10% of the peak height	µL, mL
A_r	cross sectional area	m^2
A_S	asymmetry factor,	-
B	contribution of longitudinal diffusion to plate height,	$cm^2\ hr^{-1}$
b	width the peak to the left of the maximum at 10% of the peak height	µL, mL
c	total molar concentration in the solution	moles m^{-3}
C	concentration or contribution of the resistance to mass transfer to plate height,	mg mL^{-1}, hr
C_0	concentration of protein loaded on to the column	mg mL^{-1}
C_C	concentration of Glutathione S Transferase on unlysed microbial culture	mg mL^{-1}
C_{Final}	final concentration	mg mL^{-1}
$C_{Initial}$	initial concentration	mg mL^{-1}
C_L	concentration of Glutathione S Transferase in the lysate under investigation,	mg mL^{-1}
C_S	concentration of Glutathione S Transferase in a sonicate of the microbial culture	mg mL^{-1}
d	diameter of the tube,	m
D_{AB}	binary diffusivity for system a-b	$m^2\ s^{-1}$

D_L	degree of lysis	-
d_p	particle diameter	m
dUV_A/dv	first order derivative of the UV absorbance with respect to volume	$mAu\ \mu L^{-1}$
J^*_{Ay}	molar flux of the analyte relative to the molar average velocity of the mobile phase.	$moles\ m^{-2}s^{-1}$
$L,$	length	cm, m
M_0	zeroth moment of a distribution	-
M_1	first moment of a distribution	-
M_2	second moment of a distribution	-
N	number of theoretical plates,	-
Q	steady state flowrate	$m^3\ s^{-1}$
$R_{hyd.}$	hydraulic resistance	$Pa\ s\ m^{-3}$
t_R	retention time	min
u	linear velocity	$cm\ hr^{-1}$
U_0	superficial velocity	$m\ s^{-1}$
V	volume	μL
V_R	retention volume	μL
V_{total}	total volume loaded on to the column	μL
W_h	width at half peak height	min, μL, mL

x_A	molar fraction of species a	-
α	dimensionless geometric correction factor.	-
ε	bed voidage	-
μ	viscosity	mPa s, Pa s
μ_v	mean volume	μL
ρ	density	kg m^{-3}
σ	standard deviation	-
σ^2	variance	-

DBC	dynamic binding capacity	μg μL^{-1}
HETP$_N$	non-Gaussian height equivalent to one theoretical plate,	cm
HETP	height equivalent to one theoretical plate,	cm

1 Introduction

Biopharmaceuticals form a significant and increasing proportion of the global pharmaceutical market and they are used to treat diseases ranging from cancer to diabetes (Walsh 2010; Newman & Cragg 2007). However, the development of new biopharmaceuticals is expensive; the development of a new molecular entity is estimated to cost around $1.8 Billion (Paul et al. 2010) and the process of getting a new drug to market takes a long time, approximately on average 10 years (DiMasi et al. 2003).

The function of these biological molecules is dependent on their structural detail such as correct folding and glycosylation. When used as drugs, must act on the medicinal target, without invoking an undesired immune response. The manufacturing process can have a significant impact not just on yield and purity but on product quality. For example, fermentation conditions can affect the yield and quality of proteins produced both in mammalian cell culture (Andersen & Goochee 1994) and microbial cell culture (Andersen & Krummen 2002) as can downstream processes (Kee et al. 2008)

Figure 1.1 a bioprocess flow diagram, shows the stages in the production of biopharmaceuticals. As can be seen from this diagram, a typical bioprocess consists of a fermentation/bioreactor step followed by three to six downstream processing operations, depending on whether the product is intracellular or extracellular, and the purity and formulation required. There are many different choices that can be made at each stage that affect yield, product purity and quality and these choices need to be made at a relatively early stage of process design.
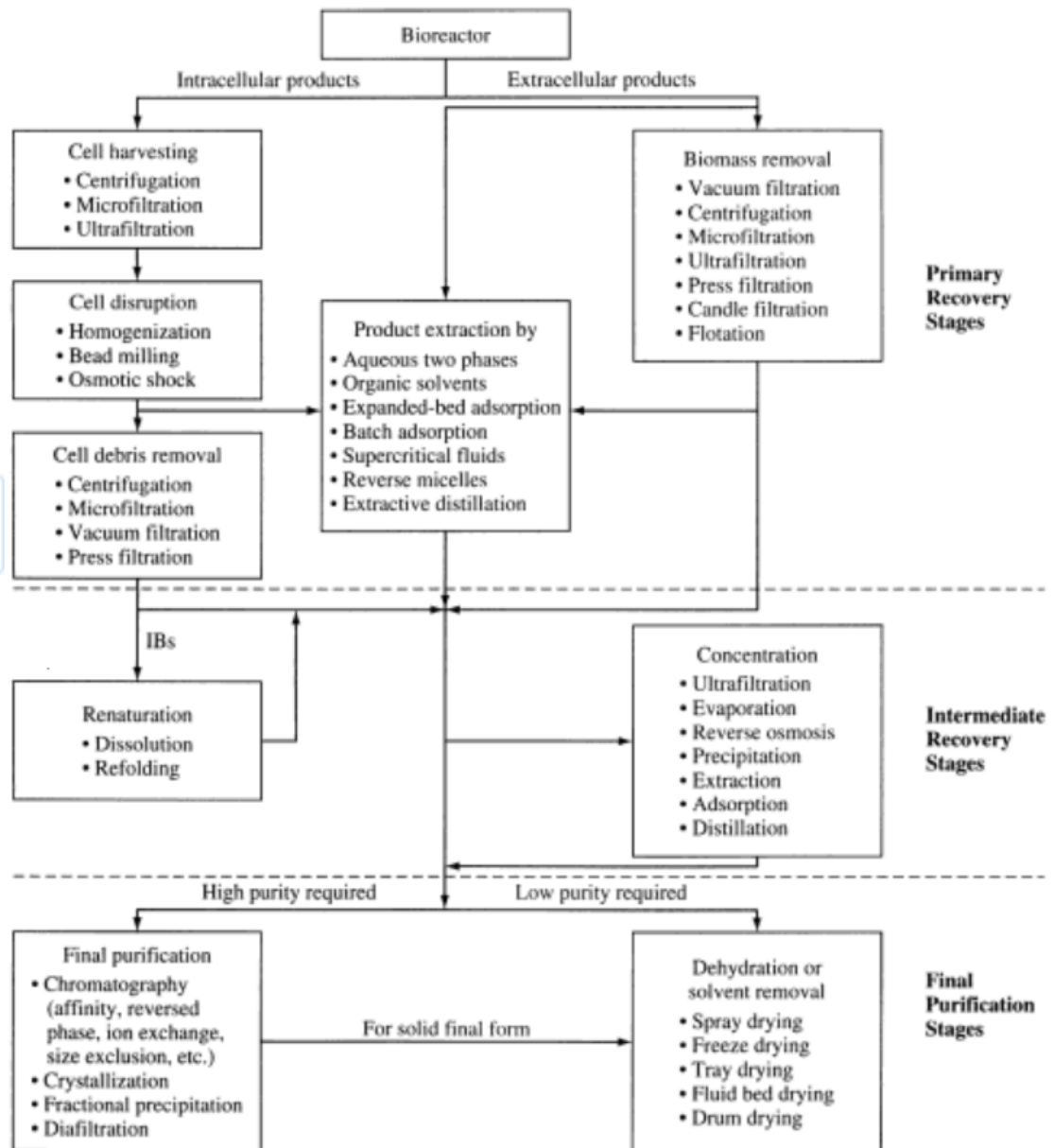
Figure 1.1 - Flow diagram of a bioprocesses taken from Harrison et al (Harrison 2003). Permission to reproduce this diagram has been granted by Oxford University Press.

Current regulatory requirements are that the process of manufacture of the biopharmaceutical is defined relatively early on in the drug discovery process i.e. before the clinical trials begin (Micheletti & Lye 2006). Consequently, there is a drive towards the use of microscale techniques to provide information to enable intelligent process design early on, without using significant quantities of expensive materials and other resources when the clinical utility of the

prospective biopharmaceutical is not clearly established. Such microscale techniques also allow parallel operations thereby enabling a number of different process conditions to be examined at the same time.

A range of microscale work on fermentation and mammalian cell culture has been undertaken primarily in miniaturised reactors (Kumar et al. 2004) and microwells (Fernandes & Cabral 2006; Micheletti et al. 2006). There has also been work on microfluidic bioreactors for fermentation (Schäpper et al. 2009) and mammalian cell culture (Hung et al. 2005; Leclerc et al. 2003). However, in order to fully realise the benefits of these microscale cell culture and microbial fermentation systems, a device capable of online sample preparation for further investigation of product quality is key. The overarching aim of this thesis is to move towards the development of a microfluidic device capable of lysing microbial cells and purifying a target protein product to a sufficient degree for further analysis. Consequently, the research will focus on the design of two compatible microfluidic devices, a lysis device and an affinity chromatography device.

1.1   Concepts of Microfluidics and its Applications

Microfluidics refers to the manipulation and analysis of fluids within micrometer-sized channels. There is a move towards the use of microfabricated devices in the biotechnology industry. This is largely due to the potential benefits that such devices may bring which include faster analysis, lower sample volumes and parallel operation of multiple analyses (Fiorini & Chiu 2005). These benefits are of direct relevance to this research which aims to move towards a microfluidic device for the preparation of pure protein from microbial cells to

enable subsequent rapid screening and monitoring of the effects of upstream and downstream processes on protein product quality.

The field of microfluidics has progressed significantly in the last 20 years since the invention of what is generally considered the first microfluidic device, in 1979, by John Terry at Stanford University. The device was fabricated using a silicon wafer to which a pyrex cover was anodically bonded and consisted of a sample injection system, 1.5m gas chromatography column, and a thermal conductivity detector (de Mello 2002).

Microfluidic devices exist either as capillaries or planar chips and can be fabricated from a range of materials such as glass, silicon, PDMS (Linder et al. 2001), and polycrystalline diamond (Björkman et al. 2001). Like John Terry's chromatography column, microfluidic devices are manufactured using methods adapted from the semiconductor and plastics industries, such as photolithography, wet-etching, micromachining, replica moulding, embossing, and injection moulding (Fiorini & Chiu 2005).

1.2   Advantages of Microfluidics

As mentioned above, microfluidic devices carry a number of advantages over larger scale processes which are mainly due to their small size (Whitesides 2006). The small size of microfluidic devices means that the distance travelled by cells, analytes or molecules of interest are generally small allowing shorter diffusion distances and hence shorter time for diffusion to occur.

A number of researchers have used the ability to reduce the diffusion distance in a microfluidic device in order to achieve faster assays. For example a

microfluidic chip to perform an Enzyme Linked Immunosorbent Assay has been developed. By virtue of reduced diffusion distances, made possible by the use of microfluidics, the incubation time needed for assay were reduced from a few hours, in microwell plates, to five minutes in the chip (Rossier & Girault 2001). Furthermore, a capillary immunoassay with electrochemical detection was developed by covalently bonding a monoclonal antibody on the internal surface of a capillary for the detection of atrazine (a pesticide) in water. The author of this work postulated that the reduced distances for diffusion would help increase the assay speed (Jiang et al. 1995)

The advantage of reduced diffusion distances is therefore a very useful property, and it is one that is of key importance to this work. This is particularly the case for the microlysis device which will work by mixing unlysed cells with a lysis reagent. Consequently the shorter the diffusion distances the quicker the lysis reagent will mix with the microbial culture and the faster lysis will occur.

The smaller dimensions of microfluidic devices also give rise to the possibility of shorter residence times in the device. The relationship between device size and residence time is intuitive. Molecules or cells travelling at a given volumetric flowrate will travel at a faster superficial velocity in a channel or capillary with a smaller diameter. This coupled with the fact that, in microfluidic devices, the length of the channel is also typically much smaller than at lab or process scale, can give rise to short residence times. In order to illustrate this principle further, Table 1.1 compares the range of superficial velocities for a capillary, of dimensions similar to those which may be found in a microfluidic device, to the superficial velocities and flowrates that might be observed in a tube at lab scale. It is of note that the range of residence times for the capillary are an order of

magnitude lower than those in the lab scale tube. However, there is significant overlap and it is of course possible to have the same residence time in a lab and microscale device. In fact this is intended to be the case for the microaffinity chromatography column, designed and characterised in this work, in order to allow comparison with lab scale column performance.

Table 1.1 - Table showing a range of superficial velocities and residence times, in tubes of typical lab and microfluidic scale dimensions, for a range of typical flowrates.

	Tube length (cm)	Flowrate	Superficial Velocity (m s^{-1})	Residence Time
100 µm	5	1- 500 µL min^{-1}	2.12 x10^{-3} – 1.06 m s^{-1}	0.0471 – 23.6s
0.5 cm	20	1 - 500 ml min^{-1}	8.49 x 10^{-4} - 0.424 m s^{-1}	0.471 - 236 s

Researchers have taken advantage of the size of microfluidics devices to increase throughput. For example a device capable of screening and sorting nematode worms (*Caenorhabditis elegans)* has been developed. The device takes advantage of the proximity of the different components to allow rapid sorting of the nematodes (Rohde et al. 2007)

Microfluidic devices also have a very small footprint and hence a number of devices can be included on one chip enabling experiments to be run in parallel. A number of researches have taken advantage of this to create high throughput devices. For a example a microfluidic device with four parallel processes, to detect insulin secretions from islets of langerhans perfused on the chip, has been developed (Dishinger & Kennedy 2006). Some work has also been done

on producing parallel ELISA assays on chip. In this work eight individual assay chambers were included on a single chip (Herrmann et al. 2006). Furthermore, researchers have created a microfluidic device containing an array of living cells to measure real time gene expression of the hepatocyte inflammatory gene. The device was able to produce a month's worth of data with a few hours preparation time. This was due to the number of investigations that could be performed at the same time on the array (King et al. 2007).

As can be seen from the examples discussed above, reduced diffusion distances, smaller device size and the ability to run microfluidic devices in parallel, together with the fact that microfluidic devices can be automated (Ichikawa et al. 2009) give microfluidic devices the potential to deliver high throughput. As mentioned previously this work aims to move towards a microfluidic device for high throughput preparation of samples, through the design of a microfluidic lysis and a microaffinity chromatography step. Since the flowrates used are likely to be somewhat limited by the optimum flowrate for the microcolumn, taking advantage of short diffusion distances, smaller device size and the ability to run devices in parallel due to the small device footprint will be critical to fulfilling the objective of achieving a high throughput device.

By virtue of the size of the of microfluidic devices, they use much smaller sample volumes and are able to reproducibly handle these small volumes of liquid. As an example of this, a microfluidic sonicator developed by researchers can be used to disrupt as little as 2.5 µL of HL-60 cells or *Bacillus subtilis* spores by virtue of the size of the sonication chamber (Marentis et al. 2005) These reduced sample volumes mean that microfluidic devices consume less reagents and they are therefore cheaper to run. It has been estimated that the

cost of a microfluidic Enzyme Linked Immunosorbent Assay, just in terms of the reagents used, is two orders of magnitude cheaper than a standard assay (Dishinger & Kennedy 2006). Therefore, because the quantities used in microfluidic devices are much less than for lab scale experiments, expensive reagents and proteins, which would not be economical at larger scales, can be used at microscale. It is worth noting as well that, even though sample and reagent volumes are small, these devices can still offer high sensitivity (Cesaro-Tadic et al. 2004; King et al. 2007)

Microfluidic devices can also consume less power than lab scale assays. As an example to illustrate this fact, a microfluidic device for carrying out polymerase chain reactions, where the temperature needs to be raised to 92°C has been developed by researchers. The device exhibits very fast thermal response times, and due to the small volumes being handled has low enough power consumption to enable it to be battery operated (Lee et al. 2004)

Microfluidic devices can be easy to manufacture (Astorga-Wells et al. 2003) and may be manufactured from cheap materials such as soda lime glass (Lee et al. 2003), PDMS and polymethylmethacrylate (F. Huang et al. 2006). They can also be bulk manufactured (Lee et al. 2004). Consequently microfluidics lends it self to the design of disposable devices and research is being done into designing such devices. For example a disposable plastic ELISA chip (Rossier & Girault 2001) and a disposable PDMS and glass immunoassay chip (Linder et al. 2001) have been developed by different research groups.

Another advantage of microfluidics is that, because of the small volumes of liquid involved, the surface chemistry of microchannel walls may be controlled

to affect separations and propel fluids without the need for pumping (Huang et al. 2006)

Flow in microfluidic devices is largely limited to the laminar regime. Whilst this can be a challenge, as discussed in the next section, it can also be advantageous. For example a microfluidic fuel cell, that utilises laminar flow to ensure that fuel and oxidant streams are kept separate but in contact, so that diffusion can occur but they are prevented them from mixing uncontrollably, has been designed by researchers (Choban et al. 2004). Researchers have also used the fact that laminar flow dominates in microfluidic devices to develop a microfluidic switch, without moving parts, that is able to alter the direction of flow as a result of actuation by applying external pressure (Ismagilov et al. 2001).

1.3 Challenges of Microfluidics

The first major challenge that microfluidics, in general, poses is the restriction of fluid flow to the laminar regime. This is due to the fact that the critical dimensions of microfluidic channels (eg the width or diameter) are of the order of a few tens to a few hundreds of micrometers which yields low Reynolds numbers. This has the effect of limiting mass transfer in microfluidic devices to diffusive transport which of course is much slower than convective mass transport (Wu et al. 2004). That said, as discussed in Section 1.2, the diffusion distances in microfluidic devices can be very small which acts to reduce diffusion time. In addition a number of technologies, such as the use of submerged liquid jets created by hydrodynamic focusing (Knight et al. 1998) and agitation by magnetic beads (Herrmann et al. 2006) have been developed to aid mixing on the microfluidic scale. It may be necessary to consider use of

some of these technologies to enhance mixing in the microlysis device if this proves to be an issue.

Another major issue in microfluidics is fouling resulting from particulates, cells, or protein molecules sticking to the walls of the device (Mukhopadhyay 2005). However there are ways in which this can be overcome. For example one group of researchers have developed a method of coating the walls of microfluidic channels with plasma polymerised tetraglyme (tetraethylene glycol dimethyl ether). The coating was stable during operation, had a shelf life over 3 months, and was able to prevent non-specific adsorption of fibrinogen which is a "sticky" protein (Salim et al. 2007).

Viscosity is another major challenge in microfluidics because of the size of the channels, and the pressures required to force more viscous substances through them. This is particularly the case with DNA which is very viscous. However, there are ways to overcome viscosity issues. For example one research group used a copolymer, which changes viscosity with temperature, to create a sieving matrix for a DNA sequencing microfluidic device. This meant that the sieve could be activated when needed, i.e. after injection of the DNA, making the injection easier (Wan et al. 2009)

Finally, because of the minute volumes involved, evaporation is a key issue in microfluidic devices. This is because it can introduce big errors by changing volumes and altering concentrations (Heo et al. 2006). However researchers have found ways to overcome the issue of evaporation for example Cesaro-Tadic *et al* used miniaturised heating and cooling elements in their microfluidic device to precisely control the rate of evaporation thus allowing long incubation

times for their miniaturised immunoassays (Cesaro-Tadic et al. 2004). Evaporation can also be a useful tool in microfluidics, for example a group of researchers has used evaporation and capillary forces to pump liquid through their microfluidic device at a flowrate of 3.02µL min^{-1} (Guan et al. 2006).

Additionally, although not of direct relevance to this work, it has been shown that flow in microfluidic devices can elongate, and potentially degrade DNA molecules by scission (Shrewsbury et al. 2001).

1.4 Fluid Dynamics and Mass Transport in Microfluidic Systems

A key consideration in microfluidics is fluid dynamics because it is critical to mass transfer. In microfluidic devices, the characteristic dimensions are typically of the order of between tens to a few hundred microns. Consequently, as described in the previous section, the associated Reynolds numbers are small and hence the flow regime is typically laminar

In this work the microfluidic geometries considered consist of circular tubes i.e. capillaries and connections, or packed capillaries. The interstitial Reynolds number for a packed bed is given by Equation 1.1 (Seguin et al. 1998a) and the Reynolds number for flow in a tube is given by Equation 1.2.

$$\mathrm{Re} = \frac{\rho U_0 d_p}{\varepsilon \mu}$$ **Equation 1.1**

$$\mathrm{Re} = \frac{\rho U_0 d}{\mu}$$ **Equation 1.2**

Where ρ is the density of the fluid, U_0 is the superficial velocity, d is the diameter of the tube, d_p is the diameter of the packing particles, ε is the bed voidage and μ is the viscosity of the fluid.

Table 1.2 below shows the calculated Reynolds number for different size capillaries in the range considered in this thesis. The fluid properties of water were used for these calculations (density 1000 kg m^{-3} and viscosity of 0.89 mPas at 25ºC) as water was lowest viscosity fluid used in this work. These Reynolds numbers presented would therefore give an idea of the highest Reynolds numbers likely to be encountered. As can be seen from the table, these calculations indicate laminar flow at flowrates of between 1 µL min^{-1} and 1 mL min^{-1} in capillaries of between 100 µm and 1000 µm diameter. At flowrates of 1mL min^{-1} in capillaries with a diameter larger than 10 µm flow remains laminar. However, when the diameter of the tube is 10µm, and the flowrate is 1 mL min^{-1}, giving rise to a superficial velocity of 175 m s^{-1} the resulting Reynolds number indicates that the flow regime is just entering into the transitional regime.

Table 1.2 - Table showing the calculated Reynolds number for a capillary of between 10 m and 1000 m in diameter. The Reynolds number ranges reflect this. The lower Reynolds numbers correspond to the 1000 m capillary and the larger Reynolds numbers correspond to the 10 m capillary.

Flowrate (µL min^{-1})	Reynolds Number	Regime
1	0.024-2.4	Laminar
10	0.24-24	Laminar
100	24 -240	Laminar
1000	240-2400	Laminar – transitional flow

The corresponding pressure drop, calculated using the Hagen Poiseuille flow equations, for a 1 cm long capillary with: a circular cross section; 10 μm internal diameter; and at a flowrate of 1 mL min^{-1} is approximately 105bar. Consequently, flow in the devices designed in this work will be laminar. The Hagen Poiseuille equations, Equation 1.3 and Equation 1.4, are set out below (Mortensen & Bruus 2006).

$$\Delta P = QR_{Hyd}$$

Equation 1.3

Where $\triangle P$ is the pressure drop across the capillary, Q is the steady state flowrate and R_{hyd} is the hydraulic resistance. The hydraulic resistance can be described by the following equation.

$$R_{hyd} = \frac{\alpha \mu L}{A_r{}^2}$$

Equation 1.4

Where A_r is the cross sectional area of the tube, L is the length of the tube, μ is the viscosity of the fluid, and α is a dimensionless geometric correction factor.

Table 1.3 shows the calculated interstitial Reynolds numbers for a column packed with spherical matrix beads between 10 μm and 640 μm in diameter over a range of typical chromatography flowrates. The fluid properties of water were used for these calculations (density 1000 kg m^{-3} and viscosity of 0.89 mPas at 25ºC) as the buffers used in the chromatography work were assumed to have properties very similar to water.

At flowrates of up to 100 cm hr^{-1} the Reynolds number is below 1 indicating Stokes flow. At 200 cm hr^{-1} to 400 cm hr^{-1} Stokes flow is maintained for matrix

beads of less than 240 µm diameter. For larger matrix beads the flow enters

the inertial regime (Gunjal et al. 2005). The mean diameter of the standard

Glutathione affinity matrix which will be used in this work is 90 µm, suggesting

that Stokes flow will be maintained in the microcolumn.

Table 1.3 Table showing the calculated interstitial Reynolds number for a column packed with beads of between 10 m and 640 m in diameter. The Reynolds number ranges reflect this. The lower Reynolds numbers correspond to the 10 m matrix beads and the larger Reynolds numbers correspond to the 640 m matrix beads.

Flowrate (cm hr^{-1})	Interstitial Reynolds Number	Flow Regime
25	0.002-0.17	Laminar Stokes flow
50	0.005-0.33	Laminar Stokes flow
100	0.010-0.66	Laminar Stokes flow
200	0.021-1.33	Laminar Stokes flow - Inertial Flow
400	0.01-2.66	Laminar Stokes flow - Inertial Flow

As discussed, flow in both unpacked capillaries and capillaries packed with

matrix beads, at the range of flowrates, dimensions and geometries that will be

investigates in this thesis will be laminar, as is the case in microfluidic devices

more generally. This has the effect of limiting mass transfer to diffusion, which

is much slower than convective mass transfer as it relies on the movement of

molecules rather than the movement of the bulk liquid. Consequently, any

mixing operations in other parts of the microfluidic system, e.g. the microlysis

device, will be limited by the rate of diffusion.

1.5   Cell Disruption Theory

Recombinant proteins can be expressed in prokaryotes, or eukaryotic hosts such as mammalian cells, plant cells or yeasts.   This section of the thesis will focus on microbial cells as this is most pertinent to the studies undertaken.

In microbial host cells, expressed recombinant proteins may either excreted, or intracellular.   However, the majority of recombinant proteins produced at present are intracellular and hence cell disruption is a key unit operation in most bioprocesses (Tkac et al. 2004).

In order to understand the different methods available for disruption of microbial cells, it is essential to have an understanding of the bacterial cell envelope. The bacterial cell envelope consists of two (gram positive bacteria) or three (gram negative bacteria) layers: the cytoplasmic membrane, the peptoglycan layer; and in gram negative bacteria the outer membrane. A schematic of these layers is shown in Figure 1.2. It is the peptoglycan layer which gives the cell wall most of it's mechanical strength and hence is a key consideration particularly in the mechanical or physical cell disruption which rely on shear to rupture the cell. In gram negative bacteria the cell membrane gives rise to chemical resistance of the cell and hence this is a key consideration for chemical lysis (Harrison 1991).

Gram negative bacteria   Gram positive bacteria

Outer membrane

Peptoglycan

Periplasm

Cytoplasmic
Membrane
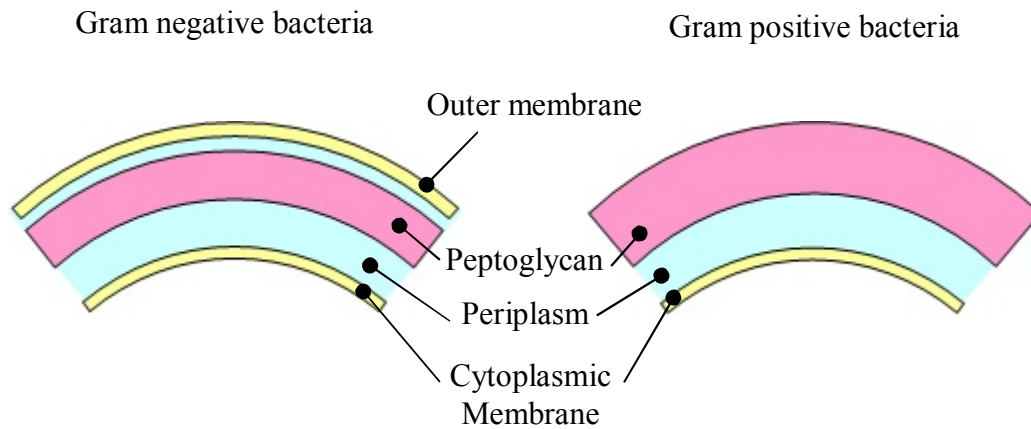
Figure 1.2 – Diagram of the bacterial cell envelope for gram negative and gram positive bacteria

The strength of the cell depends on the type of cell (e.g. bacteria or yeast), the species, the process conditions in which the cells are grown and the growth phase (Hopkins 1991). As well as the strength of the cell, the disruption method chosen will depend on a number of factors including the volume of sample to be disrupted, and the location of product within in the cell. The process of cell disruption can denature proteins leading to the loss of product. Consequently, the method and degree of lysis must be chosen carefully to optimise the amount of product.

Cell disruption can be separated broadly into two main types: mechanical cell disruption; and non-mechanical disruption (Harrison, 1991). Mechanical disruption involves the generation of shear forces. This can be achieved in a number of ways for example homogenisation creates these shear forces by causing the cell suspension to impact, under high pressure, on a surface, typically a metal impact ring. Mechanical methods can also be performed on frozen cell pastes. The main methods of mechanical disruption are:

- The colloid mill which works by producing hydrodynamic shear forces which disrupt the cells. A basic colloid mill consists of two disks separated by a small gap. One of the disks is rotated at high speed while the other is ether kept stationary or rotated at high speed in the opposite direction. In some collide mills cones are used instead of disks (Harrison, 1991);

- The high pressure homogeniser which works by forcing the cell suspension, under high pressure through a valve onto an impact ring (Harrison, 1991). It is thought that impingement on the ring causes most of the lysis (Moore et al. 1990);

- The jet mill which uses impingement of cells fired in jets against a wall or grinding of cells, fired in jets against each other, to cause disruption (Harrison, 1991);

- The bead mill, in which glass, plastic or stainless steel beads, usually between 0.2mm - 2.8mm are added to a cell suspension in a cylinder which is agitated by impellers. Impact between the cells and the beads causes the disruption of the cells (Harrison, 1991);

- The French Press which works by using a large piston, to force cells through small valve under high pressure. The hydrodynamic shear and sudden change in pressure cause the disruption of the cells and the evidence suggests that it is the rate and degree of the pressure drop which causes the disruption of cells (Brookman & Brookman 1975);

- Solid shear in which a frozen cell paste at -27ºC to -25ºC is passed through a small orifice. The shear and grinding action of the ice crystals are thought to cause the lysis of the cells (Harrison, 1991);

Mechanical methods of cell disruption are mainly used at lab and process scale. The main disadvantages of mechanical methods of cell disruption are the high capital cost of the equipment required, and the high energy costs. However, they do not generally involve adding other substances that may need to be removed by downstream purification.

Non-mechanical methods of cell disruption can be subdivided into physical, chemical and biological disruption methods. Some physical methods, like mechanical methods also rely on shear forces to rupture the cells.

Sonication of a sample causes cavitation as a result of the acoustic vibrations, while hydrodynamic cavitation occurs when cells are pumped through a constriction resulting in a local increase in velocity which causes cavitation to occur. In both cases collapse of these cavities releases mechanical energy which causes the disruption of the cells.

Osmotic shock and freeze thaw work by causing the contents of the cell to expand and hence shear open the cell. By contrast desiccation disrupts cells by permeabilisation of the membrane (Harrison, 1991).

Physical methods of cell disruption tend to require significant energy. The exception to this is disruption by osmotic shock which requires the addition of salts which usually need to be removed from the final product. That said

physical methods of cell disruption can generally be used at relatively small scales. For example, freeze thaw can be used in microwell plates.

Disruption of cells can also be achieved by chemical means. By far the most common method of lysing cells chemically is with the use of detergents such as Triton X100 and SDS to solubilise the cell membrane. Other methods of chemical lysis include the use of organic solvents such as toluene, chaotropic agents such as Guanidine Hydrochloride, and acids and bases to disrupt cells (Harrison, 1991). The main disadvantage of chemical lysis is the addition of the chemicals which must then be removed from the product. However, they do not require expensive equipment as in essence all that is needed is to mix the cells with the lysis agent. This is very attractive when it comes to microfludic cell lysis as it means that the device can be very simple.

Disruption of cells by biological means can be done by the addition of enzymes such as lysozyme to break down the peptoglycan structure in the cell wall. In gram negative bacteria, prior treatment with a non ionic detergent or chelating agent is necessary to disrupt the outer membrane. Other methods of disruption by biological means include inhibition of cell wall synthesis or addition of antibiotics to cause permeabilisation of cell (Harrison, 1991) The main advantages and disadvantages of biological lysis are similar to those of chemical lysis.

Table 1.4 summarises some of the main advantages and disadvantages for the individual methods of cell disruption outlined above. It is of note that most of the methods of mechanical disruption have high capital costs and energy requirements, and involve the use of moving parts with makes them more

complicate to miniaturise for use in a microfluidic platform. The most promising

alternatives for miniaturisation are chemical and biological lysis methods. The

next section will look at the work that has been done on microfluidic lysis to

date.

Table 1.4 -The main advantages and disadvantages of the different types of methods of cell disruption. The majority of the information in this table is taken from a review paper by Harrison in 1991 (Harrison 1991)

Category	Method	Disadvantages	Advantages
Mechanical	Colloid Mill	High Capital Cost; High Energy Cost; Excessive Heating; Denaturation at air liquid interfaces; Wear of moving parts due to high speeds.	High throughput; Continuous operation
	Homogeniser	High Capital Cost; High Energy Cost; Excessive Heating; Denaturation at air liquid interfaces	High throughput; Continuous operation
	Jet mill	High Capital Cost; High Energy Cost; Excessive Heating; Denaturation at air liquid interfaces	Continuous operation possible Good disruption of recombinant *E.coli* reported in a single pass
	Bead mill	High Capital Cost; High Energy Cost; Excessive Heating; Denaturation at air liquid interfaces; Smaller beads/multiple passes needed for microbes	Continuous operation possible; Good at releasing granular produces from the cell wall; Choice of bead size can be used to control the cell disruption i.e. larger beads can be used to release periplasmic proteins and smaller ones can be used to grind the cell wall
	French press	High Capital Cost; High Energy Cost; Excessive Heating; Not suitable for large volumes; valve prone to clogging	The Press provides a single pass through the point of maximum shear force limiting damage to delicate biological structures due to repeated shear, as occurs in other disruption methods.
	Solid Shear Devices	High Capital Cost; High Energy Cost; Low throughput	Good product preservation
Physical	Sonication	Fine cell Debris; Excessive heating can result so good cooling is required; Ionisation can cause damage to the product	Can disrupt very small quantities of cells; Can be scaled up and run continuously
	Hydrodynamic Cavitation	More suited to large scale	Less heating than sonication; Lower energy requirements than sonication ; more suited to continuous operation than sonication
	Desiccation	Low yields	Cells remain largely intact
	Osmotic shock	Not efficient in cells with a cell wall e.g. microbes and plant cells; High quantities of salt in the product stream	Relatively inexpensive
	Freeze Thaw	Slow; Low yield; High energy requirements; Detrimental effect on protein product activity.	Does not require addition of any chemical and biological agents
	Heat lysis.	Requires significant energy; Heat labile products may be damaged	Can be operated continuously
Chemical	Acid Lysis	Slow; results in precipitation of proteins; hydrolysis of proteins	Relatively inexpensive
	Alkaline lysis	Harsh conditions which would denature most proteins	Relatively inexpensive
	Chaotropic Agents	Harsh conditions which would denature most proteins	Relatively inexpensive
	Detergents	Can denature proteins	Relatively inexpensive
Biological	Enzymatic lysis	Expensive due to the cost of the enzyme; Enzyme will need to be removed from the final product.	Mild process conditions; Low energy consumption; Low capital costs

1.6 Cell Disruption on the Microfluidic Scale

A number of methods have been employed by researchers for the microscale lysis of microbial and eukaryotic cells (both mammalian and yeast cells). The lysis methods employed so far include mechanical lysis, physical and chemical methods.

Mechanical methods of cell lysis have been used on mammalian, microbial and yeast cells, Di Carlo *et al* used a microfluidic device containing a filter region with nanostructure barbs, created using modified deep reactive ion etching, to lyse mammalian cells. The device was used to lyse human leukaemia cells (HL-60) and defibrinated sheep's blood. The device required quite high flowrates up to 300 μL min^{-1} and the amount of protein released, as compared to chemical lysis was low (a maximum of 7.5%) (Di Carlo et al. 2003). Such a device would probably require significantly higher flowrates and a finer filter region to achieve lysis of *Escherichia coli* cells. These flowrates are not in a suitable range for coupling with the planned microaffinity chromatography column and the protein release is poor and so this technology is probably not suitable for the planned microlysis device.

Researchers have also used spherical particles inside a microfluidic compact disk, similar to the bead mill described earlier in Section 1.5. Whilst this device was able to achieve a reasonably good lysis of yeast cells (65% compared to a standard bead lysis protocol) no comparison to a standard protocol was presented for *Escherichia coli* lysis, The device also had a fairly large total volume (1mL) and required external equipment to rotate the device and achieve the lysis. It was also a batch process, which makes it unsuitable for further

investigation with a view to using it in the microfluidic lysis work presented in this thesis. This is because the device this work aims to move towards is a continuous device.

With regard to work on lysis by physical means, on the microfluidic scale, researchers have used a microsconicator, fabricated in a chip format using quartz and glass, to lyse mammalian cells and bacterial spores. The device was able to produce in the region of 80% lysis of HL-60 eukaryotic cells and in the region of 50% lysis of *Bacillus subtilis* spores in 3 and 30s respectively. Flowrates in the range of 5µL min^{-1} to 50µL min^{-1} were used (Marentis et al. 2005). Whilst the flowrates are of the correct order planned for this work, and the lysis of *Bacillus subtilis,* which is difficult to lyse, is good. The materials of fabrication are relatively expensive and the fabrication methods complicated.

Electric fields have also been used to lyse cells on the microfluidic scale. One example of this is a PDMS device to continuously lyse *Escherichia coli* cells in a DC field. The research group who developed this were able to achieve close to 100% lysis in a field strength of 1000-1500 V/cm (Wang et al. 2006). However, the device seems to sit somewhere between single cell lysis methods and higher throughput microfluidic lysis methods and, as such, throughput is unlikely to be sufficient for this work. Another example is the use of a microfluidic chip, fabricated from Pyrex and containing gold electrodes, to lyse human colon carcinoma HT-29 mammalian cells. The cells were lysed, and 74% lysis was achieved, using an AC field, of 8.5V at 10kHz, at a flowrate of 0.25–1 µL min^{-1} (Lu et al. 2005). Whilst the throughput of this device and flowrate would be suitable for this project, it is unclear whether this method would work for microbial cells which are more difficult to lyse than mammalian cells

A number of different methods of single cell lysis have been investigated by researchers. One group used a square wave electrical field to lyse single nonadherent human leukaemia cells in 33 ms. This was followed by on chip electrophoresis to separate cytosolic dyes. The devices was able to process 7-12 cells per minute (McClain et al. 2012).

Researches have also been able to lyse single plant cells, and have shown that lysis can be achieved by both mechanical and electrical means in the same device. A pinched-channel structure fabricated on a Pyrex substrate was able to lyse single zucchini protoplast cells larger that 45µm. Smaller cells were lysed by applying a voltage across the cell until it lysed (Ikeda et al. 2007).

Other work in the area of single cell lysis has been done. Irmia *et al* used a microfluidic device to lyse single human lymphoblast cells in a 25pL microfluidic chamber using 0.1% (w/v) and 0.2% (w/v) SDS and 3M GTC. Lysis was achieved in 0.5-1s with the GTC (Irimia et al. 2004).

Single cell lysis methods obviously have too low a throughput for exploitation in this work which aims to create relatively high quantities of purified protein. They are more suited to the cellular level physiological and pathological studies.

Chemical lysis in microfluidic devices has also been achieved. For example, a microfluidic device, fabricated from PDMS, that is capable of lysing red blood cells, HeLa (human tumor line) and Chinese Hamster Ovary (CHO) cells by local Hydroxide Generation at a cathode, has been designed by researchers. The device operated in the flowrate range of 15 µL min^{-1} to 50 µL min^{-1} and was able to lyse CHO cells in approximately 2s. However the device demonstrated

relatively low throughput and was not investigated with respect to microbial cells which are more difficult to lyse (Di Carlo et al. 2005).

Researchers have used other chemical reagents to lyse cells in microfluidic devices. One such example is the use organic solvents to lyse *Escherichia coli.* The solvents, 20% (v/v) xylene, 79% (v/v) acetone, and 1% (v/v) toluene were used lyse recombinant *Escherichia coli* expressing enhanced green fluorescent protein (EGFP) and lipase. The cells and lysis reagent were mixed in a micromixer by means of a magnetically actuated diaphragm. This lysis method is reported to have released up to 94% of the EGFP (Huh et al. 2007). However, the disadvantage of this system is the need for an external magnetic stirrer plate and the addition of organic solvents which may affect subsequent purification steps. Since the aim of this work is to develop online lysis and chromatography it is considered best to avoid the addition of organic solvents which may affect the chromatography step.

Apart from the work reviewed in this section, there does not appear to have been much other work on microfluidic chemical lysis. However, taking into account the complexity of some of the microfluidic lysis devices, using chemical lysis for the microlysis device is an attractive proposition because the device can be simpler, and unless mixing is particularly problematic, would not need external power over and above the pumping. Consequently this is the mode of lysis that will be explored in this work.

1.7   Chromatography Applications

Since its discovery, at the beginning of the 20th century, by Michael Tswett (Sakodynskii 1972) chromatography has been developed into an incredibly powerful tool for analysis, and large and small scale separation.

Most chromatography techniques are based on the fact that a molecule (or analyte) will distribute itself between two phases - this is called partitioning. The partition coefficient is the ratio of the concentration in the stationary phase to that in the mobile phase, and this is dependent on the analyte, the phases used, and the conditions such as pH and temperature (Jönsson 1987). Consequently, different analytes will distribute themselves in different proportions based on these conditions and this gives chromatography the ability to separate analytes.

The two phases described above are a mobile phase and a stationary phase. The mobile phase can either be a gas, liquid, or supercritical fluid and the stationary phase can either be a solid or a liquid. Different combinations of mobile and stationary phase give rise to the different forms of chromatography set out in Table 1.5.

As can be seen from this table there are seven different forms of chromatography. One of the most commonly used forms of chromatography, particularly in biotechnology, is liquid-solid chromatography. This is the type that will be used in this work and so this will be the focus for the rest of the introduction.

Table 1.5 – Table showing the different forms of chromatography adapted from Jönsson *et al* (Jönsson 1987)

Type	Mobile Phase	Stationary Phase
Gas Chromatography (GC)	Gas	-
Gas-Liquid Chromatography (GLC)	Gas	Liquid
Gas-Solid Chromatography (GSC)	Gas	Solid
Liquid Chromatography (LC)	Liquid	-
Liquid-Liquid Chromatography (LLC)	Liquid	Liquid
Liquid-Solid Chromatography (LSC)	Liquid	Solid
Supercritical Fluid Chromatography (SFC)	Supercritical fluid	-

1.8   Types Chromatography

Liquid-solid chromatography can be performed in a planar system, in a tube with ligands chemically bonded to its surface, or as a column packed with irregular or spherical particles.   Purification of proteins is usually performed by liquid chromatography in a packed column. Liquid chromatography can itself be divided into two main types according to the method by which the analyte is retained in the column namely: size exclusion; and adsorption chromatography

Size Exclusion chromatography, first developed by Lathe *et al* in 1956 (Lathe & Ruthven 1956) uses the protein molecules size and shape to separate them. A column packed with matrix beads, which have pores of a given diameter, is used to separate different proteins. Proteins which are larger than the pore diameter pass straight through the column, while smaller proteins are retained

as they move through the matrix pores and hence take longer to pass through the column.

Adsorption chromatography uses interactions between proteins and species immobilised on the matrix to separate proteins. These interactions cause the proteins to be adsorbed onto the column. One such example is Hydrophobic Interaction Chromatography. Hydrophobic regions on the surface of proteins are attracted to hydrophobic groups immobilised on the surface of the matrix. These interactions are enhanced by loading in a buffer with a high ionic strength. Elution is achieved by using a low ionic strength buffer which reduces the strength of the interaction between the hydrophobic regions on the protein and the immobilised groups on the matrix. Gradient or stepwise elution is usually used..

Another example of adsorption chromatography, Ion-Exchange chromatography, was developed in its modern form in 1971 (Small 2004). It uses the charged nature of proteins to separate them. A resin with immobilised ions on its surface, either positively or negatively charged, is packed into a column. Those proteins with a higher charge density (of the opposite charge to the resin) are the most strongly attracted. Proteins can then be eluted by changing the ionic strength or pH. Increasing the ionic strength of the elution buffer over a period of time (gradient elution) will result in analytes being separated based on their charge density. Alternatively, changing the pH can be used to elute specific proteins by taking advantage of the unique relationship between net surface charge and pH that proteins have.

Affinity chromatography is another type of adsorption chromatography. It is used for the separation of mixtures of biological molecules based on highly specific interactions such those between antibody and antigen e.g. Fab' and Protein A, or enzyme and substrate e.g. Glutathione and Glutathione S Transferase (GST).

Affinity chromatography was first presented by Cuatrecasas *et al*, in 1968 who used affinity chromatography to purify staphylococcal nuclease form α-chymotrypsin and carboxypeptidase A. Sepharose beads where activated by treatment with cyanogen bromide and coupled to 3'-(4-Amino-pheny1-phosphoryl)-deoxythymidine-5'-phosphate, a synthetic compound, which has a strong affinity for staphylococcal nuclease due to its inhibitory properties (Cuatrecasas et al. 1968).

Since its introduction, affinity chromatography has become so widely used that 60% of all purification protocols involve it's use (Lowe 1996). It is so widely used because of its ability to selectively capture just the protein of interest and hence yield a higher degree of purity than any other single purification step. It is this property that makes it extremely useful in microfluidic systems, which due to fouling and pressure issues, seek to use as few steps as possible. Affinity capture is able to take a particulate free crude sample and purify it sufficiently to enable further analysis. Consequently the microfluidic chromatography column presented in this work will be an affinity column.

1.9 Chromatography Theory

There are two theories commonly used to describe the process inside the chromatography column. The first, the plate theory of chromatography,

considers the chromatography column to be analogous to a fractional distillation column, and hence uses theoretical plates to describe the separation process and the concentration profile of the solute within the column. This theory assumes that equilibrium exists between the two phases in each theoretical plate, that little diffusion occurs between the plates so that motion of the mobile phase carries the solute along the column, and that the height of the theoretical plates is constant throughout the column. The faster equilibrium is reached between the mobile and the stationary phase the shorter the plate height and hence the more efficient the column Equation 1.5 (International Union of Pure and Applied Chemistry 2012) shows the relation between the column efficiency (plate number) and the variance of the peak.

$$N = \left(\frac{t_R}{\sigma}\right)^2 = \left(\frac{V_R}{\sigma}\right)^2$$

Equation 1.5

Where N is the number of theoretical plates, t_R is the retention time, σ is the standard deviation of the peak and V_R is the retention volume. Assuming that the peak is Gaussian, Equation 1.6 (Nagashima 2010) relates the width at half the peak height W_h to the standard deviation

$$W_h = 2\sigma\sqrt{2\ln 2}$$

Equation 1.6

Rearranging Equation 1.6 for σ and substituting into Equation 1.5 gives

$$N = 8\ln 2\left(\frac{t_R}{W_h}\right)^2 = 8\ln 2\left(\frac{V_R}{W_h}\right)^2$$

Equation 1.7

The height equivalent to one theoretical plate can therefore be described as shown in Equation 1.8

     Hani El-Sabbahy

$$HETP = \frac{L}{N} = \frac{L}{5.55\left(\dfrac{V_R}{W_h}\right)^2}$$

Equation 1.8

Where HETP is the height equivalent to one theoretical plate, and L is the length of the column.

The equations for calculating the HETP, which are ultimately derived from rate theory are still widely used today and will be used in this work to gain an understanding of the packing quality in the micro column. As Martin and Synge acknowledge in their work, HETP depends also on the diffusivity of the solute in the solvent, larger molecules having lower diffusivity will tend to increase HETP (Martin & Synge 1941). Consequently, a small molecule, usually acetone as this can be detected by it's absorption of UV at 280nm, is used to determine the influence of the packing quality inside the column on the HETP. Because acetone does not bind to the matrix, the HETP obtained determines the quality of the packing and its influence on HETP.

Martin and Synge suggested that the HETP depends upon the factors controlling diffusion and the flowrate of the liquid (i.e. it increases with flowrate) and postulated the existence of an optimum flowrate as diffusion between the theoretical plates becomes more important at lower flowrates increasing HETP (Martin & Synge 1941) essentially this predicts the HETP flowrate relationship presented by the rate theory of chromatography.

The rate theory of chromatography considers the processes inside the column that contribute to dispersion and hence band broadening. The van Deemter equation is the best known derived equation based on the rate theory and describes how eddy diffusion, longitudinal diffusion and mass transfer effect the dispersion in the column and hence the HETP.

$$HETP = A + \frac{B}{u} + Cu$$ **Equation 1.9**

Where u is the linear velocity of the mobile phase, A is the contribution of eddy diffusion to the plate height, B is the contribution of longitudinal diffusion and C is the contribution of the resistance to mass transfer,

Eddy diffusion, in the context of the van Deemter equation, occurs as a result of the different flow paths taken by analyte molecules as they travel through the column. Consequently, the larger the matrix particles and the more irregular they are in terms of size, the greater the difference in the length of the flow paths. Equally the quality and regularity of the packing will have an effect on eddy diffusion. For example, a poorly packed column would again increase the number of different length flow paths and hence decrease the performance of the column. Similarly less dense packing near the wall, resulting from wall effects, will provide a shorter flow path near the wall as compared to the rest of the column and hence decrease the columns efficiency.

Longitudinal diffusion occurs because of the differences that occur in the mobile phase concentration, for example at the interface between the equilibration buffer and the eluate. Because of the concentration difference, analyte molecules tend to diffuse towards the region containing a lower concentration.

This tends to dilute the sample over a larger volume and hence results in band broadening and an increase in HETP. Since diffusion is a slow process, the contribution of longitudinal diffusion to band broadening is at it highest at lower flowrates because diffusion has more time over which to occur. Molecular diffusion obeys Fick's law (Equation 1.10)

$$J^*_{Ay} = -cD_{AB}\frac{\partial x_A}{\partial y}$$

Equation 1.10

Where J^*_{Ay} is the molar flux of the analyte relative to the molar average velocity of the mobile phase, c is the total molar concentration in the solution, D_{AB} is the binary diffusivity for system A-B, and x_A is the molar fraction of species A (Bird et al. 2002). From Fick's law we can see that longitudinal diffusion is dependent on the concentration gradient and diffusivity. Diffusivity is dependent on the viscosity of the mobile phase, the mass of the analyte, and temperature. Consequently, all of these parameters will affect longitudinal diffusion.

The final term in the van Deemter equation accounts for the contribution of resistance to mass transfer. There are a number of mass transfer processes that take place inside the chromatography column between the mobile and stationary phase. These include: diffusion, adsorption, and possibly convection in the bulk (depending on flowrate). Resistance to mass transfer, in either the mobile or stationary phase, increases the amount of time it takes to reach equilibrium between the two phases and increases the difference in retention of different molecules of the same species. It is this which results in band broadening and hence increases the HETP.
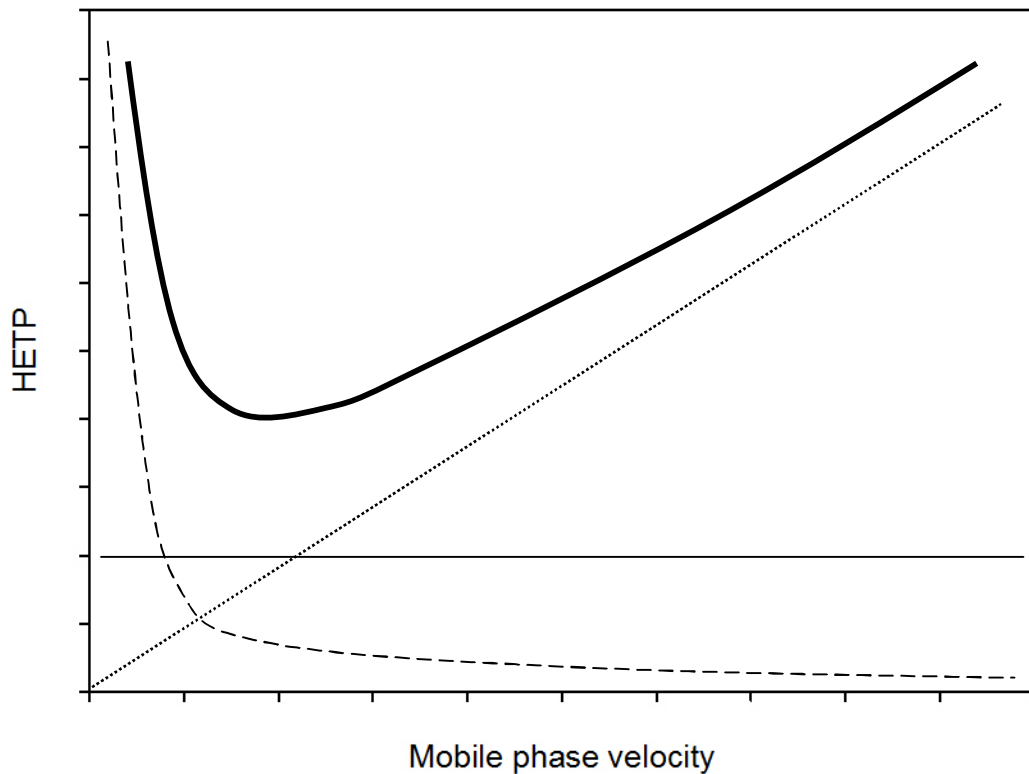
Figure 1.3 - Sketch of a typical van Deemter curve (thick solid line) showing the contribution of eddy diffusion (thin solid line) longitudinal diffusion (dashed line) and resistance to mass transfer (dotted line) to HETP.

Figure 1.3 shows a typical sketch of a van Deemter curve showing the contribution of eddy diffusion, longitudinal diffusion and resistance to mass transfer to the HETP. From the graph it can be seen that there is an optimum linear velocity at which the HETP is at a minimum. This optimum velocity may not be the best velocity to operate the column at as there is a trade off between band broadening and throughput.

In practical terms, band broadening tends to increase the width of the elute peak, which results in a poorer separation in chromatography where multiple analytes are eluted from the column (e.g. size exclusion, ion exchange, and hydrophobic interaction chromatography). This is because it can cause peaks to overlap resulting in the mixing of analytes and poorer purities. In affinity chromatography this is generally not the case due to its specificity. The ligand on the affinity matrix is designed to attract only one type of Protein e.g. Glutathione Sepharose is designed to bind to Glutathione S Transferase and Protein A is designed to bind IgG. In affinity chromatography band broadening results in two major issues. Firstly it acts to increase the time over which breakthrough occurs. This increases the quantity of feed needed to load the column. Secondly it increases the width of the elution peak meaning that the eluted product is spread over a larger volume hence reducing the concentration. Consequently, it is important to minimise band broadening through dispersion.
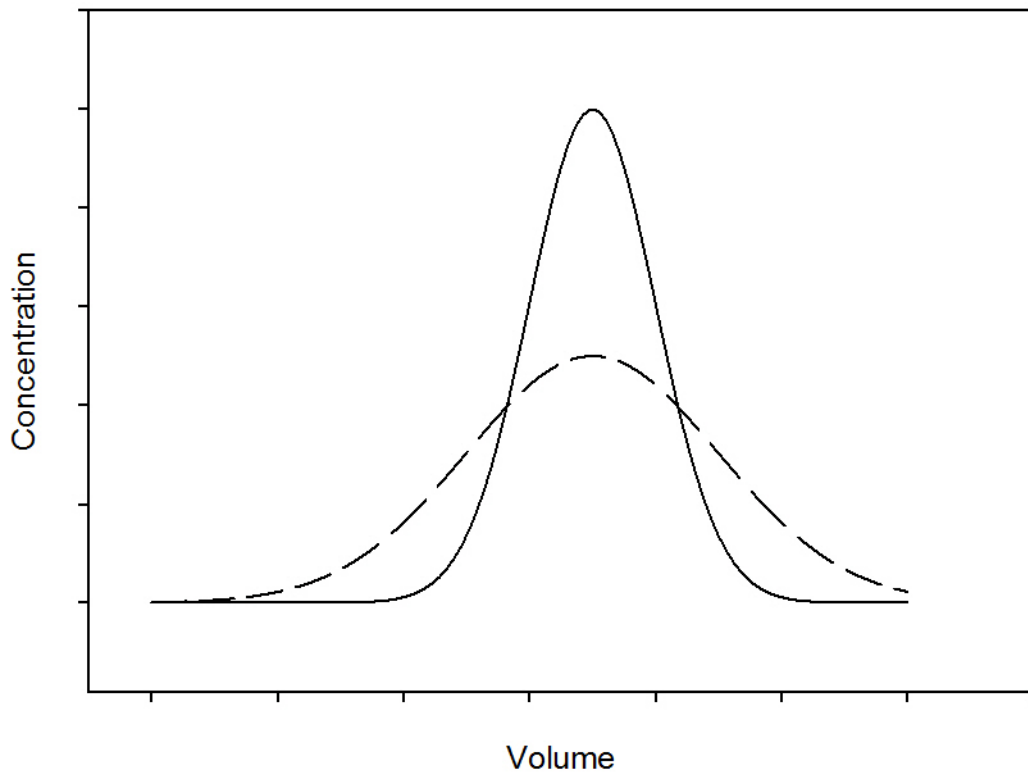
Figure 1.4 - Sketch illustrating the effect of band broadening on elution curves. The solid line curve is an elution with less dispersion resulting in a more concentrated eluate. The dashed curve is a sketch of an elution curve with greater band broadening. While the total quantity of protein eluted is approximately the same it is eluted over a larger volume and hence the concentration of the eluate is lower.

Figure 1.4 shows a sketch of two Gaussian peaks, of the ideal form that would be seen during elution from a column. Whilst both peaks are of similar area, meaning that the total quantity of protein eluted is the same, the broader peak is eluted over a larger volume resulting in a lower concentration of eluate.

HETP analysis, as described above, assumes that the peaks are Gaussian in shape. However, this is almost never the case. Consequently, a way of measuring how far the peak deviates from this is useful. Peak asymmetry is often used to assess by how much the column performance deviates from the ideal. The peak asymmetry is calculated as shown in Equation 1.11 (Dong 2006).

$$A_S = \frac{a}{b}$$

Equation 1.11

Where A_S is the asymmetry factor, b is the distance along the x axis between the maximum and the curve to the right of the maximum at 10% of the peak height, and a is the distance along the x axis between the maximum and the curve to the left of the maximum at 10% peak height. An acceptable peak asymmetry is between 0.8 and 2. An alternative way of measuring the asymmetry of the peak is by using the tailing factor which is defined at 5% of the peak height (Dong 2006).

The performance of columns which are used for capture are typically measured by dynamic binding capacity (DBC) and typically at 10% breakthrough (Carta & Jungbauer 2010). The dynamic binding capacity is the quantity of protein that binds to the column under process conditions per unit bed volume and it is equal to the area above the breakthrough curve divided by the bed volume. So for the DBC at 10% breakthrough the area below the breakthrough curve up to 10% breakthrough is integrated and this is subtracted from the total amount of protein loaded on to the column up until 10% breakthrough and divided by the column's volume.

Other methods of measuring the performance of columns such as the retention time, retention factor and selectivity are used but these are more applicable to methods of chromatography other than affinity chromatography, where more than one analyte binds to the column. As the work in this thesis focuses on affinity chromatography these will not be further elucidated here.

1.10 Microscale Chromatography

A significant amount of work has been done on microfluidic chromatography to date. Microfluidic chromatography research has mainly been in the microfluidic chip format. Some of these chips have included other methods of analysis such as mass spectrometry, as well as liquid chromatography, and have included micro devices for pumping and mixing (Xie et al. 2005; Lazar et al. 2006; Ghitun et al. 2006)

Microaffinity chromatography as an analytical tool, particularly in the field of proteomics has received a significant amount of attention in the literature. For example researchers have developed microfluidic metal affinity chromatography in a compact disk format to detect phosphorylated peptides (Hirschberg et al. 2004).   Other work on microaffinity chromatography for phosphopeptide analysis includes a multichannel titanium dioxide microfluidic column (Boulousis et al. 2011) .

Analysis and detection of small amounts of other moieties has also been achieved by microaffinity chromatography in a chip based format. For example, a microaffinity column containing polymer beads with an RNA aptamer linked to the matrix (via a UV labile linker which enabled photoelution) was able to detect 96 fm of hepatitis C virus RNA polymerase protein (Cho et al. 2004). Another example is a microfluidic chip, fabricated from PDMS, containing an affinity microcolumn for capture and on chip identification and quantitation of the FLAG epitope, by direct fluorescence measurements or fluorescence resonance energy transfer. It was reported that this device is able to potentially detect sub-femtomole quantities of antibody with a high signal to noise ratio (Buranda et al. 2002).

These analytical microfluidic chromatography devices whilst useful are designed to capture only small amounts of protein and as such are unsuitable for this work which aims to capture and purify a comparatively large amount of protein for subsequently analytical purposes.

Other research into microfluidic chromatography as an analytical tool has also been carried out. One group of researchers looked at frontal affinity chromatography in a microfluidic capillary, for use during drug discovery, to determine the binding affinity of proteins for antibodies (Schriemer et al. 1998). Another research group designed a diamond walled capillary column containing an anion exchange monolith. The column was used to successfully separate a mixture of three proteins, equine conalbumin, chicken ovalbumin and soya bean trypsin inhibitor. Separation was achieved in 20s (Björkman et al. 2001)

Microfluidic chromatography devices have also been used as a method of studying dynamic binding capacities to predict process scale performance of ion exchange columns. The dynamic binding capacities for the 1.5µL, 1 cm long column (Figure 1.5) compared well with published process scale literature (Shapiro et al. 2009). Further work by Shapiro *et al* on predicting elution behaviour from the micro column showed that the column was able to predict lab scale behaviour (Shapiro et al. 2010).
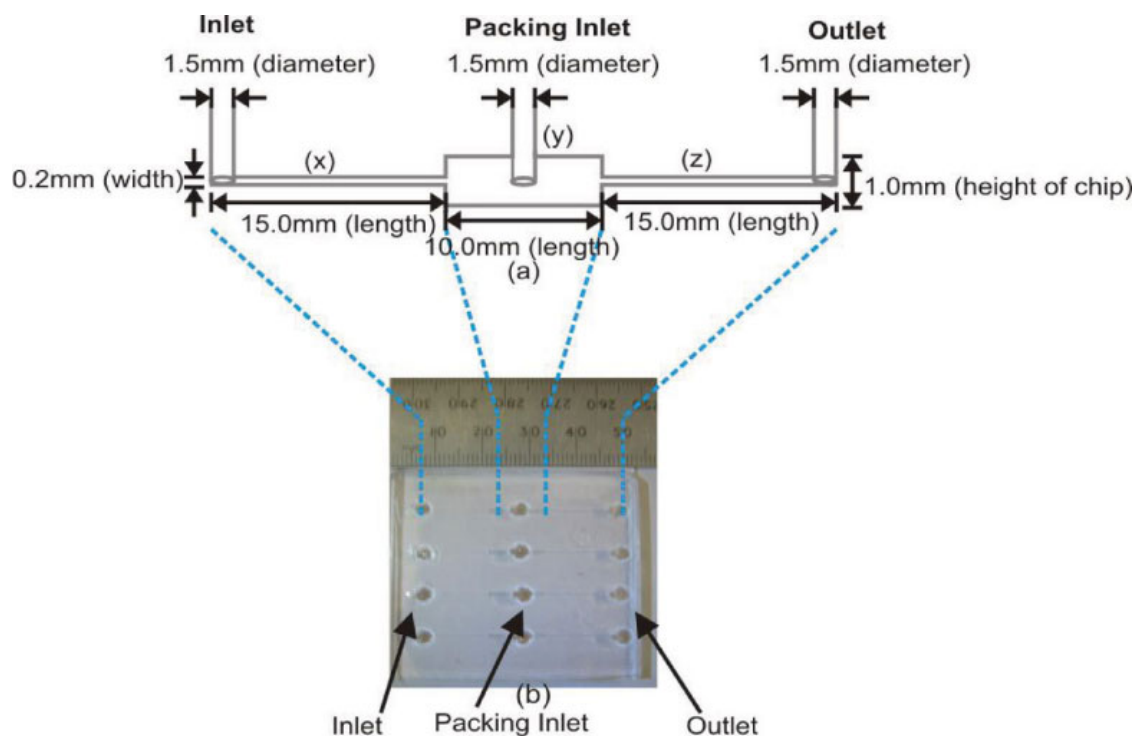
Figure 1.5 – Figure showing the design of a microfluidic ion exchange column used by Shapiro et al to study dynamic binding capacities as a prediction of process scale performance (Shapiro et al. 2009). Permission to reproduce this figure has been granted by John Wiley and Sons.

In terms of preparatory chromatography, some work has been done on the microfluidic scale. Wang *et al* were able to achieve chiral separations of racemic mixtures of tryptophan and thiopental in a PDMS, membrane chromatography, microfluidic chip. The device was able to achieve a good degree of separation and operate with only a 50 nL sample plug (Wang et al. 2002). Also negative enrichment of target cells by affinity chromatography has been conducted by researchers. This was done in a microfluidic device manufactured from PDMS and glass substrate. The internal surface of the column was modified to incorporate a mouse, antihuman, antibody and was able to achieve an increase in purity from approximately 30% to approximately 80% when a model mixture of Human T lymphocyte (Hut 78), and mouse

endothelial (RCL-2583) cells was passed through the device which captured the Hut cells (Li et al. 2011).

Some work has also been done on using microfluidic affinity chromatography for the purpose of purifying protein for further analysis. For example one research group designed a device for the capture of streptadivin. The microfluidic device they designed consisted of a channel created by PET sheets into which Poly (N-isopropylacrylamide)-Coated Beads were injected. When the temperature was raised above a certain threshold the beads were maintained in place, and were able to capture labelled streptadivin. When the temperature was lowered to room temperature the streptadivin containing beads were released from the column and the protein was thus eluted. It is not clear from this work what the quantity of protein is eluted and whilst the device was characterised with pure protein, a complex feed was not used (Malmstadt et al. 2003). Another example of preparatory microfluidic chromatography is an affinity chromatography chip, manufactured from borosilicate glass and packed with a monolithic porous polymer, which was used to selectively capture albumin from human cerebrospinal fluid . However, no work on eluting the captured albumin was reported (Li & Lee 2004).

The work planned for this project is to design and characterise a microfluidic chromatography column for the preparation of a purified protein sample, to compare the columns performance to a lab scale column, and prove that it is able to capture and elute protein from a complex feed. This is something that has not been achieved in the reviewed work on microaffinity chromatography. The column may also be able to predict larger scale performance and so could potentially be useful for scale up.

1.11 Micro Column Packing

In microaffinity chromatography, a number of different methods of packing have been employed by researchers. These include immobilising a ligand on the wall of the column, using a monolith (which is a porous material used to pack the column) or packing with particles. The method chosen will have an effect on the capacity of the column, the ease of packing, and refreshing the packing.

In a review paper (Huang et al. 2006) it was suggested that the surface chemistry of microchannel walls may be selected to promote or block ligand adsorption on the surface of a microchannel. The paper further suggests that ligands may be designed to capture target molecules and hence will selectively adsorb compounds making it possible to carry out microaffinity chromatography in those channels. As the paper recognises, the column would have to be of significant length in order to provide enough surface area to capture sufficient protein.   However, the method has been used for the negative enrichment of cells as described in Section 1.10. The microaffinity chromatography column planned for this work, however, aims to capture significant amounts of protein for further analysis and so surface modification of channel walls is not appropriate for this work.

Polymer monoliths are another type of packing that has been used to perform affinity separations. Monoliths carry the advantage of easier packing of a microfluidic channel and of course they remove the need for frits. Photo-initiated methods for the fabrication of porous polymer monoliths are ideal for microfluidic chips because the polymerisation reaction can be restricted to specific areas by using lithographic masks (de Mello 2002). Monoliths have been successfully used by researchers for affinity separations. For example,

Bedaire *et al* used a porous polymer monolith, with Concanavaline A immobilized on its surface, to provide an affinity monolith for high mannose glycans (Bedair & Oleschuk 2006). However, there are a number of disadvantages to using monoliths the most significant of which are: the lower surface area per unit volume that they provide (compared to packed beds); and the need to manufacture the monolith specifically for the intended chromatography. By contrast, affinity matrix beads are readily available with a range of ligands.

In addition to the above, bead matrices can be prepared independently from the fabrication of the microchannel allowing conditions that might affect and degrade the ligands to be avoided. As mentioned above, commercially available beads offer a number of advantages such as the fact that they are available with a number of ligands, and the bead surfaces are engineered to minimise non-specific adsorption and selectively bind the desired biomolecules. Also, beaded matrices offer increase surface area and hence have a greater adsorption capacity compared with a channel surface or a monolith (Huang et al. 2006). For these reasons, the microfluidic affinity column used in this work will be packed with a bead matrix.

Packing of columns with matrix beads has previously been achieved by dry packing (with gas), slurry packing (with solvents) or with supercritical carbon dioxide. Slurry packing is the most commonly used method and is less likely to result in plugging of the column than dry packing. The equipment for slurry packing is also less complicated than that required for supercritical fluid packing (Lancas et al. 2004).

Other technologies are also available to aid packing. For example, as described previously, thermally-responsive polymer beads that could be reversibly immobilised on microfluidic channel walls have been developed. This allowed the packing of a microfluidic affinity chromatography column at the time of use and had the advantage of enabling the packing to be changed easily to refresh the column. It also removed the need for frits to mechanically hold the matrix in place (Malmstadt et al. 2003). However, a further advantage to using readily available standard matrix beads to pack the planned microaffinity chromatography column is that the potential for the use of the column to predict lab and process scale can be explored. Consequently, this project will employ slurry packing of a readily available bead matrix.

1.12 Mass Transfer Considerations in Microfluidic Chromatography

With regard to microfluidic chromatography, the issues of diffusive versus convective transport apply and have been found to be an issue in a number of microaffinity columns, designed by researchers. For example, Piyasena *et al* found that the binding and dissociation rate constants for their FLAG peptide beads were lower than those obtained using flow cytometry measurements. They postulated that this was a result of the increased significance of diffusive transport at this scale (Piyasena et al. 2004).

Ghitun *et al* discussed how chromatographic performance can be enhanced, by reducing matrix particle size, and hence the distance across which analyte molecules must diffuse before they bind to the matrix (Ghitun et al. 2006).

Typically HPLC columns, which have an internal diameter of a few millimetres, are packed with matrix of the order of a few microns in diameter. This thesis will look at the performance of a microcolumn 700 µm in diameter, packed with beads with and average diameter of 90 µm. As described above, this type packing is advantageous because it is used at other scales. Consequently, analyte molecules will have a relatively larger distance across which to diffuse compared to a standard HPLC. It is therefore expected that diffusion within the bead will be a major factor in column performance.

1.13 Integrated Microfluidic Devices

The ultimate aim of this work is to move towards an integrated microfluidic device for online sample preparation by including a lysis and a chromatography step in one microfluidic device.

To date, a significant amount of work on integrated microfluidic devices has been undertaken on the manipulation of single cells to analyse their contents (Mellors et al. 2010; Gao et al. 2003; Gao et al. 2004; Yi et al. 2006).

Other work on integrated microfluidic devices has focussed on their potential for analysis. For example, a microfluidic device had been developed by researchers for integrating liquid chromatography and mass spectrometry. This device was designed for the analysis of complex protein digests in the field of proteomics (Ghitun et al. 2006). Another example of a microfluidic device for analysis incorporates filtration, solid phase extraction, and chromatographic separation for detection and resolution of polyaromatic hydrocarbons (Broyles et al. 2003). DNA/RNA amplification, separation, and detection has also been achieved on an integrated microfluidic device (F. Huang et al. 2006).

Some work has been done on sample preparation on the microfluidic scale. For example an integrated microfluidic cell culture and lysis device has been designed. The device was able to culture mammalian cells for 5 days and then lyse them without adding additional reagents by local hydroxide generation (Nevill et al. 2007). There is however a gap in terms of sample preparation as not much research has been done in this area (Mariella 2008). This work aims to contribute to filling this gap by moving towards a microfluidic device that is able to prepare significant quantities of purified protein sample, for further analysis, by integrating online microfluidic lysis and microaffinity chromatography.

1.14 Glutathione S Transferase as a Model Protein

Glutathione S Transferase will be used as the model protein in this work. Glutathione S Transferase is a dimeric enzyme which exists in many organisms. It catalyzes the conjugation of reduced glutathione with many diverse electrophilic substrates and is thought to play and important role in detoxification in many organisms (Zablotowicz et al. 1995). The molecular weight for one asymmetrical unit of Glutathione S transferase from *Schistosoma japonica* is 29.25KDa making the dimer 58.5kDa. Figure 1.6 shows the structure of GST from *Schistosoma japonica* which has been used to express and purify a number of proteins by creating fusion proteins (Smith & Johnson 1988).

Glutathione
Binding Site
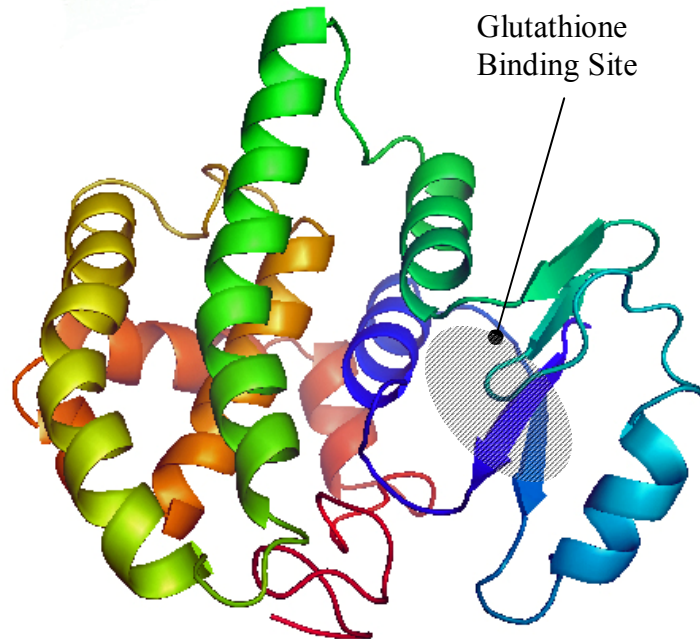
Figure 1.6 - One asymmetrical unit of GST from *Schistosoma japonicum*. The amino acid sequence was obtained from the Protein Data Bank and the diagram was produced using PyMOL software (Schrödinger, Surrey, UK). The molecular weight of the Schistosoma japonicum GST dimer is 58.5KDa

Gene fusion systems are used to provide an easy way of expressing proteins in *Escherichia coli,* addressing variability in the quantities of protein expressed and preventing the formation of inclusion bodies. The Glutathione S Transferase (GST) gene fusion systems has been reported to be one of the most successful in producing correctly folded and soluble proteins in the *Escherichia coli* cytoplasm (LaVallie & McCoy 1995). Gene fusion systems also provide a way of purifying those proteins easily, and often in a single step using affinity chromatography

GST affinity tags are a low cost way of purifying and obtaining high yields of recombinant proteins (Lichty et al. 2005), and they have been used successfully in a number of applications including vaccine production (Dempster et al. 1996; Wright et al. 1992), studies of protein-protein interactions (Peles et al. 1997) and cellular biology studies (Ellis et al. 1997). Consequently, the ability to disrupt and capture GST fusion proteins on the microscale would be useful. In

addition to this GST activity can be easily assayed by the CDNB (1-chloro-2,4-dinitrobenzene) assay. These factors combined with the fact that GST can be obtained relatively inexpensively as pure protein and can easily expressed in *Escherichia coli,* via pGex plasmid, make Glutathione S Transferase a good model protein with which to undertake the work in this thesis.

1.15 Aim and Objectives

As mentioned previously in this chapter, the overarching aim of this thesis is to move toward a microfluidic device, for the processing of microbial cell culture, to a level of purity suitable for further analysis. Two steps will be used to achieve this, a micro-lysis step and micro-affinity chromatography. The objectives of this project are therefore as follows:

- Objective 1 - Design and characterise a microfluidic device capable of lysing *Escherichia coli* microbial culture, by chemical lysis. The microlysis device needs to operate in the same flowrate range as the microfluidic chromatography step and be able to achieve a good degree of lysis when compared to standard laboratory techniques. The effectiveness of the device at lysing bacteria will be investigated by measuring the amount of active Glutathione S Transferase released from the disrupted microbial cells. This is covered in chapter 3

- Objective 2 - Design a microaffinity chromatography column, packed with standard Glutathione Sepharose beads, which is capable of capturing Glutathione S Transferase. In order to judge whether the chromatography column is suitable for further work, in terms of

characterisation, it will need to display appropriate response curves to acetone transitions. This work is covered in chapter 4.

- Objective 3 - Characterise the microaffinity chromatography column designed in chapter 4 in terms of packing quality. This will be measured by HETP analysis and asymmetry factor. This is covered in chapter 5.

- Objective 4 - Characterise the behaviour of the microaffinity column with pure protein and compare these to lab scale. This will be measured by analysis of the breakthrough and elution curves and Dynamic Binding Capacity of the column. This is covered in chapter 5.

- Objective 5 - Characterise the behaviour of the micro affinity column with 100% clarified lysate (lysate which has been fully clarified and is undiluted). This will be determined by comparison with the pure protein breakthrough curves and elution curves. This is also covered in chapter 5.

The key conclusions of the project are covered in chapter 6. The materials and methods general to more than one chapter are covered in chapter 2. The materials and methods specific to each chapter are covered in the chapter.

2 Materials and methods

This section describes the materials and methods common to the investigations undertaken in at least two of the results chapters. Unless otherwise stated, all reagents were obtained from Sigma Aldrich (Sigma Aldrich, Dorset, UK).

2.1 *Preparation of Growth Media*

2.1.1 Luria-Bertani (LB) media

1 L of LB media was prepared by adding 10 g of tryptone, 5 g of yeast extract and 10 g of sodium chloride to a large beaker containing 800 mL of deionised water and a stirrer bar. The beaker containing the mixture was placed on top of a stirrer plate and the mixture was stirred until the tryptone, yeast extract and sodium chloride had fully dissolved. The solution was then topped up with deionised water to make the volume up to 950 mL. A pH probe was then placed in the solution and the pH was measured. The pH was then adjusted, while measuring, by adding hydrochloric acid to lower the pH and sodium hydroxide to raise the pH until pH 7 was reached. The media was then topped up to a total volume of 1 L. To make 2x LB, double the weight of tryptone, yeast extract and sodium chloride were used for the same volume of water.

For shake flask fermentations, LB media with 10 g/L glycerol was used. This was made by adding 10g of glycerol when the tryptone, yeast extract and sodium chloride were added. The rest of the method of preparation was identical to above.

The LB media was then decanted into a Durant bottle, the cap was replaced and then loosened sufficiently to avoid a build up of pressure during

autoclaving. A strip of autoclave tape was placed across the cap. The Durant bottle containing the media was then autoclaved (The holding temperature for autoclaving was 121ºC and the holding time was 15 minutes). Once the autoclaving process was complete the cap was tightened.

2.1.2 Preparation of LB Agar

1 L of LB Agar was prepared by adding 10 g of tryptone, 5 g of yeast extract and 10 g of sodium chloride to a large glass beaker containing 800mL of deionised water and a stirrer bar. The beaker containing the mixture was placed on top of a stirrer plate and the mixture was stirred until the tryptone, yeast extract and sodium chloride had fully dissolved. A pH probe was then placed in the solution and the pH measured. The pH was then adjusted, while measuring, to pH7.0 by adding hydrochloric acid or sodium hydroxide. 15 g of agar was added to the LB media and the mixture was heated in the microwave to melt the agar. The hot LB agar was then placed back on the stirrer and stirred thoroughly. The LB agar was made to 1 L by adding deionised water. The LB agar was transferred to a 1 L Durant bottle with the cap on loosely. A strip of autoclave tape was placed over the cap and the LB agar was autoclaved. Once the autoclaving process was complete the cap was tightened.

2.1.3 Preparation of LB Agar Plates

LB agar was prepared as described in Section 2.1.2. The cap on the Durant bottle containing the LB agar was loosened and it was heated in the microwave until the contents melted fully. 25mL of LB agar per plate were pipetted, in a laminar flow cabinet, into sterile falcon tubes. The LB agar in the falcon tubes

was then allowed to cool down sufficiently to be able to hold them but not enough to allow the LB agar to set. This was to prevent loss of heat labile ampicillin sodium salt. 25µl of 150mg/ml ampicillin sodium salt stock solution (sterilised by passing it thought a 0.2µL syringe filter) was then added to each falcon tube. The tubes were capped and inverted several times to ensure that the antibiotic was properly mixed with the LB agar.

Petri dishes were then laid out in a laminar flow cabinet next to sterile flame. The contents of each falcon tube were then carefully poured into a single Petri dish, taking care to avoid formation of bubbles. The lid of the Petri dish was placed on the dish so that a small amount of it was uncovered. This was to prevent condensation on the inside of the lid. Once cooled and the LB agar set the lids were put on fully. The plates were stored in the fridge until needed.

2.2 Transformation with the pGEX3x Vector and Preparation of Glycerol Stocks

A water bath with temperature control was set to 42° C. One 50µL aliquot of competent *Escherichia coli* BL21 DE3 cells was thawed on ice. 1 ng of pGex 3x vector (Amersham, Buckinghamshire, UK) was then pipetted into the tube containing 50µL of competent *E.coli* and mixed by tapping. The mixture was incubated on ice for 30 min following which the eppendorf was quickly placed in a floating eppendorf stand. The tube and stand were the placed in the water bath and left for 30s. The eppendorf tube was then transferred back to the ice and left to cool for 2 mins. The transformed *E.coli* was added to 900 µL of LB in a sterile falcon tube and was grown for 1 hour at 37° C in an incubator with orbital shaker set to 250rpm. 400µL of the broth was then pipetted onto each of

two LB agar plates which were made as described in Section 2.1.3 and spread using a sterile spreader. The LB agar plates were incubated overnight at 37° C

Two sterile falcon tubes were then each filled with 5 mL of sterile LB medium and 5µL of filter sterilised, 150 mg/mL, ampicillin stock solution was added to each. Two colonies were then picked and a colony grown in each of these falcon tubes, with shaking at 200rpm, at 37ºC overnight.

Two autoclaved 100mL shake flasks were each filled with 20mL of sterile LB media in a laminar flow cabinet followed by 20µL of filter sterilised, 150mg/mL, ampicillin. Each shake flask was inoculated with 2mL of broth from an overnight culture and they were then grown in an incubator at 37ºC, with shaking at 200rpm, until the OD at 600nm had reached 1. Glycerol stocks were then made of each of theses cultures. 100µL of filter sterilised 40% glycerol (v/v) was added to sterile eppendorf tubes followed by 100µL of culture from a shake flask. The glycerol and culture were mixed gently by pipetting. Three glycerol stocks were made from each shake flask. The eppendorfs were then placed in the -80ºC freezer.

2.3   Preparation of Buffers

2.3.1 Phosphate Buffered Saline (PBS) pH7.4

1 Sachet of 0.01M Phosphate Buffered Saline powder was added to a to beaker containing 900 mL of deionised water and a stirrer bar. The beaker was placed on magnetic stirrer plate and stirred until the powder had dissolved. The beaker was then topped up to 1 L. The pH was checked using a pH meter and adjusted with 1M HCl and 1M NaOH if necessary. A 0.2µm Nalgene 595 bottle

top filter (Nalgene, New York, USA) was then placed on top of a clean dry Durant bottle, a vacuum pump was attached to the filter and the solution was filtered

2.3.2 Elution Buffer Tris HCl pH8.0 with 10mM Reduced Glutathione

0.788g of Tris HCl as added to a beaker containing 90 mL of deionised water. A stirrer bar was then placed in the beaker and the beaker was placed on top of a magnetic stirrer plate. The buffer was then stirred until the Tris-HCl had dissolved. 0.3073 g of reduced L-Glutathione was then added to the beaker and stirring was continued until it was dissolved. The volume was then topped up to 1 L and the pH was adjusted to pH 8.0 by adding sodium hydroxide and hydrochloric acid. A 0.2µm Nalgene 595 bottle top filter (Nalgene, New York, USA) was then placed on top of a clean dry Durant bottle, a vacuum pump was attached to the filter and the solution was filtered. For large scale experiments this buffer was prepared immediately before use and not stored. For microscale experiments 500µL aliquots were snap frozen in dry ice and ethanol, as described in Section 2.7, and stored at -80ºC until needed. They were defrosted immediately before use.

2.3.3 1M Potassium Phosphate Buffer pH6.5

13.61g of monobasic potassium phosphate was added to a beaker containing a stirrer and water was added to make the volume up to just below 100 mL. The beaker was placed on a stirrer plate and stirred until all the salt was dissolved. The solution was topped up to 100 mL. This was repeated for 17.42 g of dibasic potassium phosphate.

A separate beaker was filled with 50 mL of the dibasic potassium phosphate solution and monobasic potassium phosphate was added while measuring the pH until a pH of 6.5 was reached.

2.4 Fermentations of Recombinant Escherichia coli BL21 DE3 Containing the pGex-3x Vector

2.4.1 500mL Shake flask Fermentation

One vial of the *E.coli* BL21 DE3 glycerol stock was streaked out, without defrosting it, on an LB agar ampicillin plate in a laminar flow cabinet. The glycerol stock was returned quickly to the -80ºC freezer. The plate was incubated overnight at 37ºC.

In the laminar flow cabinet, 5ml of autoclaved LB media was pipetted into a sterile falcon tube followed by 5 µL of filter sterilised, 150mg/mL, Ampicillin sodium salt. The falcon tube was closed and the media and antibiotic were mixed by inverting. A single colony, from the agar plate was picked and used to inoculate the falcon tube. The falcon tube was then placed in an incubator, at 37 ºC, with orbital shaking at 200rpm and left overnight.

A 2 L baffled shake flask and 1 L measuring cylinder were sterilised. A plug of cotton wool was placed in the top of the shake flask and both the shake flask and measuring cylinder were covered with aluminium foil, taped into place with autoclave tape, and then sterilised by autoclaving. They were then left to cool in the laminar flow cabinet. In the laminar flow cabinet, the sterilised shake flask was filled with 500mL of LB media containing 10g/L glycerol using the sterilised measuring cylinder. This was followed by 500µL of filter sterilised

150mg/ml ampicillin stock solution. The shake flask was then inoculated by pipetting the 5ml overnight culture into the shake flask.
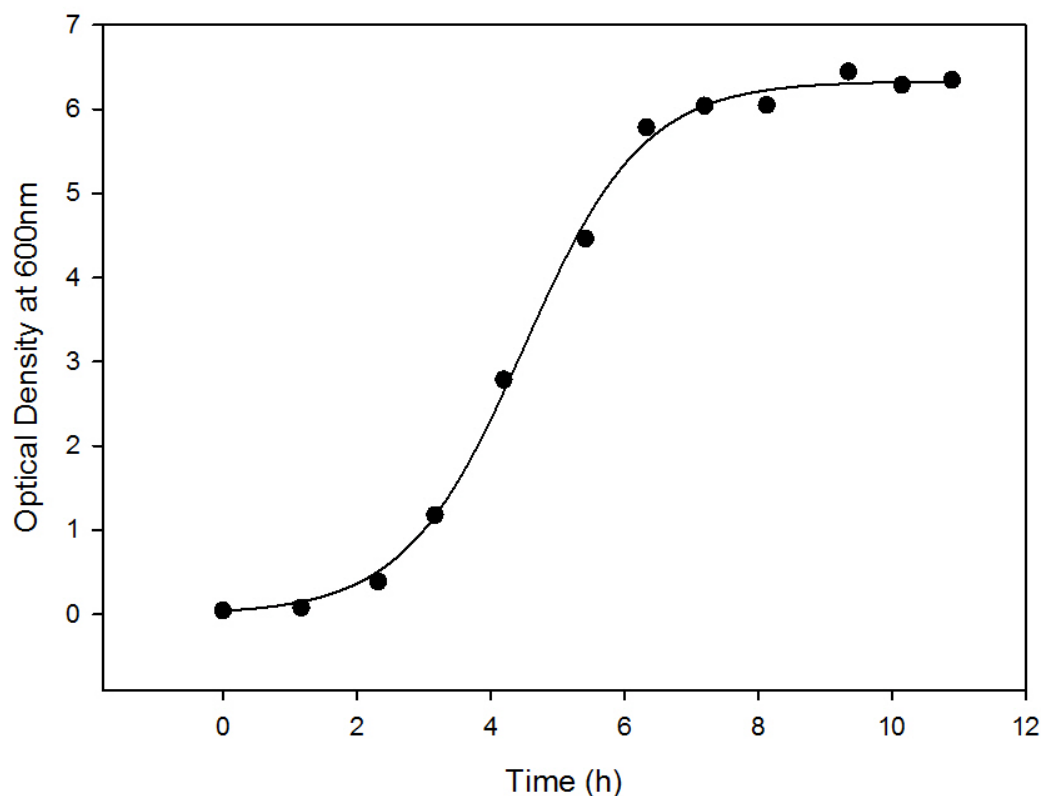
Figure 2.1 – 500 mL baffled shake flask fermentation of recombinant *Escherichia coli* expressing Glutathione S Transferase from *Schistosoma japonicum* by means of the pGex-3x vector.

Figure 2.1 shows the Optical Density versus time for an uninduced fermentation. This was performed in order to decide on the best point at which to induce the production of the protein. Subsequent shake flask fermentations, which were performed for the purpose of the microlysis experiments were induced after approximately 8 hours by adding 500µL of filter sterilised 1M IPTG to try to get the highest possible optical density as protein production takes some of the energy of the cells. The fermentation was allowed to proceed for a further 4 hours.

2.4.2 5.5 L Stirred Batch Fermentation in 7 L Fermenter

4.5L of 2xLB media was added to a 7 litre fermenter. The fermenter and ancillaries were the sterilised and assembled according to the standard operating procedure and allowed to cool to 37°C. 500 ml of filter sterilised glucose solution containing 50g of glucose was then added to the fermenter. 5.5ml of 150mg/ml filter sterilised ampicillin solution was also added to the fermenter.

The fermenter was then inoculated with the contents of a 500ml shake flask and a sample was taken. The fermentation was then allowed to proceed. The pH was maintained at 7 with ammonia and phosphoric acid and samples were taken every hour. After 3 hours and 35mins the fermentation was induced by adding 5.5 mL of filter sterilised 1M IPTG solution. The fermentation was allowed to proceed for a further 4 hours after which it was harvested. Figure 2.2 shows the key data gathered from this fermentation.

The harvested broth was centrifuged using a CARR Powerfuge P6 centrifuge. The cells were re-suspended in 120ml of PBS at pH 7.4. This was divided into 4 aliquots and disrupted by sonication.   The sonicate was then centrifuged at 4000rpm for 15mins at 4°C. This was done in an Eppendorf 5810R bench top centrifuge (Eppendorf, Cambridge, UK) using the A-4-62 swing out bucket rotor with falcon tube holders. The supernatant was decanted carefully and filtered using a 0.2µm Nalgene 595 bottle top filter. The filtered supernatant was aliquoted into 5 mL aliquots and snap frozen in dry ice and ethanol as described in Section 2.7.
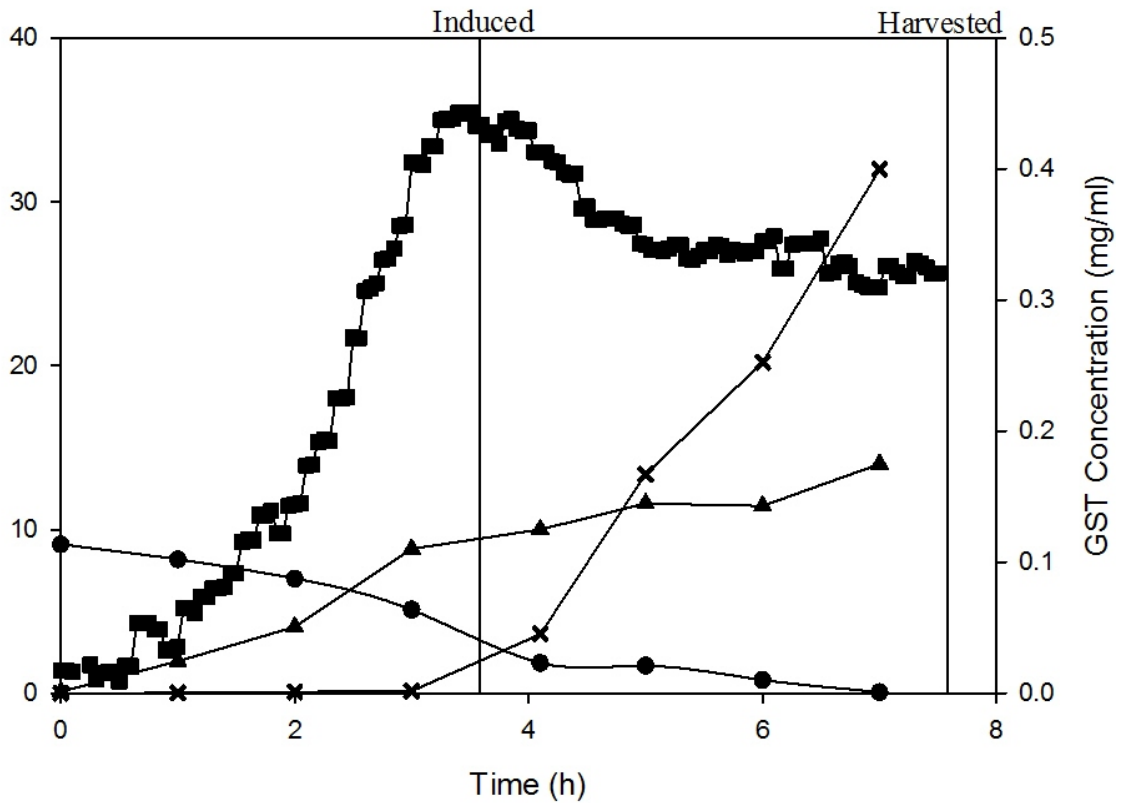
Figure 2.2 – 5.5L Fermentation of recombinant *Escherichia coli* BL21 DE3 containing the pGex- 3x vector so that it was expressing Glutathione S Transferase from *Schistosoma japonicum.* The growth media used was 2x LB with 10g/L of glucose (■) Oxygen Uptake Rate. (▲) OD at 600nm (●) Glucose concentration in (g/L) (X) Glutathione S Transferase concentration in (mg/ml). The vertical lines on the graph indicate the time of induction and havesting.

Table 2.1, below, shows a crude mass balance of GST protein at different stages in the purification process. It can be seen that a lot of protein was lost between harvesting and sonication. This may be due to incomplete cell disruption. Consequently, the preparation of 100% clarified lysate would have benefited from an alternative method of lysis.

Table 2.1 – GST content at different stages of the feedstock preparation process

Step	GST Concentration (mg/ml)	Process Volume (ml)	Total Amount of GST (mg)	Yield (%)
Harvested Broth	0.0463	5500	254.65	100
Sonicate Supernatant	0.238	120	28.56	11.2
0.2µm Filtered Supernatant	0.169	100	16.9	6.6

2.5   Microwell plate CDNB Assay

Prior to adding the samples 45µL of deionised water was added to each microwell of a 96 well microwell plate. The plate was then covered with parafilm (Bemis Company Inc. Wisconsin, USA) to prevent evaporation of the water.

A serial dilution of 0.87mg/ml Glutathione S Transferase from *Schistosoma japonicum* was made by placing 8 microfuge tubes in a rack. The first tube was left empty and 10µL of deionised water was pipetted into the remaining seven tubes. 40µL of GST was then added to the first tube. 20µL of GST was pipetted from the first tube to the second tube and the protein and water were mixed by pipetting several times. 20µL of the GST solution was taken from the second tube, pipetted into the third tube and mixed again by pipetting. This was repeated until all tubes contained GST solution in water. 5µL of each of the dilutions were then added to the plate in triplicate. In order to reduce errors from slightly different reaction times these standards were included on each

microwell plate. Figure 2.3 shows a typical standard curve obtained for the microwell plate CDNB assay.

5µL of sample was then added to each microwell and mixed by pipetting. This was repeated three times for each sample so that there would be triplicates. The microwell plate was then covered with parafilm while the sample reagents we being prepared.
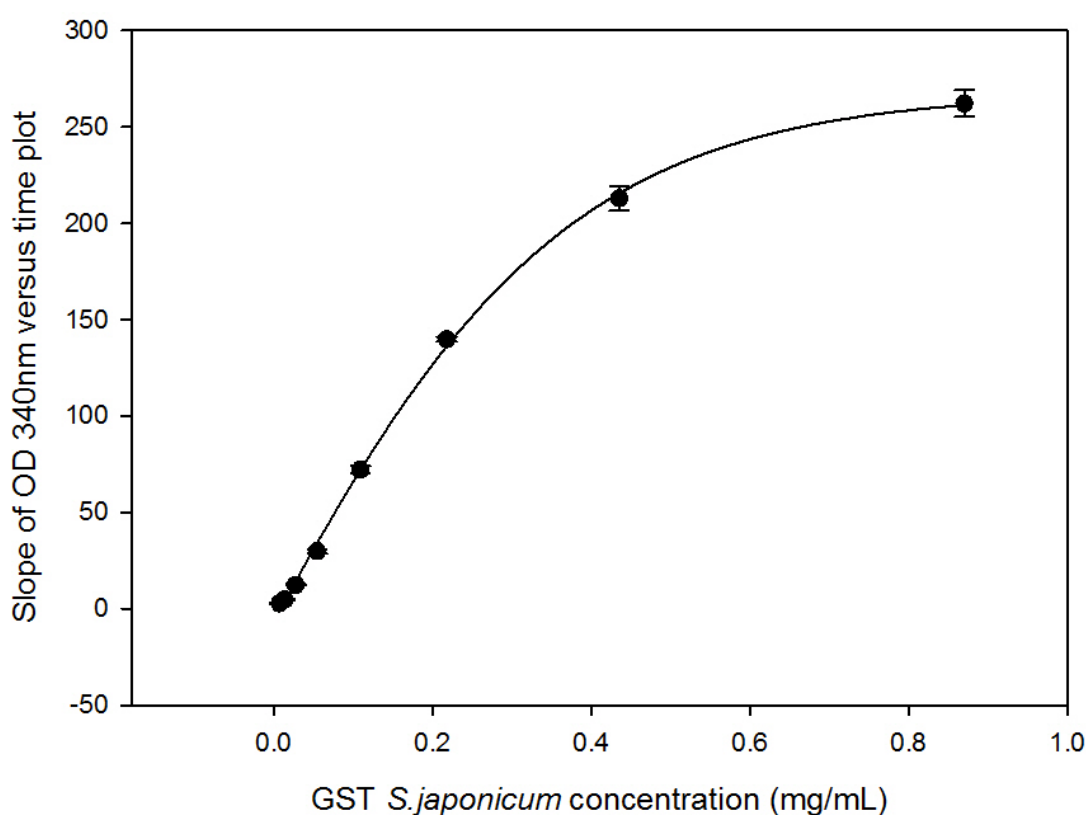
Figure 2.3 – Standard curve obtained by serial dilution of a standard solution of 0.87 mg/ml Glutathione S Transferase from *S. japonicum*

The CDNB reagent was then prepared by adding 20.3mL of deionised water to a clean a falcon tube followed by 2.9mL 1M Potassium Phosphate buffer pH6.5. 100mM CDNB in Ethanol and 100mM Reduced L-Glutathione were then prepared immediately prior to the assay. 290µL of 100mM CDNB in ethanol

and 290μL 100mM reduced glutathione in deionised water were then added quickly and the tube was closed and inverted several times to ensure thorough mixing. The resulting solution was decanted into a weighing boat and a multichannel pipette was used to pipette 205μL in to each microwell. This process was done as quickly as possible to reduce the error resulting from differences in reaction start time.

The microwell plate was then read at 340 nm at one minute intervals for 5 mins by a Tecan plate reader controlled by icontrol software (Tecan Group Ltd, Männedorf, Switzerland). The gradient for each UV absorbance versus time curve, for each sample, was then obtained by manipulation in MS Excel. The concentration of the serial diluted standard was then plotted versus the gradient to give a standard curve. The concentration of Glutathione-S-Transferase in any sample within the range 0.87 to 0 mg/mL could be obtained by reading from the standard curve.

2.6   Microwell plate Bradford Protein Assay

2.6.1 Standard Assay

Using a Bradford Assay kit (Biorad Laboratories Ltd, Hertfordshire, UK), 30 mL of Bradford reagent per 96 well plate, was decanted into a falcon tube and left for half an hour to reach ambient temperature. Seven γ-globulin standards in the 2000-125 μg/ml range where made by performing serial dilutions of the 2mg/ml γ-globulin solution provided with the kit. 5μL of each standard were pipetted into empty microwells in triplicate. 5 μL of each sample was then added to microwells, in triplicate.
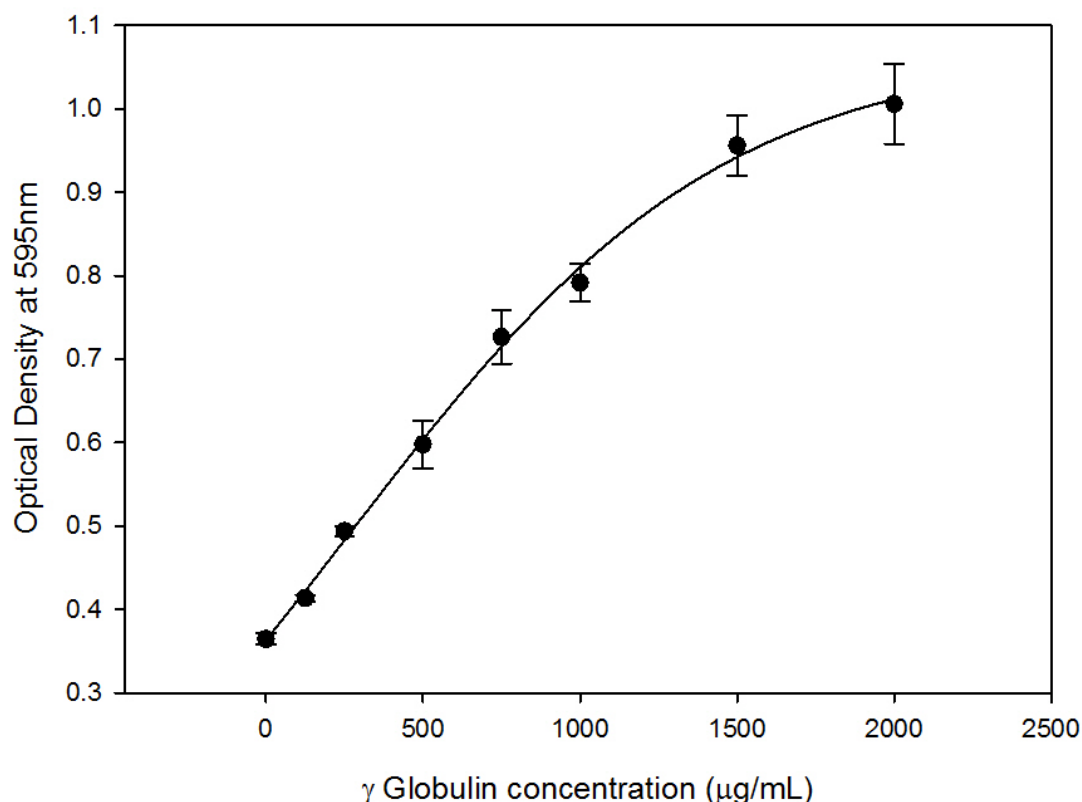
Figure 2.4 – Standard curve obtained for the standard microwell pate assay obtained by serial dilution of a standard solution of 2mg/ml γ-globulin standard

The dye reagent was then decanted into a weighing boat and a multichannel pipette was used to add 250μL of the reagent into each microwell. The sample and dye reagent where mixed together by pipetting. The microwell plate was then incubated at room temperature for 10 mins. Following this the plate was read by a Tecan plate reader control by icontrol software at 595nm. Figure 2.4 shows a typical standard curve obtained for the standard Bradford microwell plate assay.

2.6.2 Micro Assay

20 mL of Bradford reagent per 96 well plate, was decanted into a falcon tube and left for half an hour to reach ambient temperature. Seven γ-globulin standards in the 25μg/ml-1.25μg/ml range where made by diluting the 2mg/ml

γ-globulin solution provided with the kit. 150μL of each standard were pipetted into empty microwells in triplicate. 150 μL of each sample was then added to empty microwells in triplicate.

The dye reagent was then decanted into a weighing boat and a multichannel pipette was used to add 150μL of the reagent into each microwell. The sample and dye reagent where mixed together by pipetting. The microwell plate was then incubated at room temperature for 10 mins. Following this, the plate was read by a Tecan plate reader control by icontrol software at OD595. Figure 2.5 shows a typical standard curve obtained for the micro Bradford microwell plate assay.
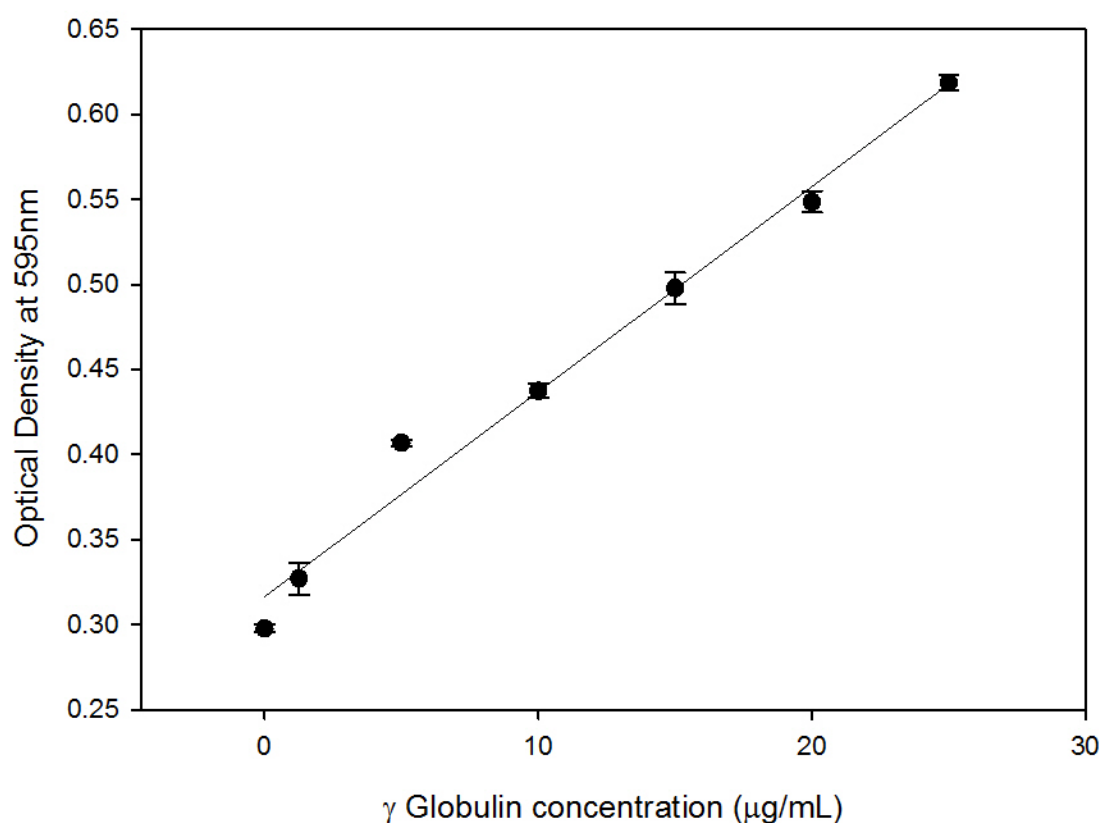
Figure 2.5 – A typical standard curve obtained for the micro microwell plate assay obtained by serial dilution of a standard solution of 2mg/ml γ-globulin standard.

2.7   Snap Freezing of Samples

A 4L Polypropylene beaker (Nalgene, New York, USA) was filled with sufficient ethanol to reach just below the top of a round floating Eppendorf tube rack (Nalgene, New York, USA) when it was placed in the beaker. Dry ice pellets were then added to the ethanol.   When the ethanol was sufficiently cold, i.e. gently bubbling but still with sufficient ice to maintain the temperature, the tube rack, containing eppendorf tubes filled with samples, was placed in the ethanol. The resulting temperature increase in the ethanol caused the ethanol to bubble more quickly as the dry ice sublimed. Once this subsided and the ethanol was bubbling gently again, the Eppendorf tube rack was removed and the tubes were kept cold on dry ice. The tubes were immediately transferred to a -80 C freezer.

2.8   Presentation of Data

The graphs in this thesis were produced using SigmaPlot (Systat Software Inc, Illinois, USA). Error bars shown on the graphs represent the standard error of the mean.

3 Micro Lysis in Capillary – Design and Characterisation

3.1 Introduction and Aims

This chapter investigates microfludic chemical lysis with the aim of designing the first step in a two stage process for high throughput lysis and separation of protein. A number of different researchers have looked at lysis on the microscale (Di Carlo et al. 2005; Schilling et al. 2002; Kim et al. 2004; Huh et al. 2007). However, to date, these have generally been low throughput and mechanical or sonic methods have tended to be used. Chemical lysis, by contrast has the advantage that simpler microfluidic devices, capable of lysing relatively large quantities of cells can be constructed and these devices do not need complicated external equipment. BugBuster Mastermix™ was chosen because BugBuster has been shown to be a reliable method for protein release for subsequent protein quantitation studies (De Mey et al. 2008) and the BugBuster Mastermix™ reagent contains a nuclease to digest the DNA released during lysis. Given that this work is on the microfluidic scale and lysed microbial cultures can be viscous because of the DNA content, it was thought that using a lysis reagent containing nuclease would reduce the potential for problems with high pressure drops and poor mixing.

This chapter begins by describing the materials and methods specific to the investigations described in it. The results and discussions section then describes the investigations undertaken in order to arrive at a final microlysis device. Finally the summary and conclusion section highlights the key findings from the work presented in this chapter and sets out the key conclusions.

The results and discussion section begins by looking at the rheological behaviour of *Escherichia coli* culture that has been disrupted in a number of different ways, as well as unlysed microbial culture, at the microlitre scale with the aim of validating the decision to use chemical lysis with BugBuster Mastermix™ in this work.

The chapter then goes on to investigate critical parameters such concentration of chemical lysis agent, residence time, flowrate and device configuration. The chapter concludes by presenting the design of a chemical lysis device for high throughput lysis of *Escherichia coli* cell cultures.

3.2   Materials and Methods

This section describes the materials and methods used which are specific to the investigations in this chapter. This covers:

- the preparation of *E.coli* cultures of specific Optical Densities;

- the disruption of the *E.coli* cultures;

- the experimental verification of the Hagen-Poiseuille flow equations;

- the microlysis experimental setup and methods;

- measurement of viscosity.

All fittings were obtained from IDEX Health and Science, Washington, USA unless otherwise stated and all reagents were purchased from Sigma Aldrich, Dorset, UK unless otherwise stated.

3.2.1 Preparation of *Escherichia coli* Cultures with Defined Optical Densities

500ml shake flask fermentations of *Escherichia coli* were undertaken as described in Section 2.4.1. The *Escherichia coli* culture was divided into 500 ml centrifuge bottles so that an even number of bottles containing the same amount of culture were produced. The culture containing bottles were loaded into a Beckman J2-M1 floor standing centrifuge (Beckman Instruments (UK) Ltd, High Wycombe, UK) fitted with a JA-10 rotor, being sure to position the bottles in opposite pairs, so that the rotor remained balanced. The *E.coli* culture was then centrifuged at 5000rpm for 30mins at 4ºC. Most of the supernatant was then decanted leaving a small amount at the bottom of each bottle.

The bottles were placed in an orbital shaker and were shaken at 300rpm until the cells were fully resuspended in the remaining supernatant. The concentrated cell culture was pipetted into falcon tubes and the Optical Density (OD) was adjusted by diluting with fresh autoclaved LB media containing 10g/L glycerol. The culture OD was measured at 600nm using a Cecil spectrophotometer (Cecil Instruments, Cambridge, UK) to check the OD. When the desired OD was reached the culture was stored in the fridge until needed.

3.2.2 Dry Cell Weight Calibration factor for *Escherichia coli* culture grown in LB Media

According to Wang *et al*, for *E.coli* BL21 DE3 cells grown in LB media, an optical density of 1 at 600nm corresponds to a dry cell weight of 0.385 g/L (Wang et al. 2009)

3.2.3 Cell Disruption of *Escherichia coli* Culture by Sonication

A 1 mL sample of *Escherichia coli* culture of the desired Optical Density was pipetted into a 2 mL eppendorf tube. The eppendorf tube was placed in a small beaker packed with ice tightly enough to hold the eppendorf tube in a vertical position. The sample was placed in a sonicator, a Soniprep 150 (MSE (UK), Ltd, London, UK), so that the sonicator probe was immersed in the sample without the probe touching the bottom or side of the eppendorf. The sonicator amplitude was set to 20µm with 10 cycles of 10 seconds on and 10 seconds off. The sonicated sample was then removed from the sonicator, the eppendorf tube was closed and the sample mixed by inverting.

3.2.4 Cell Disruption of *Escherichia coli* Culture by Homogenisation

Cell culture of the appropriate OD was prepared as described in Section 3.2.1. 40 mL of cell culture sample was then placed in a Gaulin Micron Lab 40 homogeniser (APV Gaulin GmbH, Lubeck, Germany). The sample was homogenized by passing it through the homogeniser at 500 bar. The homogenate was then decanted into an autoclaved beaker and mixed with a sterile stirrer. Using autoclaved pipette tips, 3 mL of samples was pipetted into autoclaved eppendorf tubes. The tubes were then placed in the fridge until needed.

3.2.5 Cell Disruption of *Escherichia coli* Culture by Lysis with BugBuster Mastermix™ in a Stirred Bijou

Lysis in a stirred bijou was carried out by pipetting the appropriate quantity of cell culture into an empty bijou tube. A small stirrer bar was placed inside the bijou tube and the bijou was placed on top of a magnetic stirrer plate and secured with autoclave tape. The stirrer was then started and the appropriate quantity of BugBuster Mastermix™ (Merc Millipore, Darmstadt, Germany) was added to the cell culture. The bijou tube was then covered with parafilm to minimise evaporation from the surface of the mixture.   The lysis was allowed to proceed for one hour with samples being taken for further analysis at 5, 15, 30 and 60 mins.

3.2.6 In-Capillary Lysis
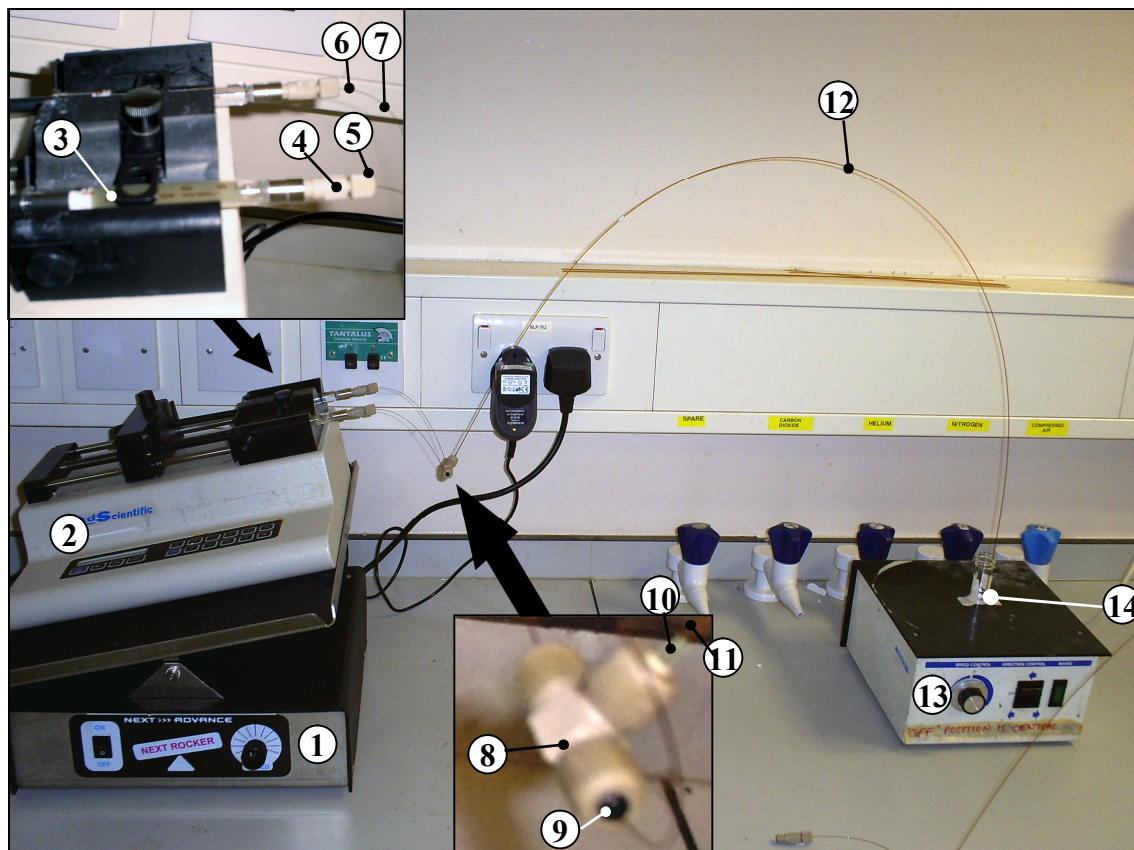
Figure 3.1 - Micro lysis experimental setup. The microlysis consisted of the following component parts: (1) Universal Rocker (New Era Pump Systems Inc, New York ,USA) (2) Syringe pump (Kd Scientific, Massachusetts, USA) (3) 2.5ml Gastight® Glass syringes (VWR, Dorset , United Kingdom), (4) P-659 syringe adaptor (IDEX Health and Science, Washington, USA); (5)F127 10-32 fingertight peek nut for 1/16" OD tubing (IDEX Health and Science, Washington, USA); (6) F-242x 395 micron 1/16" OD tubing sleeves (IDEX Health and Science, Washington, USA); (7) 150micron ID 363 micron OD fused silica capillary tubing (Polymicro technologies, Arizona, USA); (8) P-890 micro tee with 152 micron thru hole (IDEX Health and Science, Washington, USA); (9) F-152 ferrule for 360µm outer diameter tubing (IDEX Health and Science, Washington, USA) (10) F-132 ferrule for 1/16" outer diameter tubing (IDEX Health and Science, Washington, USA); (11) F267G tubing sleeves 840 micron id 1/16" OD (IDEX Health and Science, Washington, USA); (12) 700 micron inner diameter 850 µm outer diameter capillary tubing (Polymicro technologies, Arizona, USA); (13) Magnetic stirrer plate; (14) Bijou tube with magnetic stirrer bar.

The micro-lysis system was assembled as shown in Figure 3.1. One syringe was filled with 2.5ml of BugBuster Mastermix™ and the other with 2ml of recombinant *E.coli* BL21DE3 culture (containing the pGex 3x vector) and 0.5ml air. The air bubble was introduced into the syringe containing the *E.coli* in order

to provide a way of continuously mixing it, and hence prevent the *E.coli* cells from settling out of the suspension while the experiment was in progress. To achieve this mixing, the universal rocker rocked the syringe pump and syringes at a rate of 0.4 Hz causing the bubble to move up and down the syringe mixing the microbial culture.

The end of the 700µm outer diameter capillary in which the lysis took place was placed inside a bijou which contained 1.8 ml of deionised water and a small stirrer bar. This bijou was placed on top of a magnetic stirrer plate and stirred continuously in order to quench the lysis once the lysate left the device.

Once the experiment was complete with the stirrer still on, 1ml of sample was pipetted into an eppendorf tube and spun at 12000 rpm for 5mins using an eppendorf 5810R desktop centrifuge (Eppendorf UK Ltd, Stevenage, UK). The supernatant was then pipetted into another eppendorf tube and snap frozen in dry ice and ethanol as described in Section 2.7.

Investigations relating to methods of mixing the BugBuster and microbial culture were undertaken by changing the type of union used from a T-Piece with a large thru-hole to one with a small thu-hole and then to a teardrop micromixer. Experiments to determine the effect of residence time on the performance of the microlysis device were carried out by keeping the flowrate constant and varying the length of the 700 µm internal diameter capillary. When carrying out investigations into the effect of flowrate on lysis device performance the flowrate was varied on the syringe pump while changing the length of the outlet capillary to maintain a constant residence time, and keeping the type of union constant.

It is worth noting that the actual flowrate of the fluid passing through the device was double that set on the pump because of the two syringes feeding the device.

3.2.7 Measurement of Viscosity of Different types of Lysate

The viscosity of *Escherichia coli* culture, sonicate, homogenate and lysate was measured using a Brookfield Cone and Plate LVDVII programmable viscometer with the CP42 cone (Brookfield, Harlow, Essex). The results were recorded using their Wingather V3 software. The viscometer was levelled on the bench top by adjusting the height of the screw feet. To maintain a constant temperature of 20ºC, water was pumped through the sample chamber from a water bath with temperature control. The cone was removed carefully from the viscometer, and the viscometer was auto zeroed. The cone was then replaced carefully and the sample chamber was replaced, without any sample in it. The speed of the cone was then set to 10rpm and the cone and plate gap was set by turning the adjustment ring on the viscometer to bring the plate and cone close together until the torque reading was between 0% and 0.4%. The rotor was then turned off and the sample chamber removed ready for the sample to be added.

Before adding the sample, the sample chamber was cleaned - first with water and then with 70% ethanol. The cone was also cleaned carefully first with water then with 70% ethanol. 1 ml of sample was then placed inside the sample chamber, the chamber was replaced and measurements of shear stress and shear rate were taken while the cone rotation speed was varied in the range of 0 to 200rpm. Following the measurement, the sample was discarded into a

large beaker containing Tego. The chamber and cone were then cleaned as described above.

3.2.8 Experimental Verification of the Hagen- Poiseuille Flow Equations

In order to verify the Hagen-Poiseuille flow equations at the microscale, the pressure drop versus flowrate relationship for 60% glycerol (v/v) solution was investigated in capillaries of different diameters and cross sections. 60% glycerol was chosen because of its Newtonian behaviour i.e. the shear stress versus shear rate relationship is a linear one. The viscosity of the glycerol solution was measured with a Brookfield LVDVII cone and plate viscometer (Brookfield, Harlow, Essex) viscometer as described in Section 3.2.7
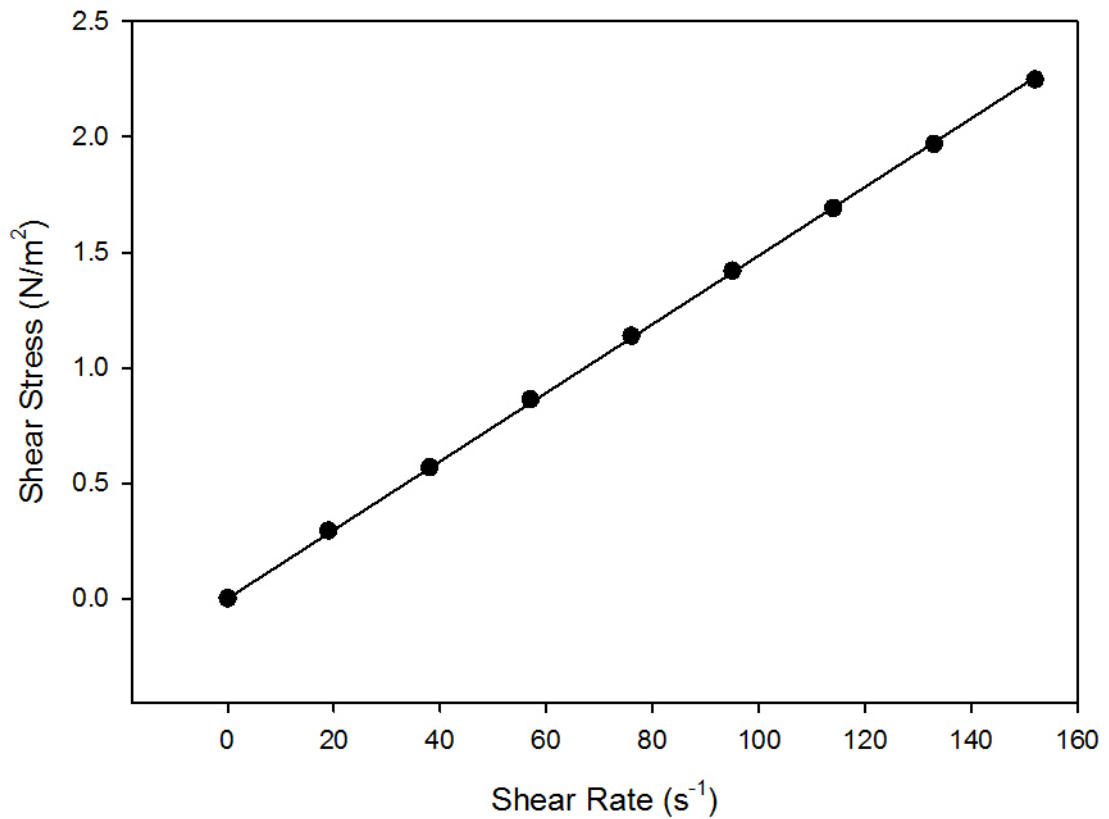
Figure 3.2 - Plot of shear stress versus shear rate for 60% glycerol (v/v) in water. Measurements were taken using a 1 mL sample of glycerol solution using Brookfield LVDVII cone and plate viscometer (Brookfield, Harlow, Essex)

Figure 3.2 shows the shear stress versus shear rate curve for 60% glycerol. As expected, the solution shows Newtonian behaviour and has a viscosity of 0.0149 Pas. In the literature the viscosity of 60% (v/v) glycerol at 20°C is reported as 10.96 cp or 0.01096 Pas. This is a little lower than the value obtained. However, the viscosity of 64% (v/v) glycerol in the literature is 14.42 cp or 0.01442 Pas (Sheely 1932). Consequently, the slightly higher than expected viscosity can be accounted for by experimental error in the preparation of the diluted glycerol solution.

The 60% glycerol solution was then used to investigate the pressure drop versus flowrate relationship in capillaries of different internal diameters and

cross sections. The change in pressure drop was measured using an Agilent HPLC with Chemstations software.   A P779 Nanotight union was attached to the end of the capillary immediately after the pressure sensor on the Agilent HPLC system. Fused silica capillaries of different cross-sections (circular and square cross sections) and different diameters/widths were obtained from Polymicro technologies (Polymicro technologies, Arizona, USA).   These capillaries were cut into 10 cm lengths.

In order to investigate the pressure drop versus flowrate relation for a capillary, firstly the glycerol solution was pumped though the system at the desired flowrate, without the capillary attached, the pressure reading was allowed to stabilise and the pressure drop reading was taken. The flow was then stopped and the 10 cm capillary was then attached to the system via the nanotight union. The flow was started and allowed to stabilize after which the pressure reading was taken again.   The flowrate was then increased and the pressure reading was allowed to stabilize after which the another pressure reading was taken. This process was repeated for different flowrates in the range of 100 µL min^{-1} to 400 µL min^{-1}. The pressure drop versus flowrate relationship of circular cross-section capillaries with internal diameters 75 µm, 100 µm and 150 µm, and square cross-section capillaries with internal diameters of 75 µm and 100 µm were investigated using this experimental technique.
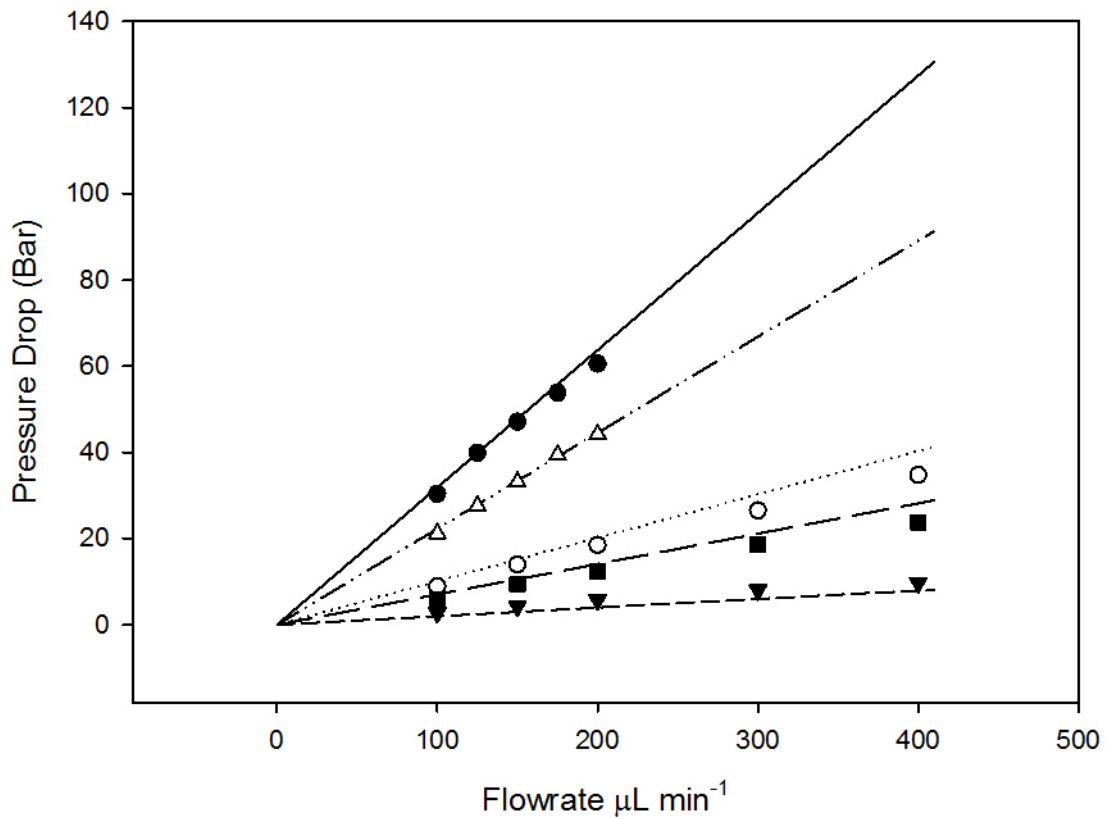
Figure 3.3 - Experimental verification of Hagen-Poiseuille flow equations for 10cm long circular and square cross section capillaries of different diameters. The data points represent the experimentally obtained data for pressure drop versus flowrate in these capillaries. The associated lines indicate the theoretical pressure drop versus flowrate relationship. The (●),(○) and (▼) indicate experimental data obtained for a 75µm, 100µm and 150µm ID circular cross-section capillaries respectively, while the solid black line, dotted line and short dashed line indicate the theoretical relationships.. The (△) and (■) indicate the experimental data obtained for a 75µm and 100µm width square cross-section capillary while t he dash-dot-dot line and long dashed line indicate the theoretical relationships

Figure 3.3 shows the experimental data obtained, as described above, compared with the theoretical pressure flowrate relationships calculated using the Hagen-Poiseuille flow equations (Equation 3.1and Equation 3.2 below) (Mortensen & Bruus 2006).

$$\Delta P = QR_{Hyd}$$ **Equation 3.1**

Where Q is the steady state flowrate and R_{hyd} is the hydraulic resistance. R_{hyd} can be described by the following equation

$$R_{hyd} = \frac{\alpha \mu L}{A_r{}^2}$$

Equation 3.2

Where A_r is the cross sectional area of the tube, L is the length of the tube, μ is the viscosity of the fluid (0.0149 Pas) and α is a dimensionless geometric correction factor.

Figure 3.3 show that there is very good agreement between the experimental results and the theoretical Hagen–Poiseuille flow equations at microscale and as such these equations may be used for calculation of the pressure drop at a given flowrate, at this scale, for Newtonian fluids.

3.3 Results and Discussion

This section begins by looking at the physical properties of BugBuster lysate in comparison with undisrupted *Escherichia coli* culture and cultures disrupted by other means. This information is used to validate the proposition to use BugBuster Mastermix™ as the lysis reagent for in-capillary lysis and to look at any potential issues this may present in a microfluidic device.

The impact of the ratio of BugBuster to broth is then investigated to identify the most appropriate mix for the micro lysis device.

Finally the impact of: a) the type of union used to bring the broth and lysis reagent together; b) the flowrate; and c) the residence time, on the performance of the lysis device, are investigated culminating in a lysis device design.

3.3.1 Comparison of the Rheological Properties of BugBuster Lysate with other Methods of Cell Disruption

The physical properties of BugBuster lysate were investigated, in comparison with undisrupted *Escherichia coli* culture and cultures disrupted by sonication, and homogenisation to understand how the BugBuster lysate is likely to behave in the microlysis device and validate its use in subsequent work. The first investigation that was undertaken was the measurement of the viscosity of BugBuster lysate as compared to undisrupted *E.coli* cell culture, sonicate and homogenate. Cell culture with an OD of approximately 8 Absorbance Units (AU) was disrupted by sonication, homogenisation and BugBuster lysis as described in Sections 3.2.3, 3.2.4 and 3.2.5 respectively.
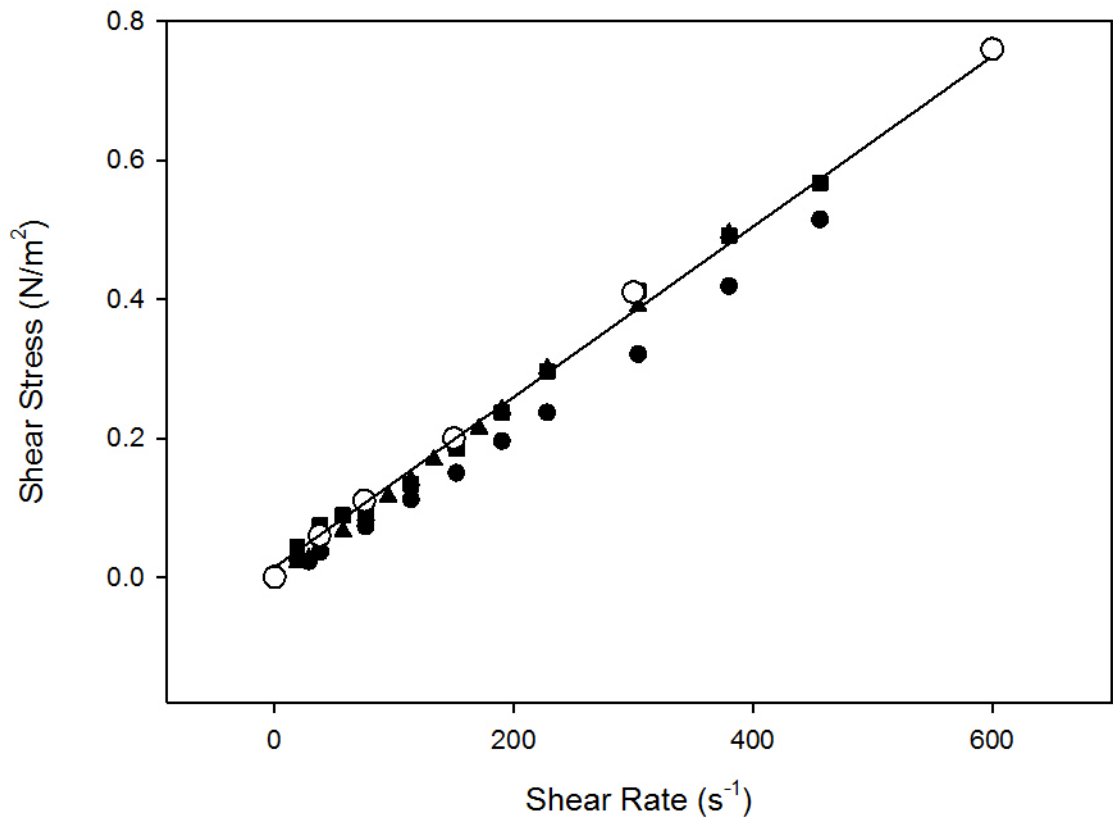
Figure 3.4 – Shear stress versus shear rate curves for *E.coli* culture OD 6.4 AU (●) sonicate of an *E.coli* culture of OD 6.4 AU (▲) homogenate of an *E.coli* cell culture with OD 9.5 AU (■) and BugBuster lysate obtained by adding equal quantities of OD 8 AU cell culture and BugBuster Mastermix™ (○). All optical densities were measured at 600nm.

Figure 3.4 shows shear stress versus shear rate curves for cell culture, homogenate, sonicate and lysate at ODs around 8 AU. From the graph it can be seen that the viscosities of the sonicate, homogenate and BugBuster lysate are similar and higher than the viscosity of the cell culture. The increased viscosity results from the release of the intracellular components of the *E.coli* in particular DNA and proteins (Ciccolini et al. 1999). From this graph the BugBuster lysate does not appear to be preferable to either the sonicate or homogenate in terms of viscosity, even though the cells are more diluted because of the addition of the BugBuster. A further study was undertaken at higher OD, as any differences in viscosity were likely to be more pronounced.
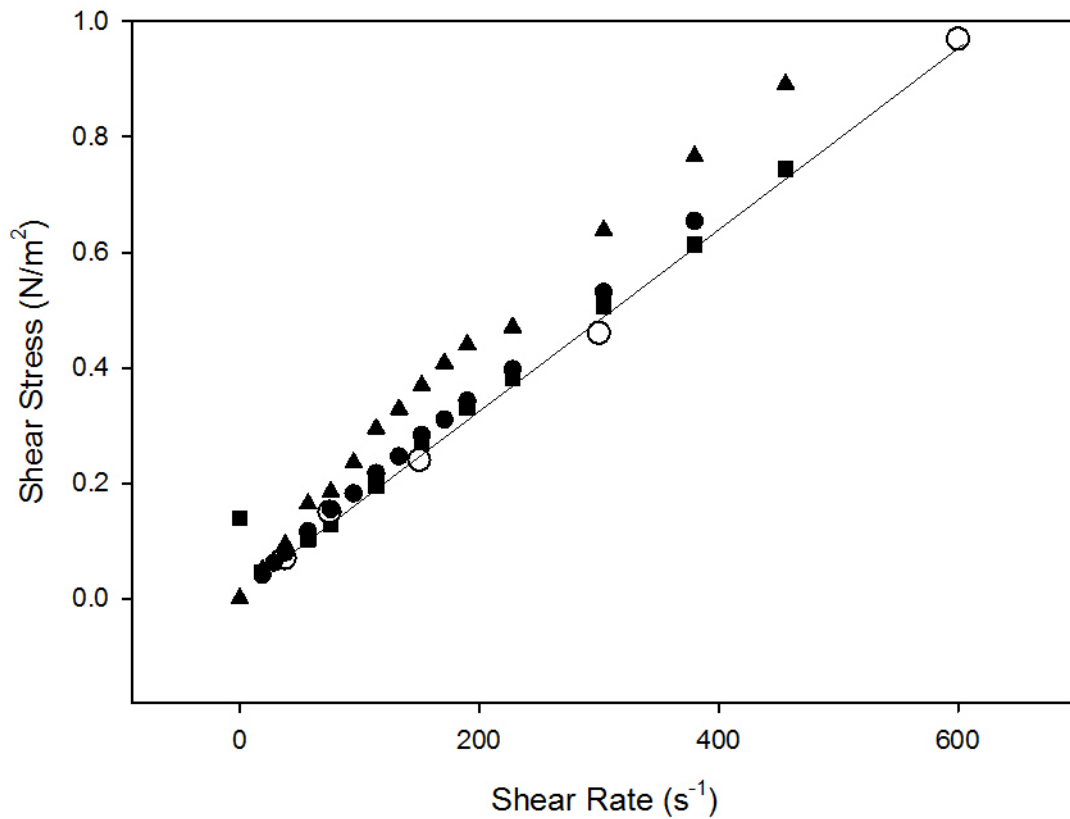
Figure 3.5 – Shear stress versus shear rate curves for *E.coli* culture OD 40 AU (●) sonicate of an *E.coli* culture of OD 41 AU (▲) homogenate of an *E.coli* cell culture of OD 41 AU (■) and BugBuster lysate obtained by adding equal quantities of OD 40 AU cell culture and BugBuster Mastermix™ (○). All optical densities were measured at 600nm.

Figure 3.5 shows shear stress versus shear rate curves for cell culture, sonicate, homogenate and BugBuster lysate for ODs of approximately 40 AU. From this graph there is a much clearer distinction between the viscosities of the samples. This is because the cell concentration is higher at higher ODs and so the protein and DNA concentrations in the disrupted sample are also be higher. It is however of note that the BugBuster lysate viscosity is very similar to that of the cell culture. This is thought to be for two reasons. Firstly, the fact that an equal volume of BugBuster to cell culture is added in order for the lysis to proceed would mean that the actual concentration of cellular material in the BugBuster lysate is significantly less than in the cell culture. The second

reason is that, it is thought that, the nuclease (approximately 25 units/mL of Benzonase) in the BugBuster Mastermix™ digests the DNA reducing the viscosity of the sample.

It is also of note that the OD40 AU BugBuster lysate shear stress versus shear rate curve in Figure 3.5 is very similar to the OD41 AU cell culture shear stress versus shear rate curve in Figure 3.8. This is because the Optical Density stated for the BugBuster lysate curve is the Optical Density before the BugBuster was added. As mentioned above, the addition of BugBuster dilutes the sample to 50% of its initial concentration.

Table 3.1 compares the apparent viscosities obtained by Ciccolini *et al* with the viscosities obtained in this research. In order to provide a basis for comparison, the wet cell concentration of 12.5g per 100mL reported in Ciccolini *et al* was divided by four to convert it to dry cell weight concentration. This factor was chosen as other researches have found the wet cell weight to be around four times the dry cell weight for the same concentration of *E.coli* cells (Veide et al. 1983). For the sonicate, homogenate and 50% BugBuster lysate, the Optical Densities were used to calculate dry cell weight using the calibration factor provided in Section 3.2.2. The dry cell weights for both 50% BugBuster lysates were then divided by two to take in to account the dilution resulting from the addition of BugBuster Mastermix™.

As can be seen in Table 3.1, viscosities found by Ciccolini *et al* are two orders of magnitude larger than those presented for the BugBuster Lysate, sonicate and homogenate obtained in this work at lower shear rates, and one order of

magnitude larger at higher shear rates. This is thought to be for two reasons. Firstly, the cell concentration used in Ciccolini *et al* work is higher than the cell concentrations used in this work. Secondly, as Ciccolini *et al* conclude, the rheology of the alkaline lysates investigated were dominated by the release and denaturation of macromolecules, particularly chromosomal DNA. This resulted in the higher viscosities and non-Newtonian behaviour of the alkaline lysate (Ciccolini et al. 1999). It is thought that nuclease in the BugBuster Mastermix ™ digests the DNA in the lysate causing it to behave as a Newtonian fluid and reducing its viscosity .

Comparing the viscosities of OD 120 AU BugBuster lysate with OD41 AU Homogenate and Sonicate in Table 3.1, it is observed that the concentration of cells in the OD120 AU 50% Bugbuster lysate is significantly higher than the concentration of cells in the OD41 AU sonicate and homogenate, but the viscosity of the BugBuster lysate is significantly lower than that of the sonicate and similar to that of the homogenate. This adds further weight to the argument that the digestion of DNA by the nuclease present in BugBuster Mastermix™ is responsible for the reduced viscosity of the BugBuster lysate.

Overall, whilst at low ODs there is little difference in the rheological properties of the *E.coli* BL21 samples disrupted by homogenisation, sonication and BugBuster Lysis, at higher ODs BugBuster lysis is preferred at the microscale because of the reduced viscosities which would lead to better mixing and lower pressure drops.

Table 3.1 – Table comparing the apparent viscosities obtained by Ciccolini *et al* with: the viscosites obtained for OD41 AU *E.coli* sonicate; OD41 AU *E.coli* homogenate; and 50% BugBuster lysates of OD 40 AU and OD120 AU *E.coli* cell cultures. The Optical densities quoted for the Bugbuster lysate are for the cell culture before the addition of BugBuster Mastermix™

	E.coli Concentration (g dry cell weight/L)	Shear rate (s^{-1})				
		46	116	367	461	581
Peak Apparent Viscosity for of alkaline lysate *E.coli* c600/ pR26 cell suspension (mPas) (Ciccolini et al. 1999)	31.3	130	110	35	30	25
Pseudo steady state viscosity of alkaline lysate *E.coli* c600/ pR26 cell suspension (mPas) (Ciccolini et al. 1999)	31.3	40	35	16	13	12
Viscosity of OD41 AU *E.coli* BL21 cell suspension homogenate (mPas)	15.8			1.65		
Apparent Viscosity of OD41 AU *E.coli* BL21 cell culture sonicate (mPas)	15.8	2.83	2.44	2.03		
Viscosity of OD40 AU *E.coli* BL21 cell culture 50% (v/v) Bugbuster Mastermix™ lysate (mPas)	7.7			1.38		
Viscosity of OD120 AU *E.coli* BL21 cell culture 50% (v/v) Bugbuster Mastermix™ lysate (mPas)	23.1			1.68		

3.3.2 *Study of the Rheological Behaviour of BugBuster Lysate over Time*

To understand how the BugBuster chemical lysis proceeds over time, and to assess whether viscosity is likely to be an issue as time progresses, the rheological behaviour of BugBuster lysate over time was investigated. In order to do this, BugBuster lysis was performed in a stirred bijou as described in Section 3.2.5. Samples were taken at 5, 15, 30 and 60 minutes and the shear stress versus shear rate relationship was measured using a Brookfield Viscometer as described in Section 3.2.7. Measurements of the Glutathione-S-Transferase activity were also taken at these sampling times using the microwell plate CDNB assay as described in Section 2.5.
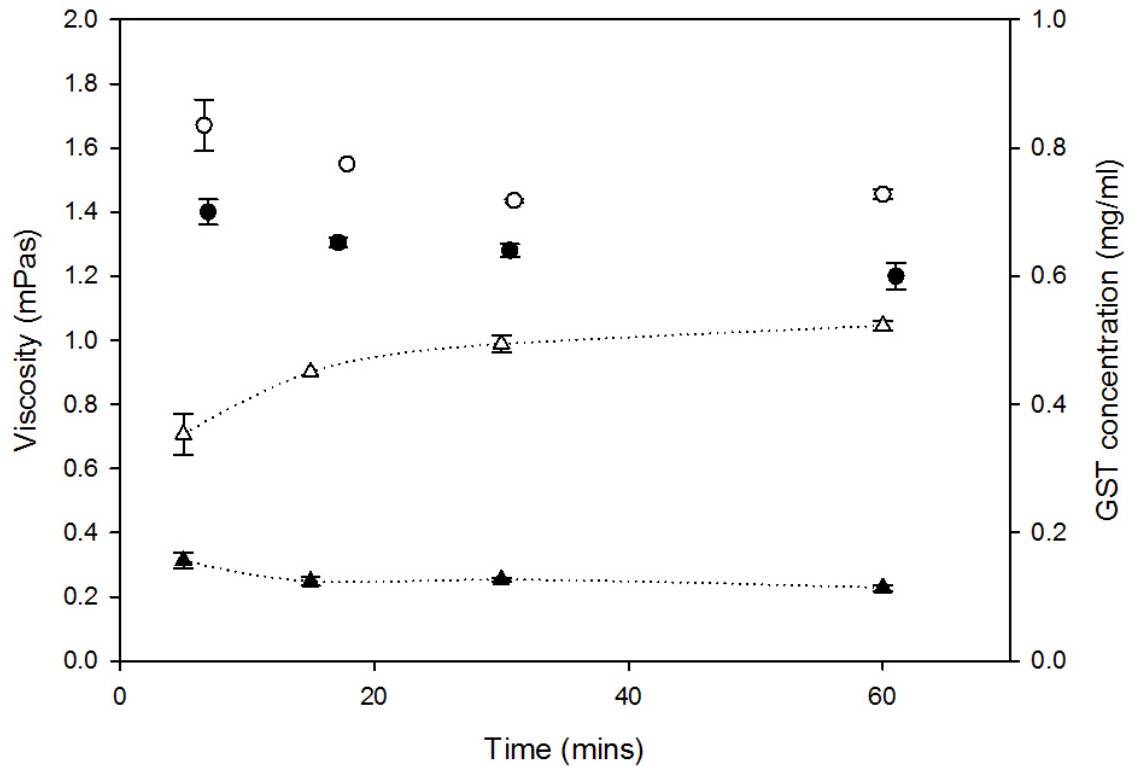
Figure 3.6 – Viscosity versus time curves for BugBuster lysis using 50% BugBuster and 50% cell culture. The (●) shows the viscosity versus time relation for OD 8 AU cell culture undergoing lysis with BugBuster. The (○) shows the viscosity versus time relation for OD 40 AU cell culture undergoing lysis with BugBuster.   The (▲) shows the how the concentration of active Glutathione S Transferase changes with time for the OD8 lysis.   The (△) shows the how the concentration of active Glutathione S Transferase changes with time for the OD 40 AU lysis.

Figure 3.6 shows the rheological behaviour of the BugBuster lysis over time.

Overall, at both ODs, the viscosity of the lysate reduces over time. It is thought

that, in this well mixed system the majority of the lysis happens in the first 5

mins, when the viscosity is at a maximum.   The subsequent decrease in

viscosity is thought to be as a result of the nuclease in the BugBuster

Mastermix™ lysis agent which digests the DNA, breaking it down, and reducing

the overall viscosity of the sample. The GST activity curves also shown on this

graph present two different profiles, for the change in protein activity, at the

different ODs.   The first, at OD 8 AU, shows reduction in protein activity over

time. It is thought that this reduction is due to the proteases in the lysate

attacking the Glutathione-S-Transferase and reducing the activity. Since the cell lysis event is essentially a reaction between the cell wall and the lysis agent, at OD 8 AU, it is thought that because of the low concentration of cells, any subsequent lysis that occurs, to cells not lysed in the first 5 mins, is not sufficient to compensate for lost GST activity due to proteolytic reactions taking place. At OD 40 AU however, the profile is different. The concentration of active GST increases with time. This is thought to be because the higher concentration of cells means that additional lysis happening after the first 5 mins is sufficient to more than compensate for the activity lost by proteolytic enzymes and hence increase the overall activity of the lysate.

Both sets of results show that after the first five minutes there are unlikely to be any viscosity problems in the microfludic lysis device. There does, however, remain some uncertainty over what happens in terms of rheological behaviour in the first 5 mins, but the practicalities of measuring the viscosity with the available equipment make it difficult to get data in this time range.

3.3.3 Rheological Behaviour of BugBuster Lysate at Different ODs

In order to investigate whether there are likely to be any pressure drop considerations in the microlysis device, rheological studies of the shear stress shear rate relationship for both cell culture and BugBuster lysate at ODs of up to 120 AU were investigated. The shear stress/shear rate relationship was measured with a Brookfield Viscometer as described in Section 3.2.7.
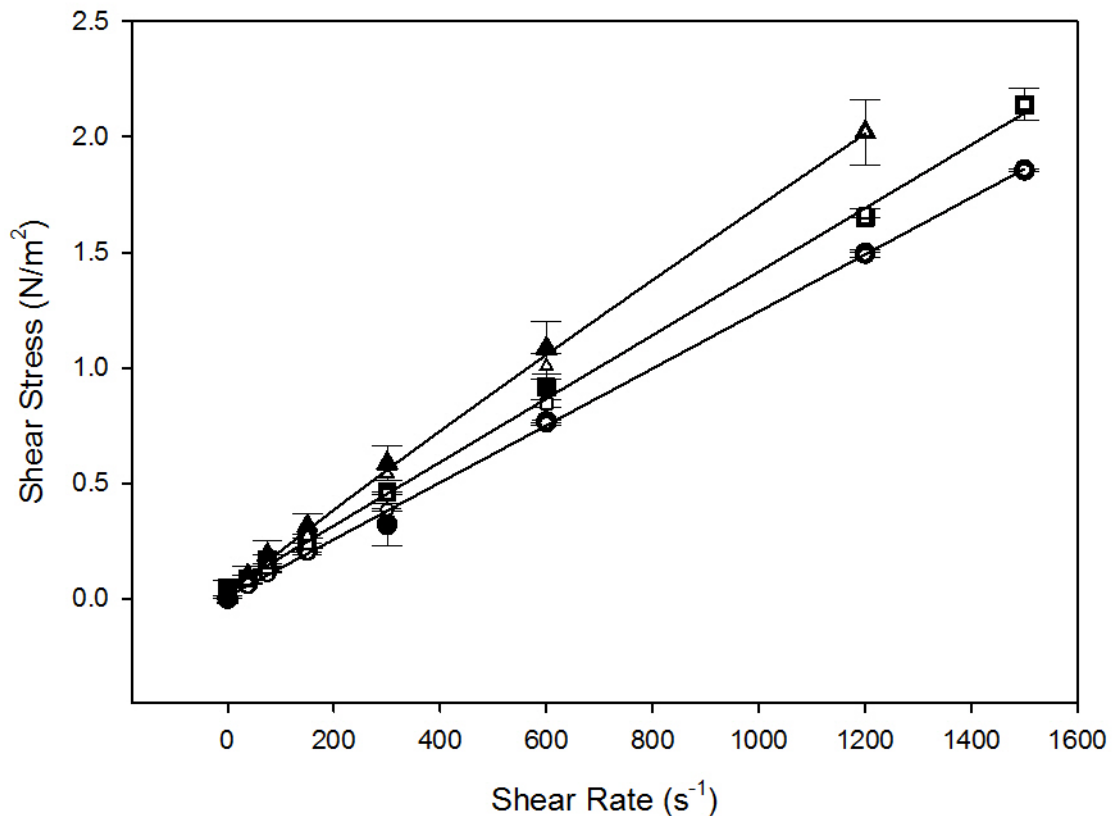
Figure 3.7 – 50% BugBuster lysate shear stress versus shear rate curves at approximately 5 mins into the lysis. The (●) shows the shear stress / shear rate relationship for OD 8 AU *E.coli* culture undergoing lysis with 50%(v/v) BugBuster Mastermix™ and 50% (v/v) OD8 AU Cell culture while the shear rate is being increased in the viscometer. The (○) shows the same shear stress /shear rate relationship while the shear stress is being decreased. The (■) shows the shear stress/shear rate relation for 50% (v/v) BugBuster and 50% OD 40 AU cell culture while shear rate is increasing and the (□) shows the same relation while shear rate is decreasing. Finally the (▲) shows the shear rate increasing shear stress/shear rate relation for 50% OD 121 AU cell culture and 50% BugBuster and the (△) shows the shear rate decreasing relation for the same OD.

Figure 3.7 shows the shear stress versus shear rate curves for BugBuster lysis

undertaken with cell cultures of ODs of 8 AU, 40 AU, and 120 AU, at 600nm. It

is of note that, at all ODs, the behaviour of the shear stress versus shear rate

curves of the BugBuster lysates can be approximated to that of a Newtonian

fluid. It is also of note that there is little difference in the shear stress/shear rate

relationship while the shear rate is increasing, as compared to the shear rate

decreasing. This indicates that no hysteresis is taking place and that the lysate

is not being damaged by the measurement process.
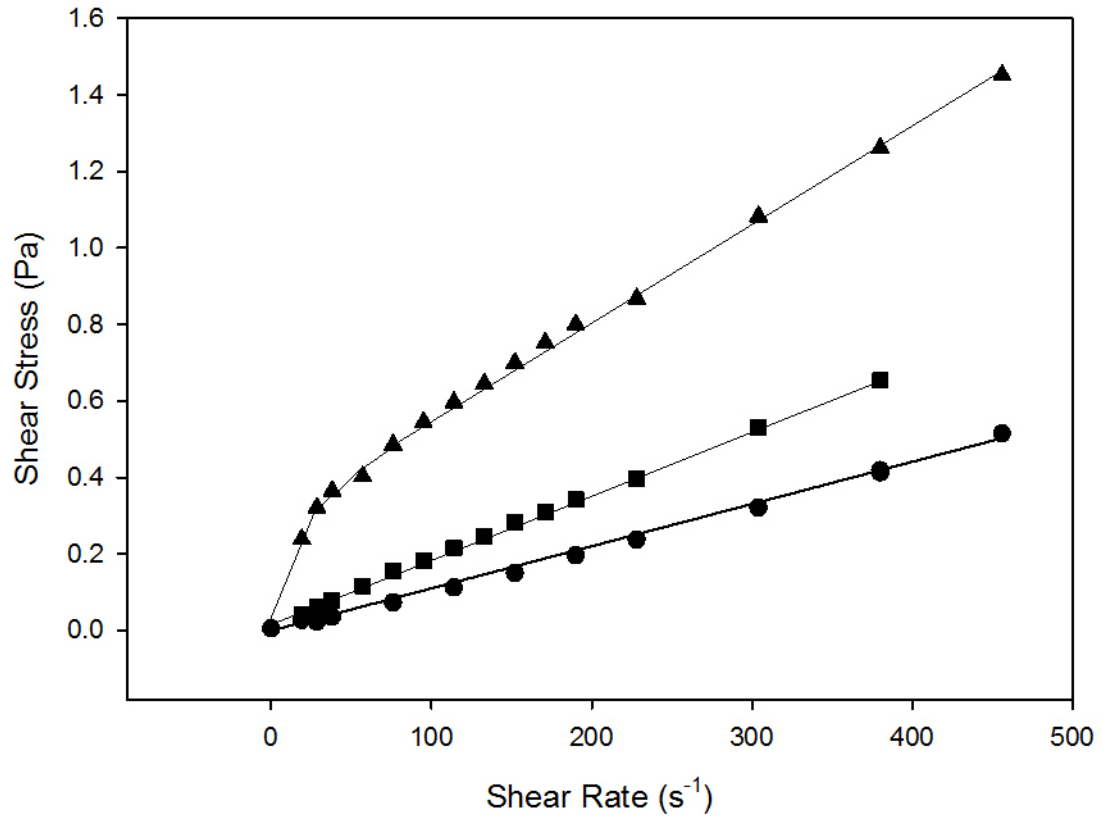
Figure 3.8 – Undisrupted *E.coli* culture shear stress versus shear rate curves. The (●) shows the shear stress/shear rate relationship for OD 6.4 AU *E.coli* culture. The (■) shows the shear stress/shear rate relationship for OD 41 AU cell culture while shear rate is increasing. Finally the (▲) shows the shear stress/shear rate relationship for cell culture OD 131 AU.

Figure 3.8 shows the shear stress versus shear rate curves for cell cultures with

ODs of 6.4 AU, 41 AU, and 131 AU at 600nm. At ODs of 6.4 AU and 41 AU the

cell culture behaves as a Newtonian fluid. However at an OD of 131 AU the

fluid behaves as a pseudoplastic fluid, i.e. viscosity decreases with increasing

shear rate. This is due to the microbial cells in suspension. Blood, which is

also essentially cells in suspension, is also a pseudoplastic fluid.

To understand which flowrates were feasible in a microfluidic lysis device with 50% BugBuster lysate or *E.coli* culture up to ODs of 131 AU, the pressure drop versus flowrate relationships were evaluated and plotted. For all ODs of BugBuster lysate and OD 6.4 AU and 41 AU of the broth, it was possible to use the Hagen-Poiseuille equations. However, because at OD 131 AU the *E.coli* culture is pseudoplastic in nature COMSOL (COMSOL Ltd, Massachusetts, USA) was used to obtain the pressure drops over the range of flowrates.
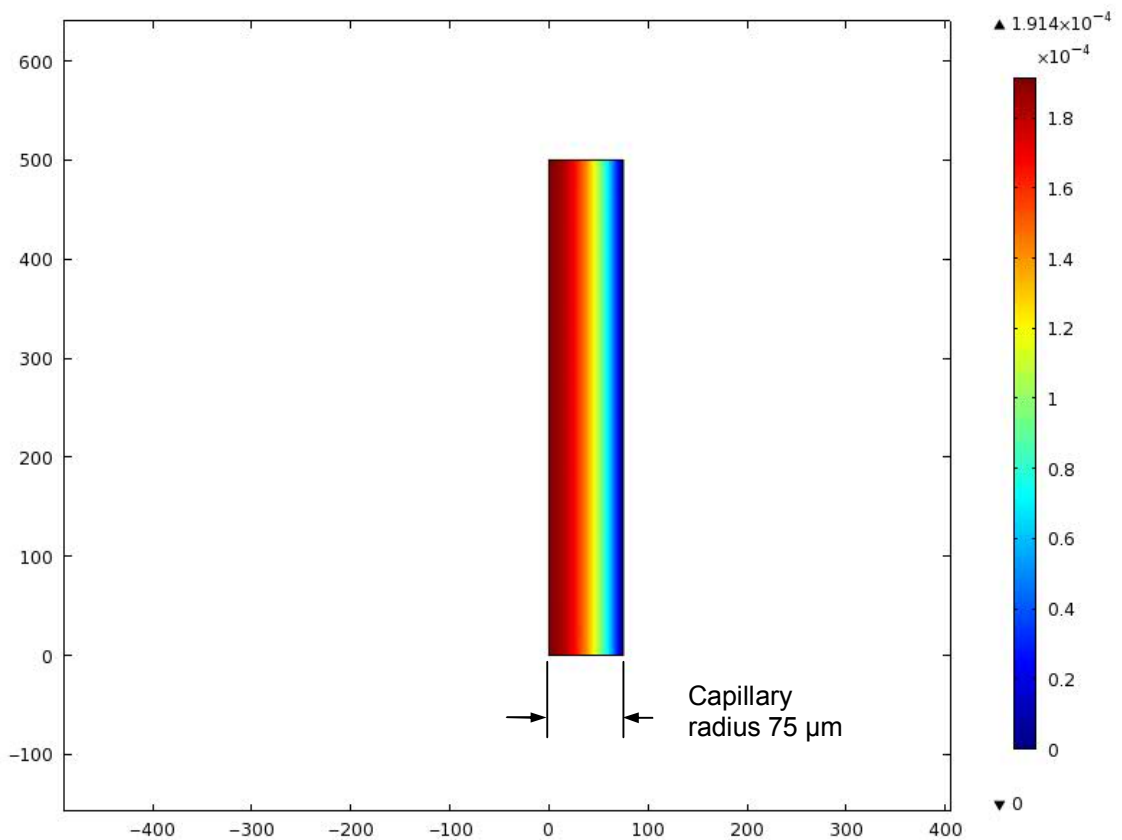
Figure 3.9 – Velocity surface plot of a 75µm by 500µm slice of 150µm internal diameter capillary used to model flow of *E.coli* cell culture with an optical density of 131 AU. The inlet flowrate for this plot is 1µL min⁻¹. The axes of the plot show the x and y dimensions in µm.

Figure 3.9 shows a typical velocity surface plot obtained for a 75µm by 500µm slice of the capillary. The pressure drop value obtained from COMSOL for each flowrate was multiplied by 2000 to give an estimate of the pressure drop across a 1 m capillary.
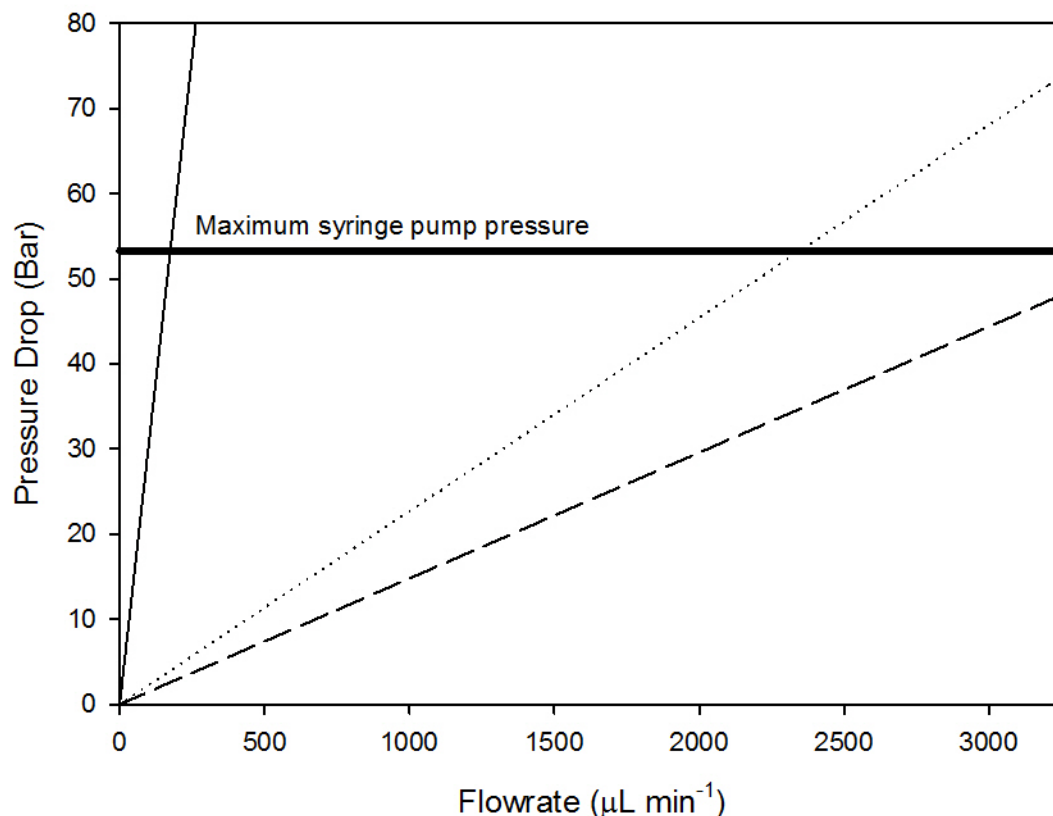
Figure 3.10 – Plot showing the pressure drop versus flowrate relationship for different OD E.coli cultures flowing in a 150 μm internal diameter capillary. The dashed line shows the pressure drop versus flowrate relationship for OD 6.4 AU cell culture. The dotted line shows the pressure drop versus flowrate relationship for OD 41 AU culture. The solid thin line shows the pressure drop versus flowrate relationship for BugBuster lysis of OD 131 AU culture. The OD 6.4 AU and OD 40 AU lines were plotted using the Hagen-Poiseuille equation. The OD 131 AU was plotted by modelling a slice of the capillary in COMSOL. The thick solid line indicates the maximum pressure the Kd scientific syringe pump used in subsequent experiments could apply when pumping using a 500μL syringe.

Figure 3.10 shows the velocity pressure drop relation for different ODs of cell culture and Figure 3.11 shows the velocity pressure drop relation for different ODs of BugBuster lysate. Both represent the pressure drop in a 150μm internal diameter capillary which is 1m in length, this capillary was chosen as this was intended to be the smallest capillary in the device, i.e. the capillary that would be delivering the feed streams to the lysis device.
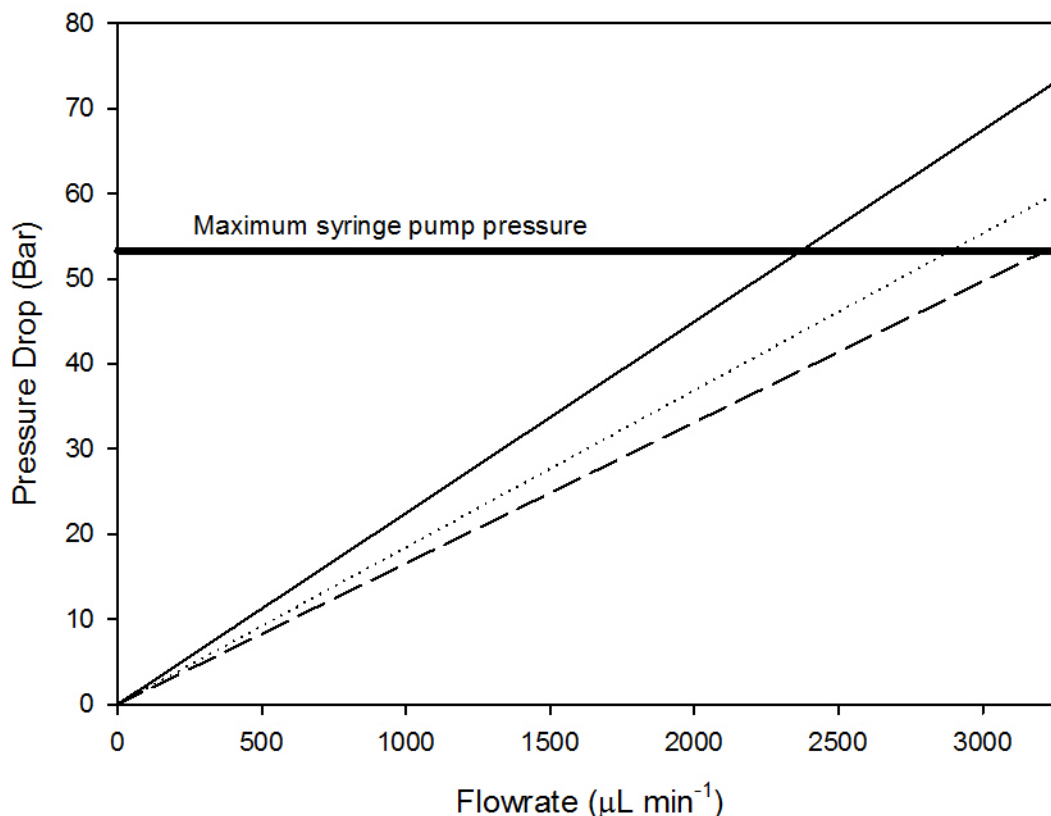
Figure 3.11 - Plot showing the pressure drop versus flowrate relationship for BugBuster lysates of different OD *E.coli* cultures flowing in a 150µm internal diameter capillary. The dashed line shows the pressure drop versus flowrate relationship for BugBuster lysis of OD 8 AU cell culture. The dotted line shows the pressure drop versus flowrate relationship for BugBuster lysis of OD 41 AU culture. The solid thin line shows the pressure drop versus flowrate relationship for BugBuster lysis of OD 121 AU culture. These relations were calculated using the Hagen-Poiseuille equation. All BugBuster lysis were undertaken using 50% *E.coli* culture and 50% BugBuster (v/v). The thick solid line indicates the maximum pressure the Kd scientific syringe pump used in subsequent experiments could apply when pumping using a 500µL syringe.

It is clear from both graphs that in order to get pressure drops sufficiently high to start causing problems with pumping and leaks, flowrates of several ml per minute are required for the BugBuster lysate and several hundred microlitre per min for the cell culture (at the highest ODs). These are both well above the intended flowrates being considered. The range of flowrates to be investigated is 0-30µL min^{-1} to enable compatibility with the chromatography step.

Consequently pressure drop in the microlysis device does not give too much cause for concern.

3.3.4 Determination of the Optimum BugBuster Concentration

In order to ascertain the optimum mixture of cell culture and BugBuster for continuous microlysis, the effect of BugBuster concentration on the degree of lysis was investigated. The degree of lysis was obtained by measuring the quantity of GST released by the BugBuster lysis using the micro CDNB assay, as described in Section 2.5. This was compared to the quantity of GST in unlysed cell culture and sonicate. Equation 3.3 shows how the degree of lysis was calculated.

$$D_L = \frac{C_L - C_C}{C_S - C_C}$$ **Equation 3.3**

Where D_L is the degree of lysis C_L is the concentration of GST in the lysate under investigation, C_C is the concentration of GST on unlysed cell culture and, C_S is the concentration of GST in a sonicate of the cell culture. The sonicate was prepared as described in Section 3.2.3
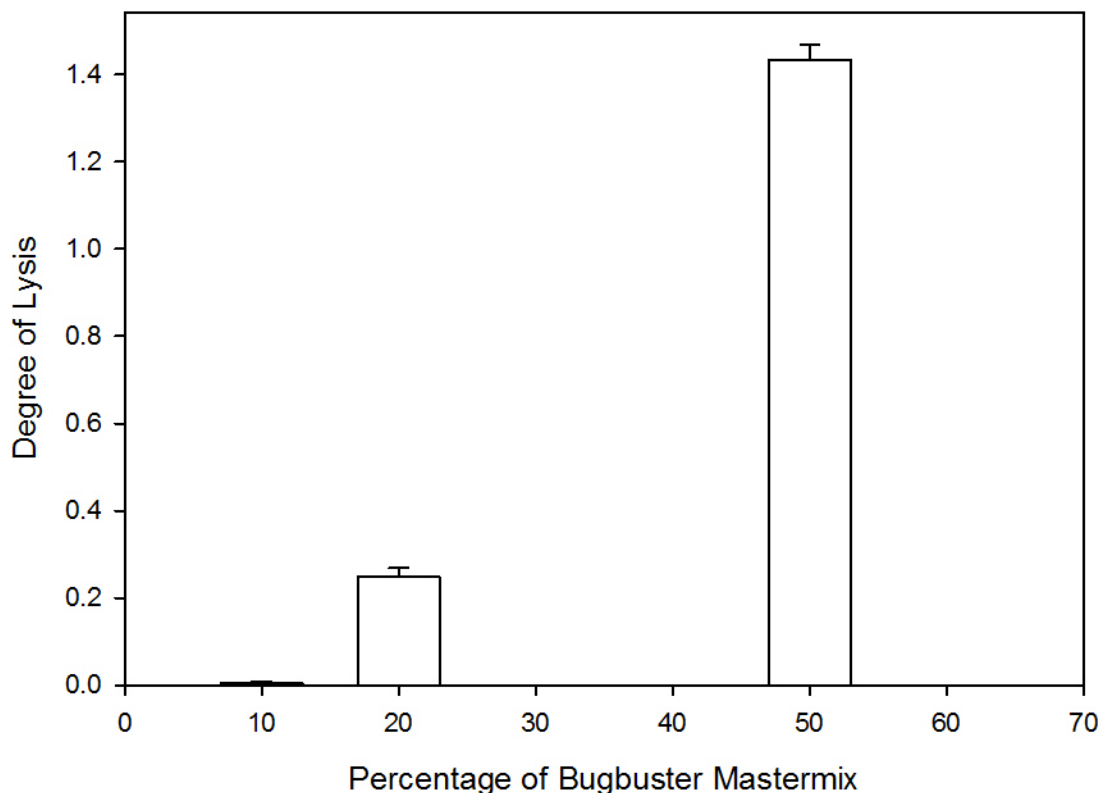
Figure 3.12 – Figure showing the degree of lysis obtained by lysing *E.coli* culture OD 4.5 AU with different concentrations of BugBuster Mastermix™. The lysis was carried out in a stirred bijou. The 10% BugBuster lysis was carried out by pipetting 1.8 mL of cell culture into an empty bijou tube. A stirrer bar was placed inside the bijou tube and the bijou was placed on top of a magnetic stirrer plate and secured with autoclave tape. The stirrer was then started and 200 μL of BugBuster Mastermix™ was added to the cell culture. The bijou tube was then covered with parafilm to minimise evaporation from the surface of the mixture. The lysis was allowed to proceed for one hour. The 20% and 50% BugBuster lysis were carried out in the same manner except 1.6mL of cell culture and 400 μL of BugBuster and 1 mL of cell culture and 1 mL of BugBuster were used respectively.

Figure 3.12 shows the degree of lysis obtained by lysing *Escherichia coli* in a

stirred bijou with different concentrations of BugBuster Mastermix™. From this

graph it is clear that lysis performed with 10% and 20% (v/v) achieved just a

fraction of the protein release of sonication. Lysis with 50% (v/v) BugBuster,

however, results in much greater protein release, even outperforming

sonication. Consequently 50% (v/v) BugBuster lysis was chosen for the continuous micro lysis experiments.

Researchers looking at the similarity of performance, by measuring percentage of soluble protein release found that BugBuster lysis and sonication were dissimilar (Listwan et al. 2010). However, their results show that for some fragments BugBuster can outperform sonication. So these results do not necessarily disagree with theirs. It also worth noting that the lysis reagent used in that research was BugBuster, and not BugBuster Mastermix™, and so did not contain Lysosyme whereas BugBuster Mastermix™ does. Lysosyme helps in the lysis of the cells by breaking down the peptoglycan structure in the cell wall.

3.3.5 Investigation of the effect of lysis device design on lysis

In order for lysis to occur, the lysis agent and cells must be well mixed and sufficient time for the lysis to proceed must be allowed. Consequently, the devices that were designed consisted of two components, a union fitting to bring together the cell culture and BugBuster streams, and a length of capillary to allow the lysis to proceed whilst flowing through the device. Fused silica capillary with a 700µm internal diameter was chosen for this as it would allow studies over the range of flowrates and residence times required, without having an unmanageable length of capillary and without an excessive pressure drop.

This first part of the investigation focuses on the type of union fitting that would achieve the best mixing and hence lysis. Three different unions were tested: A T-piece with 152µm thru-hole (Small T-Piece); a T-Piece with a 500 µm thru-

hole (Large T-Piece); and a Teardrop mixer (Micronit, Enschede, The Netherlands)
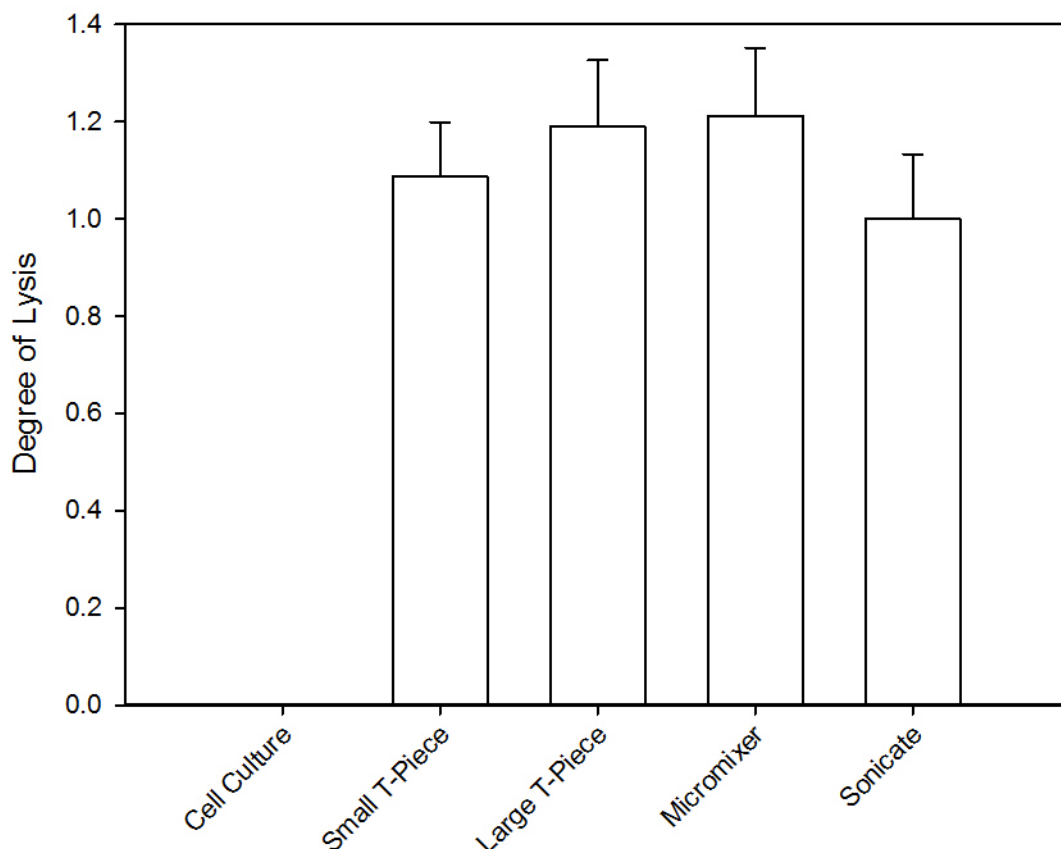
Figure 3.13 – Figure showing the degree of lysis obtained by continuous lysis with different lysis devices of OD 4.5 AU culture. The lysis device consisted of two 15cm long inlet capillaries. The union fitting for mixing of the two inlet streams was either a: Small T-Piece (P-890 micro tee with 152 micron thru hole); a Large T-Piece (P-727 tee with 0.5 mm thru-hole); or a Teardrop micromixer. The outlet capillary had an internal diameter of 700μm. The length of the outlet capillary was 100cm in order to achieve a residence time of 30 mins. The flowrate was kept constant at 12.828 μL min^{-1}.

Figure 3.13 shows the degree of lysis obtained with the three different types of union fitting. Using the Small T-Piece (with the 152μm thru-hole) results in less protein release than the other two types of union, and there is very little difference between the degree of lysis obtained with the teardrop micromixer and the Large T-piece.

In order to determine whether there is a statistically significant difference between the degree of lysis obtained using the small T-piece as compared to the other two types of union used, a t-test was performed on the results for the small T-piece and the micromixer. The p value obtained was 0.523 showing that the difference is not statistically significant. Consequently, the performance of the lysis device is insensitive to the type of union used to mix the BugBuster Mastermix™ and the *E.coli* cell culture

During experimentation the teardrop mixer did tend to block up quite frequently and was much more difficult to clean. Due to the size of the small T-Piece's through hole, 152µm, there may also be difficulties with blocking of the small T-piece. Therefore, the T-piece with 500 µm thru-hole (Large T-Piece) was chosen for further work.

3.3.6 Investigation of the effect of residence time on the degree of lysis

As described in Section 3.3.5 chemical lysis requires a length of capillary in which the lysis can proceed. The optimum length of the capillary used depends on the diameter of the capillary, the flowrate; and the effect of residence time on the degree of lysis. The effect of residence time on the degree of lysis was investigated, by measuring the quantity of protein released during lysis. For these experiments the flowrate was fixed at 12.828µL min^{-1}, the diameter of the capillary was also kept constant at 700µm. The length of the outlet capillary was varied, from 8.33cm to 2m, to result in different residence times.
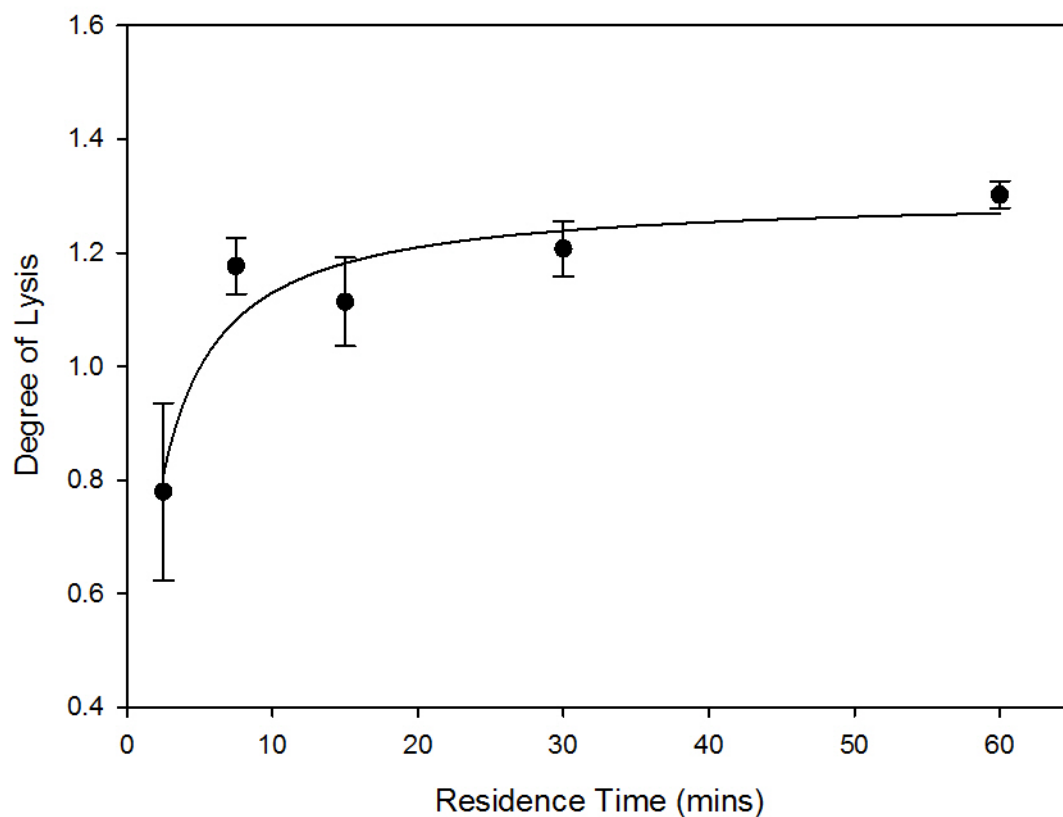
Figure 3.14 – Graph showing the effect of residence time on the degree of lysis of OD 4.5 AU culture. The lysis device consisted of two 15cm long inlet capillaries. The union of the two inlet streams was a P-727 tee with 0.5 mm thru-hole (IDEX Health and Science, Washington, USA). The outlet capillary had an internal diameter of 700μm. The length of the outlet capillary was varied in order to change the residence time. The flowrate was kept constant at 12.828 μL min^{-1}.

Figure 3.14 shows the effect of the residence time on the degree of lysis. As expected the degree of lysis appears to increase with residence time. However, the majority of lysis happens quite quickly, as the degree of lysis obtained with a residence time of 60 mins, is estimated to be only about a 14% greater than obtained with a residence time of 5 mins. It is also of note that there is quite significant error in the degree of lysis data obtained for a residence time of 2.5 mins.

In order to determine whether there is a statistically significant difference between the degree of lysis obtained as a result of different residence times in the device, a t-test was performed on the degree of lysis obtained after 2.5mins compared to that obtained after 60 mins. The p value obtained was 0.030 showing that the difference is statistically significant. However, given the large errors on the degree of lysis obtained after 2.5mins, t-tests were also obtained for: the degree of lysis obtained after 7.5mins compared to 60mins; and the degree of lysis after 15 mins also compared to 60mins. The p values obtained for these t-test were 0.084 and 0.082 respectively, which are a little large than the 0.05 threshold for rejecting the null hypothesis. Further repeats of this investigation would therefore be useful as it is possible that there may be a statistically significant relationship between residence time and degree of lysis.

Comparing the degree of lysis obtained after 60 min in the microlysis device (Figure 3.14), with the degree of lysis obtain with 50% BugBuster, after 60 min in a stirred bijou tube, shown in Figure 3.12, it is of note that the degree of lysis values obtained are similar. This suggests that the cell culture and BugBuster Mastermix™ are mixing well in the microlysis device.

Overall, any of the residence times, greater than 5 mins would give sufficient protein release. However, with the aim of minimising sample quantity and processing time, the shortest residence time possible, which would also give the lowest device volume, should be chosen. This combined with the reproducibility of results means that a residence of about 7.5mins is likely to provide the best performance.

3.3.7 Investigation of the effect of flowrate on the degree of lysis

In order to ascertain the optimum flowrate for the microlysis step, the effect of flowrate on the degree of lysis was investigated. The residence time was kept constant at 7.5 mins and the outlet capillary external diameter, as in previous experiments, was maintained at 700 μm. A residence time of 7.5 mins was chosen as this would minimise the experiment run time, and the volume of sample required, whilst still providing good lysis. The length of the outlet capillary was varied between 6.25 cm and 50 cm to allow the residence time to remain constant while the flowrate was varied between 3.207μL min^{-1} and 25.656μL min^{-1}.

Figure 3.15 shows the effect of flowrate on the degree of lysis. The graph appears to show that better lysis is achieved at higher flowrates, possibly as a result of better mixing. However, the degree of lysis obtained at the highest flowrate 25.656μL min^{-1} is only about 30% better than that obtained at the lowest flowrate, 3.207μL min^{-1}. In addition it can be seen that there is little change in the degree of lysis obtained at flowrates above approximately 10μL min^{-1}. These differences look to be within the experimental errors.

In order to determine whether there is a statistically significant difference between the degree of lysis obtained at different flowrates, a t-test was performed on the data obtained at a flowrate of 3.207μL min^{-1} as compared to that obtained at a flowrate of 25.66μL min^{-1} The resulting p value was 0.219 showing that the difference is not statistically significant. Consequently, it is concluded that the degree of lysis is insensitive to changes in the flowrate. This is probably because flow in the microlysis device is laminar over the range of flowrates investigated, resulting in mixing by diffusion only. To verify this, the

Reynolds number, at flowrate of 25.656µL min^{-1}, in a 700µm internal diameter tube, was calculated using Equation 1.2 using the properties of water. The Reynolds number was found to be 0.874. This is clearly in the laminar regime.
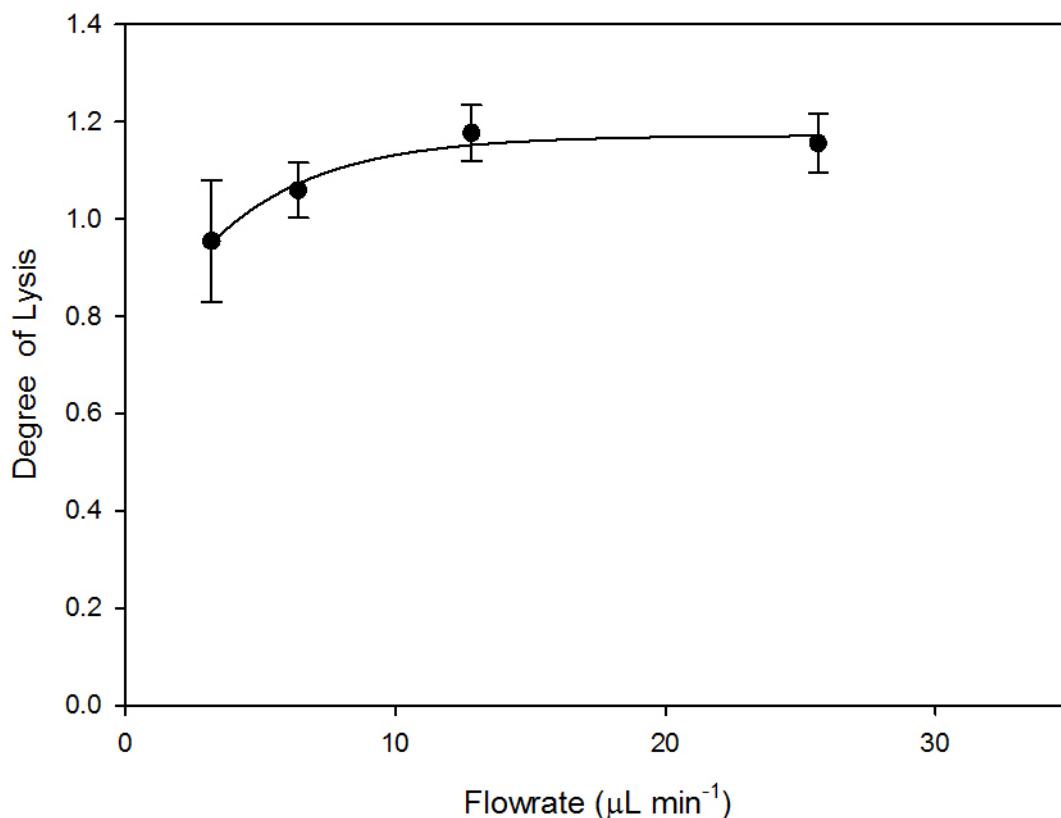
Figure 3.15 – Graph showing the effect of flowrate on the degree of lysis compared to sonication of OD4.5 culture. The lysis device consisted of two 15cm long inlet capillaries. The union of the two inlet streams was a P-727 tee with 0.5 mm thru-hole (IDEX Health and Science, Washington, USA). The outlet capillary had an internal diameter of 700µm. The length of the outlet capillary was varied in order to maintain a constant residence time of 7.5mins

Given the objective of this work to minimise processing time and sample quantity, whilst recovering sufficient sample of sufficient purity, the flowrate used in the lysis step should be minimised. This is because at lower flowrates shorter outlet capillaries will be required to achieve the same residence time. In addition, flowrates in the same range as those used in the microaffinity

chromatography column would aid joining the two devices. Consequently, flowrates in the range of 3.207 µL min^{-1} to 6.414 µL min^{-1} were chosen. Running the lysis in this range would result in a lysis device with a volume of 30 µL to 60 µL.

3.3.8 Investigation of the effect of Bugbuster Lysis on Particle Size

Initial particle size experiments were undertaken in order to investigate the impact of lysing cells with Bugbuster Mastermix™ on particle size. Preliminary particle size data obtained for *Escherichia coli* cell culture and BugBuster lysates, measured using a Zetasizer Nano ZS (Malvern Instruments Ltd, Worcestershire, UK,) did not show a significant difference in particle size. This may suggest that lysis is achieved permeabilisation of the cell wall rather than by complete disintegration which would produce a lot of fine particles. However, as this is only preliminary data, further work is needed in this area.

If perforation of the cell wall is the mechanism of lysis, it has positive implications for coupling the microlysis device with the microaffinity chromatography device, as larger particles are easier to remove by filtration or inertial forces.. The use of inertial forces and filtration to remove particulates for the purpose of coupling the microlysis and microaffinity chromatography devices is discussed further in Section 7.3.

3.4   Summary of Findings and Conclusions

In order to verify the Hagen-Poiseuille flow equations at the micro scale, the pressure drop versus flowrate relationship for 60% glycerol (v/v) solution was investigated in capillaries of different diameters and cross sections and there was shown to be good agreement between the experimental and theoretical values.

The rheological properties of BugBuster lysate were investigated, both to compare viscosity with that of homogenate and sonicate, and to look for changes in viscosity over time. BugBuster lysate compared favourably to sonicate and cell culture in terms of viscosity at OD 40 AU, and had a similar viscosity at OD 8 AU. Over time, it was found that the viscosity was greatest in the first 5 minutes after which it decreased. This indicated that viscosity was unlikely to be an issue in the microlysis device after the first 5 mins.

The proportion of BugBuster Mastermix™ to broth in the lysis reaction was also investigated and it was found that, with 50% (v/v) BugBuster, there was much greater protein release, and after adjusting for the dilution of the sample to take into account the volume of the BugBuster, it was found to outperform sonication.

Ways of mixing the BugBuster and microbial broth to allow the lysis to occur in the microlysis device were looked at. Although the micromixer device produced slightly better results, the differences between the unions was not found to be statistically significant. The issue of clogging meant that a T-Piece with 500µm thru-hole was the best option.

With regard to the effect of residence time on flowrate, t-tests were performed, and it was found that the differences between the degree of lysis obtained at different residence times were just outside the bounds of statistical significance. Further work on the effect of residence time, on the degree of lysis, in the microlysis device would therefore be useful to identify whether there is a statistically significant relationship.. That said, from the data obtained, a residence time of more than 10 mins only produced a small increase in device performance. Balancing the trade-off between reproducibility and device volume meant that a residence time of 7.5 mins would be most efficient.

The effect of flowrate was also examined, and the lysis device's performance was found that to be insensitive to flowrate. Lower flowrates carried the advantage of a smaller device, and hence smaller sample volumes, as well as being able to match the flowrate with the microaffinity chromatography step. Consequently the flowrate range of 3.207 μL min^{-1} to 6.414 μL min^{-1} was chosen.

Overall, a simple, economical and easy to make microlysis device capable of lysing *E.coli*, was designed.   The lysate residence time inside the device was 7.5mins and it was able to produce results with similar protein release efficiency to sonication. The device volume was between 30μL to 60μL.

4 Microcolumn Design

4.1 Introduction and aims

This chapter details the steps taken to arrive at the final design of a microfluidic affinity capture step. Affinity chromatography was chosen as the capture step because of its high specificity. This property is of great use when designing a device to lyse and capture a specific protein in a microfluidic platform, where volumes and pressure drops are critical, as it allows the design to include only a single capture step and hence allows a smaller device volume and shorter overall internal tubing length.. Given that a microfluidic device with a smaller volume is likely to require less sample, and a shorter device in terms of total internal channel length, will give rise to a lower pressure drops, fewer steps is a useful advantage.

The chapter will start by describing the materials and methods used for investigations that are specific to the microcolumn design work presented in it. The results and discussions section will then show the decisions and investigations undertaken to arrive at the final microaffinity chromatography column design.

Whilst there has been some work on microaffinity chromatography to date, as discussed in Section 1.10 it has mainly focused on producing a microaffinity device that works, rather than characterisation and comparison with lab scale chromatography. Consequently, there was little information available to allow a sizing of the column based on likely quantities of protein eluted, and yield. The first part of the results section focuses on the reasoning behind the critical decisions taken in producing the initial column design.

The chapter then goes on to look at how the initial device performed by looking at the columns response to an acetone transition and using this to judge what improvements in column behaviour were required. The column was then refined based on conclusions drawn from this study and further acetone transition responses measured. This process of incremental improvement lead to a final column design with an acetone transition response curve that behaved as expected.

Finally, the chapter looks at some investigations undertaken with 3D microscopy techniques. Whilst it was not possible to image all the way through the column, the images obtained provide some degree of reassurance that the column was suitable for further work in terms of characterisation. The following chapter will go on to look at this characterisation.

4.2   Materials and Methods

This section explains materials and methods used that are specific to the investigations in this chapter. It covers:

- the different methods used to pack the microaffinity column;

- the methods used to perform the acetone transitions for the different column designs;

- the methods for labelling Glutathione S Transferase (GST) with a fluorescent dye and then adsorbing the labelled protein on to the matrix packed inside the column.

 All fittings were obtained from (IDEX Health and Science, Washington, USA) unless otherwise stated, and all reagents were purchased from (Sigma Aldrich, Dorset, UK) unless otherwise stated.   Glutathione Sepharose 4b matrix was purchased from (G E Life Sciences, Buckinghamshire, UK)

4.2.1 Microcolumn Packing by Sedimentation

Syringe with plunger removed

P-659 syringe adaptor

Double winged peak nut with 1/32" ferrule

F243x Nanotight FEP tubing sleeve

Fused silica capillary

M530 Micro filter capsule

F247x Nanotight FEP tubing sleeve

50µm internal diameter PeekSil tubing

Beaker
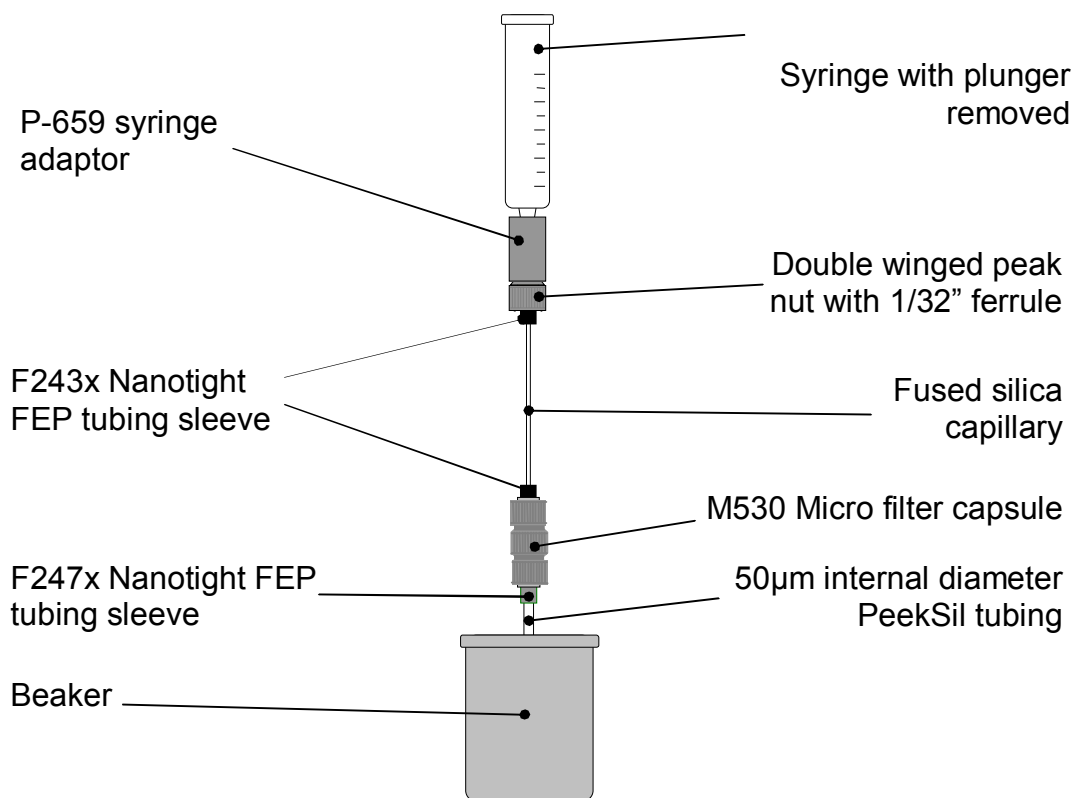
Figure 4.1 – Schematic of the apparatus and set up used for packing capillaries by sedimentation.

A 5cm length of 320µm internal diameter capillary (Polymicro, Arizona, USA) was cut. The filter capsule inside an M530 microfilter assembly was opened and the filter inside was replaced with two nylon mesh filter discs, one with an 80µm pore size, and one with 35µm pore size. The microfilter was then attached to the end of the capillary with the 35µm filter towards the column. The free end of the capillary was then attached to a P-659 syringe adaptor and this was attached to a 10ml syringe with the plunger removed. The syringe and column were then clamped in a vertical position. Figure 4.1 shows the completed apparatus set up for packing by sedimentation.

Following setup the syringe was filled with the desired dilution of matrix slurry. Either undiluted matrix slurry, or a 1:3 dilution of Glutathione Sepharose 4B matrix slurry diluted with 20% (v/v) ethanol. Both were both tried. The open end of the syringe was covered with parafilm to minimise losses from evaporation. A hole was made in the parafilm cover to allow the matrix solution to flow by gravity. Packing was allowed to proceed overnight. Following packing the column was viewed under the microscope to assess the quality of the packing.

4.2.2 Column Packing with a Nanobaume
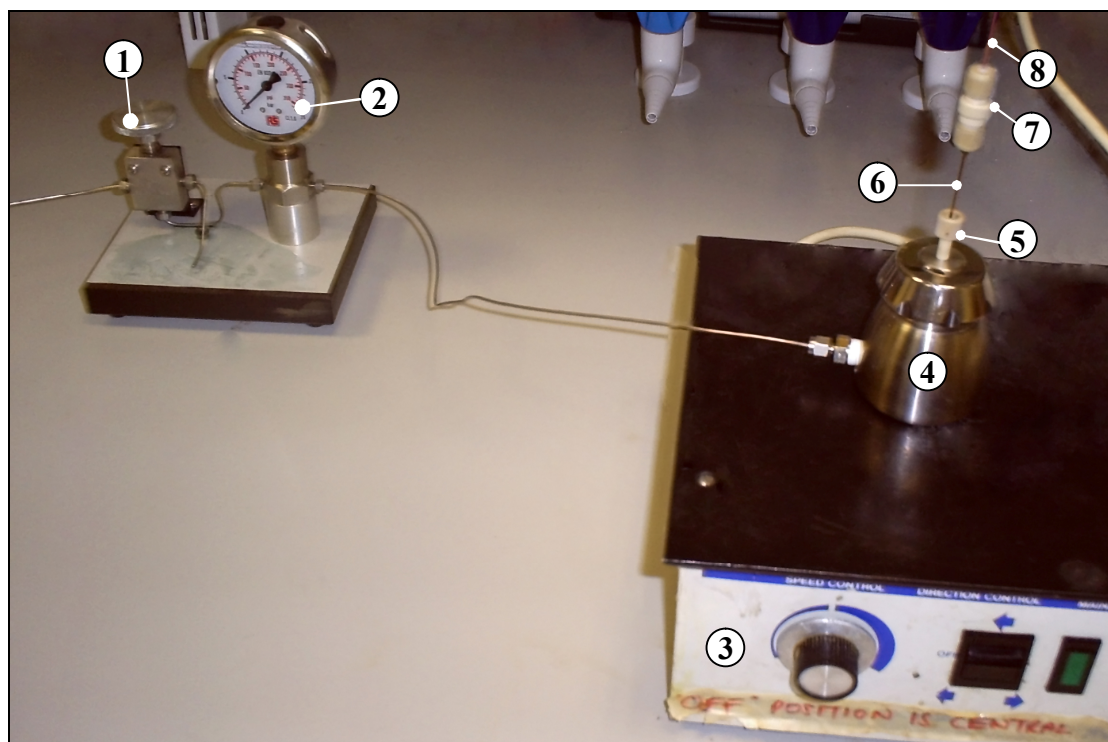
Figure 4.2 - Photograph of Nanobaume packing set up. (1) Valve; (2) Pressure gauge; (3) Magnetic stirrer plate; (4) Nanobaume (); (5) F-130 extra long 10-32 fingertight nut (IDEX Health and Science, Washington, USA); (6) 320µm micron internal diameter fused silica tubing (Polymicro technologies, Arizona, USA), (7) M530 Micro filter assembly (IDEX Health and Science, Washington, USA) (8) 100µm internal diameter PeekSil® capillary

Fused silica capillary (Polymicro technologies, Arizona, USA) with an internal diameter of 320µm was cut to a length of 15cm using a carbide cutter (IDEX

Health and Science, Washington, USA). A longer length of capillary, than that of the final column, was used. This was to enable the packing to be observed and hence to ensure that the required 5cm column had been fully packed. The filter capsule inside an M530 (IDEX Health and Science, Washington, USA) microfilter assembly was opened and the filter inside was replaced with two nylon mesh filter discs, one with an 80μm pore size, and one with 35μm pore size. The M530 filter assembly was then added to one end of the capillary, with the 35μm filter towards the column, and the other was then fed into the lid of the Nanobaume, so that the free end would be positioned just above the magnetic stirrer bar once the device was closed

900 μL of 20 % (w/v) ethanol was added to a glass vial. 100 μL of Glutathione Sepharose 4b slurry (G E Life Sciences, Buckinghamshire, UK) was then added to the same vial, followed by a small cylindrical magnetic stirrer bar which was 2.27 mm in diameter and 5.17 mm in length. The contents in the vial were not stirred prior to placing in the Nanobaume. This is because mixing the slurry increased the time it takes to pack the column, probably because the unstirred suspension has a higher density of matrix beads at the bottom and therefore more beads will enter the tube per unit time. The vial was then placed inside the Nanobaume and the Nanobaume closed. The Nanobaume was placed on a magnetic stirring table as shown in Figure 4.2

The pressure regulator on the nitrogen gas supply was then set to 3.5 bar and immediately the magnetic stirring table was switched on. The capillary was observed. When the packing inside the capillary was sufficient, i.e. when the packing was more than 5cm down the capillary, the nitrogen gas supply was turned off, and the capillary was carefully removed from the Nanobaume. The

capillary was then cut, being careful not to disturb the matrix inside, using the carbide cutter. A second micro filter assembly was then added to the free end of the capillary, with the 35μm nylon mesh filter towards the column, to complete the microcolumn.

The column was then placed in a specially designed holder, to prevent the column from breaking, and the column and holder were placed inside a falcon tube filled with 20% (v/v) ethanol to avoid evaporation of liquid from the end of the column which could change the packing characteristics.

4.2.3 Micro-column Acetone Transitions Using Agilent 1100 HPLC Pump, Injector and UV Diode Array Detector
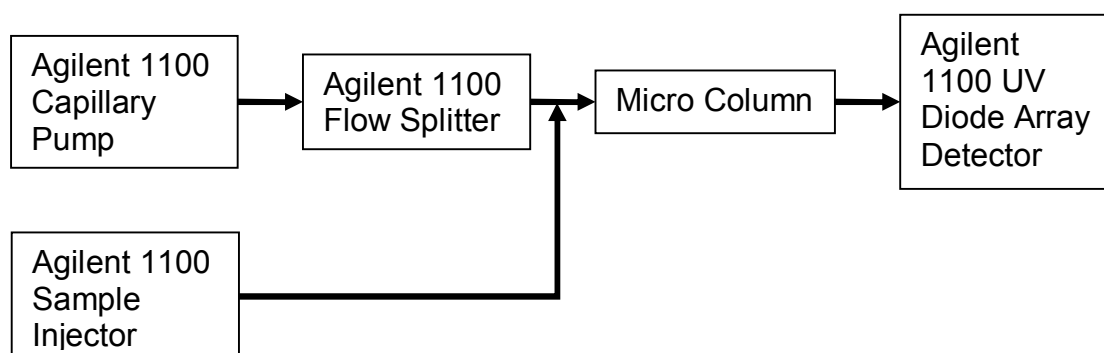
Figure 4.3 – A block diagram of the system used for acetone transitions

The system was set up as shown in Figure 4.3. A sample containing 2% acetone (v/v) acetone in PBS pH7.4 was pipetted into a glass vial and placed in the Agilent 1100 series auto sampler. The initial flowrate used was 3μL min^{-1} as this was the minimum stable flowrate that could be achieved with the HPLC capillary pump in microflow mode. The system was first equilibrated with 10 column volumes (40μL) of PBS pH7.4 at 3 μL min^{-1}. The Agilent HPLC sample injector was then instructed using the Chemstations software to inject a 40μL

sample into the system. The results were recorded using the Chemstations software and exported to Excel for analysis.

4.2.4 Micro-column Acetone Transitions Using a Syringe Pump and UV Diode Array Detector
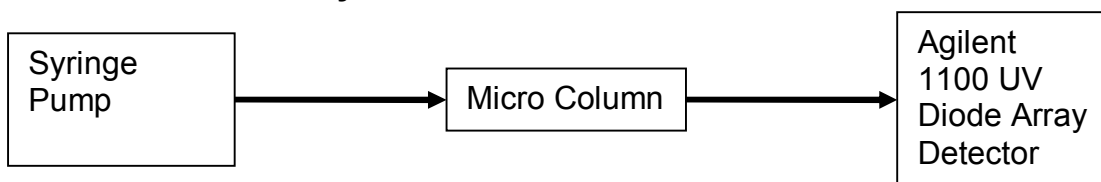
Figure 4.4 – A block diagram of the system used for acetone transitions

The system was set up as shown in Figure 4.4. The microcolumn was first equilibrated by using the syringe pump to pump 10 column volumes of PBS pH7.4 through the column at 50cm hr^{-1}. The column was then loaded, using the syringe pump, with 0.2% Acetone in PBS pH 7.4 at 50cm hr^{-1} until the UV absorbance at 280nm levelled out at its maximum value. This procedure was repeated at 75cm hr^{-1} and 100cm hr^{-1}.

4.2.5 Protein labelling for 3D microscopy

GST was labelled using an Alexa Fluor® 488 Microscale Protein Labelling Kit (Invitrogen (Life Technologies Ltd), Paisley, UK). 100 µL of 1 mg mL^{-1} GST in PBS pH7.4 was added to the reaction tube supplied with the kit and mixed with 10 µL of 1M sodium bicarbonate solution by pipetting. The reactive dye solution was prepared immediately before use by adding 10 µL of deionised water to the tube containing the reactive dye to form 11.3 nM/µL of dye solution. The dye solution was mixed thoroughly by pipetting, and 8.5 µL of the 11.3nM/µL dye solution was added to the GST and sodium bicarbonate solution. The reaction mixture was mixed thoroughly by pipetting and incubated at room temperature for 15 minutes.

The labelled protein was then purified. Two 800µL aliquots of Bio-Gel P-6 fine resin suspended in PBS pH7.2 was pipetted into two of the spin filters provided with the kit (Nanosep MF 0.2 µm centrifugation device). The gel was packed by spinning at 16000 g in a fixed angle microtube centrifuge for 15 s. 50µL of the labelled GST was then added to each spin filter and they were then centrifuged for 1 minute at 16000 g using a fixed angle microtube centrifuge.

4.2.6 Preparation of a microcolumn for imaging the packing using 3D microscopy

In order to facilitate imaging in fused silica capillaries some researchers burn off the polyamide coating (Wang et al. 2005). Therefore, for the same reasons, prior to packing as described in Section 4.2.2, a two centimetre section of the polyamide coating was burnt off from the middle of the length of capillary that would become the column. Extra care was taken when assembling and handling the column as burning off the coating made it extremely brittle and easy to break. The column was then equilibrated with 10 column volumes of PBS pH7.4 at 50 cm hr^{-1}. The protein solution, labelled as described in Section 4.2.5 was loaded on to the column, following equilibration, at 50 cm hr^{-1}. Finally the column was washed with 10 column volumes of PBS pH7.4 at the same flowrate. After placing the column in its holder and in a falcon tube containing 20% ethanol, the falcon tube was wrapped with foil to stop UV light from degrading the labelled protein.

4.3 Results and Discussion

This section begins by looking at the initial column design and explains the key decisions with regard to this design. It then goes on to discuss the development of the packing methodology, with two alternative methods of packing being examined.

The acetone transition results obtained for the initial column design are then assessed and the shape of the acetone transition curve is critically discussed. The behaviour of subsequent iterations of the microaffinity chromatography column is discussed in a similar manner.

Following arrival at a final design, 3D microscopy techniques are used to try to make a qualitative visual assessment of the quality of packing within the column.

4.3.1 Initial Column Design

(a) Agilent 1100 Series HPLC pump

M530 micro filter assembly

5cm

Agilent 1100 Series UV detector

(b) Fused silica capillary tubing 320µm internal diameter

F234x Tubing sleeve

F132 Micro ferrule

Micro-filter capsule

M530 Micro filter assemblv

F247x Tubing sleeve

50µm internal diameter PeekSil tubing
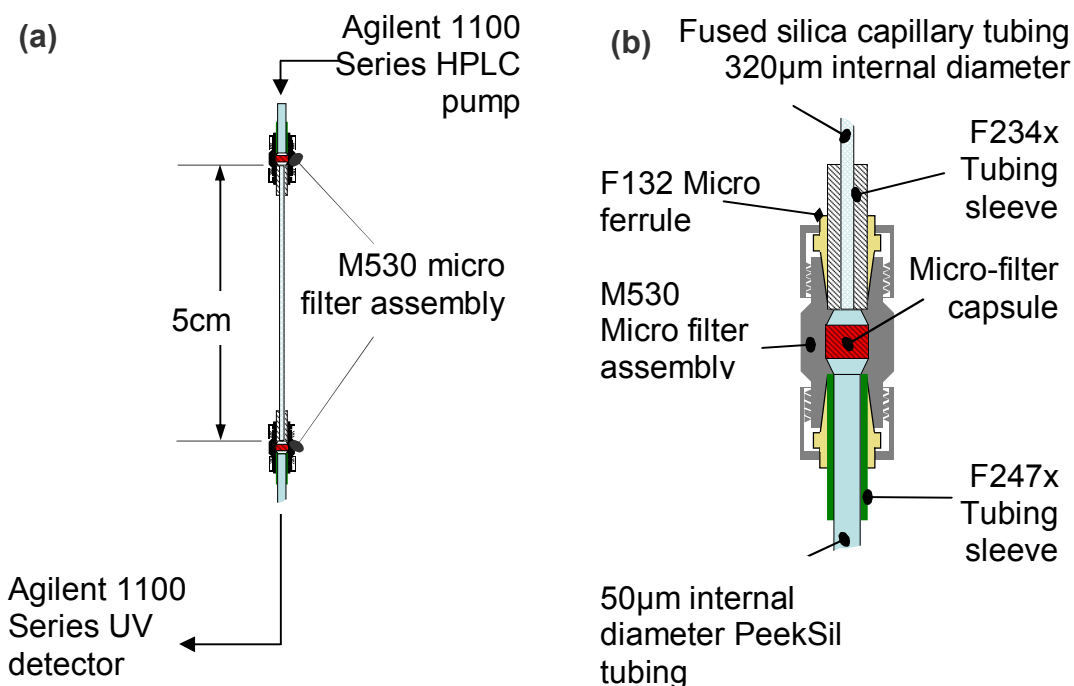
Figure 4.5 – Schematic diagram of the initial design of the capillary column. (a) shows the overall capillary column system and the length of the column. (b) shows an enlarged diagram of the column frits.

The initial column design is shown in Figure 4.5. The column length was chosen

as it was a typical bed height of a lab scale column, and was a suitable length to

include in a microfluidic chip. This specific column diameter was chosen

because it was envisaged to be the smallest possible diameter to make efficient

packing possible.
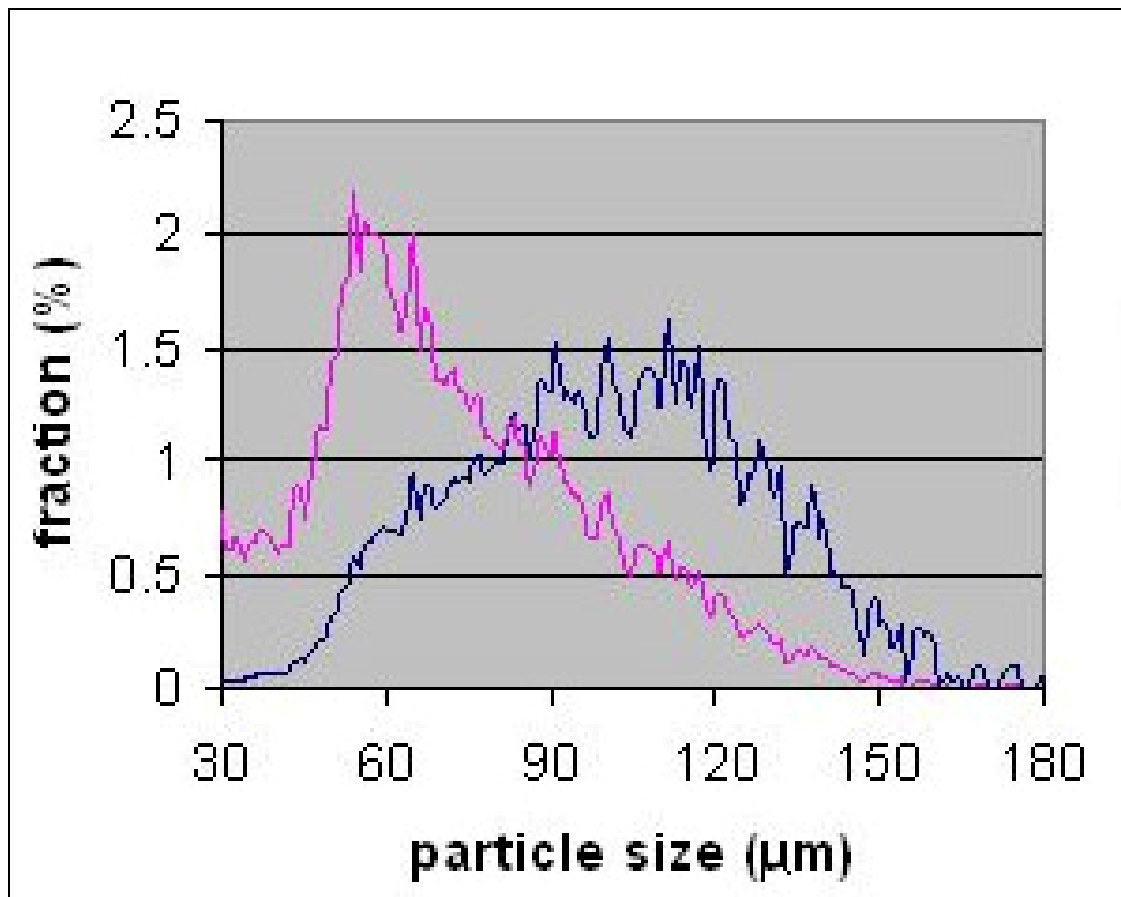
Figure 4.6 - Typical particle size distribution for Sepharose 4B base matrix (Provided by GE Healthcare Europe GmbH, Uppsala, Sweden). The blue line represents the fraction as a proportion of the total bead volume and the pink line shows the fraction as a proportion of total number of beads. The porosity of the beads is between 0.92 and 0.94. Permission to reproduce this graph has been granted by GE Healthcare.

Figure 4.6, shows a typical particle size distribution of Sepharose 4b base matrix. From this graph it can be seen that the median particle size, in terms of the total bead volume is between 90 μm and 120 μm. Modal particle diameter is estimated from this graph to be 105 μm. This was used as a basis to choose the minimum practical column diameter needed to achieve efficient packing. The two closest packing structures available to regular spheres are hexagonal close packing and face centre cubic packing.
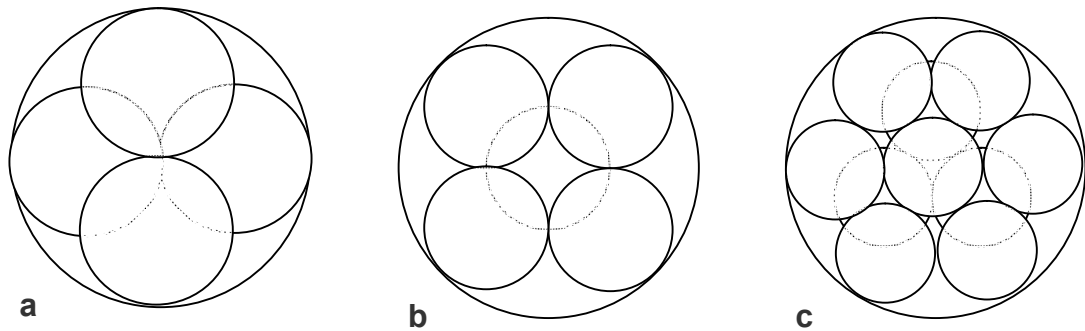
Figure 4.7 – Schematic of the various packing scenarios based on the ratio of the capillary to sphere diameter. (a) shows the likely packing scenario when a capillary twice the diameter of the packing spheres is packed with regular spheres. (b) shows the likely packing scenario when the diameter of the capillary is approximately 2.5 times the diameter of the packing spheres. (c) shows the likely packing scenario when the diameter of the capillary is three times the diameter of the packing spheres.

Figure 4.7 shows three different packing scenarios when a column is packed with regular spheres. The first scenario is when the column internal diameter is twice the diameter of the spheres. From this diagram it can be seen that the packing would amount to alternate groups of two spheres on each plane which would be perpendicular to each other. It can be envisaged from this that this type of packing would result in a large voidage. Scenario (b) is where the diameter of the capillary is just large enough to allow body centre cubic packing. Finally scenario (c) is where the capillary internal diameter is equal to three sphere diameters. On comparing scenarios (b) and (c), by qualitative assessment it can be seen that the voidage, particularly at the wall of the column is likely to be significantly less in scenario (c) i.e. with the hexagonal close packing configuration. If the capillary diameter was larger, for example equal to four sphere diameters, it is envisaged that hexagonal close packing would remain and the unit cell would start to repeat. It is acknowledged that in reality the matrix beads range quite widely in diameter, and that consequently such regular packing will not be seen in the column. However, it is thought that

on average the effect of larger and smaller beads will balance each other out. Consequently, good packing is expected at column diameters larger than or equal to three bead diameters, and hence fused silica capillary with an internal diameter of 320µm was chosen as this is the standard size closest to, but not less than, three matrix bead diameters.

4.3.2 Development of the packing methodology

Two different methods of packing the capillary were tested to determine the fastest and most reproducible packing method to pack the microaffinity chromatography column with standard Glutathione Sepharose 4b matrix (G E Life Sciences, Buckinghamshire, UK): sedimentation; and packing with a Nanobaume (Westernfluids, California, USA) - which is a device specifically designed for packing capillaries.
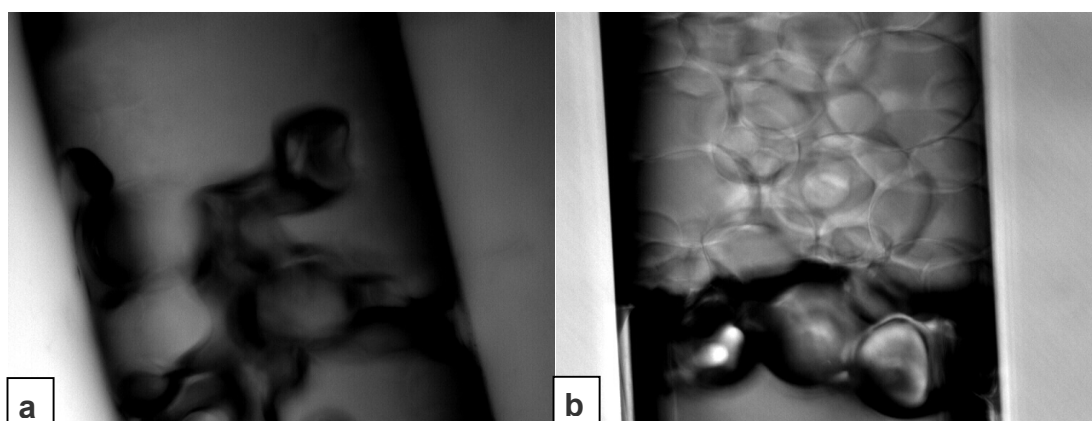
Figure 4.8 – Images of column packing by sedimentation overnight using undiluted Glutathione Sepharose 4b matrix slurry. Images taken at 20x magnification image (a) shows the top third of the column and image (b) shows the bottom of the column.

Packing by sedimentation was undertaken as described in Section 4.2.1 with 1 mL of undiluted matrix slurry in a 10 mL syringe. The resultant packing in the majority of the column, when visually inspected under the microscope, was reasonable, however there were some air bubbles in the top third of the column

which may disrupt the packing quality, and the packing did not go all the way down to the bottom of the column as shown in Figure 4.8. In addition, the remaining matrix in the syringe appeared to be packed inside the syringe with very little 20% (v/v) ethanol solution. Because there was very little liquid in the beaker used to catch the effluent, it was thought that some of the 20% ethanol was lost by evaporation. Consequently, a 1 mL syringe and 1:3 dilution of matrix slurry was used for subsequent experiments. Also, in order to try to address the issue of air bubbles inside the column the packing assembly was placed inside a universal tube and taped to the side of the tube. The Universal tube together with the column was then partially submerged in a sonicator bath, ensuring that water from the bath could not enter the tube, and taped to the side of the bath. The packing apparatus was sonicated for an hour prior to allowing packing to occur overnight.
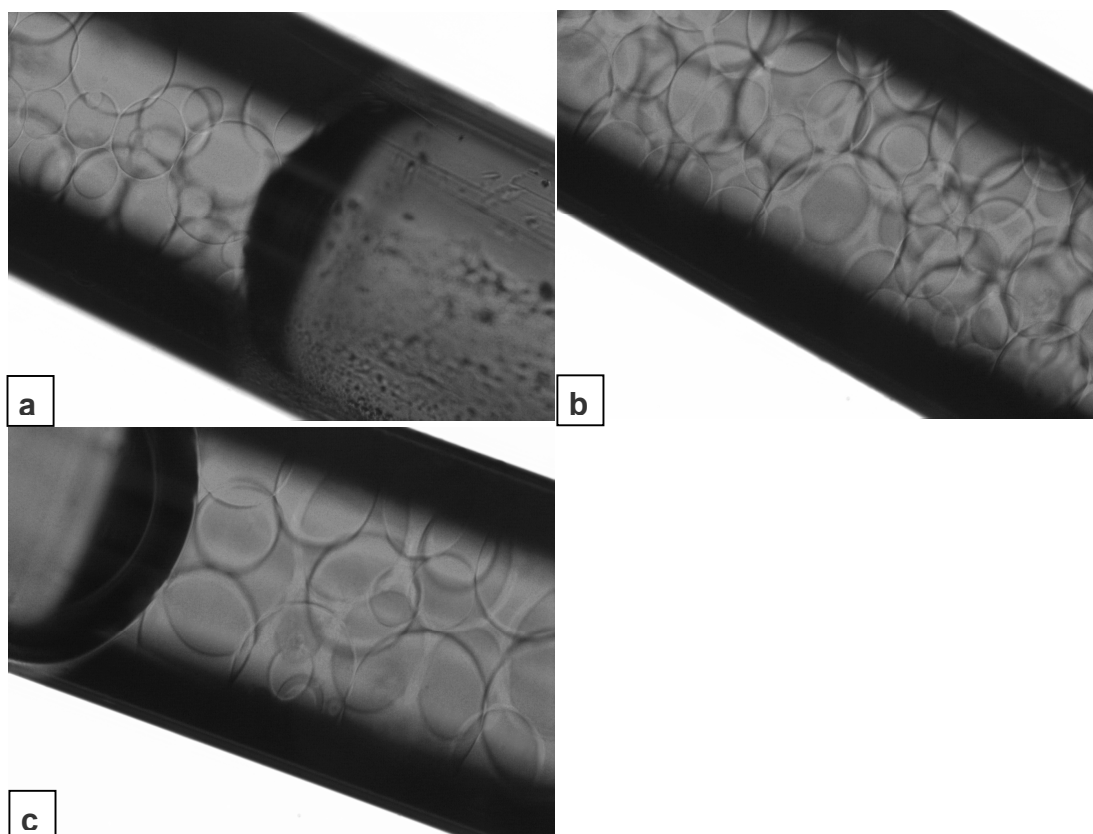
Figure 4.9 – Images of column packing by sedimentation overnight using a 1:3 dilution of Glutathione Sepharose 4b matrix slurry with sonication. Images taken at 20x magnification image (a) shows the top of the column and image (b) shows the middle of the column and (c) shows the bottom of the column

Figure 4.9 shows images of the best packing obtained by sedimentation. On removal of the fittings from the end of the glass capillary for imaging, which was done very carefully, the meniscus of the liquid inside the capillary retreated approximately 3 mm down the column taking the packing with it. This is thought to be due to capillary action and is likely to be due to the loose packing observed in Figure 4.9 (a) and (c), at the top and bottom of the column. These results show that packing by sedimentation is feasible but that pressurisation of the column to ensure denser bed packing is probably necessary, and hence these results are consistent with the findings of other researchers (Reynolds & Colón 1998). Given that speed and simplicity of the packing protocol were

considered important, it was decided that further packing methods should be investigated. Consequently packing with the Nanobaume was investigated.

For packing fused silica capillaries with the Nanobaume, a packing pressure of 3.5 bar has been used successfully by other researchers to pack a column with Sepharose beads. However, higher packing pressure potentially results in faster and closer packing. That said, if the packing pressure is too high it can result in compression of the chromatography bed. In order to validate 3.5 bar as a suitable packing pressure and to investigate whether a significantly higher packing pressure would produce good packing, a 15cm length of 320µm internal diameter fused silica capillary was packed using a Nanobaume as described in Section 4.2.2 at 3.5 bar, 6 bar and 10 bar. The capillary was then cut to the correct length i.e. 5cm and a microfilter assembly was fitted to the free end. The packing was then qualitatively evaluated by imaging using an optical microscope.
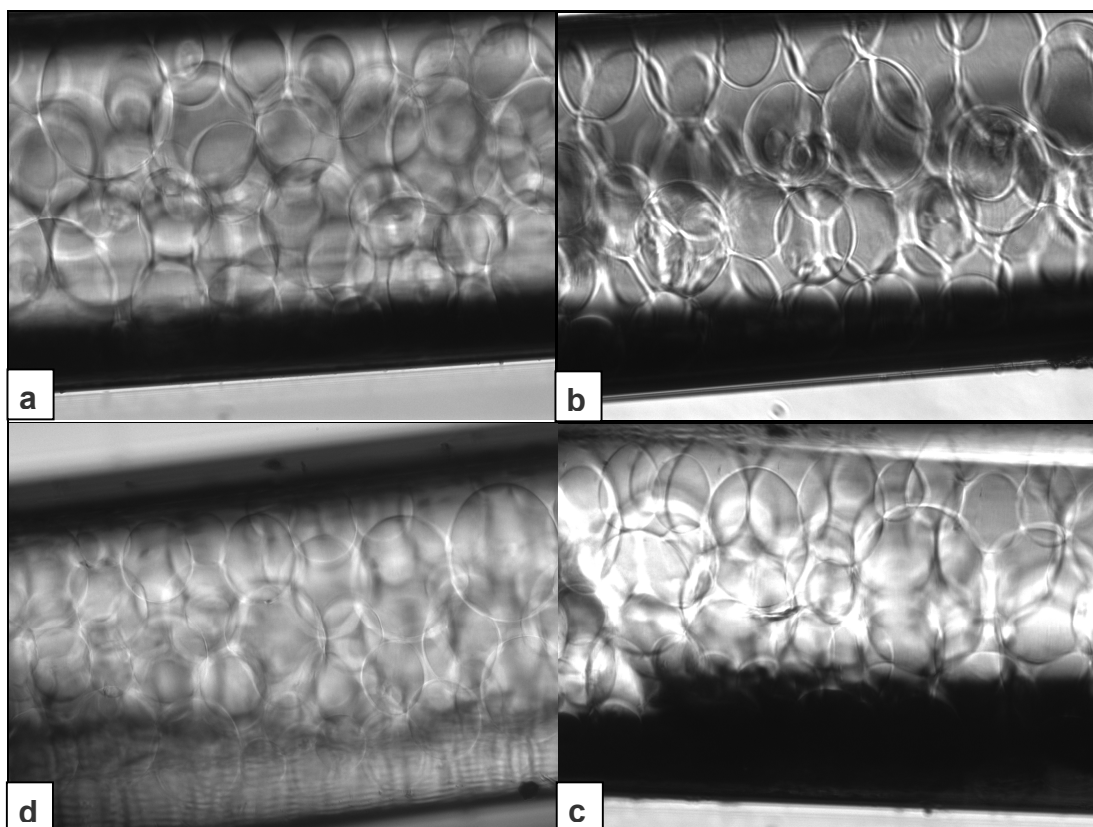
Figure 4.10 – Photographs of Glutathione Sepharose 4B packing inside the capillary micro-column with an internal diameter of 320µm at 20x magnification. (a) Microcolumn packed at 3.5 bar using the Nanobaume. The beads in this column can be seen as roughly circular geometries (b) Microcolumn packed at 6 bar using the Nanobaume. (c) Microcolumn packed at 10 bar using the Nanobaume. The beads in this column can be seen as elliptical shaped geometries. (d) Microcolumn packed at 3.5 bar using the Nanobaume following flow through the column at 10µL min^{-1}. The beads in this column can be seen a roughly circular geometries

Figure 4.10 shows the columns packed at different pressures. Figure 4.10a shows the matrix inside the column packed at 3.5 bar. The matrix beads appear almost circular and the very slight non-sphericity seen is thought to be due to the diffraction effects as a result of viewing the beads through the curvature of the capillary. Figure 4.10b shows the matrix inside the column packed at 6 bar. The matrix beads in this column are elliptical in geometry indicating that the beads are compressed. Figure 4.10c shows the matrix beads inside the column packed at 10 bar. These beads exist as oval geometries with the tips of the oval appearing to point towards the column wall

and the base appearing to point towards the centre of the column. This orientation of the oval shaped beads is thought to result from the larger voidage that exists close to wall. As the pressure is increased it is thought that the beads are forced outward to fill this voidage.

In order to ensure that the column would operate over the range of flowrates to be investigated, without irreversible bed compression, PBS pH7.4 was pumped through the column at 10 µL min^{-1}. The column was then imaged under the microscope. Figure 4.10d shows the packing in the column following flow at 10µL min^{-1}. When compared with Figure 4.10a, the shape of the beads is very similar indicating that compression of the bed is unlikely to have occurred.

It was decided that packing would be performed using the Nanobaume as this resulted in better and faster packing than sedimentation, without the need for post packing pressurisation of the bed.

4.3.3 Micro affinity chromatography column initial design

The initial column design, as described in Section 4.3.1, was tested with acetone transitions in order to check the quality of the packing and ensure that the system was behaving as expected. The acetone transitions were performed as described in 4.2.3.
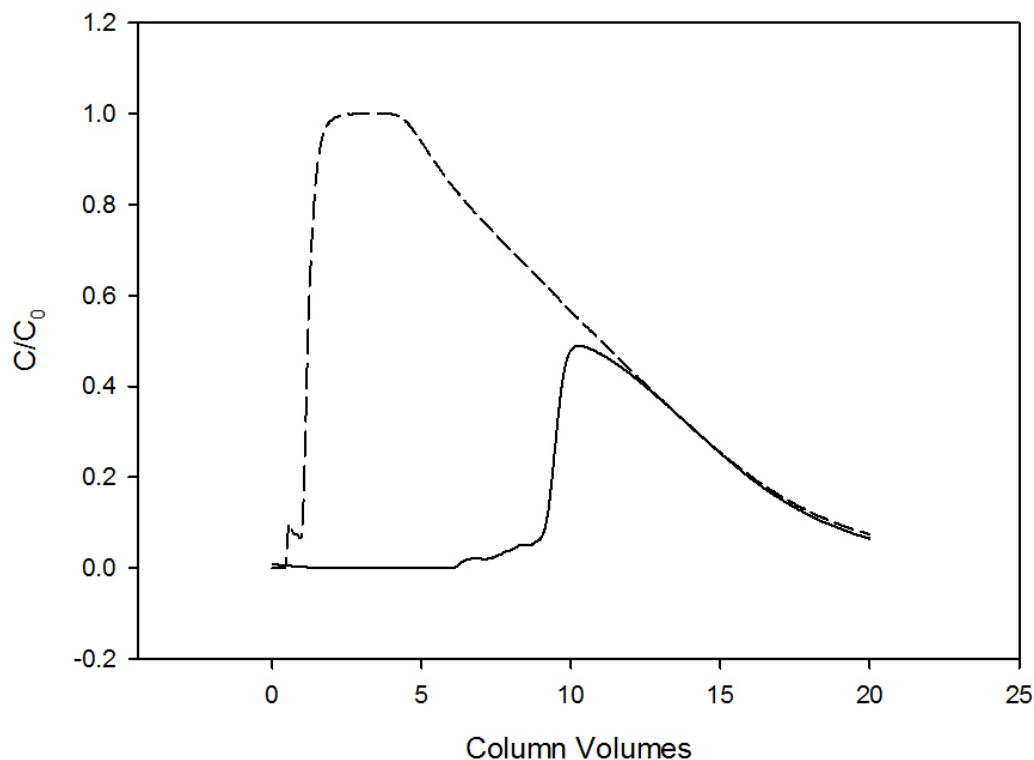
Figure 4.11 – Graph of acetone transitions performed in the presence and absence of the microcolumn at 3µL min^{-1}. The capillary column was run using an Agilent 1100 HPLC machine. The acetone transition was created by injecting a 40 µL pulse of 2% acetone into the column. The solid line shows the acetone transition for the 320µm internal diameter 5cm long capillary column constructed with fittings from Presearch. The dashed line shows the acetone transition obtained without the micro column.

Figure 4.11 shows the acetone transitions obtained with and without the column in place. The curve obtained without the column has a flat peak which is as expected. This flat peak top occurs because initially, when flow is started, just PBS is passing through the column so the C/C_0 value will be zero. The boundary between the 2% acetone plug and the PBS buffer will start to mix in the tubing and while passing through the column. This will cause the C/C_0 to rise until the maximum concentration ($C/C_0 = 1$) is reached, where 2% acetone is flowing through the column. This $C/C_0 = 1$ will be maintained until the end of the 40µL plug is reached where again mixing will cause the C/C_0 to decrease until it reaches 0. The faster the transition from $C/C_0 = 0$ to $C/C_0 = 1$ the less

mixing there is occurring in the column and tubing in the system, and the better the resolution that the column will provide. However, there is significant tailing of the peak indicating band broadening is taking place i.e. the end of the acetone plug is undergoing significant mixing. This band broadening is thought to result from diffusive mixing occurring as the acetone transition travels along the capillary tubing. Comparing the transition observed with the column in place, to the transition without the column, it is observed that the transition for the capillary column does not plateau and has a much shorter and narrower peak which starts much later. This is contrary to expectations as the acetone pulse injected onto the column is equal to approximately 10 column volumes and acetone should not be binding to the matrix. It is believed that the peaking effect observed is the result of dead volume capacities in the micro column. It is postulated that as the acetone is injected into the column it collects in these capacities, delaying it from reaching the detector which results in the later peak. As flow continues it is thought that the acetone is slowly washed out of the capacities thereby reducing its concentration. In order to solve this problem the fittings were redesigned to reduce the dead volume.

4.3.4 Reduction of the dead volume capacity

After an analysis of the system it was found that the likely location of the dead volume capacity as in the microfilter frits.
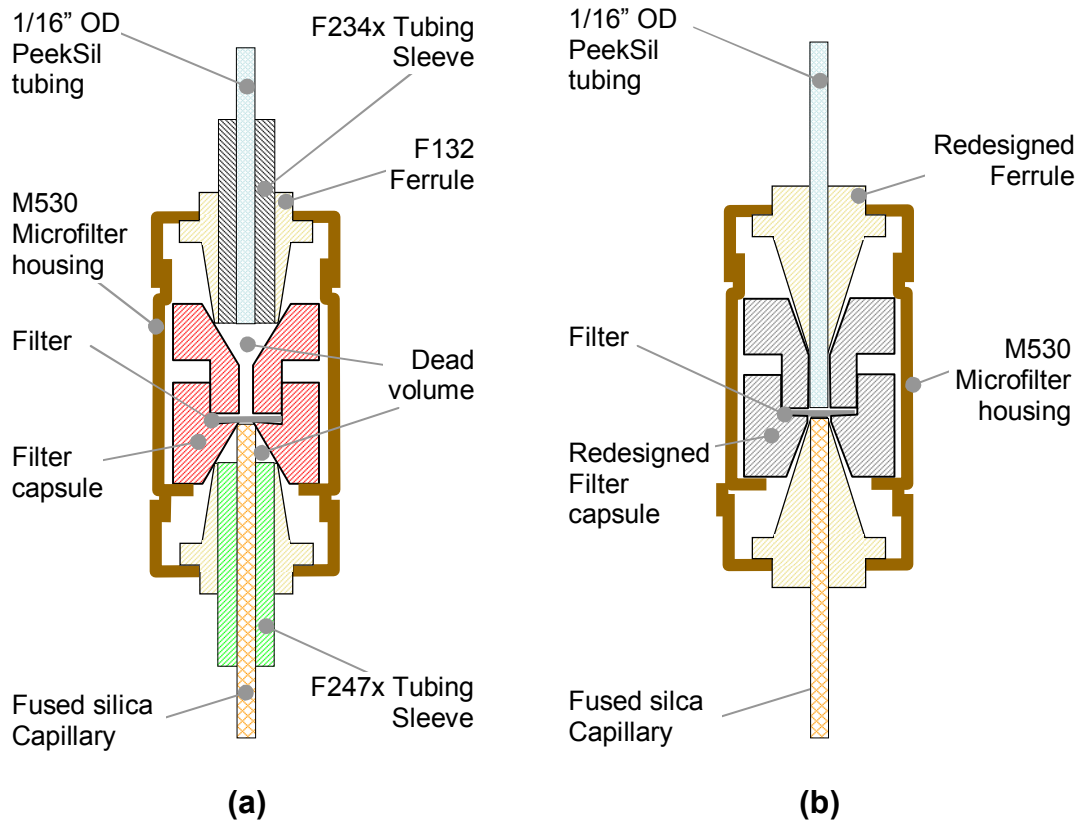
Figure 4.12 - Diagram showing the standard fittings used as frits in the initial design (a) compared with the redesigned fittings (b)

Figure 4.12(a) shows the unmodified fittings. From the diagram, two dead volume capacities can be observed between the ferrules and the filter capsule. This problem was solved by redesigning the filter capsule and ferrules to remove the need for tubing sleeves and so that they fit together tighter. A schematic of the redesigned fittings is shown in Figure 4.12 (b), a computer generated image of the fittings is shown in Figure 4.13, and the engineering drawings for the fittings are in Annex A
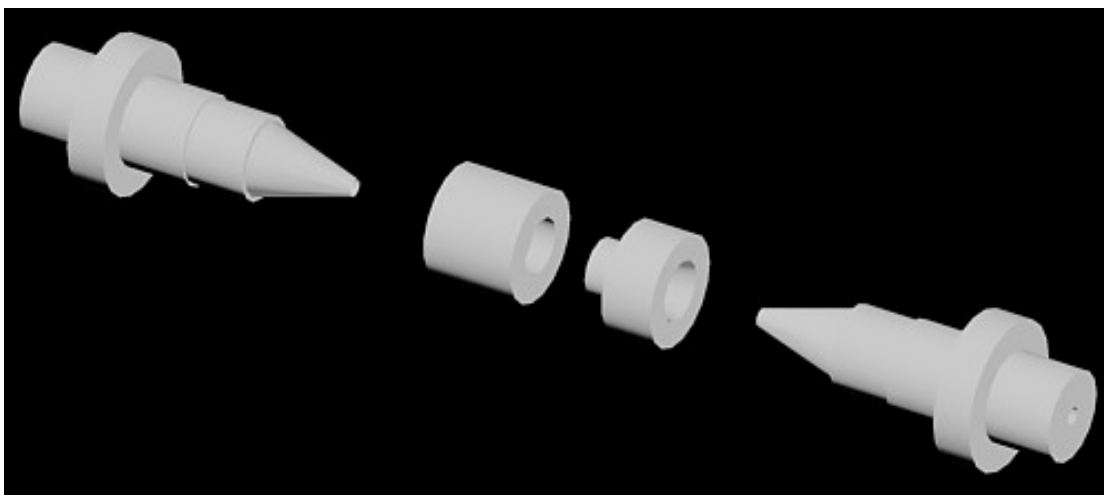
Figure 4.13 - Image of the redesigned Delryn fittings generated using AutoCAD.

The modified column was then tested by performing acetone transitions at 3µL min^{-1} with 0.2% acetone. The resulting transition curves show a marked improvement in the performance of the column which whilst not ideal is closer to the expected response curve.
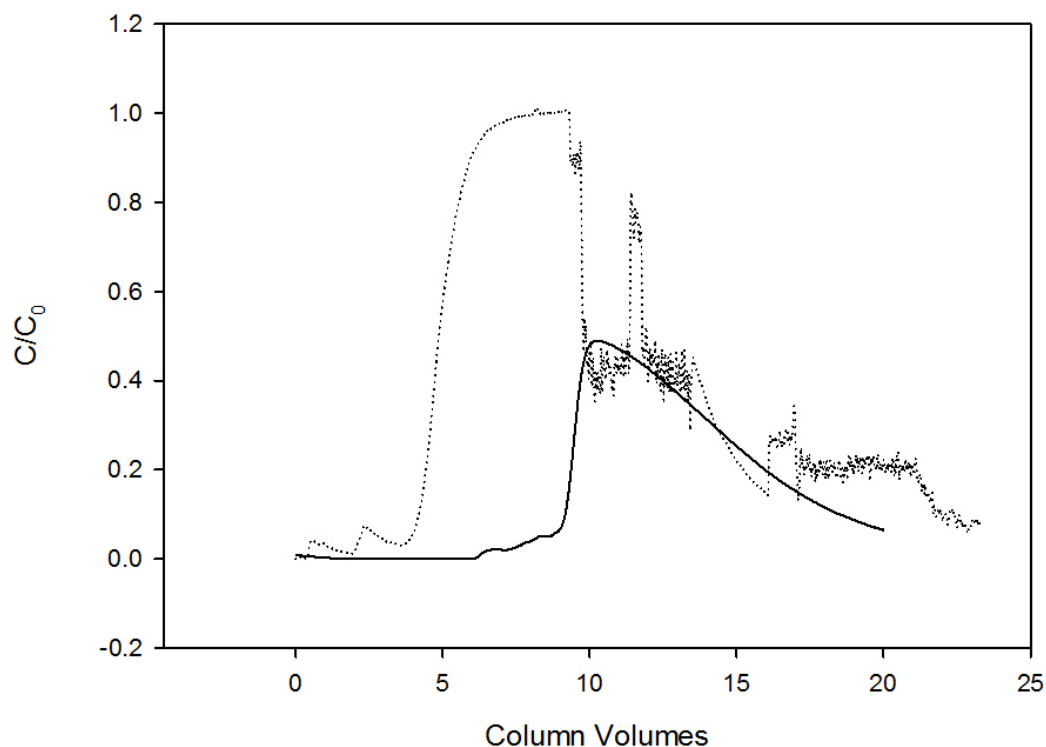
Figure 4.14 – Graph comparing acetone transitions performed on the microcolumn with standard fittings with the acetone transition on a microcolumn with reduced dead volume fittings. The capillary column was run using an Agilent 1100 HPLC machine (Agilent Technologies, Berkshire, UK). The acetone transition was created by injecting a 40microlitre pulse of 0.2% acetone into the column. The solid line shows the acetone transition for the 320µm internal diameter 5cm long capillary column constructed with M530 microfilter assembly and F132 ferrule fittings from Presearch. The dotted line shows the acetone transition obtained using the microcolumn with the new custom made reduced dead volume fittings column.

Figure 4.14 compares the acetone transitions obtained with the initial design as compared with the reduced dead volume design. The acetone transition obtained with the micro column containing the reduced dead volume fittings is clearly closer to what is expected from an acetone transition i.e. the transition reaches a plateau and the volume over which the transition occurs is of the correct order. There are however, a number of issues with the acetone transition that warrant further work to improve the performance of the microaffinity chromatography system.

The most significant issue of note in the transition curve is that a lot of noise appears on the chromatogram at around 10 column volumes. It is thought that this noise results from trapped air bubbles in the system. The noise is intermittent, interrupts the readings but does not appear to influence the underlying chromatogram and at some points the UV absorbance readings are lower than expected from the chromatogram and at others they are higher. The first two observations suggest small quantities of an immiscible substance are interrupting the flow of UV light and the final point suggests that this substance is able to transmit UV. Consequently, the most likely explanation is that this noise is caused by air bubbles getting into the system.
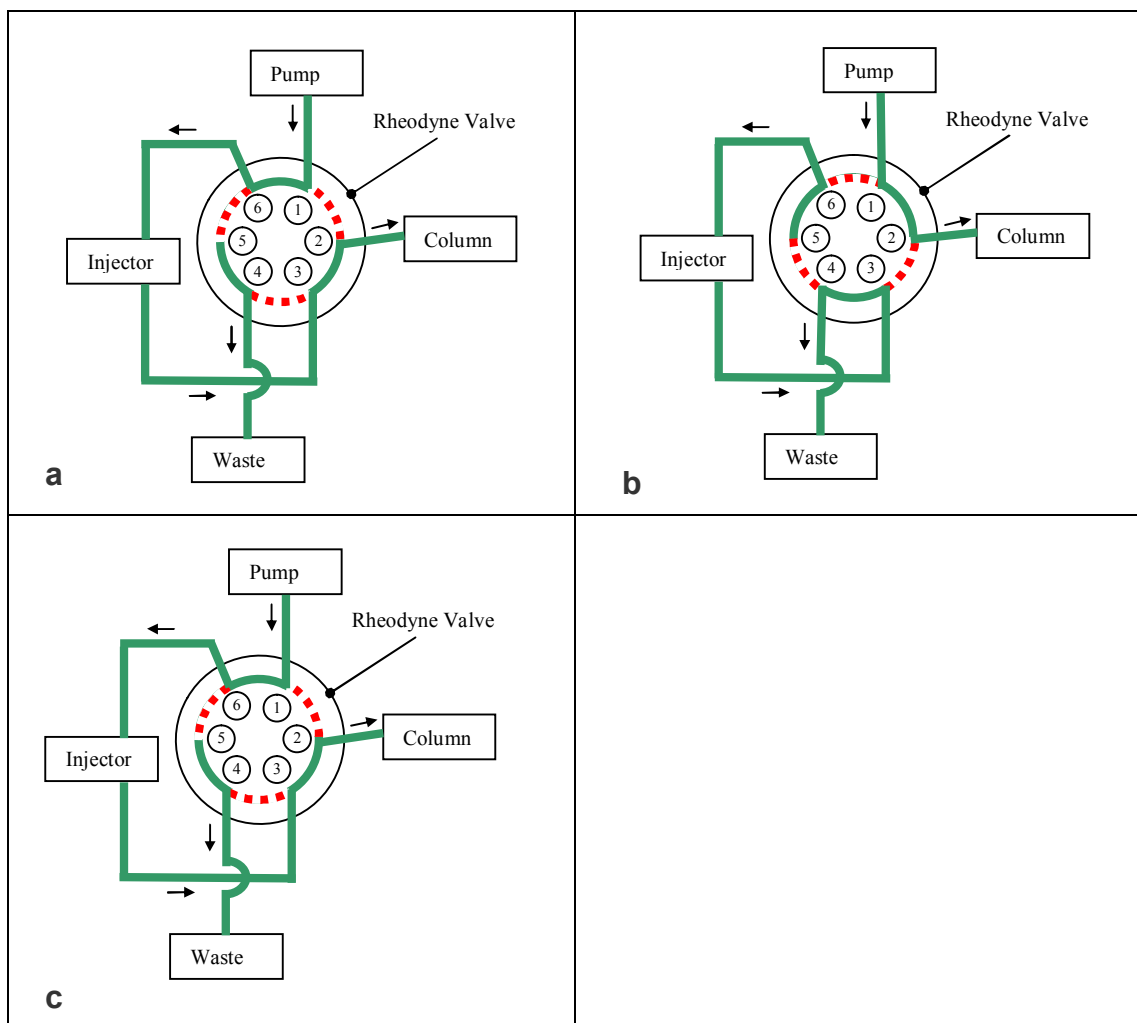
Figure 4.15 - During normal operation, the Rheodyne valve is in position a. The buffer flows through the injection loop to the column. When a sample sequence is started the Rheodyne valve switches to position b, bypassing the injection loop to allow sample to be drawn into the loop. This switching is accompanied by a moderate drop in pressure. When the sample is loaded into the injection loop, the Rheodyne valve is switched back to position 1 and the sample is allowed to flow back through the column. This switching is accompanied by a much larger drop in pressure that, at low system pressure drop's, results in flow becoming unstable.

It is postulated that this air is introduced during the switching of the Rheodyne valve in the Agilent HPLC system. Figure 4.15 shows the switching sequence of the Rheodyne valve. During normal flow, flow passes from the pump, through the injector to the column. Once an injection is started, the valve switches so that the injector is bypassed while the sample is being draw up. The sample is drawn up through a needle. The needle is then placed in a seat and some of the sample is pushed through to waste leaving the desired sample

volume. It is postulated that it at this point, when large sample volumes are being used, that air is introduced into the system perhaps because the volume of the sample pumped to waste is not sufficient enough to flush out any air bubbles.
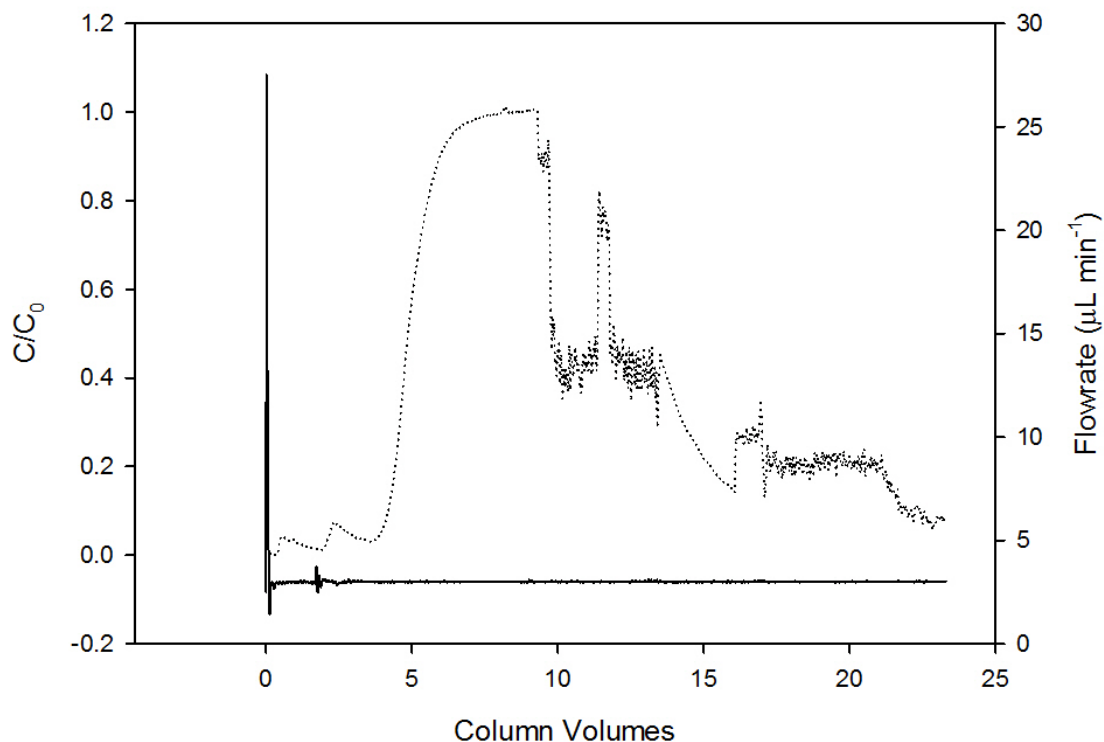
Figure 4.16 – Showing an acetone transition performed on the microcolumn against flowrate. The capillary column was run using an Agilent 1100 HPLC machine. The acetone transition was created by injecting a 40microlitre pulse of 0.2% acetone into the column. The dotted line shows the acetone transition obtained using the microcolumn with the new custom made reduced dead volume fittings column. The solid line shows the fluctuations in flowrate during the experiment.

The second issue with the acetone transition is the existence of two small peaks before the transition begins. Figure 4.16 shows the acetone transition and flowrate during the transition plotted on the same curve. It can be seen from this that the peaks occur roughly the same time after two peaks in the flowrate and are therefore perhaps caused by the increase in pressure resulting from the change in flowrate. As described in Figure 4.15 these changes in flowrate are

caused by the change in pressure drop when the Rheodyne valve is switched and as such are a property of the system. This in combination with the fact that stable flow was not possible at low flowrates meant that finding an alternative method of driving the flow was necessary.

4.3.5 Changing pump from HPLC pump to syringe pump

For the reasons described above, it was decided to use a syringe pump instead of the Agilent HPLC pump and injector. Since the syringe pump was able to provide stable flow at much lower flowrates than the Agilent HPLC pump, it was decided to begin these investigations at a lower flowrate, 50cmhr^{-1}. The system was set up, and investigations were performed as described in Section 4.2.4
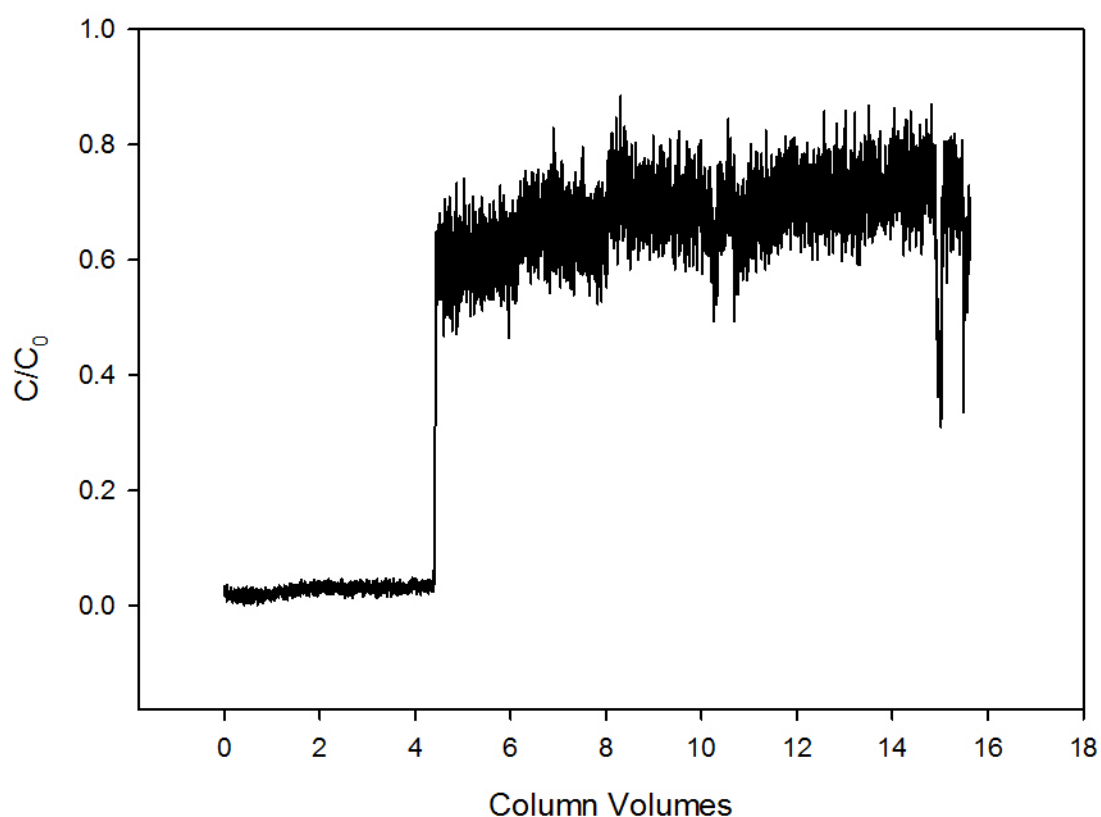
Figure 4.17 – Acetone transition performed at 50cmhr^{-1} using a syringe pump to drive flow through the system

Figure 4.17 shows a typical acetone transition obtained using the microcolumn with the new fittings and a syringe pump to drive the flow. The resulting chromatogram is of the correct shape. However there is a significant amount of noise in the signal. This is thought to be as a result of the low flowrate used. The syringe pump works by turning a threaded shaft which is used to drive a block against the syringe plunger. The rate at which the threaded shaft turns determines the flowrate of the fluid emerging from the syringe. However, the rotation of the shaft is not continuous, as a stepper motor is used. Consequently, at low flowrates, steps are taken infrequently and hence the flow is stop-start in nature. It is thought that this stop-start nature of the flow gives rise to the noise seen on this curve. In order to overcome this issue, higher flowrates need to be used.

4.3.6 Final Column Design

In order to allow the use of higher flowrates, and hence eliminate the noise problem in the acetone transition chromatogram, it was decided that the diameter of the column should be increased. A larger diameter column would allow the volumetric flowrate to be increased whilst maintaining the same linear velocity, thus increasing the flowrates available over the operating range of the column. An internal diameter of 700µm was chosen. The acetone transitions were performed with a packed and unpacked column and the investigations were performed as described in Section 4.2.4
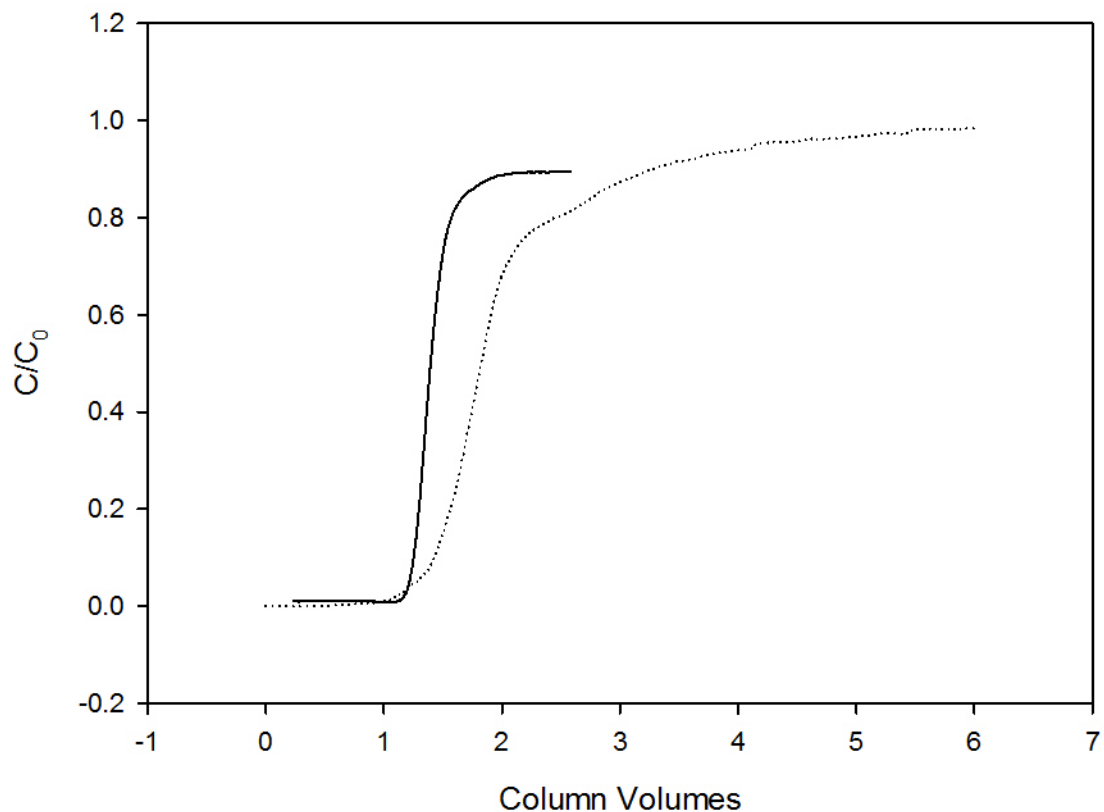
Figure 4.18 – Graph showing the acetone transitions obtained with a packed and unpacked column at 50cm hr^{-1}. The solid line shows an acetone transition obtained with a packed 700µm internal diameter column packed with Glutathione Sepharose 4b matrix. The dotted line shows an acetone transition obtained with an unpacked 700µL internal diameter column.

Figure 4.18 shows the acetone transitions obtained with the larger 700µm internal diameter column. Acetone transitions were performed both on an unpacked column initially to check whether the noise problem had been resolved. A packed column was then used. It can be seen from these chromatograms that the transition behaviour of both the packed and unpacked columns is much closer to the expected shape. The only slight deviation from this is the fact that neither curve reaches a normalised concentration value of 1. On closer inspection the unpacked column appears to get closer to this value. The initial concentration values were measured without a column in place and it is thought that the difference in pressure drop resulting from adding an

unpacked column causes a lower maximum concentration reading and hence a maximum normalised concentration of less than one. Replacing the unpacked column with a packed column further increases the system pressure drop and hence further decreases the maximum concentration reading resulting in a lower maximum normalised concentration. Comparing the shape of the acetone transitions, for the packed and unpacked column, the notable difference is that the curve is much steeper for the packed column. It is thought that this is because the matrix retards diffusive transport hence reducing band broadening.

Given these results, it is clear this system design behaves in the right manner from the flow point of view. That said, it was decided that a visual investigation of the packing quality was worth performing to qualitatively assess the packing quality prior to further work characterising the column.

4.3.7 Qualitative Assessment of Using 3D Microscopy Techniques

In order to make a qualitative assessment of the packing inside the column, confocal microscopy was used to try to build up a 3D image of the packing in a section of the column. These investigations were undertaken by first labelling the protein with AlexaFluor dye as described in Section 4.2.5 and then binding the protein to the matrix and washing any excess labelled protein as described in Section 4.2.6.
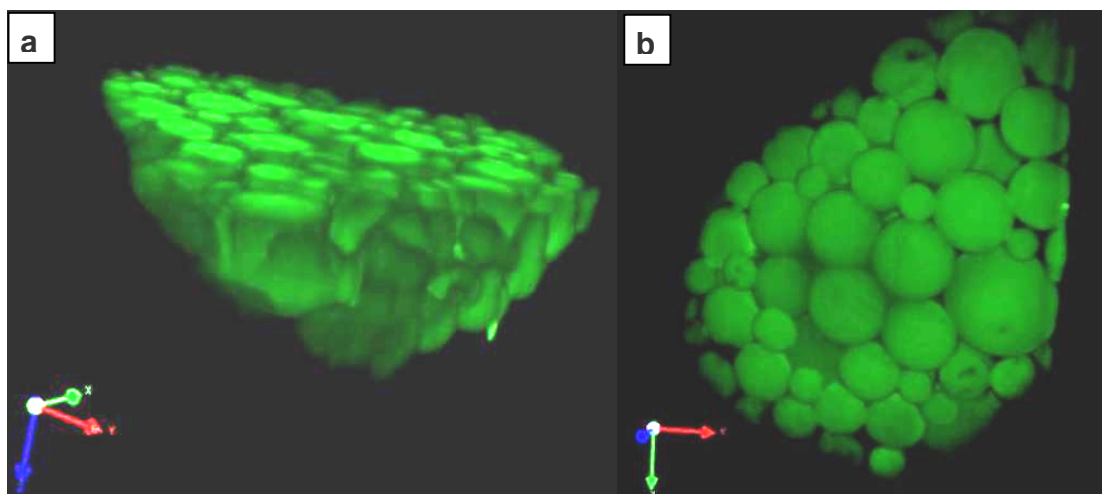
Figure 4.19 - 3D rendered confocal microscopy images at 20x magnification of the 700µm internal diameter micro affinity column (a) shows a longitudinal cross section (b) shows a side view of the column

Figure 4.19 above show images of packing inside the capillary column obtained using confocal microscopy. Whilst a good view was obtained of the first layer of beads the image lost quality with depth into the column making it impossible to image far enough of the column to get a good 3D image of the packing inside.

An alternative technique, two photon microscopy was attempted to try to resolve the issue of losing image quality with depth, and consequently to try to image deeper inside the micro column. Because two photon microscopy excites using two infrared photons it is able to image further through objects. In order to take these images the protein was labelled and bound to the column in the same way as for the confocal microscopy.
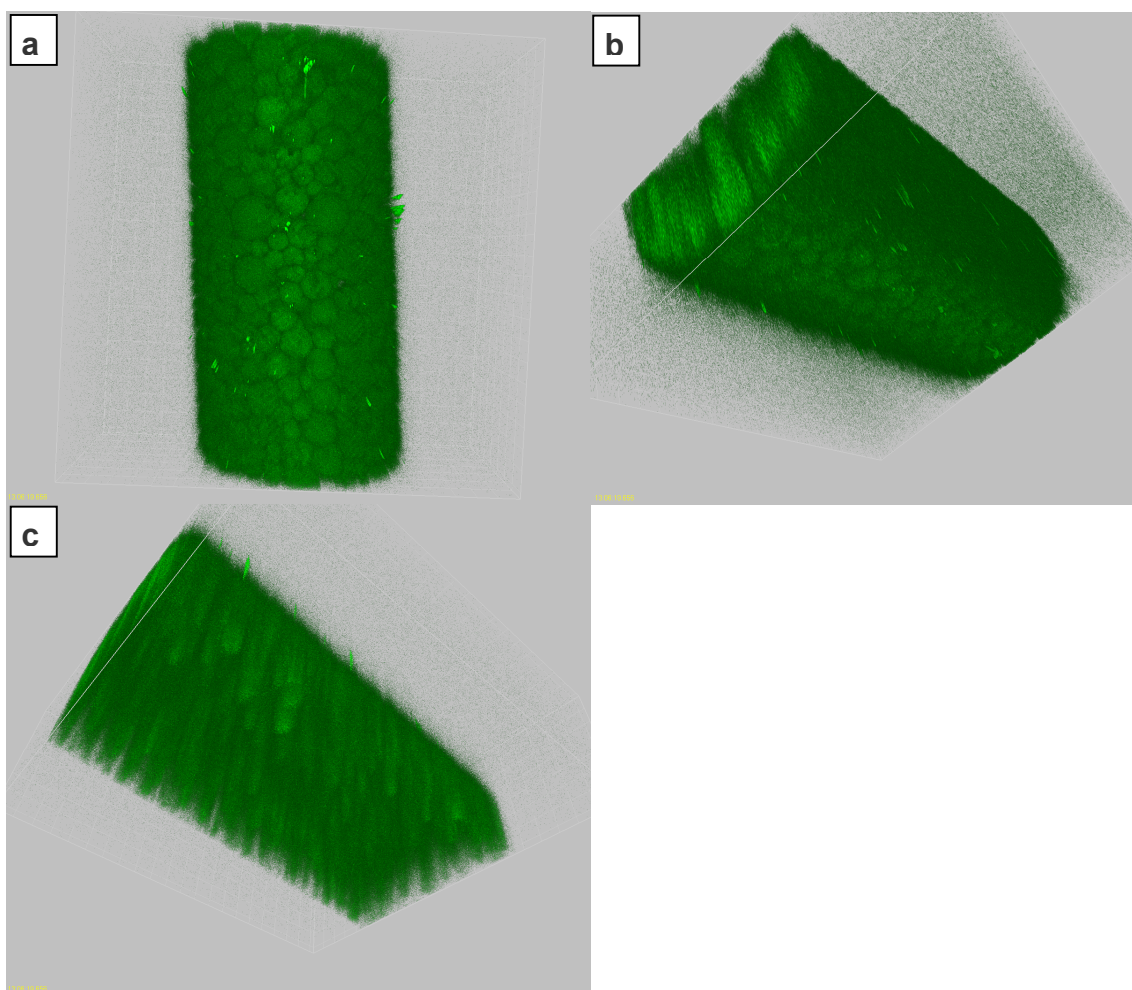
Figure 4.20 – 3D rendered two photon microscopy image of the 700µm internal diameter column at 5x magnification (a) shows a side view of the column (b) shows an axial cross section of the column and (c) shows a longitudinal cross section of the column.

Figure 4.20 shows the images obtained with two photon microscopy. As with confocal microscopy a loss in image quality was observed after the first layer of beads. Whilst it was possible to image further through the column the images were not of sufficient quality to render into a meaningful 3D image. It is thought that because of the cylindrical shape of the capillary, and spherical shape of the beads, diffraction and internal reflection inside the column may have resulted in the poor image quality of the layers below the surface. Alternative techniques of imaging inside the column such as Magnetic Resonance Imaging and Computed Tomography were considered as alternative ways of imaging inside the column. However, it was decided that the confocal and two photon

microscopy images pointed to sufficiently good packing inside the column to warrant using the column for further characterisation work.

4.4   Summary of Findings and Conclusion

In this chapter an investigation of two different methods of packing a capillary was undertaken. It was found that packing by Nanobaume was both the quickest and the most reproducible method of packing the capillary for the microaffinity chromatography column.

The initial column design and reasoning were presented, and through a process of incremental improvements an appropriate microcolumn design for further characterisation was arrived at. The key issues that needed to be overcome were dead volume capacity, instability of flow and the introduction of air bubbles into the system which all had a detrimental affect on the shape of the acetone transition curves. In order to address these issues the fittings were redesigned to reduce the dead volume capacity, the pumping method was altered and the column diameter was increased. The resulting column design produced acetone transitions of the correct shape. The final micro column design for subsequent characterisation work has an internal diameter of 700 μm, a length of 5 cm, a bed volume of approximately 19 μL and is packed with polydisperse standard Glutathione Sepharose 4b matrix.

3D microscopy was undertaken on the final column with a view to qualitatively assessing the packing.   Whilst a 3D image of the packing right the way through the column was not possible by either confocal or two photon microscopy. The images obtained did provide a certain degree of assurance that the column was properly packed.

5 Micro Affinity Chromatography - Characterisation of the system

5.1 Introduction and Aims

Having arrived at a chromatography column design in the previous chapter, this chapter concentrates on quantitative investigations to characterise the behaviour of the column and system in terms of packing quality, critical system parameters such as voidage and dead volume, behaviour of the column with a pure Glutathione-S-Transferase (GST) feed, and behaviour of the column with recombinant *Escherichia coli* lysate expressing GST from *Schistosoma japonicum*

The first section, materials and methods, describes the specific experimental materials and techniques used to characterise the microaffinity chromatography system in terms of critical system volumes, column packing and behaviour with both pure protein and 100% clarified lysate feeds.

The second section, results and discussion, is divided into four subsections. The first subsection defines the system in terms of critical system properties such as dead volume and column voidage. The second subsection characterises the packing of the microaffinity column in comparison with packing in a lab scale column. The third subsection investigates the breakthrough and elution performance of the column with pure protein, and compares this to the behaviour of a lab scale column with the same feedstock. Finally the chapter goes on to explore the microcolumn's behaviour when loaded with a 100% clarified *Escherichia coli* lysate.

The concluding section of this chapter draws out the key findings from these investigations in terms of the usefulness of this microaffinity column for rapid one step purifications of complex feeds, and looks at what further work may be necessary in this area.

A number of methods are available to characterise chromatography columns. These are described in Section 1.9 and include HETP analysis, peak asymmetry factor, tailing factor and the dynamic binding capacity. HETP analysis and peak asymmetry are typically used to characterise the packing quality in the column. These quantities are estimated from a peak created by injecting a quantity of a solution, containing a small non-binding molecule (that can be detected e.g. by a UV detector) on to the column. Acetone is usually used for this and the quantity of solution that is injected is typically less than 5% of the column's volume. This presents challenges with fluid handling at the microfluidic scale (where the column volume is typically of the order of a few microliters to a few tens of microliters) as the quantity of acetone solution required to create the pulse is very small.

Measurement of the dynamic binding capacity is used to characterise the column's performance with respect to how well it captures the analyte, under flow conditions. However, it is assessed from the breakthrough curve, and noise in breakthrough measurements can have a significant impact on the calculated dynamic binding capacity. Accurate determination of the dynamic binding capacity is therefore a challenge in microfluidics as errors may be caused by:

- the small volumes involved which mean that evaporation may cause inaccuracy in readings by changing concentrations;

- the sensitivity of instrumentation and assays used to quantify small amounts of analytes;

- and the significant impact of fluctuations in flow at low flowrates.

However, it may be possible to overcome some of these challenges by designing experiments well and using appropriate techniques.

A number of research groups have used the dynamic binding capacity as a way to characterise microfluidic chromatography column performance (Shapiro et al. 2009; Deshpande et al. 2012). Deshpande *et al* used dynamic binding capacity to characterise their microfluidic metal affinity column's performance over a range of flowrates and compare this to the equilibrium binding capacity of the adsorbent (Deshpande et al. 2012), and Shapiro *et al* used dynamic binding capacity to characterise the performance of a 1.5µL ion exchange column and compare it with data for large columns from the literature. However, there are some significant errors in the dynamic binding capacities obtained (Shapiro et al. 2009) and these are probably due to some of the factors described above.

5.2   Materials and Methods

This section outlines the materials and methods used which are specific to this chapter i.e. those specific to characterisation of the microaffinity chromatography system in terms of critical system volumes, column packing, and column behaviour with both pure protein and 100% clarified lysate feeds.

Where there are differences in the methods used for lab and microscale columns, these are specifically stated. Otherwise, methods for both scales were the same.

Unless otherwise stated, all reagents were obtained from Sigma Aldrich, Dorset, UK.

5.2.1 Microcolumn Packing
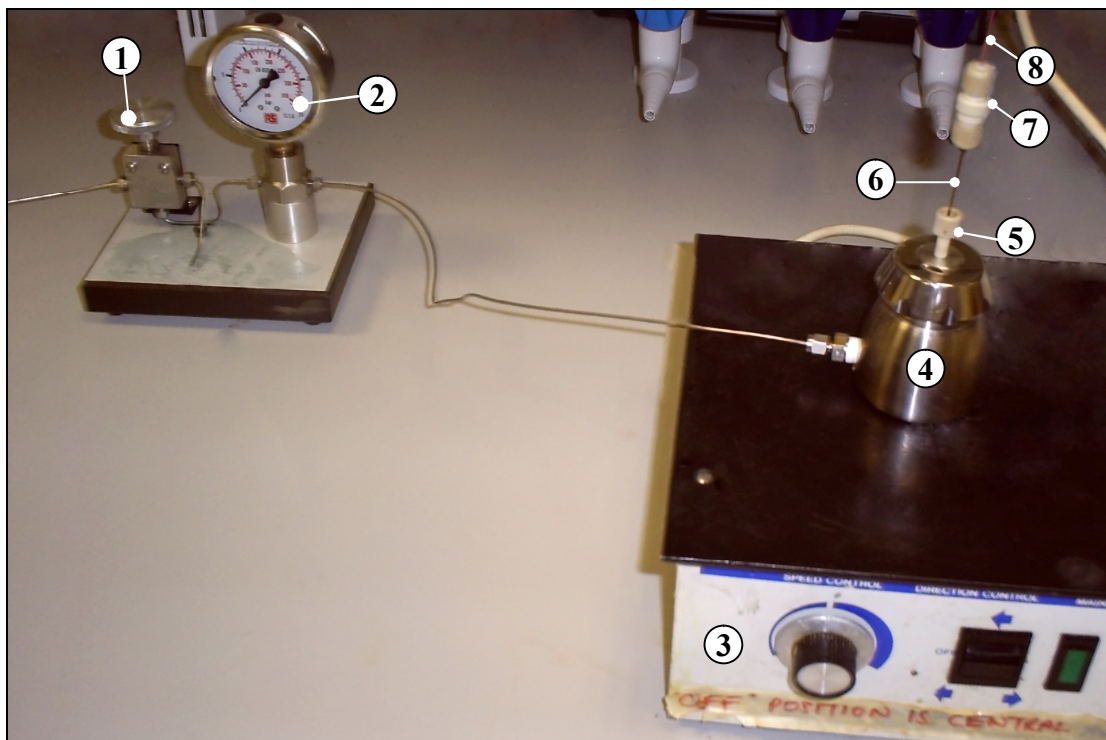
Figure 5.1 - Photograph of Nanobaume packing set up. (1)Valve; (2) Pressure gauge; (3) Magnetic stirrer plate; (4) Nanobaume (); (5) F-130 extra long 10-32 fingertight nut (IDEX Health and Science, Washington, USA); (6) 700µm internal diameter fused silica tubing (Polymicro technologies, Arizona, USA), (7) M530 Micro filter assembly (IDEX Health and Science, Washington, USA) (8) 100µm internal diameter PeekSil® capillary

Fused silica capillary (Polymicro technologies, Arizona, USA) with an internal diameter of 700µm was cut to a length of 15 cm using a carbide cutter (IDEX Health and Science, Washington, USA) - a longer length of capillary than that of the final column was used. This was to enable the packing to be observed and hence to ensure that the required 5 cm column had been fully packed.   A filter assembly (IDEX Health and Science, Washington, USA) was then added to one end of the capillary and the other was then fed into the lid of the Nanobaume, so that the free end would be positioned just above the magnetic stirrer once the device was closed.

The ferrules and filter capsule inside the assembly were specially made as described in Section 4.3.4 in order to minimise any dead volume capacities inside the column. The filter capsule contained two nylon mesh filters one 35 µm on the column side and one 80 µm mesh on the inlet/outlet side.

1350 µL of 20 %(w/v) ethanol was added to a glass vial. 150 µL of Glutathione Sepharose 4b slurry (G E Life Sciences, Buckinghamshire, UK) was then added to the same vial, followed by a small cylindrical magnetic stirrer bar which was 2.27mm in diameter and 5.17 mm in length. The contents in the vial were not stirred prior to placing in the Nanobaume. This is because mixing the slurry increased the time taken to pack the column. The reduced packing time was probably because the unstirred suspension had a higher density of matrix beads at the bottom and therefore more beads would enter the capillary per unit time. The vial was then placed inside the Nanobaume and the Nanobaume was closed. The Nanobaume was placed on a magnetic stirring table as shown in Figure 5.1.

The pressure regulator on the nitrogen gas supply was then set to 3 bar and immediately the magnetic stirring table was switched on. The capillary was observed. When the packing inside the capillary was sufficient, i.e. when the packing was more than 5cm down the capillary, the nitrogen gas supply was turned off, and the capillary was carefully removed from the Nanobaume. The capillary was then cut, being careful not to disturb the matrix inside, using a carbide cutter. A second micro filter assembly was then added to the free end of the capillary to complete the microcolumn.

The column was then placed in a specially designed holder, to prevent it from breaking. The column and holder were then placed inside a falcon tube filled with 20% (V/V) ethanol to avoid evaporation of liquid from the end of the column which could have changed the packing characteristics.

5.2.2 Lab Scale Column Packing

A syringe was used to fill the top and bottom adaptors of an XK16/20 column (G E Life Sciences, Buckinghamshire, UK) with PBS pH7.4 - being careful to ensure there were no air bubbles trapped under the frits. The outlet of the bottom adaptor tubing was capped, the adaptor was placed in the bottom of the column and the o-ring adaptor seal was closed.

The column was filled with sufficient Glutathione Sepharose 4b 75% slurry (G E Life Sciences, Buckinghamshire, UK) to make a 10 mL bed when packed i.e. one bottle. This was done by shaking the bottle to resuspend the matrix and pouring the slurry down the inside wall of the column to avoid introducing any air bubbles. The column was topped up with PBS pH7.4 until it was three quarters full. The inlet adaptor was placed into the column at a 45° angle to ensure that no air bubbles were introduced into the column. The top adaptor o-ring was then sealed just below the level of the buffer.

PBS pH7.4 was pumped into the column at a starting flowrate of 1 mL min^{-1} for 100mins (10 column volumes). The flowrate was then increased to 2 mL min^{-1} and this flowrate was maintained for 50mins. Finally the flowrate was increased to 2.5 mL min^{-1} for 40mins. The bead height was marked on the outside of the column. The flow was then turned off, the top adaptor seal was loosened and the adaptor was then gently eased down the column to the bed height marking.

The adaptor o-ring was resealed and the flow was started at 2.5 mL min^{-1} again to ensure that the top adaptor positioning was correct.

5.2.3 Measurement of HETP for the Microcolumn
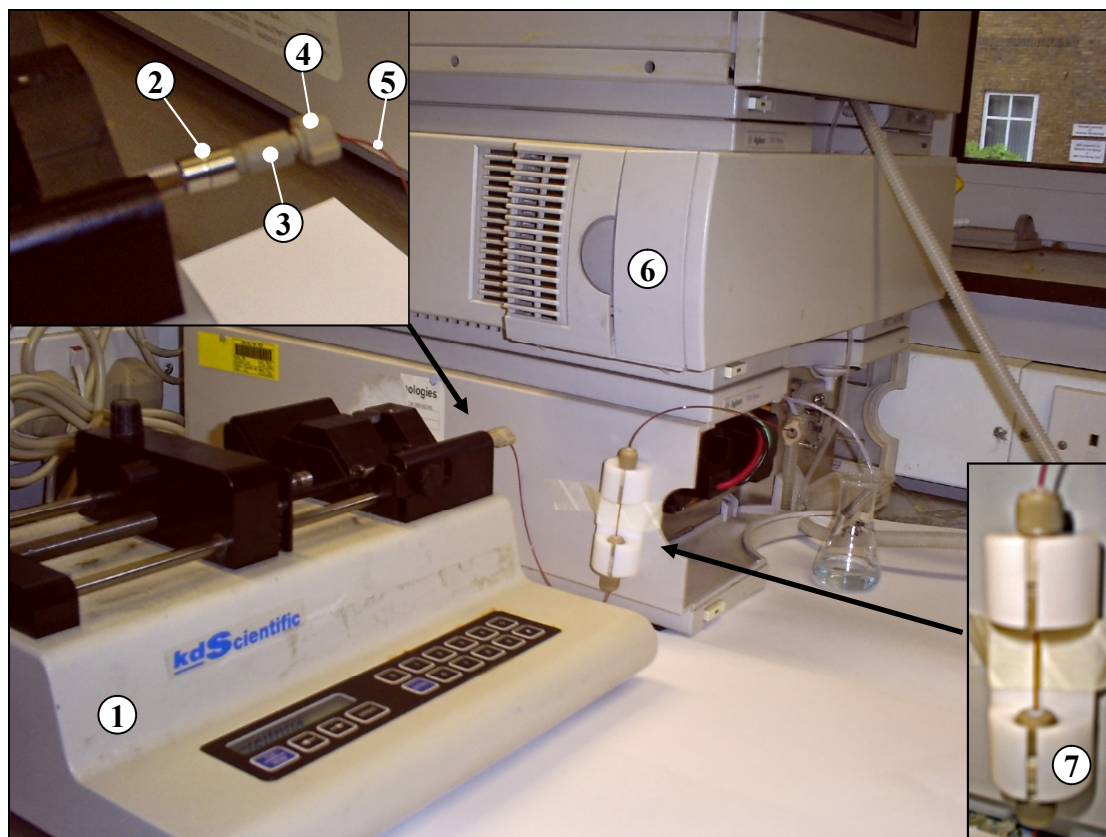
Figure 5.2 – Microscale chromatography experimental set up. The system comprised of the following: (1)Syringe pump (Kd Scientific, Massachusetts, USA); (2)Gastight® Glass syringe (VWR, Dorset , United Kingdom); (3) P-659 syringe adaptor (IDEX Health and Science, Washington, USA); (4) double winged peak nut with 1/32" ferrule (Agilent Technologies, Cheshire, UK); (5) PeekSil tubing 100µm internal diameter, 1/32" external diameter (IDEX Health and Science, Washington, USA); (6) Agilent 1100 HPLC diode array detector using a semi-micro flowcell (Agilent Technologies, Cheshire, UK), (7) Microcolumn in holder.

Figure 5.2 shows the experimental set up used for the microcolumn experiments. The concentration at the outlet of the column was measured at 280nm with an Agilent 1100 HPLC diode array detector using a semi-micro flowcell.   Results were recorded using Chemstations software (Agilent Technologies, Cheshire, UK)

The microcolumn was first equilibrated by using the syringe pump and 250µL glass syringe to pump 10 column volumes of PBS pH7.4 through the column at 50cm hr^{-1}. The column was then loaded, using the syringe pump, with 0.2% Acetone in PBS pH 7.4 at 50cm hr^{-1} until the UV absorbance at 280nm levelled out at its maximum value. This procedure was repeated at 75cm hr^{-1} and 100cm hr^{-1}

5.2.4 Measurement of HETP for the Lab Scale Column

The 10 mL XK16 packed was operated using an ÄKTA Basic chromatography machine with UNICORN software (G E Life Sciences, Buckinghamshire, UK). The bed was first equilibrated with 10 column volumes of PBS pH7.4 at 50 cm hr^{-1}. The column was then injected with 360 µL of 0.2% Acetone in PBS pH 7.4 using a 360 µL injection loop (verified by volumetric syringe). The UV absorbance reading was monitored and the run was stopped once the reading had returned to the baseline. This procedure was repeated at 25 cm hr^{-1}, 75 cm hr^{-1}, 85 cm hr^{-1}, and 100 cm hr^{-1}.

5.2.5 Measurement of Dead Volume in the Microcolumn

The system was set up as shown in Section 5.2.3. However, the column was removed from the system and the inlet and outlet capillaries were connected using a P779 Nanotight union (IDEX Health and Science, Washington, USA), which was chosen because it only has and 8 nL swept volume. PBS pH7.4 was passed through the system for 5 mins at 50cm hr^{-1} to flush the system. This was then followed by 1 mg/mL (w/v) Blue Dextran in PBS pH 7.4 at 50 cm hr^{-1}.

5.2.6 Measurement of Extra Bead Volume in the Microcolumn

The system was set up as described in Section 5.2.3. The column was first equilibrated with 10 column volumes of PBS pH7.4 at 50 cm hr^{-1}. The column was then loaded with 1 mg/mL (w/v) Blue Dextran in PBS 7.4 at 50 cm hr^{-1} until the UV absorbance at 280 nm levelled out at its maximum value. This procedure was repeated at 75 cm hr^{-1} and 100 cm hr^{-1}.

5.2.7 Measurement of Void Volume in the Lab Scale Column

The system was set up as described in Section 5.2.4. The bed was first equilibrated with 10 column volumes of PBS pH7.4 at 50 cm hr^{-1}. The column was then injected with 360µL of 1 mg/ mL (w/v) Blue Dextran in PBS pH7.4. The UV absorbance reading was monitored and the run was stopped once the reading had returned to the baseline.

5.2.8 Microscale and Lab Scale Pure Protein Runs

The systems for microscale and lab scale runs were set up as described in Section 5.2.3 and 5.2.4 respectively. In both cases, the column was first equilibrated with 10 column volumes of PBS pH7.4. The column was then loaded with 1 mg/mL (w/v) GST, from equine Liver, in PBS pH 7.4. Following loading, the column was then washed with 10 column volumes of PBS pH7.4. The protein was eluted with 10mM reduced glutathione in Tris-HCl pH8.0.

The difference in retention time at lab and microscale was used to adjust the breakthrough and elution curves for dead volume in the lab scale system.

5.2.9 Microscale and Lab Scale Column Cleaning

Between runs, the column was cleaned with two column volumes of 6M Guanidine Hydrochloride to denature and remove any non-specifically bound proteins, followed immediately by five column volumes of PBS pH7.4. This was followed by two column volumes of 70% ethanol to remove any hydrophobically bound proteins, followed immediately by 10 column volumes of PBS pH7.4.

5.2.10 Column Care

When either the lab or the microscale column were left overnight, they were washed with 10 column volumes of 20% (v/v) ethanol. This was to ensure no microbial growth on the column and particularly for the microcolumn to ensure no crystallisation of salts from the buffer, which could clog up the column.

5.2.11 Microcolumn Storage

Following the 20% ethanol wash, the column and holder were placed inside a falcon tube filled with 20% (v/v) ethanol. This was done to avoid evaporation of liquid from the end of the column which could change the packing characteristics.

5.2.12 Protein Reuse for Large Scale Chromatography Runs

All output from the lab scale column, over the run cycle, was collected. The resulting solution was mixed and aliquoted, in 20 mL aliquots, to an even number of 10KDa PES membrane spin filters (Sartorius, Surrey, UK). The spin filters were spun at 3220 RCF for 15mins at 4°C. This was done in an Eppendorf 5810 R bench top centrifuge (Eppendorf, Cambridge, UK) using the A-4-62 swing out bucket rotor with falcon tube holders.

The retentate from the spin filters was pipetted into a falcon tube, and made up to 10 mL (if below this). A length of a 10KDa molecular weight cut off Snakeskin dialysis tubing (Thermo Scientific, Illinois, USA) was then wetted in PBS pH 7.4. One end of the tubing was then tied and clamped using dialysis tubing clips. The GST solution was pipetted into the dialysis tubing. The open end of the tubing was then tied and clamped with a dialysis tubing clip.

The tubing containing the GST solution was then placed in to a stirred beaker containing 1L of PBS pH7.4 and left to dialyse over night in a fridge. The following day the PBS was discarded and replaced by 1L of fresh PBS and the dialysis was allowed to proceed for a second night.

Following dialysis the GST solution was either adjusted to the correct concentration and re-used, or snap frozen and stored at -80°C for later use.

Batches of twenty aliquots of protein solution were snap-frozen at a time. Twenty 2 mL Eppendorf tubes (Eppendorf, Cambridge, UK) were placed in a round floating Eppendorf tube rack (Nalgene, New York, USA). 1.5 mL of protein solution was aliquoted into each tube. The tubes were closed and the lids were labelled. The aliquots were then snap frozen as described in Section 2.7.

5.3 Results and Discussion

This section investigates the behaviour of the microaffinity chromatography system in terms of critical system properties: such as dead volume and column voidage and critically examines the packing quality in the column compared to a lab scale column. It then goes on to look at how the microcolumn performed with a pure protein feed and compares performance to a lab scale column. Finally the chapter looks at microcolumn performance with a 100% clarified *Escherichia coli* lysate feed.

5.3.1 Microaffinity Chromatography System Volumes

The microaffinity chromatography studies in this chapter were carried out on a 5cm long 700 μm internal diameter column packed with Glutathione Sepharose 4B matrix (GE Life Sciences, Buckinghamshire, UK). The column was packed according the protocol outlined in Section 5.2.1.

As discussed in Section 1.14, Glutathione Affinity Chromatography was chosen because:

- GST affinity tags are a low cost way of purifying and obtaining high yields of recombinant proteins (Lichty et al. 2005);

- GST affinity tags have been used successfully in vaccine production (Dempster et al. 1996; Wright et al. 1992), studies of protein-protein interactions (Peles et al. 1997) and cellular biology studies (Ellis et al. 1997);

- GST activity can be easily and directly assayed by the CDNB (1-chloro-2,4-dinitrobenzene) assay;

- GST can be obtained relatively inexpensively as pure protein and can easily expressed in *Escherichia coli,* via pGex plasmid.

For the purpose of describing system volumes, the chromatography system comprised of:

- inlet and outlet capillaries to the column;

- the column;

- the detector flowcell;

- and the detector inlet capillary.

Table 5.1 shows the critical system volumes of the microaffinity chromatography system which was used for subsequent experiments.

It is recognised in the literature that minimising dead volume plays an important role in ensuring good chromatography performance (Maynard & Grushka 1972), (Jönsson 1987) (Ishii et al. 1977).   Ishii *et al* reported that by minimising dispersion resulting from extra column volumes, chromatographic performance similar to standard HPLC was obtainable in micro HPLC columns with a diameter of between 500 µm and 1mm.

When designing the system, it was decided that because the volume of the column was so small, dead volume would have a significant effect on

performance and so the minimum practical capillary diameters and lengths were chosen in order to minimise this effect. That said, the calculated total dead volume was still 6.65µL which, compared to the column volume of 19.24 µL, was still significant. Therefore, it was considered important to verify this dead volume experimentally and to take it into account when investigating the behaviour of the microcolumn.

Table 5.1 – Volumes of the different components of the microcolumn system

	Length (cm)	Diameter (µm)	Volume (µL)
Column Inlet Capillary	20 ± 0.05	100 ± 3	1.57 ± 0.063
Microcolumn	5 ± 0.20	700±10	19.24 ± 1.3
Column Outlet Capillary	20 ± 0.05	100 ± 3	1.57 ± 0.063
Detector Inlet Capillary	31 ± 0.05	120 ± 3	3.51 ± 0.052
Flow cell	0.6	1030	5.00
Dead volume	-	-	6.65 ± 0.17

Experimental Verification of Dead Volume

In order to estimate the system dead volume, 1 mg/mL blue dextran transitions were obtained at a linear flowrate of 50 cm hr^{-1}, with the column removed, as described in Section 5.2.5. A typical blue dextran transition is shown in Figure 5.3.
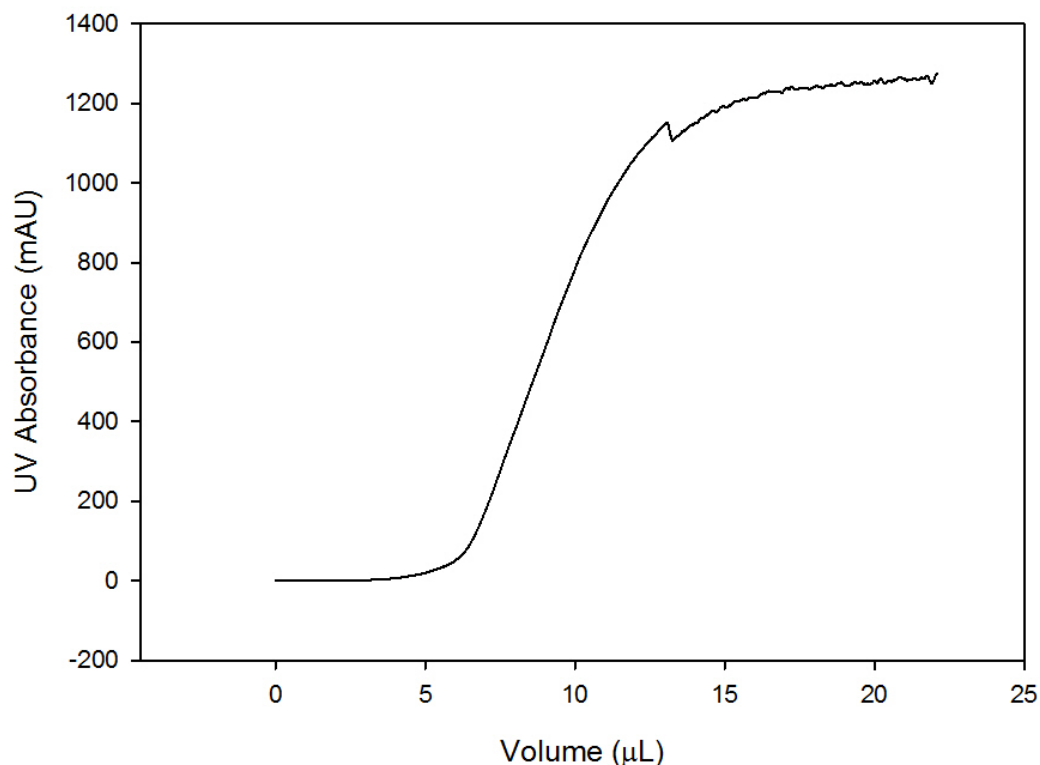
Figure 5.3 – A typical blue dextran transition curve, obtained at a flowrate of 50 cm hr^{-1}, without the micro column in place. The system was first flushed with PBS pH7.4 and then loaded with 1 mg/mL Blue dextran 2000 in PBS pH7.4.

The first order derivatives of these transitions were computed using SigmaPlot (Systat Software Inc, Illinois, USA). Figure 5.4 shows a typical first order derivative curve. The curve has a flattened peak, though this property is more visible in the blue dextran transitions performed with the column in place (Figure 5.6).

The location of the flattened peak was estimated by fitting the curve to a modified 4-parameter Weibull distribution (Equation 5.1(Yang 2008)), in SigmaPlot, to predict the maximum. A Weibull distribution was used rather than a Gaussian distribution because the blue dextran derivative curves exhibit tailing properties and hence it was possible to get a better fit.

$$f(x,a,x_0,b,c) = \frac{ac}{b}\left(\frac{x-x_0}{b}\right)^{(c-1)} e^{-\left(\frac{x-x_0}{b}\right)^c}$$

Equation 5.1

The dashed line in Figure 5.4 shows the Weibull distribution fitted to the experimental data. The Weibull distribution fits the data well.
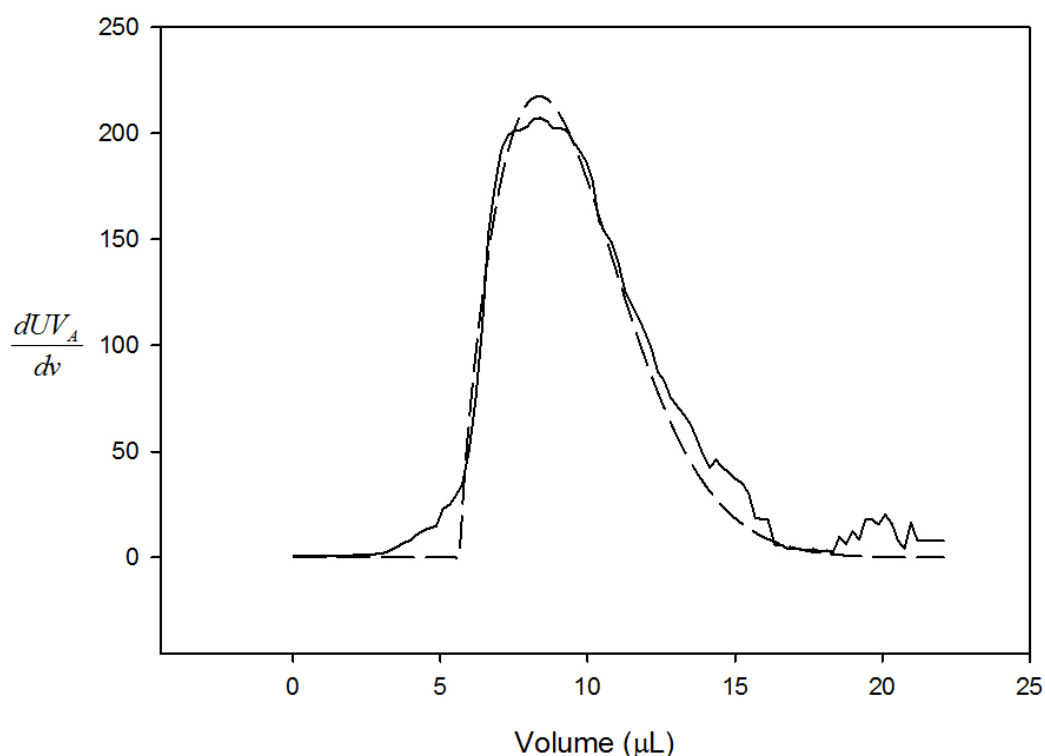
Figure 5.4 – A typical blue dextran transition derivative curve, with the micro-column removed, fitted to a Weibull distribution. The derivative curve shown (solid line) is for the blue dextran transition at 50cm hr^{-1}. The dashed line represents the predicted derivative curve when the data is fitted to a Weibull distribution

The dead volume estimated by blue dextran transition derivative is 8.54μL ±0.17 μL. This is higher than the calculated dead volume reported in Table 5.1. It is thought that this discrepancy is due to the inaccuracies caused by the detector volume, which made it difficult to locate the maxima on the truncated

peak. Consequently, the calculated dead volume in Table 5.1 was used to adjust the chromatograms.

Extra bead volume

In order to calculate the voidage of the microcolumn and confirm that flowrate, over the range used in these investigations, would have little effect on the void volume of the micro column, the extra-bead volume, which includes the dead volume, was estimated by using blue dextran 2000 transitions at different flowrates, with the column in place. Blue dextran has been used by researchers to measure the void volume of affinity columns (Katoh et al. 1978). It is used because it is too large to enter the pores of the matrix beads, and is not expected to bind to the matrix.

1 mg/ mL blue dextran transitions were obtained at linear flowrates of 50 cm hr^{-1}, 75 cm hr^{-1} and 100cm hr^{-1} as described in Section 5.2.5. Figure 5.5, shows blue dextran transition data at a linear flowrate of 50 cm hr^{-1}.
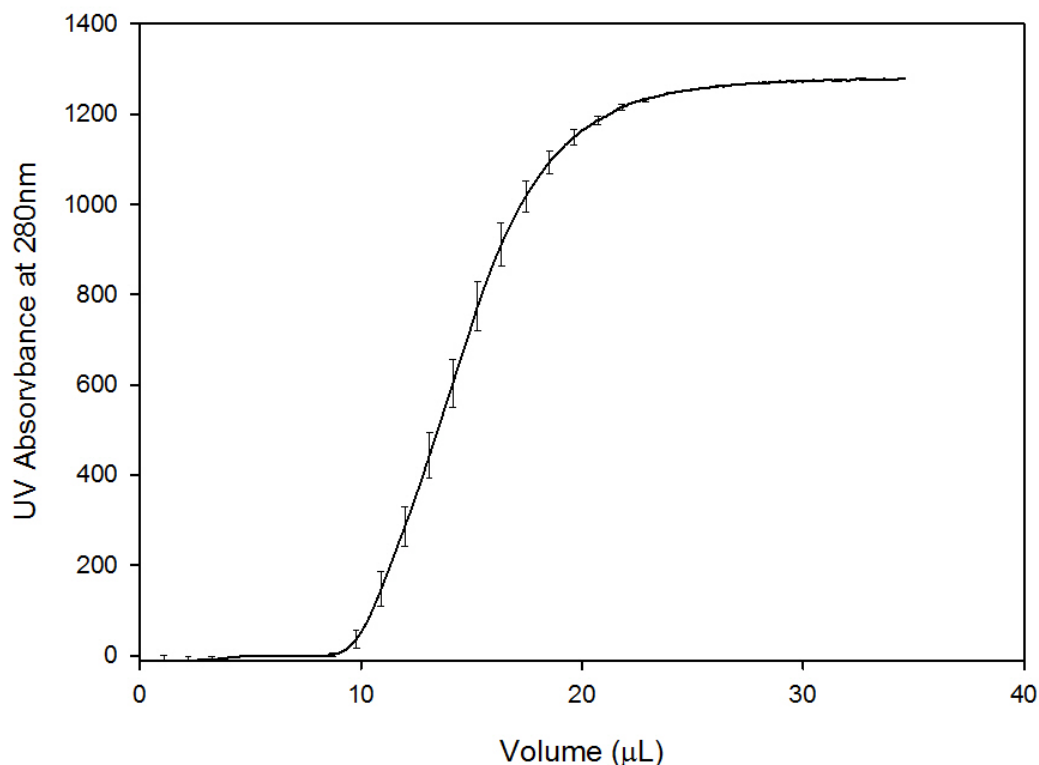
Figure 5.5 – Blue dextran transition curve obtained at a flowrate of 50 cm hr⁻¹. The column was first washed with PBS pH7.4 and then loaded with 1 mg/ mL Blue dextran 2000 in PBS pH7.4

As for the dead volume, the first order derivatives of these transitions were computed using SigmaPlot (Systat Software Inc, Illinois, USA). Figure 5.6 shows these first order derivative curves. As with the first order derivatives obtained without the column in place, these curves have an almost flat peak. However, the flattening of these peaks is more pronounced and it is therefore easier to estimate their width, which is of the order of 5µL - similar to that of the volume of the detector flowcell. It is therefore thought that the flat peak exhibited by these curves is due to residence time in the flowcell.
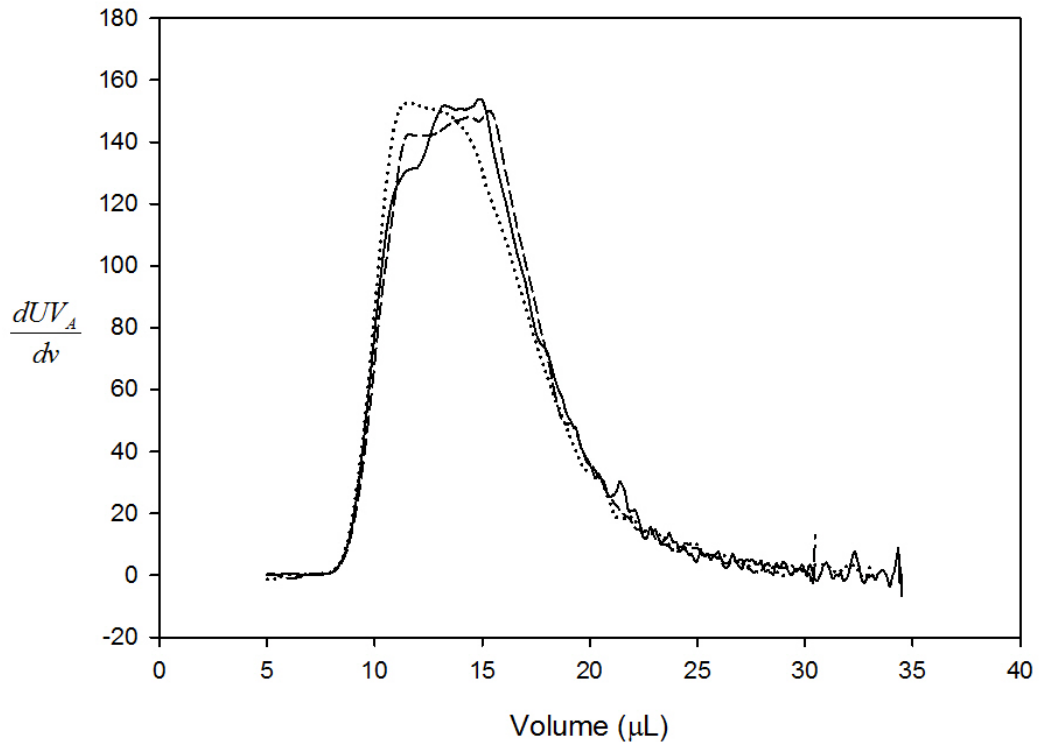
Figure 5.6 - First order derivatives of the averaged blue dextran transitions. 1 mg/ mL blue dextran 2000 was loaded on to the column at different flowrates and the resulting transitions for each flowrate were averaged and differentiated to give the above curves. The solid line is the first order derivative of the averaged blue dextran transitions obtained at a linear velocity of 50 cm hr^{-1} the dashed line is the first order derivative of the averaged blue dextran transitions obtained at is 75 cm hr^{-1} and the dotted line is the first order derivative of the averaged blue dextran transitions obtained at 100 cm hr^{-1}

As for the estimation of dead volume, the location of the truncated peak was estimated by fitting the curve to a Weibull distribution in SigmaPlot, to predict the maximum.

Figure 5.7 shows an example derivative curve (solid line), for the 50 cm hr^{-1} blue dextran transition. The dashed line shows the Weibull distribution that was fitted to the derivative curve. A good fit is evident from the graph.
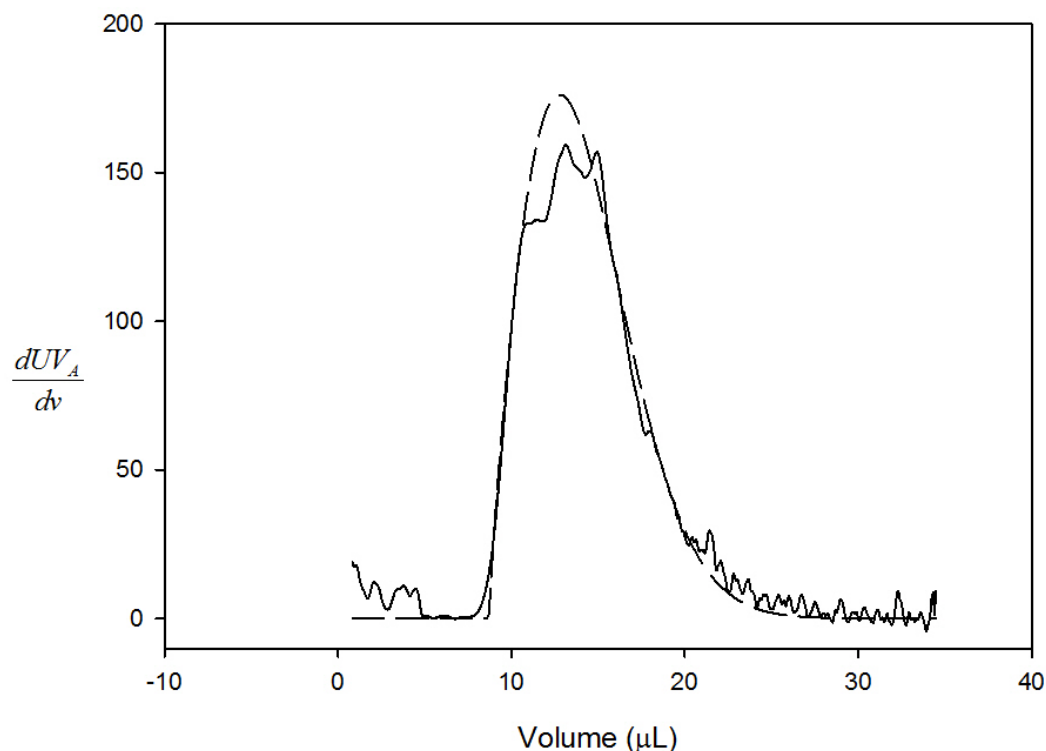
Figure 5.7 – Typical blue dextran transition derivative curve showing the estimation of the void volume by fitting the curve with a Weibull distribution. The derivative curve shown is for the blue dextran transition at 50 cm hr⁻¹. The dashed line represents the predicted derivative curve when the data is fitted to a Weibull distribution

Table 5.2 shows the estimated extra bead volumes at the different flowrates investigated. These extra bead volumes include a proportion of the detector volume as well as the column inlet, column outlet, detector inlet capillary volumes, and the bed voidage. There is very little difference in the extra bead volume at different flowrates. This is to be expected as any slight bed compression would be so small that it would be very difficult to measure.

Table 5.2 - Estimated extra bead volume at different flowrates

Flowrate (cm hr^{-1})	Extra Bead Volume (µL)
50	13.10 ± 0.31
75	13.2 ± 0.32
100	12.7 ± 0.22

Voidage

The voidage of the micro column was estimated by subtracting the dead volume (8.52µL) from the extra bead volume (13.10µL). In order to provide a basis for comparison, the voidage of the lab scale column was estimated by blue dextran pulse as described in Section 5.2.7.

Table 5.3, below, compares the voidage of the 5 cm micro column with that of a 5 cm lab scale XK 16 column. A packed bed of spherical particles would typically be expected to have a voidage of approximately 0.3. As can be seen, the voidage of the lab scale column is 0.35 which is slightly higher than might be expected. However, this increased voidage could be due to dead volume in the column inlet and outlet tubes. By contrast, the micro column displays a significantly smaller voidage than the lab scale column.   There is significant error in the voidage value of the micro-column with the voidage potentially ranging from 0.2 to 0.28.   This larger error can be attributed to the errors resulting from estimation of the maxima of the truncated blue dextran derivative peaks which were used to estimate the column voidage.

Table 5.3 - Table comparing voidage of the microcolumn and the XK 16 lab scale column

Column	Voidage
Micro Column	0.24 ± 0.041
Lab Scale	0.35 ± 0.002

However, whilst it is difficult to say with certainty that the void fraction in the microcolumn is lower than expected, the results do suggest a lower than expected void fraction and this could be due to wall effects. Shalliker *et al* suggested that, in conventional chromatography columns, two wall effects exist due to radial packing variability. Immediately against the wall, matrix beads are unable to form a close packing arrangement. As a result there is a higher void fraction and hence a higher mobile phase velocity close to the wall. The local void fraction is highest closest to the wall, tending to unity at the wall, the void fraction then drops to it's lowest value at one bead diameter from the wall (Shalliker et al. 2000)(Kaltenbrunner et al. 1997). A thicker layer exists inside the first one, with a lower void fraction than the bulk of the column due to higher packing density near the wall. Guiochon suggested that this layer was caused by the high radial stress applied by the bed to the wall as a consequence of friction between particles (Guiochon et al. 1997) and (Knox et al. 1976) suggested that this region was of the order of thirty beads across. The micro affinity column has an internal diameter of approximately 700µm. The mean diameter of the matrix particles is 90µm. That means, on average the column is just over seven beads across. Consequently, it is thought that both wall effects exist inside the micro-column.

While the first wall effect tends to increase the voidage in the column, the second wall effect tends to give rise to tighter packing in the centre of the column than in a conventional column. This would result in a loose outer core and tighter inner core to the column. Because the inner core of the column is larger in volume than the outer core it is thought that overall this would result in a lower voidage and this would seem to fit with the results.

5.3.2 Characterisation of the packing

Height of Theoretical Plates

In order to assess the quality of the packing, the height of theoretical plates (HETP) was estimated for both the lab scale and micro columns. Measurement of HETP is done by injecting a solution containing a non-binding substance, most commonly acetone, on to the column. A non-binding substance allows dispersion effects to be examined separately from binding effects. Acetone is used because it is a small molecule and hence can enter the pores of the matrix beads. It can also be easily detected by measuring UV absorbance, at the column outlet, at 280nm.

The HETP of the lab scale column was determined experimentally by injecting an acetone pulse on to the column and measuring the UV absorbance at 280nm as the pulse comes off the column, as described in Section 5.2.4. The values of Gaussian HETP and asymmetry were calculated from the acetone peaks obtained, using Unicorn software (G E Life Sciences, Buckinghamshire, UK). Figure 5.8 shows a typical acetone pulse obtained at lab scale.
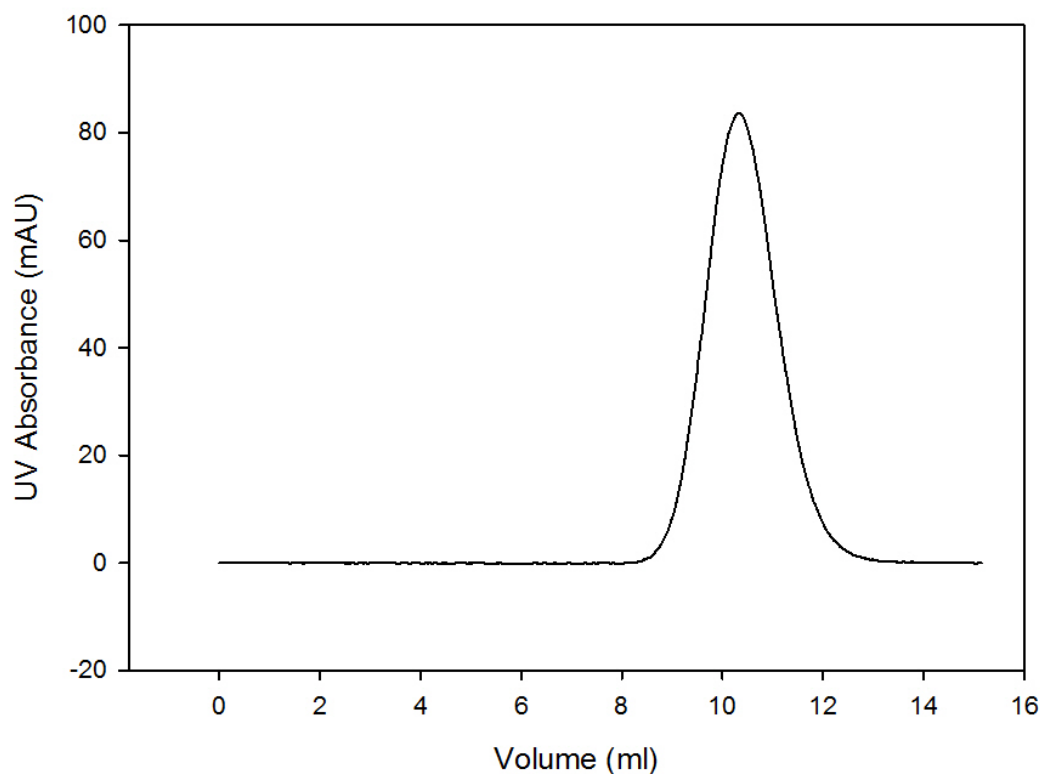
Figure 5.8 - Typical acetone pulse. A 360µL 0.1% acetone (v/v) in PBS pH7.4 was loaded on to the 10 mL XK16 column at 50cm hr^{-1}.

When performing chromatography, particularly at the micro scale, it is critical to ensure there are no air bubbles introduced into the system and that the error in ascertaining the start time is kept to a minimum (these are the two main sources of error). The volume of an acetone pulse injected on to the column to ascertain the HETP typically needs to be less than 5% of the column volume For the microaffinity column, with a bed volume of approximately 19 µL, to measure HETP by injecting an acetone pulse, the volume of acetone solution injected onto the column would need to be less than 1µL. Injecting less than 1µL was not feasible with the experimental system in use for these experiments. This is because this quantity of acetone solution, would need a syringe with a volume of 10µL or less to accurately dispense this amount of liquid. Consequently, it was decided that performing acetone pulses on the micro column would introduce too much error from both the start time estimation and

the inclusion of air bubbles. The data for estimating the HETP was therefore obtained by acetone transition as outlined in Section 5.2.3.
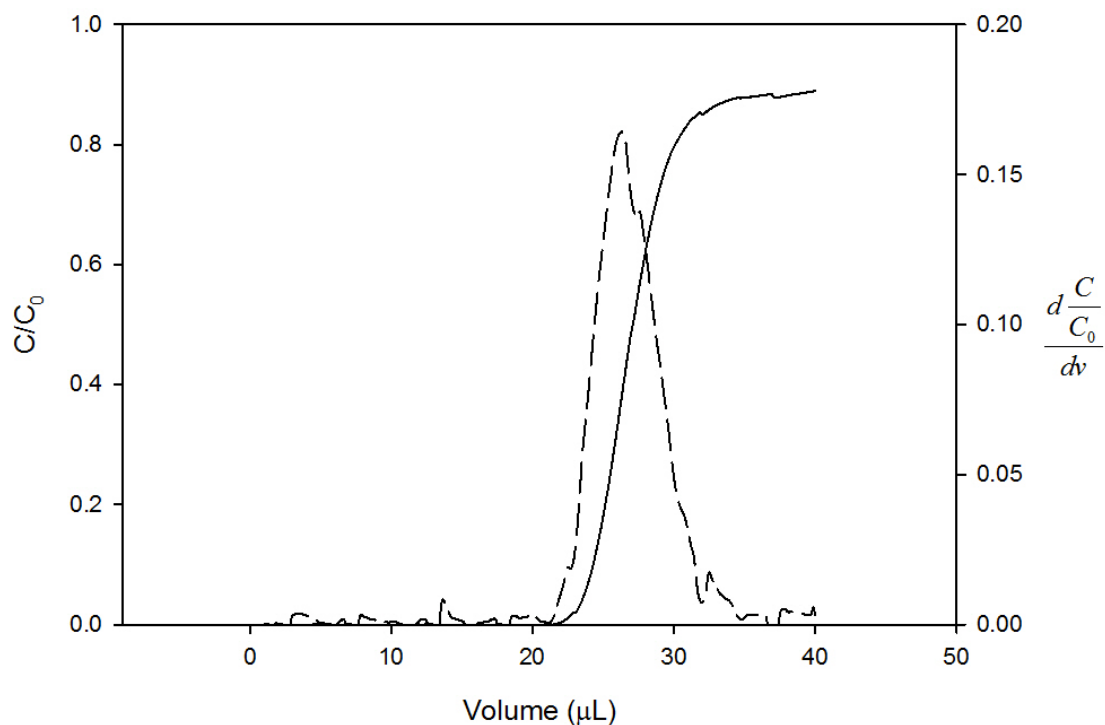
Figure 5.9 - 0.2% acetone transition with its first order derivative. The transition was performed 100 cm hr^{-1} by switching flow between PBS pH7.4 and 0.2% (v/v) acetone in PBS pH7.4.

Figure 5.9, shows a typical acetone transition, performed at 100 cm hr^{-1}, and its first order derivative which was computed using SigmaPlot. The acetone transitions were differentiated and used to calculate the Gaussian HETP and the peak asymmetry using Equation 5.2 and Equation 5.3.

$$HETP = \frac{L}{N}$$

Equation 5.2

Where L is the length of the column and N is the number of plates. The number of plates is given by

$$N = \left(\frac{V_R}{\sigma}\right)^2 = 5.55\left(\frac{V_R}{W_h}\right)^2$$ **Equation 5.3**

Where V_R is the retention volume, σ is the standard deviation of the peak, and W_h is the width at half the peak height. The retention volume and width at half the peak height were estimated graphically.

Non-Gaussian HETP is given by Equation 5.4 (Larson et al. 2003). The non-Gaussian HETP takes into account the entire shape of the curve.

$$HETP_N = \frac{L\sigma^2}{\mu_V^2}$$ **Equation 5.4**

Where L is the length of the column, σ^2 is the variance is given by Equation 5.5 and μ_v, the mean volume, is given by Equation 5.6 (McCue et al. 2007)

$$\sigma^2 = \frac{M_2}{M_0} - \left(\frac{M_1}{M_0}\right)^2$$ **Equation 5.5**

$$\mu_V = \frac{M_1}{M_0}$$ **Equation 5.6**

Where M_0, M_1 and M_2 are the zeroth, first and second moments of the distribution. The moments that result from a step change at the column inlet are defined in Equation 5.7

$$M_j = \int_0^{V_{total}} V^j \frac{dC}{dV} dV$$ **Equation 5.7**

Solving these equations (solution shown in Annex B) gives Equation 5.8 and Equation 5.9 which were used to estimate µ and σ^2 respectively (McCue et al. 2007). Calculations were performed in Excel and the average of every ten data points was taken to reduce the impact of random error on the result

$$\mu_V \approx \frac{\sum_0^i V_i \Delta C_i}{C_{Final} - C_{Initial}}$$ **Equation 5.8**

$$\sigma^2 \approx \frac{\sum_0^i (V_i - \mu_V)^2 \Delta C_i}{C_{Final} - C_{Initial}}$$ **Equation 5.9**

Table 5.4 shows the Gaussian HETP values for the micro scale column compared to those of the lab scale XK 16 column. The micro column HETPs are around five to ten times higher than those for the lab scale column. Larson observed that HETP values obtained, when calculating Gaussian HETP from transition data, were of the order of five times larger than those obtained from pulse analysis (Larson et al. 2003). Whilst these results are in general agreement with the findings of Larson *et al*, they are still larger than might be expected. However, there was a significant dead volume in the system, and given that variance is additive (Boussenadji et al. 1993) (Poe et al. 1997), this dead volume could explain this discrepancy.

$$\sigma^2_{Total} = \sigma^2_{column} + \sigma^2_{Tubing}$$ **Equation 5.10**

Where σ^2_{Total} is the total variance of the system, and σ^2_{column} and σ^2_{tubing} are the variances resulting from the column and the extra column dead volume respectively.

In order to take account of dispersion resulting from extra-column effects, acetone transitions were performed without the column in place and the variance was estimated from the width at half peak height of the derivative curves using Equation 1.6. This was subtracted from the total variance and used to calculate the corrected HETPs, shown in the final column of Table 5.4. These HETP's are around 2 – 6 times higher than that of lab scale column, and in better agreement with the findings of Larson *et al*, confirming that extra column dispersion is responsible for the higher than expected HETPs for the micro column.

Table 5.4 - Table showing HETPs of the micro affinity chromatography column compared with the XK 16 lab scale column

Flowrate (cm hr^{-1})	Lab Scale Column HETP (cm)	Microscale Column HETP (cm)	Microscale Column HETP (cm) corrected
25	0.038 ± 0.010	-	
50	0.021 ± 0.012	0.35 ± 0.016	0.13 ± 0.035
75	0.024 ± 0.023	0.34 ± 0.0085	0.10 ± 0.017
85	0.026 ± 0.0050	-	
100	0.029 ± 0.0088	0.32 ± 0.0011	0.073±0.0055

Given that HETP values obtained by transitional analysis are significantly higher than those obtained by acetone pulse, direct comparison of HETP values for the lab and micro scale columns impossible. However, comparison of the shape of HETP versus flowrate curves may allow the relative contribution of: longitudinal diffusion; eddy diffusion; and resistance to mass transfer, to column

performance at lab and micro scales, to be compared. Equation 5.11, the van Deemter equation (van Deemter et al. 1956), describes the way in which eddy diffusion, longitudinal diffusion and resistance to mass transfer contribute to the HETP.

$$HETP = A + \frac{B}{u} + Cu$$

Equation 5.11

Where u is the linear velocity of the mobile phase, A is the contribution of eddy diffusion to the plate height, B is the contribution of longitudinal diffusion and C is the contribution of the resistance to mass transfer.

Figure 5.10 - Plot of HETP versus flowrate. The (●) show Gaussian HETP versus flowrate for the 10 mL XK16 lab scale column. The (○) show Gaussian HETP versus flowrate for the 19µl micro column which was calculated using Equation 5.2 and Equation 5.3. The (△) shows corrected Gaussian HETP versus flowrate for the 19µL micro column, these HETP values were corrected to remove extra column dispersion using Equation 5.10 to calculate the variance resulting from the column by subtracting the extra column variance from the total variance. The (□) shows non-Gaussian HETP versus flowrate for the 19µl micro column calculated using Equation 5.4, Equation 5.8 and Equation 5.9.

Figure 5.10 shows van Deemter plots for the lab scale column and the microcolumn. It can be seen from this graph that the lab scale column displays typical van Deemter behaviour. At flowrates below 50cm hr^{-1}, longitudinal diffusion is the dominant cause of band broadening whilst at flowrates above 60 cm hr^{-1}, resistance to mass transfer becomes most dominant.

In Figure 5.10, three van Deemter plots are shown for the micro column – one showing the Gaussian HETP versus flowrate, one showing the corrected Gaussian HETP (corrected by subtracting the extra column variance from the

total variance), and one showing the non-Gaussian HETP versus flowrate (calculated using Equation 5.4, Equation 5.8 and Equation 5.9). Previous research (Larson et al. 2003) has shown that Gaussian HETP, obtained by transitional analysis is not able to show breaches in column integrity when they occur, while the non-Gaussian HETP is. Therefore, the non-Gaussian HETP has been included in order to show that no such breaches occurred during these experiments. A breach is indicated by a much higher HETP and as can be seen this did not occur.

All HETP versus flowrate curves for the micro column showed quite different properties to the van Deemter plot for the lab scale column. Both non-Gaussian HETP and uncorrected Gaussian HETP remain almost constant over the flowrate range investigated, 50 cm hr^{-1} to 100cm hr^{-1}, varying by around 0.002cm in both cases. This is thought to be because the HETP values obtained are dominated by extra column dispersion. This conclusion is supported by the work of Kaltenbrunner et al who found that even in 1 mL columns extra column effects contribute as much as 60% to dispersion (Kaltenbrunner et al. 1997).

Given the large errors, at low flowrates, in the corrected Gaussian HETP, it is difficult to drawn conclusions regarding the shape of the HETP versus flowrate curve. That said, it seems to be dominated by eddy diffusion/longitudinal diffusion effects.

Table 5.5 shows the asymmetry values obtained for the micro column, by transition analysis, compared with those obtained for the lab scale column by acetone pulse. Previous research has shown that asymmetry values obtained

by transitional analysis are much higher than those obtained by standard methods (Larson et al. 2003). However, whilst the asymmetry values for the micro column are higher than those obtained at lab scale at lower flowrates, they decrease with increasing flowrate. In fact the asymmetry value achieved on the micro column is better than that exhibited by the lab scale column at 100cm hr^{-1}. This is not in agreement with the work of Larson. Asymmetry values greater than one result from peak tailing which is attributed to mixing in the pre-column dead volume. Given that this is a microfluidic system, and flow is consequently laminar in the inlet capillary, these results may be explained by the shorter time available for diffusion at 100cm hr^{-1}. However, taking into account the findings of the HETP analysis, i.e. that extra column dispersion dominates in the microscale system, these asymmetry values are also likely to be dominated by extra column dispersion.

Table 5.5 - Table comparing the peak assymetries at obtained from the 0.2% acetone peaks at lab and micro scales

Flowrate (cm hr^{-1})	Peak Asymmetry	
	XK 16 Lab Scale Column	Micro Column
50	1.21 ±0.012	1.38 ±0.11
75	1.19 ±0.023	1.28 ±0.056
100	1.21 ±0.0088	1.12 ±0.066

5.3.3 Characterisation of performance of the column with pure protein

Breakthrough Performance of the Column
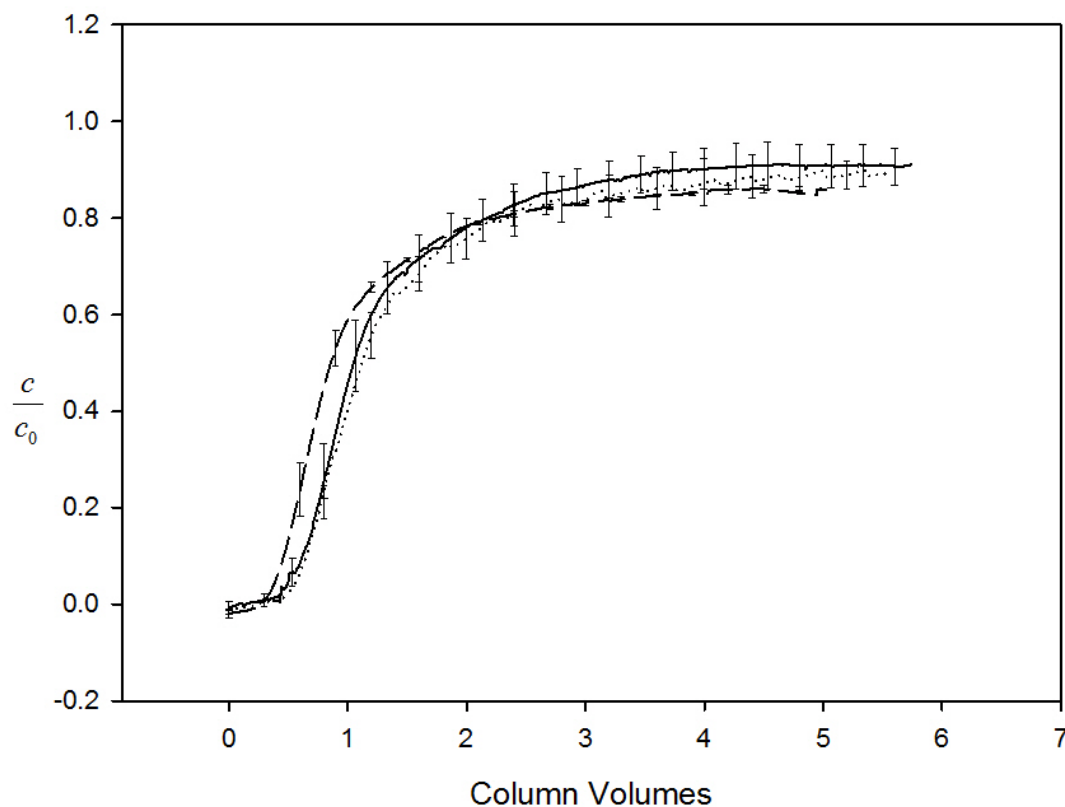
Figure 5.11 - Averaged breakthrough curves obtained by loading the micro column at different flowrates. The solid line is the breakthrough curve obtained when the column is loaded at 50cm hr^{-1}. The dashed line is the breakthrough curve obtained when the column was loaded at 75cm hr^{-1}. The dotted line is the breakthrough curve obtained when the column was loaded at 100cm hr^{-1}. In all cases the column was loaded with 1 mg/ mL pure GST in PBS pH7.4.

In order to investigate the breakthrough behaviour of the microcolumn at different flowrates, the column was loaded with 1 mg/ mL pure GST from equine liver in PBS pH 7.4, as described in Section 5.2.8. A pure protein feed was chosen in order to enable the concentration of GST to be monitored at the column outlet directly by measuring UV absorbance at 280nm with a UV detector. A concentration of 1 mg/mL passed directly through the detector, without a column, gave a reading on 296 mAU at 280nm. This concentration

was chosen because it was the minimum concentration of protein which ensured that noise did not have a significant effect on readings.

Figure 5.11 shows the averaged breakthrough curves obtained when loading the micro-column with pure GST, in PBS pH7.4 at a concentration of 1 mg/mL. It is of note that breakthrough starts very early, at approximately half a column volume, at all three flowrates. In addition, the curves are very similar in that there is very little difference in the gradient of the linear portion of the curves. These results appear to show that the protein concentration loaded is high enough to negate the difference in flowrate, this is consistent with observations of Chase. Chase observed that the shape and position of the breakthrough curve is constant when the concentration of the adsorbate is much greater than the dissociation constant of the adsorbant-matix complex (Chase 1984). Further to this, Glutathione S Transferase is a relatively small protein, and smaller molecules have better diffusivity i.e. they will diffuse faster. Since diffusion is the slowest mass transfer event, faster diffusion also acts to reduce the effect of flowrate on the shape and position of the breakthrough curve.

Another key feature of these breakthrough curves is that, following the region of linear increase in outlet protein concentration, the time taken to approach close to 100% breakthrough is comparatively long. It is thought that this is likely to be due to the time taken for the GST to diffuse into the beads, particularly the larger beads as the matrix bead size range is broad (30-180µm). The binding sites in the small beads and outer portions of the larger beads fill up quickly, as diffusion to these binding sites is relatively easy, while the binding sites in the inner portions of the larger beads take longer to fill up. This is because diffusion deep within these pores is more difficult due to the distance of travel required to

reach the deeper binding sites. Also, the postulated denser packing in the inner core of the column may lead to preferential flow along the wall and lead to a more tortuous path for the protein to travel to get to the available binding sites within this core. This would result in longer times for protein to reach the beads in the centre of the column.
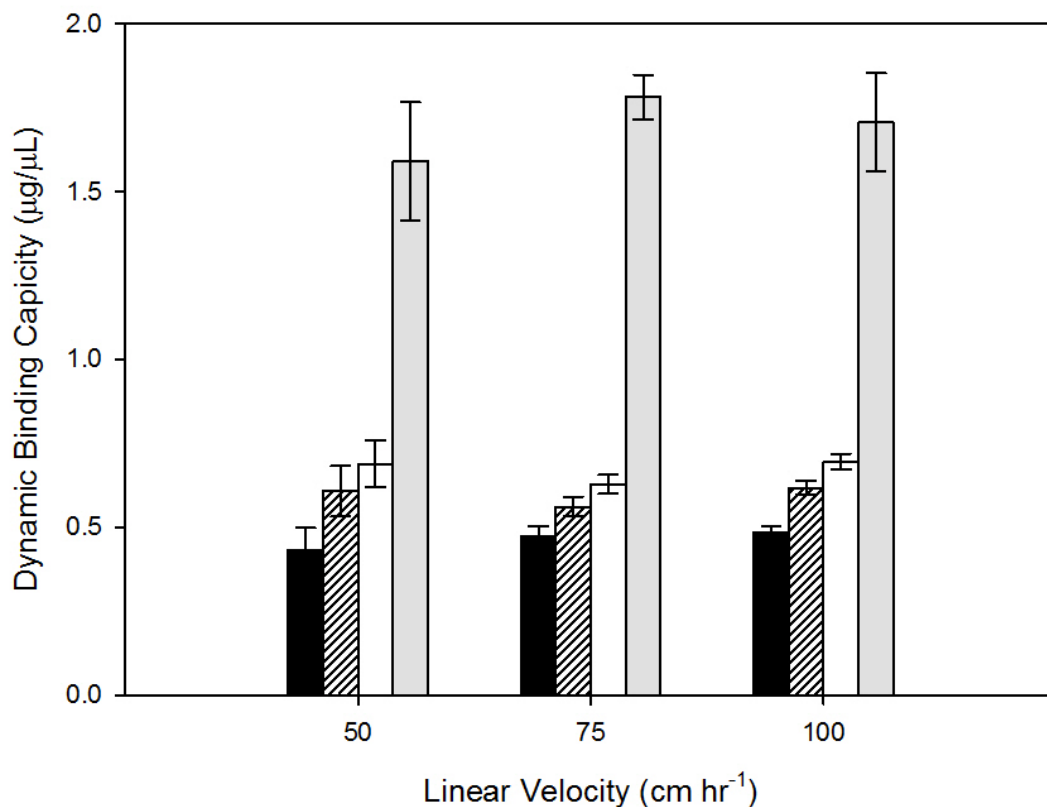
Figure 5.12 - Dynamic binding capacities in µg of GST per µL of bed volume. These dynamic binding capacities where obtained from the breakthrough curves obtained at 50 cm hr^{-1}, 75 cm hr^{-1} and 100 cm hr^{-1}. The black bars represent the dynamic binding capacities at 1% breakthrough. The hashed bars represent the dynamic binding capacities at 5% breakthrough. The white bars represent the dynamic binding capacities at 10% breakthrough. The grey bars represent the dynamic binding capacities at 100% breakthrough. The dynamic binding capacities were evaluated by calculating the area above the breakthrough curve at the 1%, 5% 10% and 100% breakthrough

Figure 5.12 shows the dynamic binding capacities obtained from the breakthrough studies that were preformed. The dynamic binding capacities at 100% breakthrough were calculated after 4.5 column volumes. This point was chosen as there was no significant increase in protein concentration above this point. However, the breakthrough curves on the micro column did not always reach 296mAU, the UV absorbance reading corresponding to the feed concentration, possibly due to the preferential flow along the wall of the column,

as discussed earlier. Therefore the dynamic binding capacities at 100% breakthrough may be an underestimation.

These dynamic binding capacities, shown in Figure 5.12 support the above conclusion that the concentration of protein loaded onto the column was much higher than the dissociation constant for the matrix-adsorbent complex as the dynamic binding capacities do not vary significantly with flowrate.

Comparison of Micro and Lab Scale Column Performances
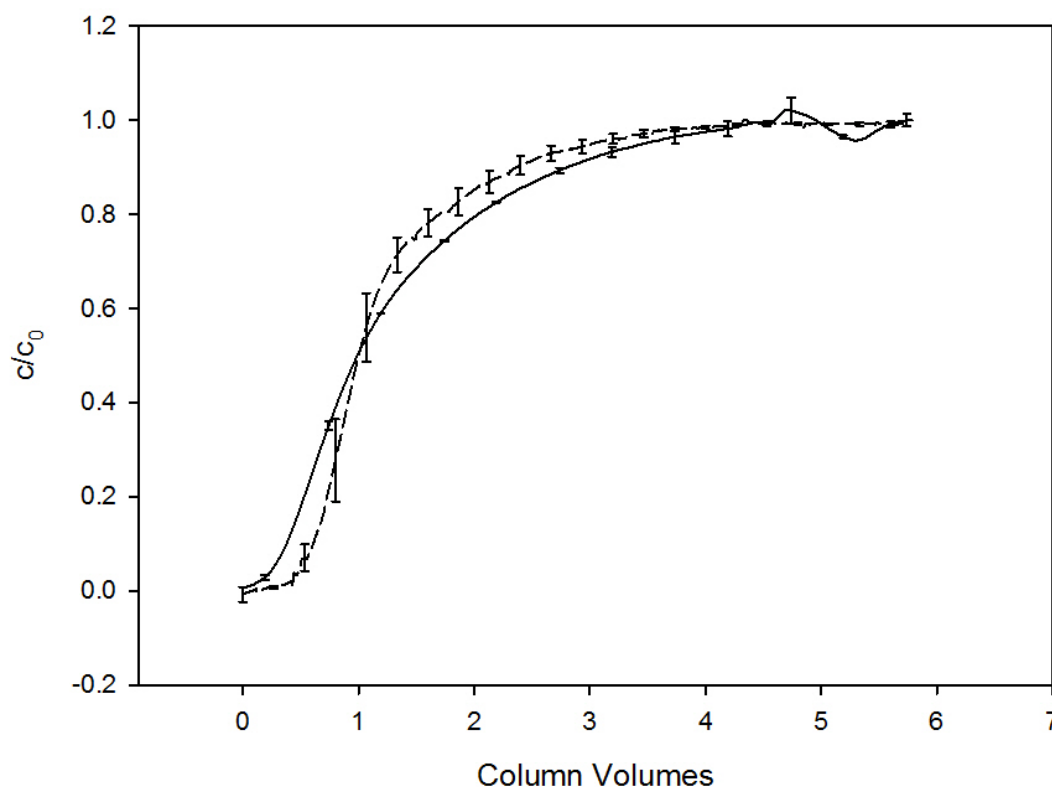
Figure 5.13 - Averaged breakthrough curves obtained by loading with 1 mg/mL pure GST, in PBS pH7.4, at 50 cm hr^{-1}. The solid line is the breakthrough curve obtained for the XK16/20 10 mL column (5cm bed height). The dashed line is the breakthrough curve obtained for the 19 L micro-column (5cm bed height).

The breakthrough behaviour of a lab scale column at loading flowrate of 50 cm hr^{-1} was investigated as a basis for comparison with the microcolumn. This was

done in order to assess whether the microcolumn behaves differently to a lab scale column during breakthrough. The lab scale XK16 column was loaded at 50 cm hr^{-1} with 1 mg/mL pure GST in PBS pH 7.4 as described in Section 5.2.8. Figure 5.13 shows the breakthrough curves at 50 cm hr^{-1} for the lab scale and micro scale columns. The linear portions of both breakthrough curves have similar gradients indicating that the rate of adsorption of protein per unit volume of feed passing through the column is similar.

As discussed in the previous section, following the region of linear increase in outlet protein concentration, the time taken to approach close to 100% breakthrough is comparatively long for both lab and microscale. This is thought to be due to the large variation in matrix particle size and consequently the longer time taken for diffusion into the large matrix beads.

Overall the shapes of the breakthrough curves are remarkably similar and the majority of the difference between the breakthrough curves can be attributed to experimental error. Consequently the affinity microcolumn shows promise for predicting larger scale chromatography. That said, the slightly steeper breakthrough curve for the microcolumn may, in part be due to the lower voidage, and hence the larger number of beads per unit volume This would lead to higher dynamic binding capacities at microscale as there are more binding sites available for the GST. This conclusion is supported by the dynamic binding capacities at 1%, 5%, 10% and 100% breakthrough, for the lab and microscale columns shown in Figure 5.14.
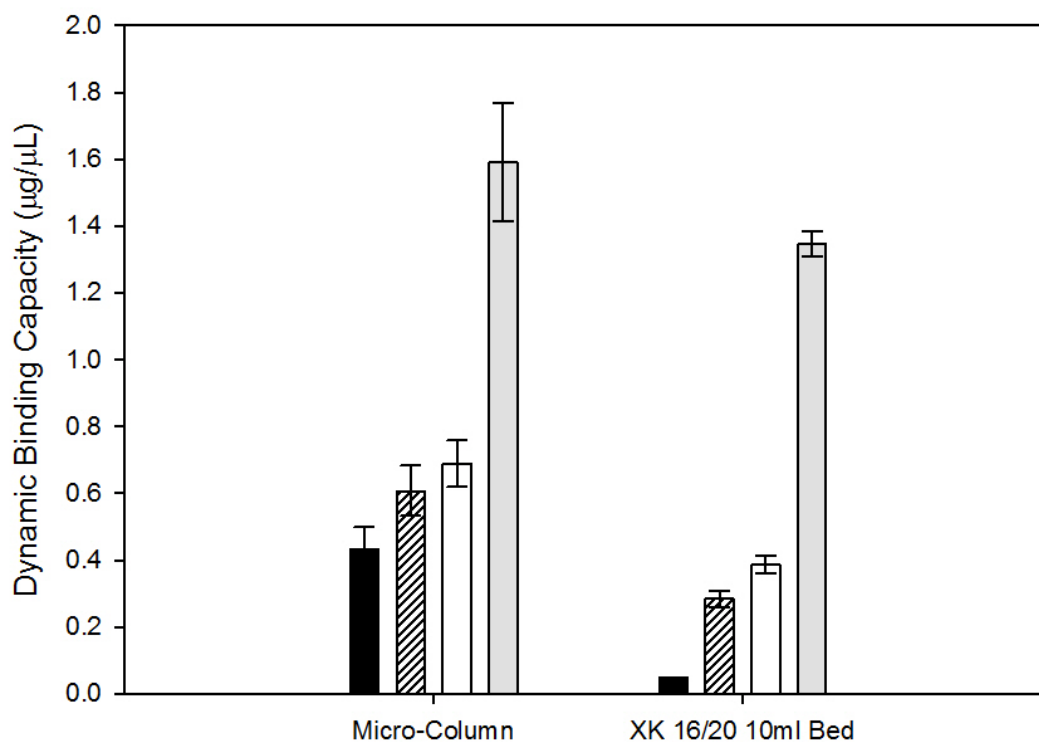
Figure 5.14 -Dynamic binding capacities in µg of GST per µL of bed volume. These dynamic binding capacities where obtained from the breakthrough curves generated by loading at 50 cm hr^{-1}. The black bars represent the dynamic binding capacities at 1% breakthrough. The hashed bars represent the dynamic binding capacities at 5% breakthrough. The white bars represent the dynamic binding capacities at 10% breakthrough. The grey bars represent the dynamic binding capacities at 100% breakthrough

Effect of Loading Flowrate on Quantity of Protein Eluted

The effect of loading flowrate, on the quantity of protein eluted, was investigated to determine whether loading at faster flowrates reduced the quantity of protein captured on the column, and hence confirm the earlier finding that the concentration of protein loaded onto the column was much higher than dissociation constant, resulting in the insensitivity of breakthrough to loading flowrate. To achieve this, the micro column was loaded at different flowrates, i.e. 50 cm hr^{-1}, 75 cm hr^{-1} and 100 cm hr^{-1}, this was followed by a wash with

PBS pH7.4 and elution with 10mM reduced Glutathione in Tris HCl pH8.0 both

at a constant flowrate of 75 cm hr^{-1}, as described in Section 5.2.8.
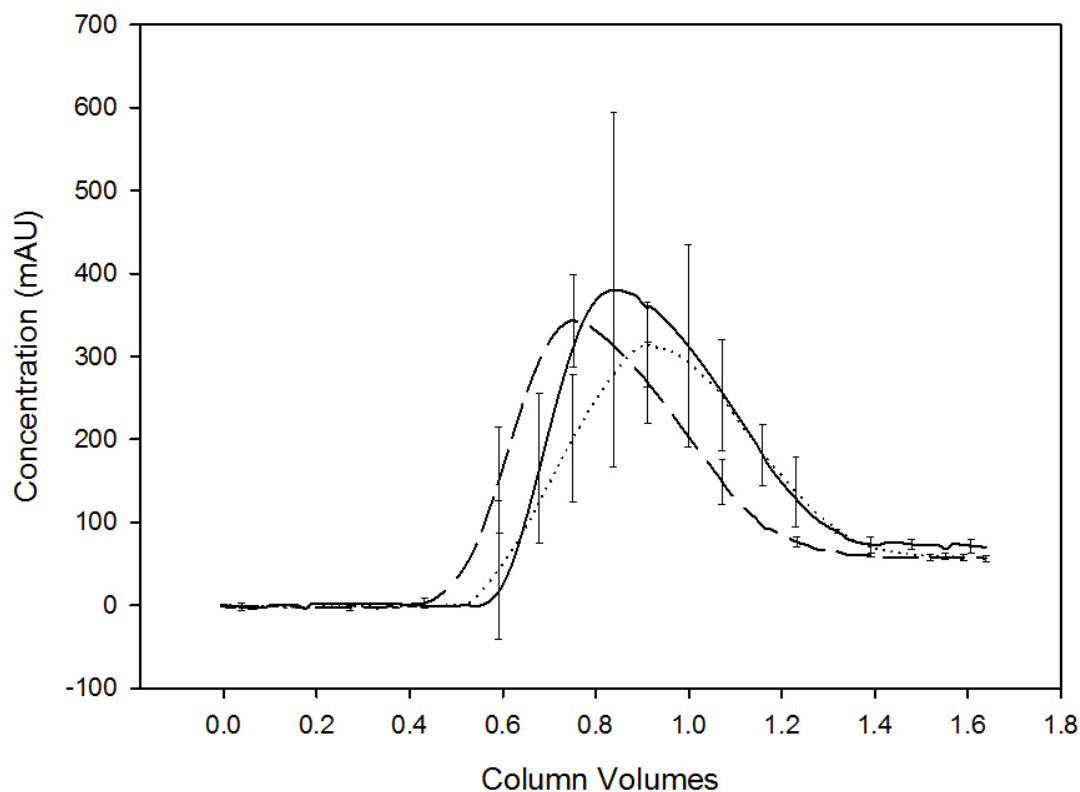
Figure 5.15 - Averaged elution curves obtained following loading at different flowrates. The solid line is the elution curve obtained when the column is loaded at 50 cm hr^{-1}. The dashed line is the elution curve obtained when the column was loaded at 75 cm hr^{-1}. The dotted line is the elution curve obtained when the column was loaded at 100 cm hr^{-1}. Following loading the column was washed with 10 columns of PBS pH 7.4 at a flowrate of 75 cm hr^{-1} and eluted with 10 mM reduced glutathione in Tris-HCl buffer pH 8.0 at a flowrate of 75 cm hr^{-1}.

Figure 5.15 shows the averaged elution curves obtained following loading at

different loading flowrates. There is significant variability in the point at which

elution begins. Elution appears to start earlier when the loading flowrate was 75

cm hr^{-1}. However, this is likely to be due to experimental error resulting from

the experimental method used.

Chemstations® software was used to record the UV absorbance at 280nm at the outlet of the system. The software was started by the operator by performing a blank injection, to waste. The recording of the results from the diode array detector began shortly afterwards. The operator had to start the syringe pump at exactly the same time that recording began, in order to ensure the start time was properly recorded. This introduced error in the start point of the elution. In addition, because the syringe pump was driven by a rotating screw thread, on occasion it would jump slightly, either forward or backward, introducing further error in determining the start of elution.
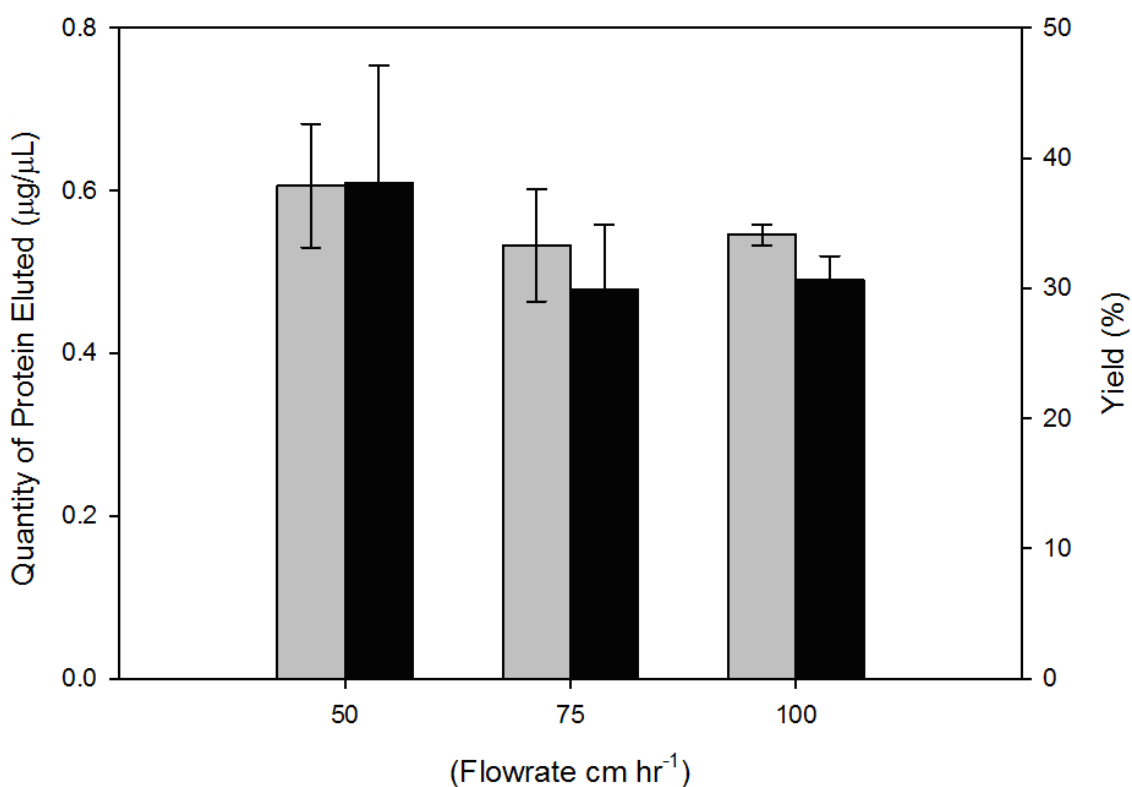
Figure 5.16 – The grey bars show the average quantities of protein eluted following loading at flowrates of 50cm hr^{-1}, 75cm hr^{-1} and 100cm hr^{-1}. Following loading, the column was washed with 10 column volumes of PBS pH7.4 at a flowrate of 75 cm hr^{-1} and eluted with 10 mM reduced glutathione in Tris-HCl buffer pH 8.0 at a flowrate of 75 cm hr^{-1}. The black bars show the yields obtained after eluting at 75 cm hr^{-1} following loading at flowrates of 50cm hr^{-1}, 75cm hr^{-1} and 100cm hr^{-1}

Figure 5.16 shows the average quantities of protein eluted after loading at different flowrates. The quantities of protein eluted are very similar and, whilst there appears to be a decreasing trend with lower quantities of protein eluted at higher loading flowrates, these differences are likely to be due to experimental error.

When comparing Figure 5.15 and Figure 5.16, it is interesting to note that the errors in Figure 5.16 are much less than in Figure 5.15. This is explained by the previously mentioned errors in recording the start point of the elution, i.e. offsetting elution peaks of similar areas gives rise to the larger errors in the averaged peak than in the average quantity of protein eluted.

The yields obtained are between 30% and 40% with the highest yield obtained at the lowest loading flowrate. This compares well to the literature with 40.8% quoted for GST fusion proteins (Lichty et al. 2005).

Overall, these results show that the quantity of protein eluted is insensitive to the elution flowrate. Further work would be needed to eliminate the error in determining the elution start point in order to improve the reproducibility of the elution results.

Effect of Elution Flowrate on Quantity of Protein Eluted
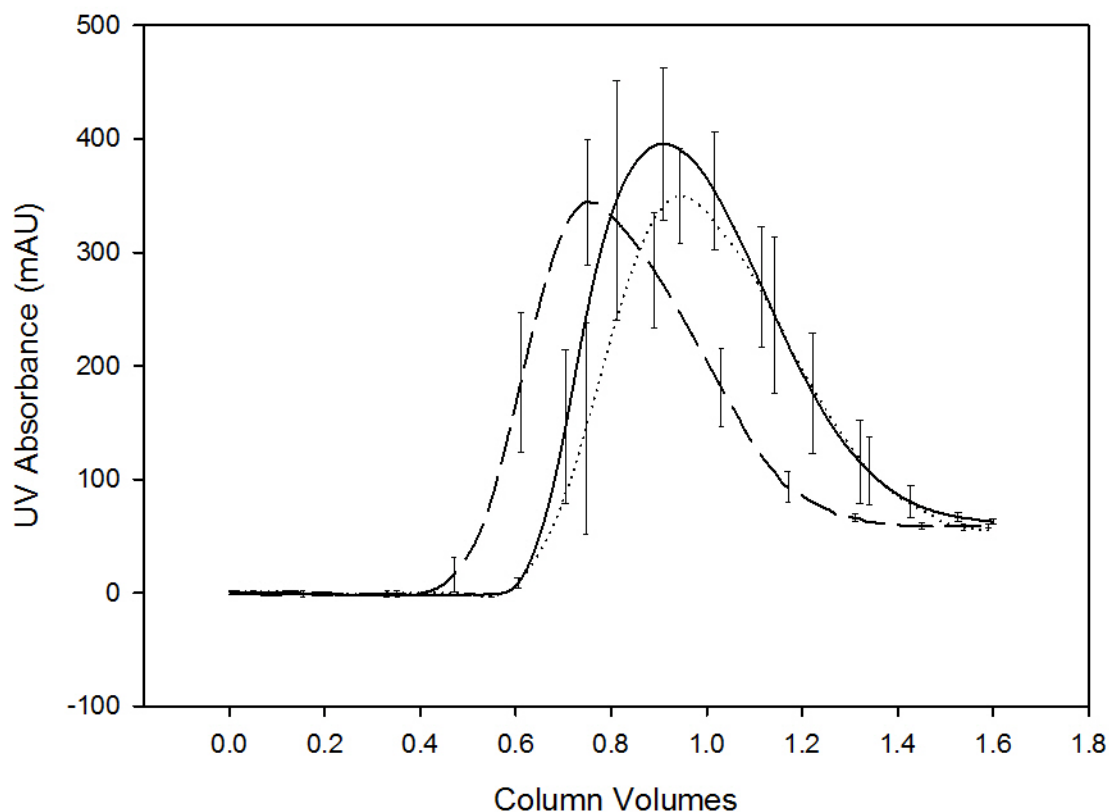
Figure 5.17 - Averaged elution curves obtained at different elution flowrates. The solid line is the elution curve obtained when the column was eluted at 50 cm hr^{-1}. The dashed line is the elution curve obtained when the column was eluted at 75 cm hr^{-1}. The dotted line is the elution curve obtained when the column was eluted at 100 cm hr^{-1}. The flowrate during loading was kept constant at 75 cm hr^{-1}. Following loading the column was washed with 10 column volumes of PBS pH 7.4 at a flowrate of 75 cm hr^{-1} and eluted with 10 mM reduced glutathione in Tris-HCl buffer pH 8.0.

The effect of elution flowrate on the quantity of protein eluted was investigated to determine whether the quantity of protein eluted from the column was sensitive to elution flowrate and to ascertain the optimum elution flowrate. The column was loaded at a constant flowrate of 75 cm hr^{-1} and the elution was repeated at different flowrates: 50 cm hr^{-1}, 75 cm hr^{-1}; and 100 cm hr^{-1}. These column runs were performed as outlined in Section 5.2.8. The loading flowrate was chosen to get the best throughput. Ideally this would have been 100 cm hr^{-}

[1]. However, at 100 cm hr^{-1} there were sometimes some artefacts in the breakthrough curve, which were probably due to jerking in the motion of the syringe pump, so 75 cm hr^{-1} was chosen.

Figure 5.17 shows the averaged elution peaks at the different elution flowrates. It is noteworthy that the volume over which the elution occurs is approximately the same at all three flowrates. The elution peaks are also all of similar area suggesting that the elution flowrate does not have a significant impact on the quantity of protein eluted. This can be seen more clearly in Figure 5.18, which shows that whilst on average there appears to be a slightly higher quantity of GST eluted at 50 cm hr^{-1}, and hence a higher yield, this difference may simply be due to experimental error.

Overall the effect of elution flowrate on the quantity of protein eluted, and yield, does not seem to be that significant, therefore in practice the column could be operated at 100 cm hr^{-1} without reducing the yield significantly. This would enable throughput to be doubled whilst maintaining the columns performance.
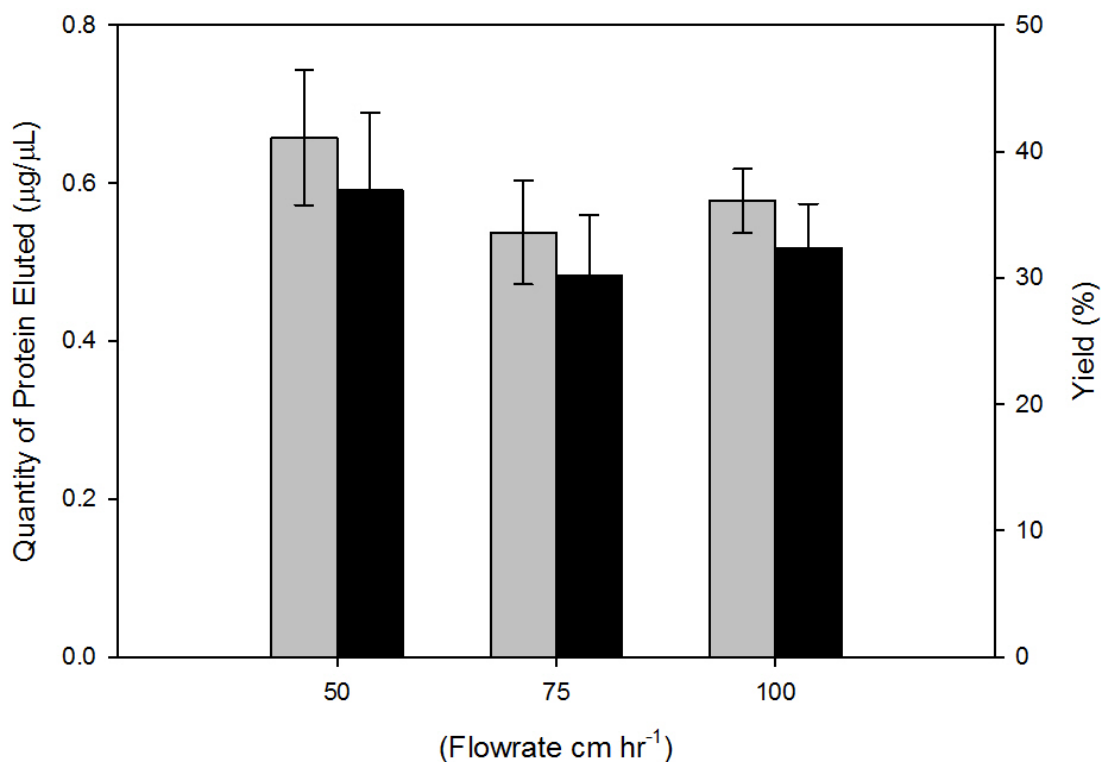
Figure 5.18 - **The grey bars show the average quantities of protein eluted at flowrates of 50 cm hr^{-1}, 75 cm hr^{-1} and 100 cm hr^{-1}. Following loading at 75cm hr^{-1} the column was washed with 10 column volumes of PBS pH7.4 at a flowrate of 75 cm hr^{-1} and eluted with 10mM reduced glutathione in Tris-HCl buffer pH8 at a flowrate of 75 cm hr^{-1}. The black bars show the yields obtained by eluting at 50cm hr^{-1}, 75cm hr^{-1} and 100cm hr^{-1} following loading at flowrates 75 cm hr^{-1}.**

Comparison of elution behaviours of Lab and Microscale columns

Representative chromatography runs were preformed at lab scale in order to provide a basis for comparison with microscale. Both columns were loaded with 1 mg/mL GST from equine liver in PBS pH 7.4 at 75 cm hr^{-1}. The columns were then washed with 10 column volumes of PBS and eluted at 50 cm hr^{-1} with 10 mM reduced glutathione in Tris-HCl pH8.
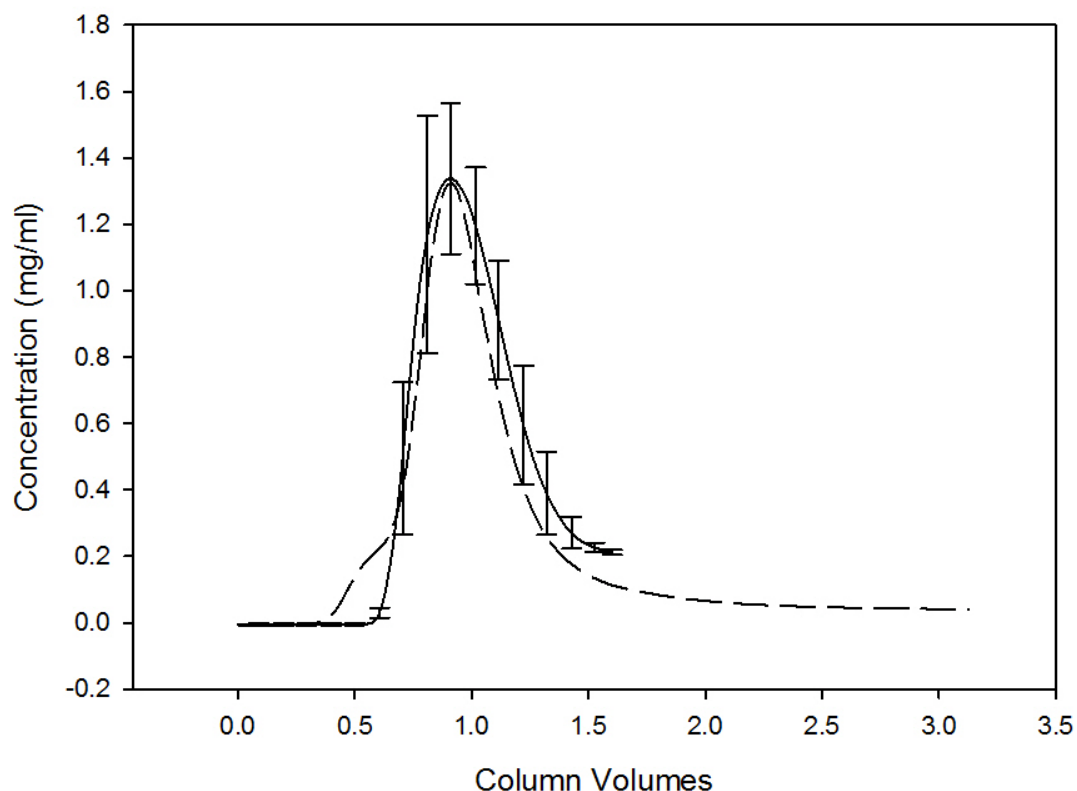
Figure 5.19 – Elution peaks obtained at lab and microscale. The solid line is the elution curve obtained when the microcolumn was eluted at 50cm hr^{-1}. The dashed line is the elution curve obtained when the XK16 10 mL column was eluted at 50 cm hr^{-1}. Both elutions are following loading at 75 cm hr^{-1} with 1 mg/ mL pure GST solution.

Figure 5.19 shows the elution curves obtained at lab and microscale. The elution curves are very similar in height and width showing that similar quantities of protein per unit bed volume are eluted from the columns. The area below the curves was estimated by integrating both peaks. Figure 5.20 shows the quantity of protein eluted at lab and microscale per unit bed volume and the yields obtained. These results show that the elution behaviour of the lab and microscale columns is very similar. Whilst, as discussed earlier, the yields agree with the literature, further work to optimise elution conditions may help to improve microcolumn yield performance.
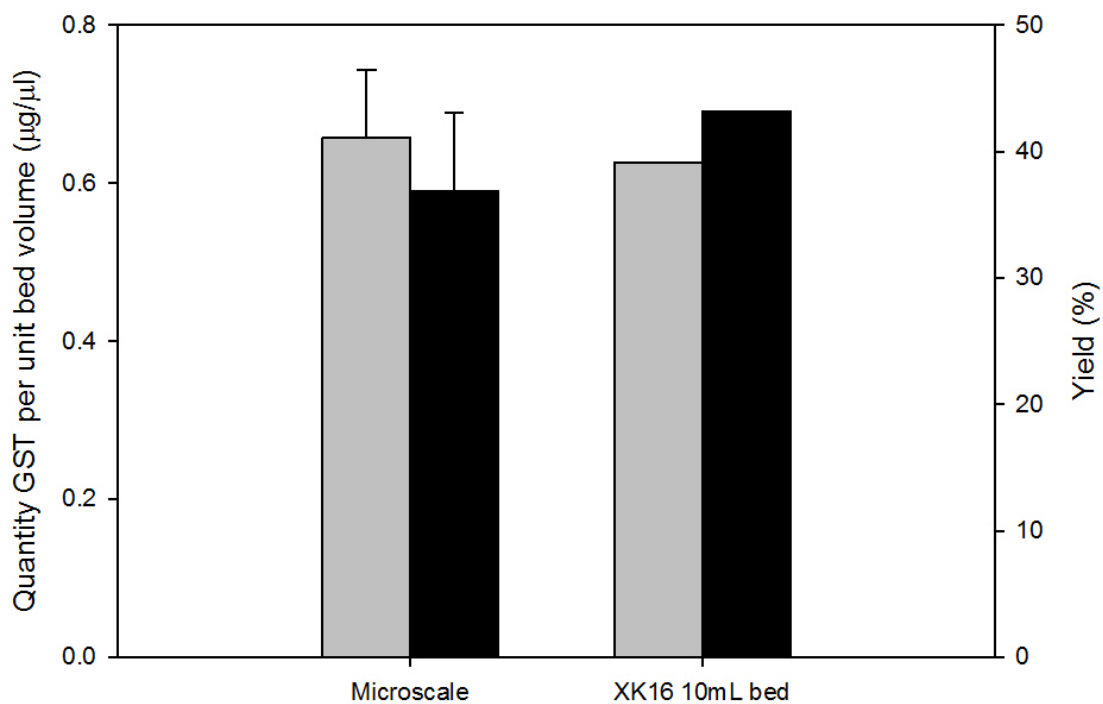
Figure 5.20 - Comparison of the quantity of protein eluted per unit bed volume at lab and microscale. The grey bars show the quantity of protein eluted per unit bed volume for the 19 L microcolumn and 10 mL XK16 lab scale column. The black bars show the yields obtained for both columns.

Column Ageing
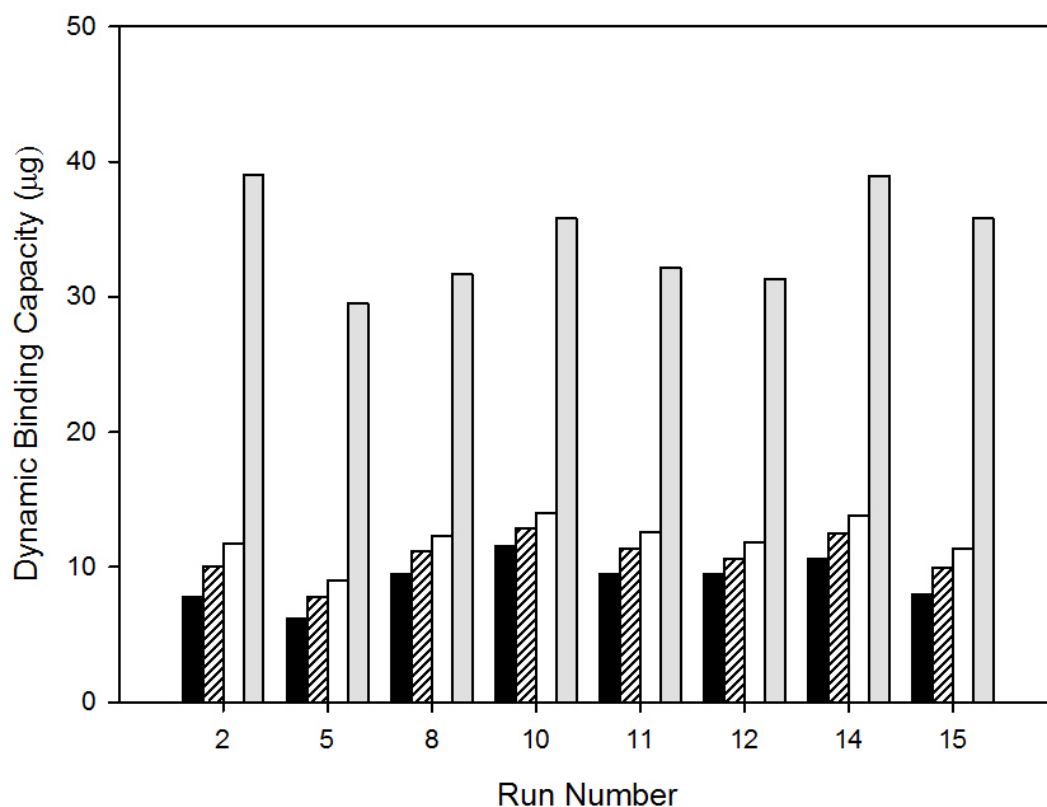
Figure 5.21 – The effect of column age on performance. The black bars represent the dynamic binding capacities at 1% breakthrough. The hashed bars represent the dynamic binding capacities at 5% breakthrough. The white bars represent the dynamic binding capacities at 10% breakthrough. The grey bars represent the dynamic binding capacities at 100% breakthrough

Figure 5.21 shows the effect of column age on dynamic binding capacity. Although there is some variability in the dynamic binding capacities achieved, the column does not appear to show a downward trend in performance over the 15 runs investigated. This is likely to be at least in part due to the column cleaning procedure that was used between each run. The detail of the wash protocol is outlined in the materials and methods 5.2.9. The 6M Guanidine Hydrochloride was used to denature and remove any non-specifically bound proteins. This would include any proteins bound to the internal surfaces of the

column. The 70% ethanol is to remove any hydrophobically bound substances from the matrix. Again, this would include substances hydrophobically bound to the internal surfaces of the column. So in addition to regeneration of the matrix, the cleaning protocol served to remove foulants from the internal surfaces of the column.
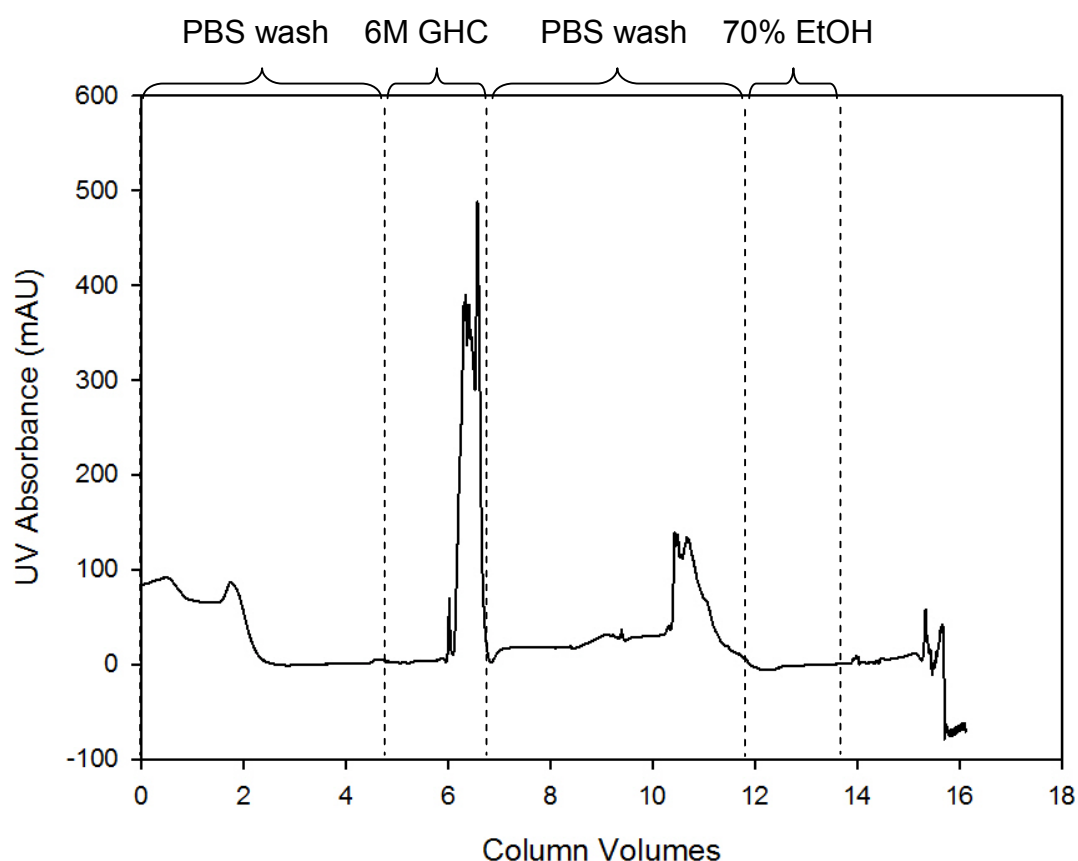
Figure 5.22 - A typical cleaning cycle. A cleaning cycle at 75 cm hr-1 was performed between each run. The column was first washed after elution with five column volumes of PBS pH7.4. The column was then cleaned with two column volumes of 6M Guanidine Hydrochloride immediately followed by a wash with five column volumes of PBS pH7.4. The column was then cleaned with two column volumes of 70% ethanol. This was followed immediately by equilibration with ten column volumes of PBS pH7.4. This cleaning cycle was taken after a pure protein run.

Figure 5.22, shows a typical post run cleaning cycle on the affinity microcolumn. Following injection of 6M Guanidine hydrochloride, a peak at UV 280 can be observed. This is the majority of denatured protein coming off the column. The

column is then washed with PBS; at the end of the wash another peak can be observed, coming off the column. This likely to be more denatured protein. However, it is clearly taking longer to pass through the column, therefore, the rate of its diffusion is likely to be lower. This could be unfolded GST that has previously bound to the column during breakthrough but was not subsequently eluted. After cleaning with 70% ethanol there appears to be oscillation in the UV 280nm readings. This cleaning protocol also serves to remove any fouling from the internal surfaces of the column.

Overall, the column does not appear to significantly loose performance over 15 runs.

5.3.4 Column Performance with Complex Feed and Comparison with Pure Protein

This section looks at the microcolumn performance with a complex feed. It was decided that 100% clarified *Escherichia coli* lysate, containing GST expressed from the pGex-3x plasmid, would enable the effectiveness of the system, with a realistic feed, to be examined.

One Hundred Percent Clarified Lysate Feed

In order to assess and compare the performance of the microcolumn with a realistic feedstock, chromatography runs were performed with 100% clarified *Escherichia coli* lysate. The lysate was made from a cell culture in which the *Escherichia coli* was transformed with the pGex3x vector to express recombinant GST from *Schistosoma japonicum.* The lysate was prepared and clarified as described in Section 2.4.2.

The 100% lysate was loaded at 50cm hr-1. The runs were performed as outlined in Section 5.2.8 except that a 10 cm, length of 100μm internal diameter capillary was attached to the end of the diode array detector outlet. A microwell plate with 45μL of deionised water in each microwell was prepared and covered with parafilm. The run was started and after 5mins and 17s the outlet capillary was placed in the first microwell. This was done in order to take account of the system dead volume. After 55s the microwell was stirred with the end of the capillary for a further 5 seconds. The outlet capillary was then transferred to the next microwell. This was repeated every minute for the duration of loading.

Figure 5.23, shows the breakthrough curve obtained for 100% clarified lysate, loaded at 50cm hr^{-1}, as compared with the breakthrough curve obtained with 1 mg/mL pure GST from equine liver loaded at 50cm hr^{-1}.   There are a number of key differences in these breakthrough curves.

Firstly, the breakthrough curve for the 100% clarified lysate feed does not start at zero. This breakthrough curve was obtained by performing the microwell plate CDNB assay (Section 2.5) on the effluent from the column at one minute intervals. The zero error is likely to be due to the lack of sensitivity of this assay at very low concentrations.
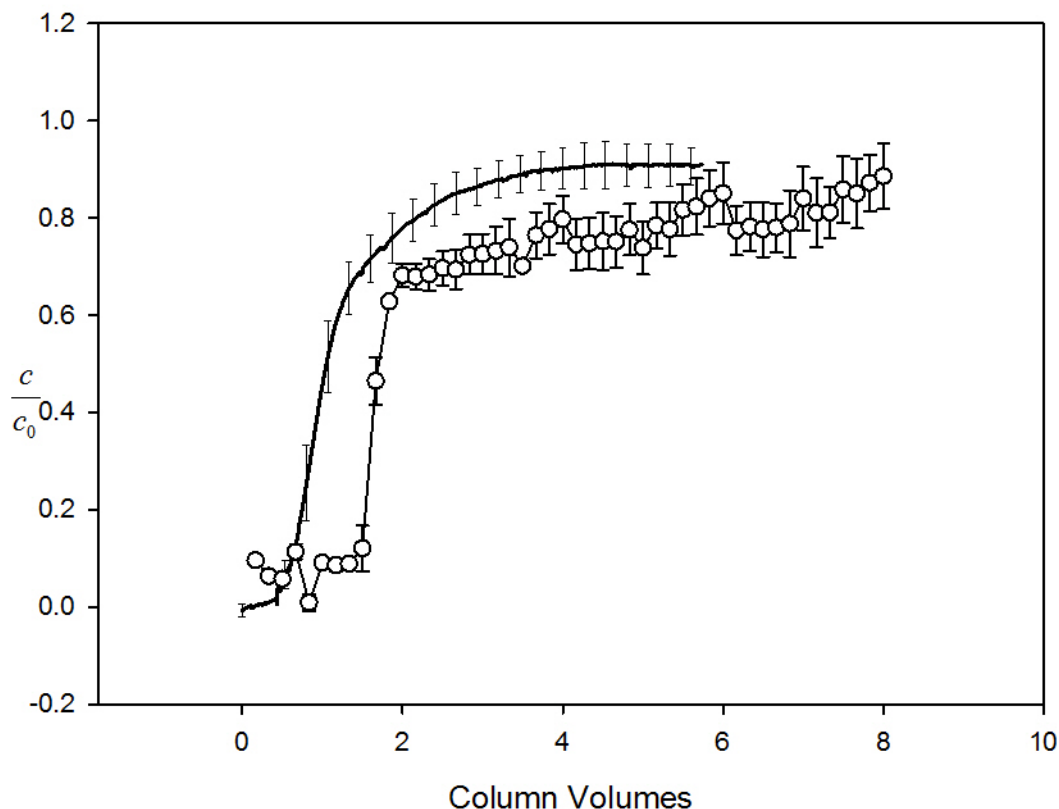
Figure 5.23 - Comparison between the breakthrough curves obtained with 1 mg/mL pure GST from equine liver at a loading flowrate of 50 cm hr^{-1} (solid line) and 100% clarified *Escherichia coli* lysate containing expressed 0.155 mg/mL GST from *Schistosoma japonicum* at a loading flowrate of 50 cm hr^{-1} (O).

Secondly, the breakthrough curve for the 100% clarified lysate feed starts off later and is slightly steeper than that for the pure protein, and then takes longer to reach 100% breakthrough. A sharper breakthrough curve is indicative of a stronger affinity of the GST from *Schistosoma japonicum* for the matrix, as compared to the GST from equine liver. Given that the concentration of GST in the 100% clarified lysate feed is lower than that in the pure protein feed, this strengthens the argument that GST from *S. japonica* has a stronger affinity for glutathione because, if the affinities were similar, a lower feed concentration would lead to a less steep breakthrough curve. The later breakthrough is explained by the lower feed concentration of GST from *S.japonicum* thus

requiring a greater volume to be loaded on to the column in order to fill up the binding sites.

Thirdly the 100% clarified lysate curve takes much longer to reach 100% breakthrough. This could result from the lower concentration of GST from *S. japonicum* and higher molecular weight. The GST dimer from equine liver is approximately 51kDa (D'Silva 1990) and the GST dimer from *S.japonicum* is 58.5kDa (according to G E Life Sciences the manufacturer of the pGex 3x vector). The larger protein would diffuse more slowly particularly into the centre of the larger beads and possibly into the centre of the column (which may be more densely packed). This would act to increase the time it takes to reach 100% breakthrough.
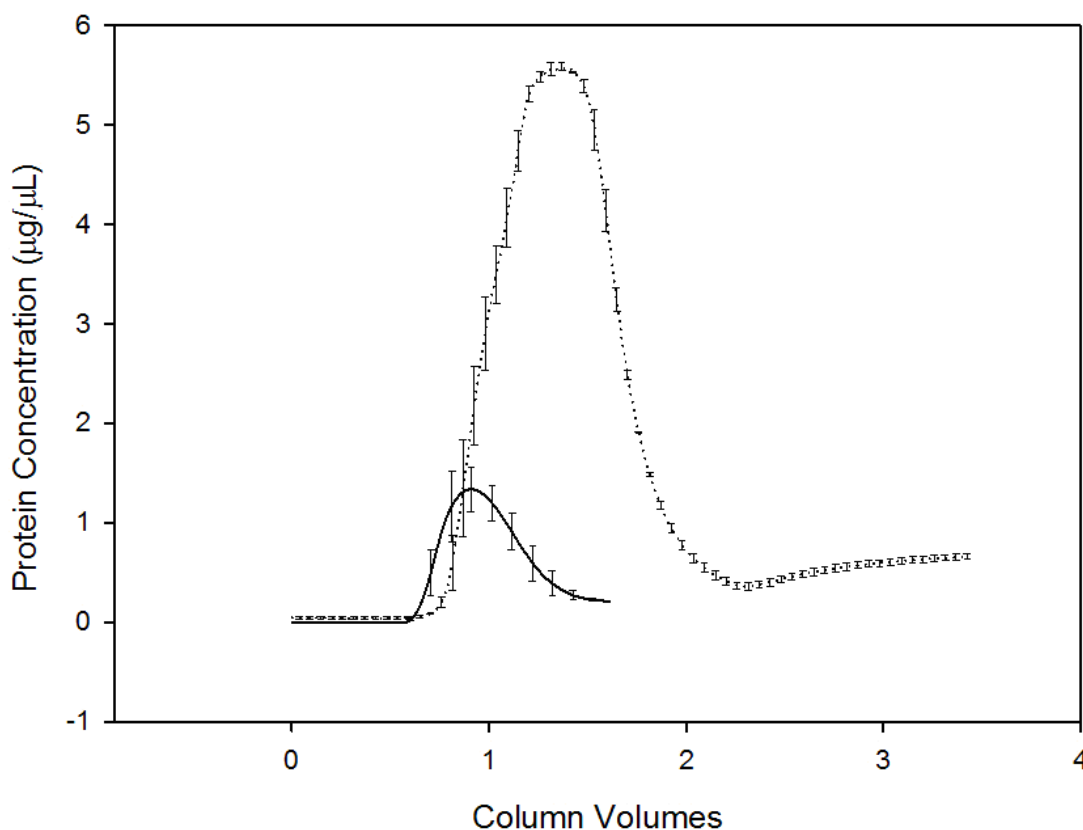
Figure 5.24 - Averaged elution curves obtained by elution with 10mM reduced glutathione in Tris-HCl pH8 at 50 cm hr⁻¹. The solid line is the elution curve obtained when the microcolumn was loaded with 1 mg/ mL of pure GST from equine liver. The dotted line is the elution curve obtained when the column was loaded with 100% clarified lysate containing recombinant GST from Schistosoma japonicum. Elution for the pure protein occurs within approximately 9 mins while for the GST from S.japonica elution is complete within approximately 12 mins.

Figure 5.24 shows the elution curves obtained when the microcolumn was loaded with pure GST from equine liver and 100% clarified *Escherichia coli* lysate expressing recombinant GST from *S. japonica*. Both elutions were performed at 50cm hr⁻¹ with 10mM reduced Glutathione in Tris-HCl buffer pH8.

Elution for the lysate occurs slightly later than that for the pure protein (It takes approximately 12 mins to complete the elution of lysate compared to 9 mins for pure protein). It is of note that the elution time, and more generally the run time

for chromatography, in this microaffinity device is the same as for lab scale. Consequently, increases in throughput are mostly possible from running several devices in parallel.

Also the quantity of GST eluted, as shown in Figure 5.25, is about three times higher than the quantity of protein eluted when the column was loaded with pure GST from equine liver and about 1.5 times the dynamic binding capacity at 100% breakthrough for pure GST from equine liver.
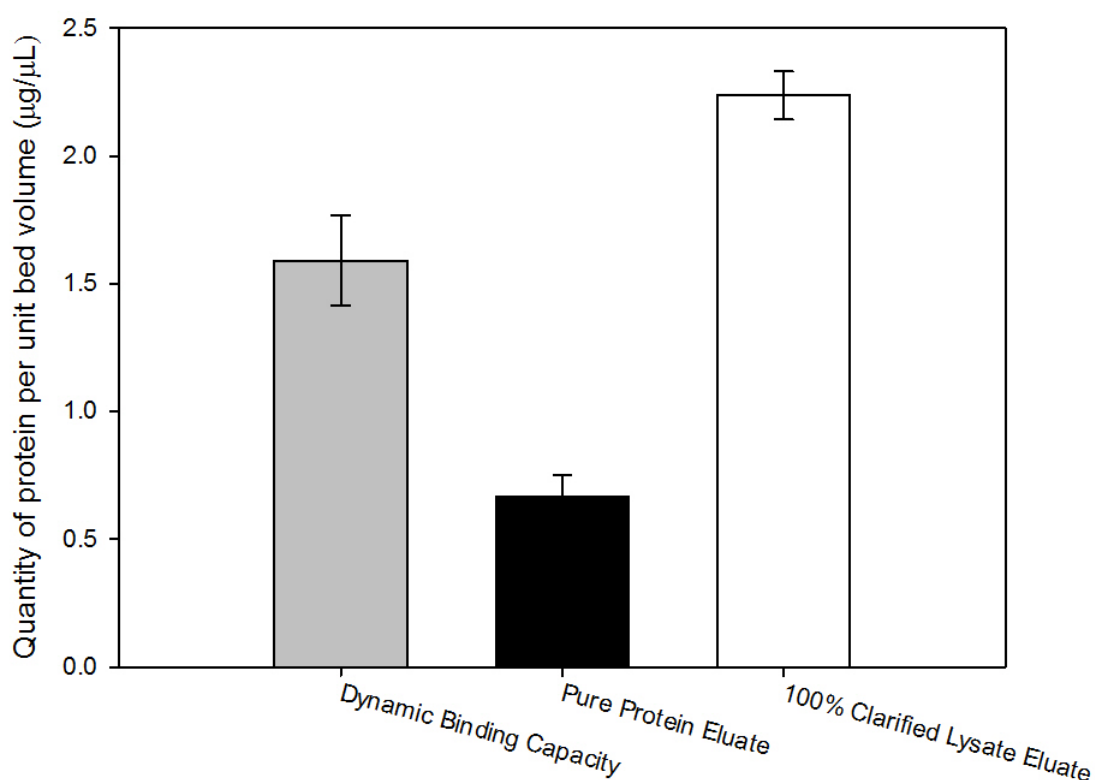
Figure 5.25 - Graph comparing the quantities of protein eluted, per unit bed volume, when the column was loaded with pure GST from equine liver (black bar) and with 100% clarified *Escherichia coli* lysate containing expressed GST from *Schistosoma japonicum* (white bar). In both cases the column was eluted at 50 cm hr^{-1} with 10mM reduced glutathione in Tris HCL pH8.0. The dynamic binding capacity of the microcolumn when loaded with pure GST in PBS pH7.4 at 50 cm hr^{-1} is represented by the grey bar.

The purity of the eluate obtained from the 100% clarified lysate chromatography was calculated by dividing the GST concentration, obtained by CDNB assay, by the total protein concentration, obtained by the microwell plate Bradford protein assay as described in Section 2.6. The purity was found to be 55% ± 6%. Poor purities have been obtained by other researchers (eg Lichty et al. 2005) using the GST affinity chromatography to purify GST fusion proteins. In addition, the poor purity can be accounted for by the fact that the CDNB assay, used to measure the GST concentration, is an activity assay, so some GST activity may have been lost. This loss could be due to the high pH of the elution buffer, or during the snap freezing process (eluate samples were snap frozen when it was not possible to measure the GST and total protein concentrations immediately).

That said, the later elution and greater quantity of protein eluted adds weight to the argument that the affinity of GST from *S. japonica* for Glutathione Sepharose 4B is higher than GST from equine liver at the conditions used and that the elution conditions used are better for GST from *S.japonicum.* The later elution could also be explained by the slower mass transfer resulting from the larger size of *S. japonica* GST molecule.

5.4   Summary of Findings and Conclusions

In this chapter an investigation of key properties such as voidage and quality of packing was undertaken. The dead volume of the microaffinity chromatography system was measured by blue dextran transition with, and without the column, and was also calculated. The measured dead volume (8.54 µL) was found to be larger than the calculated dead volume (6.65 µL). This difference was thought arise from inaccuracies resulting from the need to estimate the maxima of the truncated blue dextran first order derivative peaks.   The microcolumn displayed a significantly smaller voidage (0.2-0.28) than the lab scale column (0.35).   The large error on the obtained value for microcolumn voidage was also thought to be due to the error in estimating the position of the truncated blue dextran derivative peaks. The influence of the two wall effects found by other researchers, and its impact on the density of packing, was postulated as a potential reason for a lower void fraction.

HETP versus flowrate curves for the microcolumn were significantly different to the van Deemter curve, and it was suggested that this difference was as a result of the dominant contribution of extra column dispersion to HETP. The peak asymmetry for the lab scale column was almost constant around 1.2 while the asymmetry for the microcolumn was 1.38 at 50 cm hr^{-1} and 1.12 at 100 cm hr^{-1}. The asymmetry values were also thought to be dominated by extra column dispersion.

Studies with pure GST from equine liver showed good loading and elution behaviour. Both loading and elution were insensitive to flowrate over the range of flowrates investigated. This was thought to be due to the concentration of protein in the feed being much higher than the dissociation constant of the

adsorbent-matrix complex, essentially saturating the column. The GST feed concentration was chosen to ensure that noise did not significantly affect the data. The yields obtained, approximately 30%-40%, compared well to the literature. Further work, with more sensitive instrumentation is worth doing to investigate the effect of flowrate on breakthrough at lower feed protein concentrations.

When compared with a lab scale column of the same bed height, the shape of the breakthrough curves were remarkably similar. The majority of the difference between the breakthrough curves was thought to be due to experimental error. Consequently the affinity microcolumn is believed to show promise for predicting larger scale chromatography. The quantity of protein eluted compared favourably, with the microcolumn eluting 0.67 µg/µL, and the lab scale column eluting 0.63 µg/µL. This was significantly lower than the dynamic binding capacities at 100% breakthrough giving yields of 37% and 43% respectively, and it was concluded that further work to optimise the elution conditions, to elute more of the bound protein, was worth undertaking.

Comparison of breakthrough and elution behaviour for pure GST from equine liver to 100% clarified *E.coli* lysate containing GST from *S.japonicum* showed that, at the conditions used, the latter appeared to have a stronger affinity for the Glutathione Sepharose matrix but slower mass transfer due to its larger mass. However, a much larger quantity of GST from *S.japonicum* was eluted showing that the elution conditions were more favourable for GST from *S.japonicum*.

Hani El-Sabbahy

Whilst this purity is a little low for further analysis to determine product quality attributes, overall, proof of concept has been achieved. The micro affinity column presented in this work is capable of capturing GST from a realistic impure feed and releasing it in a purer concentrated form (2.24mg/ml with a purity of 55%). Further work to increase the purity of the product, perhaps by mixing the product stream with a buffer to reduce its pH and hence avoid loss of activity would be worthwhile. It is also likely, that if the column was packed with other affinity resins such as protein A or protein G better purities could be achieved. The column designed can also potentially be linked directly to the micro lysis device described in chapter 3 as it operates over the same range of flowrates.

6 Conclusions

This section summarises the key resulting from work described in this thesis, and uses them to draw the key conclusions.

The initial design of the microfluidic lysis device was undertaken by characterising the rheological behaviour of microbial culture and different types of lysate at eppendorf scale. This data was used to understand the limitations of design with respect to pressure drop and to validate the decision to use BugBuster in the lysis device. The BugBuster lysate had a similar viscosity to the microbial culture at OD 8 AU, and lower viscosity than the microbial culture, homogenate, and sonicate at OD 40 AU probably due to: the dilution caused by the addition of the BugBuster; and the digestion of released DNA by the nuclease in the BugBuster Mastermix™. The Hagen-Poiseuille flow equations were then experimentally verified at the microscale validating calculations made to determine the operating limits of the initial design. Excellent agreement between the experimental results and theoretical calculations was obtained.

The proportion of BugBuster to broth in the lysis reaction was investigated and it was found that this was a critical parameter with efficient lysis only occurring with the addition 50% (v/v) BugBugster.

Devices for mixing the BugBuster and microbial broth, to allow the lysis to occur in the microlysis device, were compared. The degree of lysis achieved was not sensitive to the type of mixer used with only a 13% difference between the best and the worst. This difference was not found to be statistically significant but problems with clogging meant that a T-piece with 500µm thru-hole was the best option.

Lysis was insensitive to flowrate, with lysis at the highest flowrate 25.65µL min^{-1} being 20% higher than at the lowest flowrate of 3.207µL min^{-1}. Again, this difference was not found to be statistically significant. This was probably due to the fact that mixing was by diffusion. That said, the advantage of smaller sample volumes, and the matching of flowrates to the microaffinity chromatography device, were key factors in the decision to operate the device in the range of 3.207 µL min^{-1} to 6.414 µL min^{-1}

The effect of residence time on the device's performance was investigated at it was found that lysis performance was approximately 14% higher after 60mins than after 5 mins. The results were deemed to be just outside the bounds of statistical significance. However, there was agreement with the eppendorf scale results which showed that the majority of lysis occurred in the first five minutes. Balancing the trade-off between reproducibility and device volume meant that a residence time of 7.5 mins was most efficient.

The final device design consisted of two 150 µm internal diameter capillaries feeding into a T-Piece with 500µm thru hole connected to 700µm internal diameter capillary whose length was 6.25cm for flowrates of 3.207µL min^{-1} and 12.5cm for flowrates of 6.414 µL min^{-1}. The device volume was 30µL to 60µL and it was able to successfully lyse cells with similar protein release to sonication. The resulting device is useful as a small scale device for the preparatory lysis of microbial cells and therefore as the first in a two stage microfluidic process for continuous cell lysis and purification of a specified protein.

The second step in the two step process for microfluidic sample preparation was microaffinity chromatography. The column was successfully packed using a Nanobaume, which proved to be the most robust packing method. The column design and system were refined until the column was able to produce the right shape acetone transition response. The final micro column design for subsequent characterisation work had an internal diameter of 700μm, a length of 5cm which is the same length as a typical lab scale Glutathione Affinity column, a bed volume of approximately 19μL and was packed with polydisperse standard Glutathione Sepharose 4b matrix. Qualitative assessment of the packing using 3D microscopy showed that the packing inside the column was probably good.

The microcolumn packing quality was examined in terms of HETP and asymmetry factor. The HETP versus flowrate curves for the microcolumn were significantly different to that of the lab scale column probably as result of the dominance of extra column dispersion effects in the microscale system. The lab and microscale column had similar asymmetry factors but the microcolumn asymmetry factor decreased at higher flowrates. However, given the dominance of extra column dispersion in the micro affinity chromatography system it was difficult to draw conclusions from this.

The microcolumn voidage was 20% - 43% smaller than the lab scale column. The influence of the two wall effects found by other researchers, and its impact on the density of packing, was postulated as a potential reason for a lower void fraction.

Studies with pure GST from equine liver showed good loading and elution behaviour but both were insensitive to flowrate over the range of flowrates investigated. This was thought to be due to the relatively high concentration of protein in the feed, essentially saturating the column. The GST feed concentration was chosen to ensure that noise did not significantly affect the data. Further work, with more sensitive instrumentation, is worth doing to investigate the effect of flowrate on breakthrough, with lower protein concentrations in the feed, for the purpose of scale-up predictions at microscale

When the microcolumn was compared with a lab scale column of the same bed height, the shape of the breakthrough curves were remarkably similar. The majority of the difference between the breakthrough curves was thought to be due to experimental error. The elution curves for both columns were also very similar. Consequently, the microaffinity column is believed to show promise for predicting larger scale chromatography performance. For lab and microscale columns yields were 43% and 37% respectively and so further work on optimising elution conditions is necessary.

Comparison of breakthrough and elution behaviour for pure GST from equine liver, to 100% clarified *Escherichia coli* lysate containing Glutathione S Transferase from *Schistosoma japonicum,* showed that, at the conditions used, the latter appear to have a stronger affinity for the Glutathione Sepharose matrix but slower mass transfer perhaps due to its larger mass. However a much larger quantity of GST from *S.japonicum* was eluted showing that the elution conditions were more favourable for GST from *S.japonicum*.

The 100% clarified lysate feed investigation demonstrated that the microaffinity column performed well with a complex feed and is capable of capturing GST from a realistic impure feed and eluting it in a purer concentrated form (2.24mg/ml with a purity of 55%). Further work, to increase the purity of the product, perhaps by microfluidic dialysis to exchange the buffer and hence avoid loss of activity would be worthwhile. Whilst this purity is a little low for further analysis to determine product quality attributes, overall, proof of concept has been achieved. It is also likely, that if the column was packed with other affinity resins such as protein A or protein G better purities could be achieved, and, given that the column operates at the same flowrate range as the micro lysis device, it has the potential to be connected directly to it to allow online lysis and chromatography at the microfluidic scale.

7 Future Work

This chapter describes areas of further work, worth exploring, to build on what has been achieved in this thesis. The first section will look at further work in relation to the microfluidic lysis device designed and characterised in chapter 3. The next section will look at further work in relation to the microaffinity chromatography column designed and characterised in chapters 4 and 5. The final section will describe further work that can be undertaken in relation to the integration of the microlysis and microaffinity chromatography devices.

7.1 Further Work on Micro Lysis

The work presented in chapter 3 focuses on one particular diameter outlet capillary which is relatively large. This was done to reduce the length of the capillary required to investigate residence times of up to 1 hour. By reducing the diameter of this outlet capillary, distances across which the BugBuster Mastermix™ and the microbial cells must diffuse, in order to achieve mixing, will also be reduced and hence lysis could occur more rapidly. This would enable the volume of the device to be further reduced, allowing smaller sample volumes to be lysed. Consequently, further work investigating the effect of the outlet capillary internal diameter, on degree of lysis, would worthwhile.

7.2   Further Work on Microfluidic Chromatography

The work in chapter 4 focused on arriving at a column design which produced correctly shaped acetone transition responses.   Consequently the packing pressure was not optimised. Further work on optimising the packing conditions, by quantitatively investigating the quality of packing at differently packing pressures, would be valuable.

Work on optimising the elution buffer to allow elution of more of the protein bound to the column would also be of value. As a starting point, increasing the concentration of reduced glutathione, and optimising the pH of the elution buffer, would be good areas for investigation. This kind of work illustrates one of the benefits of this microaffinity column, as the small column footprint would allow multiple investigations to be performed in parallel, with the use of appropriate UV detectors.

Using more accurate pumps and more sensitive UV detection would also allow similar investigations to those presented in this work with smaller diameter capillaries.   This would have the advantage reducing the sample volume required.

Comparison of breakthrough and elution behaviour with pure protein and 100% clarified lysate was difficult given that different GST enzymes were used. Further work, using purified GST from *S.japonica* would be useful as it would enable the effect of feed purity on column performance to be investigated.

Also the small column size, and consequently the relatively small number of beads, lends itself to bead by bead modelling using computation fluid dynamics

to determine the flowrate and concentration profiles around the beads. This could then be compared to experimental data to better understand how local irregularities such as wall effects and different bead sizes affect column performance.

Finally, studies using other matrices such as Sepharose fast flow matrices would enable a larger range of flowrates to be investigated, and studies using matrices with different ligands are also likely to enable higher levels of product purity.

7.3   Integrated microlysis and chromatography

Some initial work was undertaken on coupling the lysis and chromatography devices designed in this thesis, and running them as one device. The aim of this work was to investigate whether online lysis and chromatography could be achieved without the need for filtration between the two devices. It was recognised in doing this that, were it successful, the resulting device could only be used once due to fouling of the column by the lysate.

Whilst a small elution peak was obtained the quantity of protein eluted was not measurable by the microwell plate CDNB assay. Also, despite measuring the GST activity from the outlet of the device, until the device had been loading for over 100 mins, there was no measurable activity. There are two possible reasons for this. Firstly, the GST concentration at the output of the microlysis device was lower than that used in the 100% clarified lysate experiments. Secondly the bubble in the *E.coli* syringe (used for mixing) was observed to shrink as the experiment proceeded, implying that the pressure drop was increasing due to clogging of the device by cellular debris. This indicates a problem with blocking of the column, and also indicates that the driving force applied by the syringe pump was used to compress the bubble resulting a flowrate lower than the selected flowrate. This could be addressed by replacing the air bubble with a rigid plastic sphere.

To address the issue of clogging of the device with *E.coli* cellular debris, a method of removing the debris is necessary. Filtration is the obvious choice, and there has been some work microfluidic filtration, although for most of the devices the filter pores themselves are microfabricated with pore sizes too large for cellular debris (He et al. 1999; Chen et al. 2008). An alternative is to use

inertial forces to separate particles. This has been done successfully for particles just over 500 nm in diameter (Bhagat et al. 2009)

Another way of removing *E.coli* cellular debris post lysis, is by using the centrifugal forces resulting from fluid flowing round a circular channel to speed up sedimentation of cellular debris. Figure 7.1 shows the initial design of a device for "microfluidic centrifugation". The device includes triangular recesses in the curved channel sections to capture sedimented debris.

The time taken for this debris to migrate to these recesses would depend on: the viscosity of the fluid; the density of the debris, the critical dimensions of the device; and operating parameters such as the width of the channel; the radius of the curved sections of the channel; and the flowrate. Consequently, it should be possible, to design a chip capable of clarifying the lysate produced by the microlysis device. However, whether this device is practical to operate e.g. in terms of flowrates and pressure drops would need to be explored. This is an area that warrants further work.
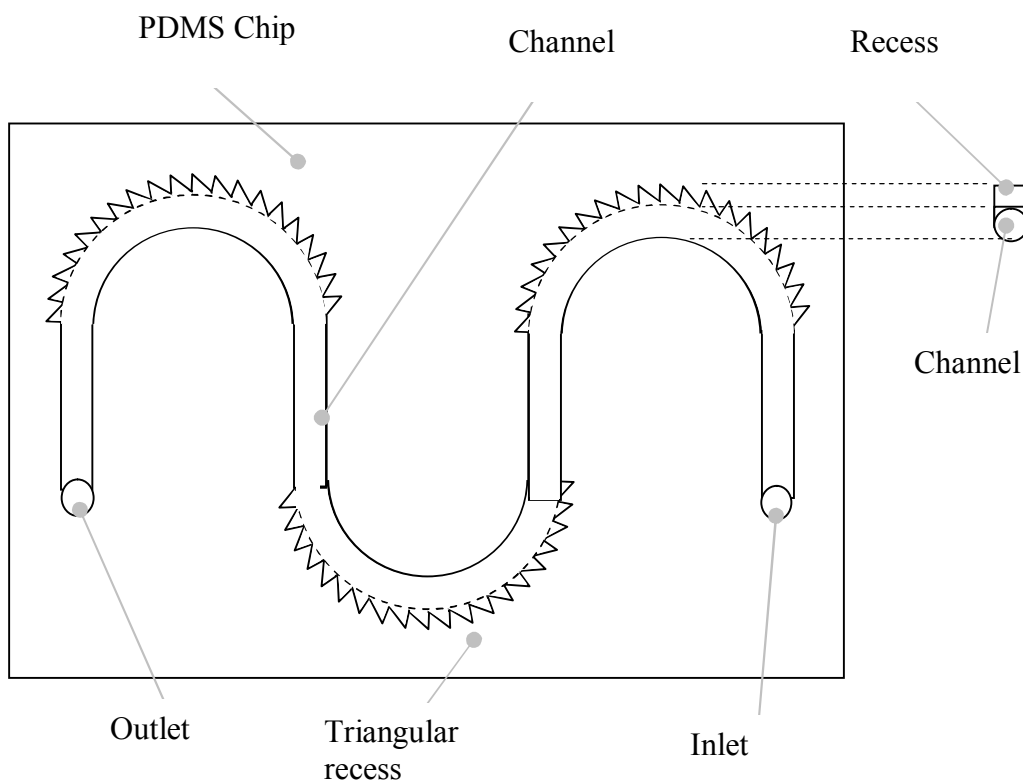
Figure 7.1 – Initial design a microfluidic device to clarify lysates using centrifugal forces created by flow round a curved channel "a microfluidic centrifugation device"

Finally, whilst the manufacturer's information says that BugBuster Mastermix™ is compatible with affinity matrices. Inclusion of microfluidic dialysis step may be useful for removing the BugBuster reagent and exchanging the buffer. Xu *et al* have developed such a device which was able to desalt effectively in 2 mins with a flowrate of 0.5 µL min^{-1} (Xu et al. 1998). Whilst these flowrates are a little low in comparison to the operating flowrates of the devices designed in thesis. The device could be scaled up by including 7 channels instead of 1. This would bring the operating flowrates in line with the microlysis and microaffinity chromatography devices.

8 References

Andersen, D.C. & Goochee, C.F., 1994. The effect of cell-culture conditions on the oligosaccharide structures of secreted glycoproteins. *Current Opinion in Biotechnology*, 5(5), pp.546–549.

Andersen, D.C. & Krummen, L., 2002. Recombinant protein expression for therapeutic applications. *Current Opinion in Biotechnology*, 13(2), pp.117–123.

Astorga-Wells, J., Jörnvall, H. & Bergman, T., 2003. A Microfluidic Electrocapture Device in Sample Preparation for Protein Analysis by MALDI Mass Spectrometry. *Anal. Chem.*, 75(19), pp.5213–5219.

Bedair, M. & Oleschuk, R.D., 2006. Lectin affinity chromatography using porous polymer monolith assisted nanoelectrospray MS/MS. *The Analyst*, 131(12), pp.1316–1321.

Bhagat, A., Kuntaegowdanahalli, S. & Papautsky, I., 2009. Inertial microfluidics for continuous particle filtration and extraction. *Microfluidics and Nanofluidics*, 7(2), pp.217–226.

Bird, R.B., Stewart, W.E. & Lightfoot, E.N., 2002. *Transport Phenomena* 2nd ed., New York: John Wiley & Sons.

Björkman, H. et al., 2001. Diamond microchips for fast chromatography of proteins. *Sensors and Actuators B: Chemical*, 79(1), pp.71–77.

Boulousis, G. et al., 2011. TiO2 Affinity Chromatography Microcolumn on Si Substrates for Phosphopeptide Analysis. *Procedia Engineering*, 25(0), pp.717–720.

Boussenadji, R., Porthault, M. & Berthod, A., 1993. Microbore liquid chromatography with electrochemical detection for the control of phenolic antioxidants in drugs and foods. *Journal of Pharmaceutical and Biomedical Analysis*, 11(1), pp.71–78.

Brookman, J.S.G. & Brookman, J.S.G., 1975. Further studies on the mechanism of cell disruption by extreme pressure extrusion, Further studies on the mechanism of cell disruption by extreme pressure extrusion. *Biotechnology and Bioengineering*, 17(4), pp.465–479.

Broyles, B.S., Jacobson, S.C. & Ramsey, J.M., 2003. Sample Filtration, Concentration, and Separation Integrated on Microfluidic Devices. *Analytical Chemistry*, 75(11), pp.2761–2767.

Buranda, T. et al., 2002. Biomolecular recognition on well-characterized beads packed in microfluidic channels. *Analytical Chemistry*, 74(5), pp.1149–1156.

Di Carlo, D. et al., 2005. On-chip cell lysis by local hydroxide generation. *Lab on A Chip*, 5(2), pp.171–178.

Hani El-Sabbahy

Di Carlo, D., Jeong, K.-H. & Lee, L.P., 2003. Reagentless mechanical cell lysis by nanoscale barbs in microchannels for sample preparation. *Lab on a Chip*, 3(4), pp.287–291.

Carta, G. & Jungbauer, A., 2010. *Protein Chromatography: Process Development and Scale-Up*, Federal Republic of Germany: John Wiley & Sons.

Cesaro-Tadic, S. et al., 2004. High-sensitivity miniaturized immunoassays for tumor necrosis factor α using microfluidic systems. *Lab Chip*, 4(6), pp.563–569.

Chase, H.A., 1984. Prediction of the performance of preparative affinity chromatography. *Journal of Chromatography A*, 297, pp.179–202.

Chen, X. et al., 2008. Microfluidic chip for blood cell separation and collection based on crossflow filtration. *Sensors and Actuators B: Chemical*, 130(1), pp.216–221.

Cho, S. et al., 2004. Microbead‐based affinity chromatography chip using RNA aptamer modified with photocleavable linker. *Electrophoresis*, 25(21‐22), pp.3730–3739.

Choban, E.R. et al., 2004. Microfluidic fuel cell based on laminar flow. *Journal of Power Sources*, 128(1), pp.54–60.

Ciccolini, L.A.S. et al., 1999. Rheological properties of chromosomal and plasmid DNA during alkaline lysis reaction. *Bioprocess and Biosystems Engineering*, 21(3), pp.231–237.

Cuatrecasas, P., Wilchek, M. & Anfinsen, C.B., 1968. Selective enzyme purification by affinity chromatography. *Proceedings of the National Academy of Sciences*, 61(2), pp.636 –643.

D'Silva, C., 1990. Inhibition and recognition studies on the glutathione-binding site of equine liver glutathione S-transferase. *Biochemical Journal*, 271(1), pp.161–165.

Van Deemter, J.J., Zuiderweg, F.J. & Klinkenberg, A., 1956. Longitudinal diffusion and resistance to mass transfer as causes of nonideality in chromatography. *Chemical Engineering Science*, 5(6), pp.271–289.

Dempster, R.P., Robinson, C.M. & Harrison, G.B.L., 1996. Parasite vaccine development: large-scale recovery of immunogenic Taenia ovis fusion protein GST-45W(B/X) from *Escherichia coli* inclusion bodies. *Parasitology Research*, 82(4), pp.291–296.

Deshpande, A.G. et al., 2012. In situ fabrication of a microfluidic device for immobilised metal affinity sensing. *New Biotechnology*, 29(4), pp.494–501.

DiMasi, J., Hansen, R.. & Grabowski, H., 2003. The price of innovation: New estimates of drug development costs. *Journal of Health Economics*, 22(2), pp.151–185.

Dishinger, J.F. & Kennedy, R.T., 2006. Serial Immunoassays in Parallel on a Microfluidic Chip for Monitoring Hormone Secretion from Living Cells. *Anal. Chem.*, 79(3), pp.947–954.

Dong, M.W., 2006. *Modern HPLC for Practicing Scientists*, Hoboken, New Jersey: John Wiley & Sons.

Ellis, D.J. et al., 1997. GST-lamin fusion proteins act as dominant negative mutants in Xenopus egg extract and reveal the function of the lamina in DNA replication. *Journal of Cell Science*, 110(20), pp.2507–2518.

Fernandes, P. & Cabral, J.M.S., 2006. Microlitre/millilitre shaken bioreactors in fermentative and biotransformation processes – a review. *Biocatalysis and Biotransformation*, 24(4), pp.237–252.

Fiorini, G.S. & Chiu, D.T., 2005. Disposable microfluidic devices: fabrication, function, and application. *Biotechniques*, 38(3), pp.429–446.

Gao, J. et al., 2003. Single cell injection and lysis on a microfluidic chip. *Chemical Journal of Chinese Universities-Chinese*, 24(9), pp.1582–1584.

Gao, J., Yin, X.F. & Fang, Z.L., 2004. Integration of single cell injection, cell lysis, separation and detection of intracellular constituents on a microfluidic chip. *Lab on A Chip*, 4(1), pp.47–52.

Ghitun, M. et al., 2006. Integrated microfluidic devices with enhanced separation performance: Application to phosphoproteome analyses of differentiated cell model systems. *Journal of Separation Science*, 29(11), pp.1539–1549.

Guan, Y.-X. et al., 2006. The use of a micropump based on capillary and evaporation effects in a microfluidic flow injection chemiluminescence system. *Talanta*, 68(4), pp.1384–1389.

Guiochon, G. et al., 1997. Consolidation of particle beds and packing of chromatographic columns. *Journal of Chromatography A*, 762(1-2), pp.83–88.

Gunjal, P.R., Ranade, V.V. & Chaudhari, R.V., 2005. Computational study of a single-phase flow in packed beds of spheres. *AIChE Journal*, 51(2), pp.365–378.

Harrison, R.G., 2003. *Bioseparations science and engineering*, New York: Oxford University Press.

Harrison, S.T.L., 1991. Bacterial cell disruption: A key unit operation in the recovery of intracellular products. *Biotechnology Advances*, 9(2), pp.217–240.

He, B., Tan, L. & Regnier, F., 1999. Microfabricated Filters for Microfluidic Analytical Systems. *Analytical Chemistry*, 71(7), pp.1464–1468.

Hani El-Sabbahy

Heo, Y.S. et al., 2006. Characterization and Resolution of Evaporation-Mediated Osmolality Shifts That Constrain Microfluidic Cell Culture in Poly(dimethylsiloxane) Devices. *Anal. Chem.*, 79(3), pp.1126–1134.

Herrmann, M., Veres, T. & Tabrizian, M., 2006. Enzymatically-generated fluorescent detection in micro-channels with internal magnetic mixing for the development of parallel microfluidic ELISA. *Lab on a Chip*, 6(4), pp.555–560.

Hirschberg, D. et al., 2004. Detection of phosphorylated peptides in proteomic analyses using microfluidic compact disk technology. *Analytical Chemistry*, 76(19), pp.5864–5871.

Hopkins, T.R., 1991. Physical and chemical cell disruption for the recovery of intracellular proteins. *Bioprocess Technology*, 12, pp.57–83.

Huang, F. et al., 2006. An integrated microfluidic chip for DNA/RNA amplification, electrophoresis separation and on‐line optical detection, An integrated microfluidic chip for DNA/RNA amplification, electrophoresis separation and on‐line optical detection. *Electrophoresis*, 27(16), pp.3297–3305.

Huang, Mosier, N.S. & Ladisch, M.R., 2006. Surface engineering of microchannel walls for protein separation and directed microfluidic flow. *Journal of Separation Science*, 29(12), pp.1733–1742.

Huh, Y.S. et al., 2007. Microfluidic cell disruption system employing a magnetically actuated diaphragm. *Electrophoresis*, 28(24), pp.4748–4757.

Hung, P.J. et al., 2005. A novel high aspect ratio microfluidic design to provide a stable and uniform microenvironment for cell growth in a high throughput mammalian cell culture array. *Lab on a Chip*, 5(1), pp.44–48.

Ichikawa, A. et al., 2009. Fluorescent monitoring using microfluidics chip and development of syringe pump for automation of enucleation to automate cloning. In *Robotics and Automation, 2009. ICRA '09. IEEE International Conference on*. pp. 2231 –2236.

Ikeda, N. et al., 2007. On-chip single-cell lysis for extracting intracellular material. *Japanese Journal of Applied Physics Part 1-Regular Papers Brief Communications & Review Papers*, 46(9B), pp.6410–6414.

International Union of Pure and Applied Chemistry, 2012. *Compendium of Chemical Terminology Gold Book*, p1138.

Irimia, D., Tompkins, R.G. & Toner, M., 2004. Single-cell chemical lysis in picoliter-scale closed volumes using a microfabricated device. *Analytical Chemistry*, 76(20), pp.6137–6143.

Ishii, D. et al., 1977. A study of micro-high-performance liquid chromatography: I. Development of technique for miniaturization of high-performance liquid chromatography. *Journal of Chromatography A*, 144(2), pp.157–168.

Ismagilov, R.F. et al., 2001. Pressure-Driven Laminar Flow in Tangential Microchannels: an Elastomeric Microfluidic Switch. *Anal. Chem.*, 73(19), pp.4682–4687.

Jiang, T. et al., 1995. Capillary Enzyme Immunoassay with Electrochemical Detection for the Determination of Atrazine in Water. *J. Agric. Food Chem.*, 43(4), pp.1098–1104.

Jönsson, J.Å., 1987. *Chromatographic theory and basic principles*, New York: Dekker.

Kaltenbrunner, O., Jungbauer, A. & Yamamoto, S., 1997. Prediction of the preparative chromatography performance with a very small column. *Journal of Chromatography A*, 760(1), pp.41–53.

Katoh, S. et al., 1978. Performance of affinity chromatography columns. *Biotechnology and Bioengineering*, 20(2), pp.267–280.

Kee, G.S., Pujar, N.S. & J. Titchener‐Hooker, N., 2008. Study of Detergent‐Mediated Liberation of Hepatitis B Virus‐like Particles from S. cerevisiae Homogenate: Identifying a Framework for the Design of Future‐Generation Lipoprotein Vaccine Processes. *Biotechnology Progress*, 24(3), pp.623–631.

Kim, J. et al., 2004. Cell lysis on a microfluidic CD (compact disc). *Lab on A Chip*, 4(5), pp.516–522.

King, K.R. et al., 2007. A high-throughput microfluidic real-time gene expression living cell array. *Lab on a Chip*, 7(1), pp.77–85.

Knight, J.B. et al., 1998. Hydrodynamic Focusing on a Silicon Chip: Mixing Nanoliters in Microseconds. *Physical Review Letters*, 80(17), pp.3863–3866.

Knox, J.H., Laird, G.R. & Raven, P.A., 1976. Interaction of radial and axial dispersion in liquid chromatography in relation to the 'infinite diameter effect'. *Journal of Chromatography A*, 122, pp.129–145.

Kumar, S., Wittmann, C. & Heinzle, E., 2004. Review: Minibioreactors. *Biotechnology Letters*, 26(1), pp.1–10.

Lancas, F.M., Rodrigues, J.C. & Freitas, S.D., 2004. Preparation and use of packed capillary columns in chromatographic and related techniques. *Journal of Separation Science*, 27(17-18), pp.1475–1482.

Larson, T.M. et al., 2003. Use of process data to assess chromatographic performance in production-scale protein purification columns. *Biotechnology Progress*, 19(2), pp.485–492.

Lathe, G.H. & Ruthven, C.R.J., 1956. The separation of substances and estimation of their relative molecular sizes by the use of columns of starch in water. *Biochemical Journal*, 62(4), pp.665–674.

LaVallie, E.R. & McCoy, J.M., 1995. Gene fusion expression systems in *Escherichia coli. Current Opinion in Biotechnology*, 6(5), pp.501–506.

Lazar, I.M., Trisiripisal, P. & Sarvaiya, H.A., 2006. Microfluidic Liquid Chromatography System for Proteomic Applications and Biomarker Screening. *Analytical Chemistry*, 78(15), pp.5513–5524.

Leclerc, E., Sakai, Y. & Fujii, T., 2003. Cell Culture in 3-Dimensional Microfluidic Structure of PDMS (polydimethylsiloxane). *Biomedical Microdevices*, 5(2), pp.109–114.

Lee, D.-S. et al., 2004. Bulk-micromachined submicroliter-volume PCR chip with very rapid thermal response and low power consumption. *Lab Chip*, 4(4), pp.401–407.

Lee, G.-B. et al., 2003. Microfluidic chips for DNA amplification, electrophoresis separation and on-line optical detection. In *Micro Electro Mechanical Systems, 2003. MEMS-03 Kyoto. IEEE The Sixteenth Annual International Conference on*. pp. 423 – 426.

Li, C. & Lee, K.H., 2004. Affinity depletion of albumin from human cerebrospinal fluid using Cibacron-blue-3G-A-derivatized photopatterned copolymer in a microfluidic device. *Analytical Biochemistry*, 333(2), pp.381–388.

Li, P., Gao, Y. & Pappas, D., 2011. Negative Enrichment of Target Cells by Microfluidic Affinity Chromatography. *Anal. Chem.*, 83(20), pp.7863–7869.

Lichty, J.J. et al., 2005. Comparison of affinity tags for protein purification. *Protein Expression and Purification*, 41(1), pp.98–105.

Linder, V. et al., 2001. Surface biopassivation of replicated poly(dimethylsiloxane) microfluidic channels and application to heterogeneous immunoreaction with on-chip fluorescence detection. *Analytical Chemistry*, 73(17), pp.4181–4189.

Listwan, P. et al., 2010. The optimization of in vitro high-throughput chemical lysis of *Escherichia coli*. Application to ACP domain of the polyketide synthase ppsC from Mycobacterium tuberculosis. *Journal of Structural and Functional Genomics*, 11(1), pp.41–49.

Lowe, C.R., 1996. Analytical biotechnology - Editorial overview. *Current Opinion in Biotechnology*, 7(1), pp.1–3.

Lu, H., Schmidt, M.A. & Jensen, K.F., 2005. A microfluidic electroporation device for cell lysis. *Lab on A Chip*, 5(1), pp.23–29.

Malmstadt, N. et al., 2003. A smart microfluidic affinity chromatography matrix composed of poly(N-isopropylacrylamide)-coated beads. *Analytical Chemistry*, 75(13), pp.2943–2949.

Marentis, T.C. et al., 2005. Microfluidic sonicator for real-time disruption of eukaryotic cells and bacterial spores for DNA analysis. *Ultrasound in Medicine and Biology*, 31(9), pp.1265–1277.

Mariella, R., 2008. Sample preparation: the weak link in microfluidics-based biodetection. *Biomedical Microdevices*, 10(6), pp.777–784.

Martin & Synge, 1941. A new form of chromatogram employing two liquid phases: A theory of chromatography. 2. Application to the micro-determination of the higher monoamino-acids in proteins. *Biochemical Journal*, 35(12), pp.1358–1368.

Maynard, V. & Grushka, E., 1972. Effect of dead volume on efficiency of a gas chromatographic system. *Analytical Chemistry*, 44(8), pp.1427–1434.

McClain, M.A. et al., 2012. Microfluidic Devices for the High-Throughput Chemical Analysis of Cells. *Anal. Chem.*, 75(21), pp.5646–5655.

McCue, J.T. et al., 2007. Use of an alternative scale-down approach to predict and extend hydroxyapatite column lifetimes. *Journal of Chromatography A*, 1165(1-2), pp.78–85.

De Mello, A., 2002. On-chip chromatography: the last twenty years. *Lab on a Chip*, 2(3), p.48N–54N.

Mellors, J.S. et al., 2010. Integrated Microfluidic Device for Automated Single Cell Analysis Using Electrophoretic Separation and Electrospray Ionization Mass Spectrometry. *Analytical Chemistry*, 82(3), pp.967–973.

De Mey, M. et al., 2008. Comparison of protein quantification and extraction methods suitable for *E. coli* cultures. *Biologicals*, 36(3), pp.198–202.

Micheletti, M. et al., 2006. Fluid mixing in shaken bioreactors: Implications for scale-up predictions from microlitre-scale microbial and mammalian cell cultures. *Chemical Engineering Science*, 61(9), pp.2939–2949.

Micheletti, M. & Lye, G.J., 2006. Microscale bioprocess optimisation. *Current Opinion in Biotechnology*, 17(6), pp.611–618.

Moore, E.K., Hoare, M. & Dunnill, P., 1990. Disruption of baker's yeast in a high-pressure homogenizer: New evidence on mechanism. *Enzyme and Microbial Technology*, 12(10), pp.764–770.

Mukhopadhyay, R., 2005. When Microfluidic Devices Go Bad. *Anal. Chem.*, 77(21), p.429 A–432 A.

Nagashima, Y., 2010. *Elementary Particle Physics: Volume 1: Quantum Field Theory and Particles*, Federal Republic of Germany: John Wiley & Sons.

Newman, D.J. & Cragg, G.M., 2007. Natural Products as Sources of New Drugs over the Last 25 Years⊥. *J. Nat. Prod.*, 70(3), pp.461–477.

Paul, S.M. et al., 2010. How to improve R&D productivity: the pharmaceutical industry's grand challenge. *Nature Reviews Drug Discovery*, pp.203–214.

Peles, E. et al., 1997. Identification of a novel contactin-associated transmembrane receptor with multiple domains implicated in protein–protein interactions. *The EMBO Journal*, 16(5), pp.978–988.

Piyasena, M.E. et al., 2004. Near-simultaneous and real-time detection of multiple analytes in affinity microcolumns. *Analytical Chemistry*, 76(21), pp.6266–6273.

Poe, D.P. et al., 1997. Supercritical fluid chromatograph for studies of retention and efficiency with a brief study of n-alkanes showing evidence of significant temperature drop with pressure drop. *Journal of Chromatography A*, 785(1-2), pp.135–148.

Reynolds, K.J. & Colón, L.A., 1998. Capillary electrochromatography in columns packed by gravity.Preliminary study. *Analyst*, 123(7), pp.1493–1495.

Rohde, C.B. et al., 2007. Microfluidic system for on-chip high-throughput whole-animal sorting and screening at subcellular resolution. *Proceedings of the National Academy of Sciences*, 104(35), pp.13891 –13895.

Rossier, J.S. & Girault, H.H., 2001. Enzyme linked immunosorbent assay on a microchip with electrochemical detection. *Lab on a Chip*, 1(2), pp.153–157.

Sakodynskii, K., 1972. The life and scientific workds of Michael Tswett. *Journal of Chromatography A*, 73(2), pp.303–360.

Salim, M. et al., 2007. Non-fouling microfluidic chip produced by radio frequency tetraglyme plasma deposition. *Lab Chip*, 7(4), pp.523–525.

Schäpper, D. et al., 2009. Application of microbioreactors in fermentation process development: a review. *Analytical and Bioanalytical Chemistry*, 395(3), pp.679–695.

Schilling, E.A., Kamholz, A.E. & Yager, P., 2002. Cell Lysis and Protein Extraction in a Microfluidic Device with Detection by a Fluorogenic Enzyme Assay. *Anal. Chem.*, 74(8), pp.1798–1804.

Schriemer, D.C. et al., 1998. Micro-Scale Frontal Affinity Chromatography with Mass Spectrometric Detection: A New Method for the Screening of Compound Libraries. *Angewandte Chemie International Edition*, 37(24), pp.3383–3387.

Seguin, D., Montillet, A. & Comiti, J., 1998a. Experimental characterisation of flow regimes in various porous media - I: Limit of laminar flow regime. *Chemical Engineering Science*, 53(21), pp.3751–3761.

Shalliker, R.A., Broyles, B.S. & Guiochon, G., 2000. Physical evidence of two wall effects in liquid chromatography. *Journal of Chromatography A*, 888(1–2), pp.1–12.

Shapiro, M.S. et al., 2009. Design and characterization of a microfluidic packed bed system for protein breakthrough and dynamic binding capacity determination. *Biotechnology Progress*, 25(1), pp.277–285.

Shapiro, M.S. et al., 2010. Microfluidic Chromatography for Early Stage Evaluation of Biopharmaceutical Binding and Separation Conditions. *Separation Science and Technology*, 46(2), pp.185–194.

Sheely, M.L., 1932. Glycerol Viscosity Tables. *Industrial & Engineering Chemistry*, 24(9), pp.1060–1064.

Shrewsbury, P.J., Muller, S.J. & Liepmann, D., 2001. Effect of Flow on Complex Biological Macromolecules in Microfluidic Devices. *Biomedical Microdevices*, 3(3), pp.225–238.

Small, H., 2004. Ion Chromatography: An Account of Its Conception and Early Development. *J. Chem. Educ.*, 81(9), p.1277-1284.

Smith, D.B. & Johnson, K.S., 1988. Single-step purification of polypeptides expressed in *Escherichia coli* as fusions with glutathione S-transferase. *Gene*, 67(1), pp.31–40.

Tkac, J., Vostiar, I. & Mandenius, C.-F., 2004. Evaluation of disruption methods for the release of intracellular recombinant protein from *Escherichia coli* for analytical purposes. *Biotechnology and Applied Biochemistry*, 40(1), pp.83–88.

Veide, A., Smeds, A.-L. & Enfors, S.-O., 1983. A Process for large-scale isolation of β-galactosidase from *E. coli* in an aqueous two-phase system. *Biotechnology and Bioengineering*, 25(7), pp.1789–1800.

Walsh, G., 2010. Biopharmaceutical benchmarks 2010. *Nat Biotech*, 28(9), pp.917–924.

Wan, F. et al., 2009. Reduced matrix viscosity in DNA sequencing by CE and microchip electrophoresis using a novel thermo‐responsive copolymer. *Electrophoresis*, 30(14), pp.2488–2498.

Wang, G. et al., 2005. Direct observation of frits and dynamic air bubble formation in capillary electrochromatography using confocal fluorescence microscopy. *Journal of Chromatography A*, 1062(2), pp.275–283.

Wang, H., Wang, F. & Wei, D., 2009. Impact of oxygen supply on rtPA expression in *Escherichia coli* BL21 (DE3): ammonia effects. *Applied Microbiology and Biotechnology*, 82(2), pp.249–259.

Wang, H.Y., Bhunia, A.K. & Lu, C., 2006. A microfluidic flow-through device for high throughput electrical lysis of bacterial cells based on continuous dc voltage. *Biosensors & Bioelectronics*, 22(5), pp.582–588.

Wang, P.-C., Gao, J. & Lee, C.S., 2002. High-resolution chiral separation using microfluidics-based membrane chromatography. *Journal of Chromatography A*, 942(1–2), pp.115–122.

Whitesides, G.M., 2006. The origins and the future of microfluidics. *Nature*, 442(7101), pp.368–373.

Wright, I.G. et al., 1992. The development of a recombinant Babesia vaccine. *Veterinary Parasitology*, 44(1–2), pp.3–13.

Wu, Z., Nguyen, N.-T. & Huang, X., 2004. Nonlinear diffusive mixing in microchannels: theory and experiments. *Journal of Micromechanics and Microengineering*, 14(4), pp.604–611.

Xie, J. et al., 2005. Microfluidic Platform for Liquid Chromatography−Tandem Mass Spectrometry Analyses of Complex Peptide Mixtures. *Analytical Chemistry*, 77(21), pp.6947–6953.

Xu, N. et al., 1998. A Microfabricated Dialysis Device for Sample Cleanup in Electrospray Ionization Mass Spectrometry. *Analytical Chemistry*, 70(17), pp.3553–3556.

Yang, X., 2008. *Effects of Sucrose on the Foaming and Interfacial Properties of Egg White Protein and Whey Protein Isolate*. Thesis (Ph.D). North Carolina, USA: NC State University.

Yi, C. et al., 2006. Microfluidics technology for manipulation and analysis of biological cells. *Analytica Chimica Acta*, 560(1–2), pp.1–23.

Zablotowicz, R.M. et al., 1995. Glutathione-S-Transferase Activity and Metabolism of Glutathione Conjugates by Rhizosphere Bacteria. *Applied and Environmental Microbiology*, 61(3), pp.1054–1060.

Annex A – Engineering Drawings of the Reduced Dead Volume Fittings Used in the Microaffinity Chromatography Work
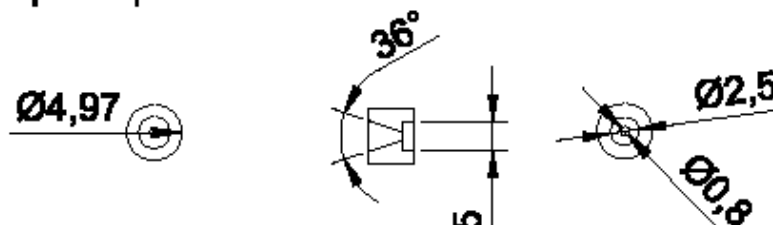
Ferrule
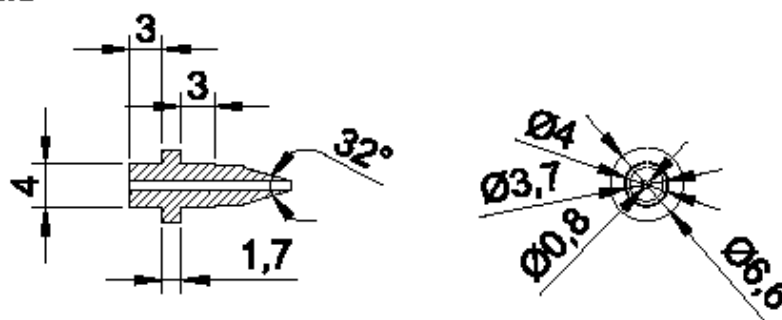
Filter capsule part #1
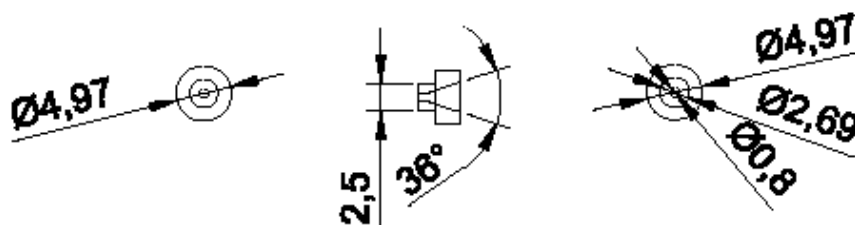
Filter capsule part #2

Annex B – Solution for Zeroth, First and Second Moments of a Frequency Distribution

$$M_j = \int_0^{V_{total}} V^j \frac{dC}{dV} dV$$

Finding the zeroth moment $M_0 = \int_{C_{Initial}}^{C_{Final}} V^0 dC$

$$M_0 = C_{Final} - C_{Initial}$$

Finding the first moment $M_1 = \int_{C_{Initial}}^{C_{Final}} V dC$

$$M_1 = \int_{C_{Initial}}^{C_{Final}} V dC$$

Finding the second moment $M_2 = \int_{C_{Initial}}^{C_{Final}} V^2 dC$

$$\mu = \frac{M_1}{M_0}$$

$$\boxed{\mu = \frac{\int_{C_{Initial}}^{C_{Final}} V dC}{C_{Final} - C_{Initial}}} \rightarrow \boxed{\mu \approx \frac{\sum_0^i V_i \Delta C_i}{C_{Final} - C_{Initial}}}$$

$$\sigma^2 = \frac{M_2}{M_0} - \left(\frac{M_1}{M_0}\right)^2$$

$$\sigma^2 = \frac{\int_{C_{Initial}}^{C_{Final}} V^2 dC}{C_{Final} - C_{Initial}} - \mu^2$$

$$\sigma^2 = \frac{\int_{C_{Initial}}^{C_{Final}} V^2 dC}{C_{Final} - C_{Initial}} - 2\mu^2 + \mu^2$$

$$\sigma^2 = \frac{\int_{C_{Initial}}^{C_{Final}} V^2 dC}{C_{Final} - C_{Initial}} - \frac{2\mu \int_{C_{Initial}}^{C_{Final}} V dC}{C_{Final} - C_{Initial}} + \frac{\mu^2 (C_{Final} - C_{Initial})}{C_{Final} - C_{Initial}}$$

$$\sigma^2 = \frac{\int_{C_{Initial}}^{C_{Final}} V^2 dC}{C_{Final} - C_{Initial}} - \frac{2\mu \int_{C_{Initial}}^{C_{Final}} V dC}{C_{Final} - C_{Initial}} + \frac{\mu^2 \int_{C_{Initial}}^{C_{Final}} 1 dC}{C_{Final} - C_{Initial}}$$

$$\sigma^2 = \frac{\int_{C_{Initial}}^{C_{Final}} V^2 dC}{C_{Final} - C_{Initial}} - \frac{\int_{C_{Initial}}^{C_{Final}} 2\mu V dC}{C_{Final} - C_{Initial}} + \frac{\int_{C_{Initial}}^{C_{Final}} \mu^2 dC}{C_{Final} - C_{Initial}}$$

$$\sigma^2 = \frac{\int_{C_{Initial}}^{C_{Final}} V^2 - 2\mu V + \mu^2 dC}{C_{Final} - C_{Initial}}$$

Factorising the numerator $\boxed{\sigma^2 = \dfrac{\int_{C_{Initial}}^{C_{Final}} (V - \mu)^2 dC}{C_{Final} - C_{Initial}}} \rightarrow \boxed{\sigma^2 \approx \dfrac{\sum_0^i (V_i - \mu)^2 \Delta C_i}{C_{Final} - C_{Initial}}}$